

Manganese-catalyzed synthesis of polyketones using hydrogen-borrowing approach.

KULYABIN, P.S., MAGDYSYUK, O.V., NADEN, A.B., DAWSON, D.M.,
PANCHOLI, K., WALKER, M., VASSALLI, M. and KUMAR, A.

2024

© 2024 The Authors. Published by American Chemical Society. Supplementary materials are appended after the main text of this document.

Manganese-Catalyzed Synthesis of Polyketones Using Hydrogen-Borrowing Approach

Pavel S. Kulyabin, Oxana V. Magdysyuk, Aaron B. Naden, Daniel M. Dawson, Ketan Pancholi, Matthew Walker, Massimo Vassalli, and Amit Kumar*



Cite This: *ACS Catal.* 2024, 14, 10624–10634



Read Online

ACCESS |



Metrics & More



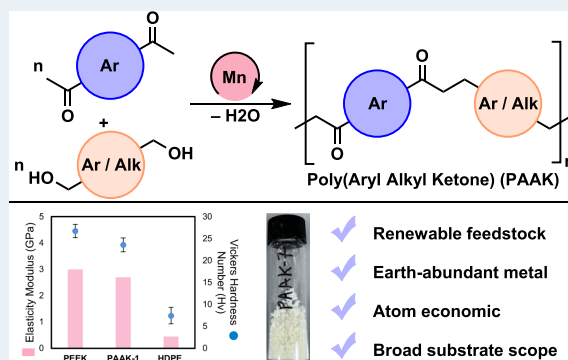
Article Recommendations



Supporting Information

ABSTRACT: We report here a method of making polyketones from the coupling of diketones and diols using a manganese pincer complex. The methodology allows us to access various polyketones (polyaryllalkylketone) containing aryl, alkyl, and ether functionalities, bridging the gap between the two classes of commercially available polyketones: aliphatic polyketones and polyaryletherketones. Using this methodology, 12 polyketones have been synthesized and characterized using various analytical techniques to understand their chemical, physical, morphological, and mechanical properties. Based on previous reports and our studies, we suggest that the polymerization occurs via a hydrogen-borrowing mechanism that involves the dehydrogenation of diols to dialdehyde followed by aldol condensation of dialdehyde with diketones to form chalcone derivatives and their subsequent hydrogenation to form polyaryllalkylketones.

KEYWORDS: manganese, polyketones, dehydrogenation, diketone, hydrogen-borrowing



INTRODUCTION

Polyketones are high-performance thermoplastics with a wide range of applications in the automotive, electronics, electrical, and medical industries.^{1,2} Compared with the structure of polyolefins, polyketones contain additional C=O groups in the polymer backbone chains which due to its polarity imparts excellent mechanical properties, crystallinity, hydrophilicity, and surface properties.³ Compared with polyamides, polyketones lack the NH group in the polymer backbone chain, which makes it much less hygroscopic and less sensitive to moisture. Despite the excellent properties of polyketones, this class of polymer has been relatively less studied. Aliphatic polyketones (POKs) are made from the reaction of late transition-metal-catalyzed coupling of ethene and/or propene with carbon monoxide (Figure 1A).⁴ Although the seminal reports on the synthesis of aliphatic polyketones (POK) date back to the 1940s and 1950s using nickel,^{5,6} and the 1980s using palladium,⁷ it was only in 1996 that POK was first commercialized by the Shell. However, the product was discontinued in 2000 due to reasons such as low demand and difficulty in polymer processing. Nevertheless, due to the demand of the POK, the product was relaunched in 2015 by Hyosung (a company in South Korea). Another class of polyketones is aromatic polyketones that also contain ether linkages and is known as polyaryletherketone (PAEK).⁸ The most common types of polymers from this class are polyetheretherketone (PEEK) and polyetherketoneketone (PEKK). These polymers have been commercialized since the

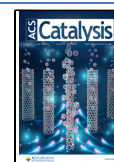
1980s and exhibit exceptional mechanical properties and chemical resistance. Their performance is considered the highest among all thermoplastics, and as a result, they are used in demanding applications such as aerospace, oil and gas drilling, and medical implants.^{1,2} Nevertheless, these polymers are difficult to process, and there is an ongoing need to develop new materials of this class bearing higher processability and keeping similar levels of thermal and mechanical properties. Additionally, in comparison to aliphatic polyketones (POK), aromatic polyketones or polyaryletherketones (PAEK) are around 10 times more expensive due to the use of more expensive feedstock/reagents. For example, polyetheretherketone (PEEK) is made from the nucleophilic substitution of 4,4'-difluorobenzophenone by the disodium salt of hydroquinone in the presence of a polar aprotic solvent such as diphenylsulfone at 300 °C (Figure 1B). Similarly, PEKK (polyetherketoneketone) is made via electrophilic polycondensation of diphenyl ether with mixtures of terephthaloyl chloride in the presence of AlCl₃ catalyst (Figure 1C). Another drawback of these methodologies is limited substrate scope due to the lack of commercial or

Received: May 22, 2024

Revised: June 7, 2024

Accepted: June 11, 2024

Published: June 28, 2024



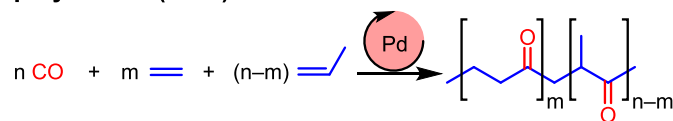
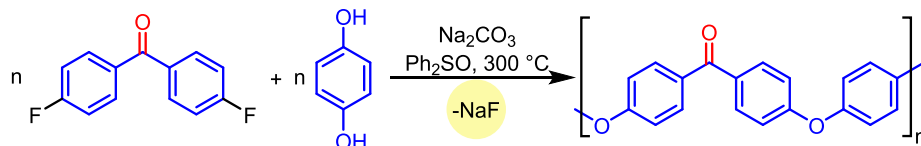
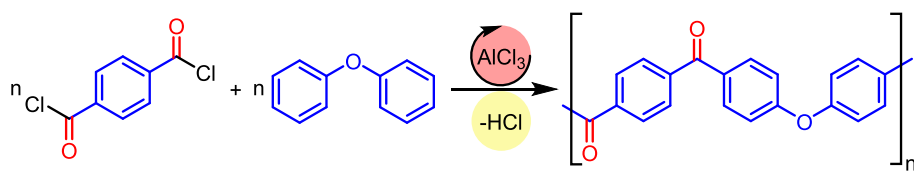
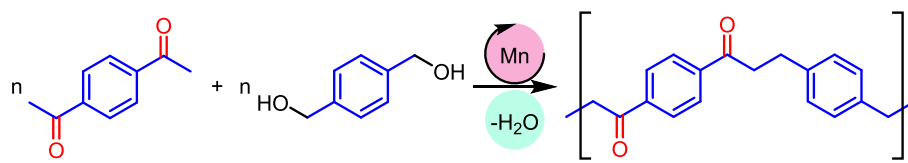
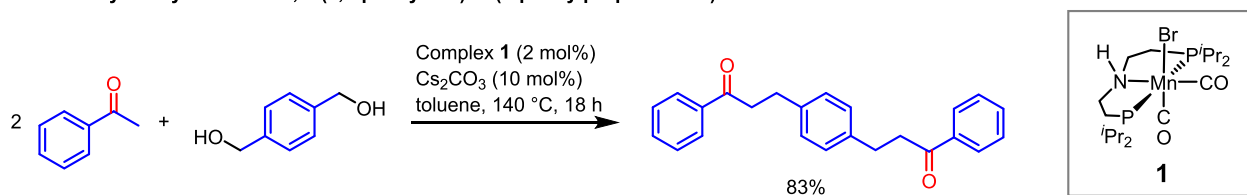
A. Aliphatic polyketone (POK)**B. Polyetheretherketone (PEEK)****C. Polyetherketoneketone (PEKK)****D. *This work*: Polyaryllalkylketone (PAAK)**

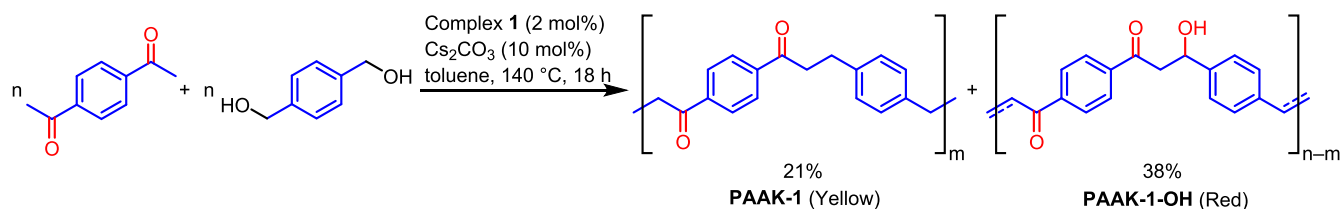
Figure 1. Methods for the synthesis of previously reported polyketones: aliphatic polyketone (POK), polyetheretherketone (PEEK), polyetherketoneketone (PEKK), and the polyketone reported herein: polyaryllalkylketone (PAAK).

Scheme 1. Coupling of Acetophenone (A) or 1,4-Diacetylbenzene (B) with 1,4-Benzenedimethanol in the Presence of the Precatalyst 1

A. Mn-catalysed synthesis of 3,3'-(1,4-phenylene)bis(1-phenylpropan-1-one)



B. Mn-catalysed coupling of 1,4-benzenedimethanol and 1,4-diacetylbenzene in toluene



inexpensive functional monomers of this type. It is noteworthy that polyaryllketones have been considered for several emerging applications in the recent past such as in the containment vessel for nuclear power plants,^{9,10} cryogenic hydrogen storage,¹¹ and separators for batteries.¹² Thus, there is a need to develop new methods to access diverse polyaryllketones that could offer excellent thermal, physical, and mechanical properties and can be produced and processed economically.

It has been suggested in the past that the presence of alkyl chains in the aliphatic ketones provides the necessary flexibility

for desirable processing whereas the presence of aromatic groups in polyaryllketones (PAEK) provides the exceptional mechanical properties.¹³ Therefore, a polyketone containing both aryl and alkyl groups, polyaryllalkylketone (PAAK) could potentially fill the gap between the properties of aliphatic and aromatic polyketones.

The concept of acceptorless dehydrogenative catalysis (where H₂ gas is released as a byproduct) and borrowing hydrogen catalysis (where the released H₂ is utilized to hydrogenate an intermediate in the reaction) are atom-economic approaches for

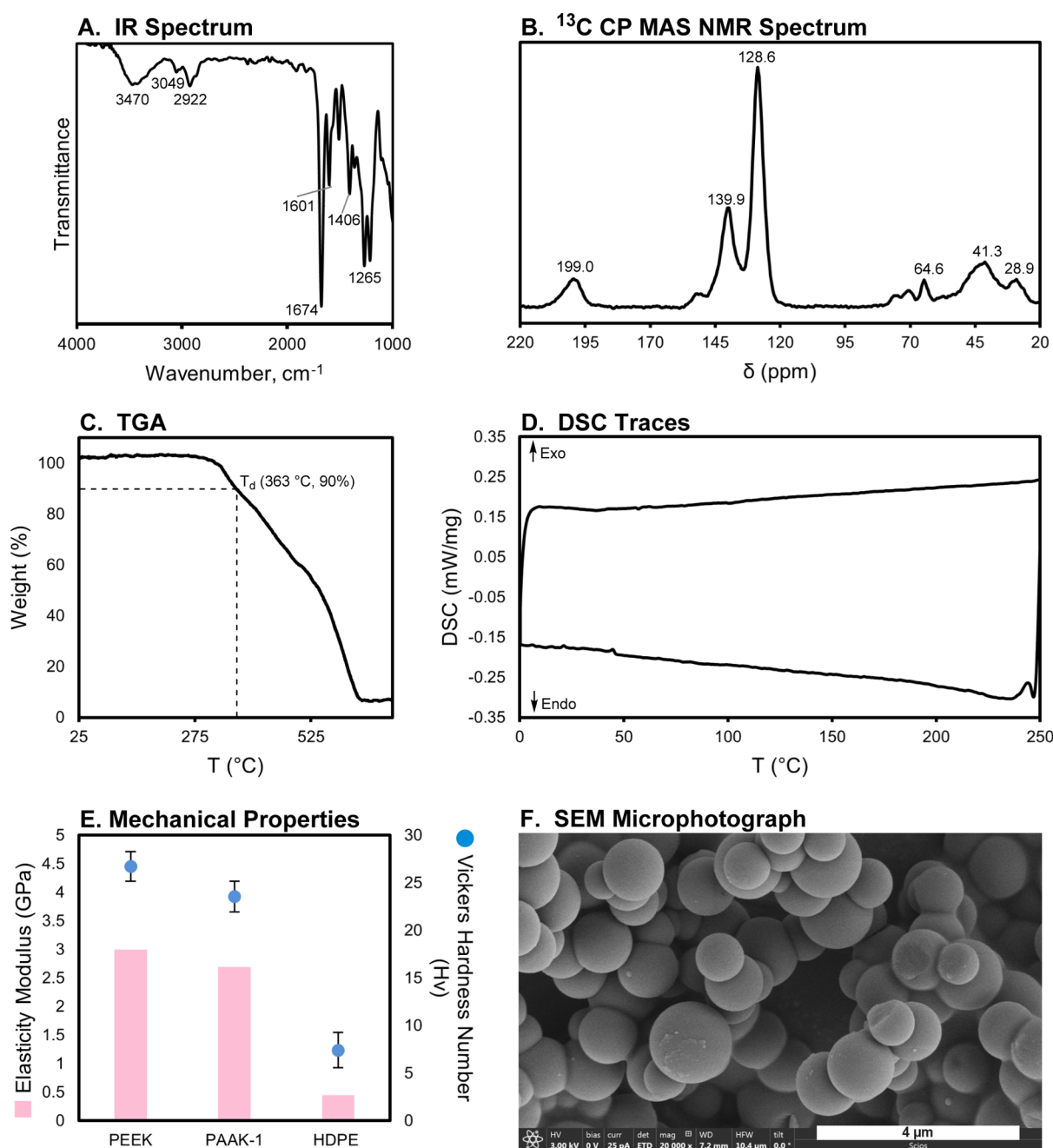


Figure 2. Characterization of PAAK-1. (A) Infrared spectrum (ATR-FTIR). (B) ^{13}C CP MAS NMR spectrum. (C) Mass loss as a function of temperature. (D) DSC plot. (E) Elasticity modulus and Vickers hardness number of commercial PEEK, polyketone PAAK-1, and HDPE. (F) SEM microphotograph.

the synthesis of organic compounds.¹⁴ The area has led to the discovery of several green transformations to make prevalent functional groups/compounds such as ketones,^{15,16} esters,¹⁷ amides,^{18–20} carboxylic acids,²¹ carbamates,^{22,23} ureas,^{24–26} amines,^{27,28} acetals,²⁹ imines,^{30,31} and heterocycles.³² These strategies have also been utilized for the synthesis of polymers such as polyesters^{33,34} and polyamides,^{34–36} and more recently polyureas^{37–39} and polyethylenimines⁴⁰ by us and others. Directly relevant to this report is the C-alkylation of ketones using alcohols that has been reported to undergo a borrowing hydrogen pathway by a number of transition metal catalysts such as ruthenium, manganese, and iron as recently reviewed by several groups.^{41–47} Despite several reports on this chemical

transformation, the study has remained limited to the synthesis of small molecules. We envisioned that this strategy might allow us to make the hypothesized polyaryllalkylketones (PAAK) from the metal-catalyzed coupling of diacetylaryls and diols for the first time. Since some diols can be prepared from renewable feedstocks, this approach can also allow us to make semi-renewable aromatic polyketones for the first time.

RESULTS AND DISCUSSION

We started our investigation by studying a model reaction: coupling of acetophenone (0.4 M) with 1,4-benzenedimethanol (0.2 M) in the presence of 2 mol % complex 1 and 10 mol % Cs_2CO_3 in toluene (140 $^{\circ}\text{C}$, 18 h). The choice of our initial

Table 1. Optimization of Catalytic Conditions for the Coupling of 1,4-Diacetylbenzene and 1,4-Benzenedimethanol^a

entry	complex	conc. (M)	Cs ₂ CO ₃ (mol %)	time (h)	yield ^b (%)	T _d ^c (°C)
1 ^d	1 (2 mol %)	0.2	10	18	89	338
2 ^d	2 (2 mol %)	0.2	10	18	<5	n.d.
3 ^d	3 (2 mol %)	0.2	10	18	51	353
4 ^d	4 (2 mol %)	0.2	10	18	17	319
5 ^d	1 (1 mol %)	0.2	10	18	87	356
6 ^d	1 (0.5 mol %)	0.2	10	18	70	348
7	1 (1 mol %)	0.1	10	18	85	373
8 ^e	1 (1 mol %)	0.05	10	18	86	342
9 ^f	1 (1 mol %)	0.1	10	18	73	342
10	1 (1 mol %)	0.1	20	18	90	369
11	1 (1 mol %)	0.1	3	18	80	335
12 ^g	1 (1 mol %)	0.1	10	18	67	328
13	1 (1 mol %)	0.1	10	2	89	363
14	1 (1 mol %)	0.1	10	1	81	343
15	none	0.1	10	18	8	396
16	1 (1 mol %)	0.1	none	18	none	n.d.
17 ^h	1A (1 mol %)	0.1	1	18	none	n.d.
18 ^h	1A (1 mol %)	0.1	2	18	<5	n.d.
19	Mn(CO) ₅ Br (1 mol %)	0.1	10	18	<5	n.d.
20	Mn(CO) ₅ Br (1 mol %)/PPh ₃ (3 mol %)	0.1	10	18	<5	n.d.

1

2

3

4

1A

^aGeneral reaction conditions: 1,4-diacetylbenzene (0.5 mmol), 1,4-benzenedimethanol (0.5 mmol), 100 mL ampule with J-Young's valve, temperature 140 °C, *t*AmOH. ^bAll yields are isolated yields. ^cT_d stands for the decomposition temperature calculated from TGA (thermogravimetric analysis) as a temperature of 10% weight loss. N.d. stands for not detected. ^d1 mmol of 1,4-diacetylbenzene and 1,4-benzenedimethanol was used. ^e10 mL of *t*AmOH was used. ^fReaction in 15 mL pressure vessel. ^gReaction at 110 °C. ^hThe activated complex 1A was prepared with 1 or 2 equivalents of KO^tBu. See SI (Page S27–S28) for details. ⁱThe activated complex 1A was prepared with 1 or 2 equivalents of KO^tBu. See SI (Page S27–S28) for details.

catalytic conditions was inspired by the previous reports⁴¹ on the transition-metal-catalyzed C-alkylation of ketones using alcohols especially the one by Beller where reactions in toluene were as effective as that in 1,4-dioxane and *tert*-amyl alcohol.⁴⁸ Remarkably, this led to the formation of the expected diketone in 83% isolated yield, which was characterized by NMR and IR spectroscopy (Scheme 1A). Motivated by this initial result, we studied the coupling of 1,4-diacetylbenzene (0.2 M) with 1,4-benzenedimethanol (0.2 M) under identical reaction conditions. The reaction led to the isolation of a mixture of yellow (21% yield) and red (38% yield) solids that could be physically separated (Scheme 1B). Both of these solids were found to be insoluble in common solvents such as toluene, DCM, acetone, chloroform, tetrahydrofuran (THF), chlorobenzene, water, dimethylformamide (DMF), dimethyl sulfoxide (DMSO), and trifluoroacetic acid, because of which we could not employ solution-state NMR spectroscopy to analyze the chemical structure of these materials. The IR spectrum of the yellow solid (Figure 2A) showed signals at 3049 and 2922 cm⁻¹ corresponding to aromatic and aliphatic C–H stretching frequencies. The presence of aromatic rings was further

confirmed by signals at 1601 and 1508 cm⁻¹ characteristic of aromatic C=C stretches. A sharp signal at 1674 cm⁻¹ characteristic of an aromatic C=O (ketone) stretching frequency was observed. A broad signal at 3470 cm⁻¹ can be assigned to the O–H group, presumably the end group of the polymer. These spectral assignments are suggestive of the structure of the polymer to be PAAK-1 (Scheme 1B) and are also in agreement with a reported polyketone made from the reaction of styrene and CO that contained phenyl groups, CH₂ linkages, and ketone groups.⁴⁹ The IR spectrum of the red solid (Figure S5, see SI) looked very similar to that of the yellow solid except for the two distinctive signals at 1605 and 1373 cm⁻¹ which are attributed to olefinic C=C and C–O bonds, respectively. Additionally, a much broader signal at 3348 cm⁻¹ corresponding to the O–H stretch was also observed. Based on these observations, we suggest that the red solid is a polyaryllalkylketone with some double bonds and O–H groups characterized to be PAAK-1-OH (Scheme 1B).

We hypothesized that the elimination of water from PAAK-1-OH might be facilitated by the presence of a proton source in the reaction mixture that would convert the hydroxy group into a

Table 2. Substrate Scope for the Synthesis of Polyketones from Diketones and Diols

$$n \text{ (diketone)} + n \text{ (diol)} \xrightarrow[2-18 \text{ h, } 140^\circ\text{C, } t\text{AmOH}]{\text{1 (1 mol\%), base (10-100 mol\%)}} \left[\text{polyketone} \right]_n + \text{H}_2\text{O}$$

Entry	Diketone	Diol	Yield ^d (%)	M _w , ^c (kDa)	<i>Đ</i> ^c	T _d ^f (°C)	Morphology
1 ^a			89 95 ^g	51.1 1.5	1.6 1.3	363, 397 ^g	Spherical (size ~1.5 μm)
2 ^a			77	54.1 1.2	1.6 1.2	351	Spherical (size ~0.5 μm)
3 ^{a,b}			41	52.9 1.6	1.7 1.3	369	Spherical (size ~3 μm)
4 ^a			98	51.1 1.4	1.7 1.3	350	Spherical agglomerates (0.2-2 μm)
5 ^a			97	53.7 2.1	1.6 1.6	365	Spherical agglomerates (0.1-2 μm)
6 ^{a,b}			99	59.6	1.6	380	Spherical agglomerates (0.1-1 μm)
7 ^a			93 99 ^g	58.5 2.4	1.8 1.4	362, 371 ^g	Spherical (size ~2 μm)
8 ^a			79	53.9 1.6	1.4 1.3	365	Spherical (size ~1 μm)
9 ^{a,b}			71	53.4	1.7	383	Non-homogeneous agglomerates
10 ^c			57	621.6 ^h	109 ^h	363	Spherical (size ~2 μm)
11 ^c			64	899.1 ^h	149 ^h	375	Non-homogeneous agglomerates
12 ^c			52	53.6 3.0	1.7 1.3	381	Non-homogeneous agglomerates

^aReaction conditions: diketone (0.5 mmol), diol (0.5 mmol), **1** (2.5 mg, 0.005 mmol), Cs₂CO₃ (16.5 mg, 0.05 mmol) in a 100 mL J-Young's flask, temperature 140 °C, 2 h. All yields are isolated yields. ^b18 h. ^c*t*BuOK (56 mg, 0.5 mmol), 18 h. ^dAll yields are isolated yields. ^ePolymer samples were heated in Cl₂CHCOOH at 120 °C overnight, filtrated, diluted with CHCl₃, and then GPC analysis was performed in CHCl₃/Cl₂CHCOOH = 8/2 mixture at 35 °C. ^fT_d corresponds to the temperature of 10% weight loss. ^gReaction is conducted under H₂ atmosphere. ^hGPC showed polymodal distribution.

better leaving group (water) or by using a polar protic solvent. Indeed, performing the reaction in *tert*-amyl alcohol (*t*AmOH) solvent resulted in the selective formation of PAAK-1 in 89% yield (Table 1, entry 1). Performing the same reaction in the presence of ruthenium^{50,51} and iridium⁴⁷ complexes, **2**–**4** that have been previously reported for the catalytic dehydrogenative transformations led to relatively lower yields of PAAK-1 (Table 1, entries 2–4). We then studied the effect of various catalytic conditions, e.g., concentration of starting materials and base, and size of the reaction vessel, on the yield of the reaction.

Interestingly, using **1** mol % complex **1** also led to the isolation of PAAK-1 in 87% yield (entry 5). Further reducing the catalytic loading to 0.5 mol % led to a lower but still very good, isolated yield (70%) of PAAK-1 (entry 6). Conducting a reaction at 0.1 M concentration of 1,4-diacetylbenzene and 1,4-benzenedimethanol led to the formation of PAAK-1 in 85% yield which is similar to that conducted at 0.2 M concentration (entry 5) although a higher T_d (decomposition temperature, 373 °C, entry 7) was observed in the case of 0.1 M concentration in comparison to that of 0.2 M concentration (T_d = 356 °C, entry

5). Decreasing the concentration further to 0.05 M did not make any significant difference in the yield or T_d of the isolated polymer, in comparison to that of 0.1 M (entry 8). Changing the size of the reaction vessel from 100 to 15 mL did not make any significant difference in the yield and thermal stability of the polymer (entry 9). Increasing the amount of Cs_2CO_3 to 20 mol % (entry 10) led to a slight increment in yield (90%), whereas decreasing the amount of Cs_2CO_3 reduced the yield (80%, entry 11), suggesting the significance of base in the coupling process. Lowering the temperature to 110 °C reduced the yield to 67% (entry 12). Interestingly, studying the time profile of the reaction suggested that the reaction reaches completion in 2 h leading to 89% yield of the PAAK-1, whereas 81% yield is obtained in 1 h (entries 13, 14). Finally, when the reaction was conducted in the absence of complex **1** and by using just Cs_2CO_3 (10 mol %), 8% of the solid was isolated (entry 15). Based on the IR spectrum and thermal studies of the isolated material, we suggest that the obtained product is a polymer resulting from the self-condensation of 1,4-diacetylbenzene (see SI, Figures S44 and S45). At the same time, no conversion of any starting material was obtained when the reaction was conducted in the presence of complex **1** without using any base (entry 16). Another control experiment was carried out using the preactivated catalyst **1A**; however, although it resulted in the transfer hydrogenation of diketone through the dehydrogenation of diol, it did not result in the formation of the expected polyketone suggesting the significance of the role of base in polymer chain propagation (entries 17, 18). Additionally, conducting the reaction in the presence of $\text{Mn}(\text{CO})_5\text{Br}$ (1 mol %) and the combination of $\text{Mn}(\text{CO})_5\text{Br}$ (1 mol %) + PPh_3 (3 mol %) resulted in only less than 5% yield of the polyketone material (entries 19 and 20) suggesting that the manganese-MACHO pincer complex (**1**) is important in the catalytic process. Thus, the optimized catalytic conditions are complex **1** (1 mol %), Cs_2CO_3 (10 mol %), 1,4-diacetylbenzene (0.1 M), 1,4-benzenedimethanol (0.1 M), 140 °C, 2 h, *t*AmOH (entry 13).

The structure of PAAK-1 was further corroborated by a solid-state $^{13}\text{C}\{^1\text{H}\}$ CP MAS NMR spectrum that showed signals at δ 29–50, 128–151, and 199 ppm characteristic of alkyl, aryl, and ketone regions, respectively, confirming the structure of PAAK-1 (Figure 2B, corresponding to Table 1, entry 13). Additionally, analysis of the mother liquor upon precipitation of polymer in the case of Table 1, entry 6, by ^1H and $^{13}\text{C}\{^1\text{H}\}$ NMR spectroscopy showed the presence of phenylcarbonyl, phenylenemethanol, acetophenonyl, and 1-phenyl-ethanol end groups and 1,3-diphenylpropanone fragments (see Section 1.4 in the SI). Further analysis of mother liquor by electrospray-ionization-mass spectrometry (ESI-MS) confirmed the presence of oligomers containing ketone and alcohol components (see section 1.13 in the SI). These intermediates support the structure of PAAK but it is possible that the polymer is irregular with randomly distributed keto and hydroxy groups and double bonds along the polymer chain.

Thermal properties of the polymer were investigated by thermogravimetric analysis (TGA) and differential scanning calorimetry (DSC), which revealed that the PAAK-1 is a thermoset material with a decomposition temperature of 363 °C (T_d , 10% weight loss) as no melting temperature could be observed (Figure 2C,D). This was further confirmed by the powder X-ray diffraction (XRD) study that revealed that the polymer is amorphous in nature (Figure S39, SI). According to

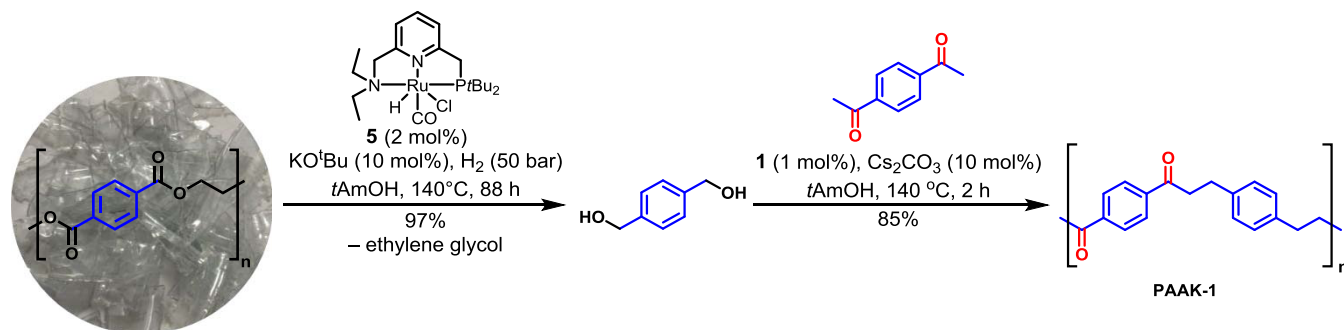
DSC analysis, the newly synthesized PAAK-1 does not have glass transition point (T_g) (Figure S49, SI).⁵²

To get some understanding of the mechanical properties of the synthesized polyketone (PAAK-1), we processed the polymer using hot compression to prepare a film of 2 mm thickness, which was used to study the load–displacement curve using nanoindentation. The elasticity modulus and Vickers hardness of the PAAK-1 were measured to be 2.7 GPa and 23.6 HV, respectively (Figure 2E). For comparison, the nanoindentation study was conducted with a commercial sample of PEEK and HDPE (high-density polyethylene) under identical conditions. Remarkably, the elasticity modulus and Vickers hardness number of the PAAK-1 were found to be comparable with the commercial sample of PEEK (3 GPa, and 26.7 HV), and higher than those measured for the HDPE (0.45 GPa and 7.4 HV). These numbers are also consistent with previous reports in the literature on the measurement of elasticity modulus and Vickers hardness of commercial PEEK and HDPE.^{53,54}

The morphology of polymers plays important roles in polymer processing and their applications and spherical particles are desirable for various processing techniques such as selective laser sintering which is used for 3-D printing or additive manufacturing which can also be used to process polyketones.⁵⁵ Polyketones can also be used in engineered powder, as was recently demonstrated by an electronics manufacturing company, Jabil Inc., which has launched PK5000 for additive manufacturing. This polyketone has desirable chemical and mechanical properties such as high impact strength and high abrasion resistance in comparison to nylons.^{56,57} A study of the morphology of PAAK-1 (made using Table 1, entry 9) using scanning electron microscopy (SEM) showed granular structures composed of small spherical particles of size around 1.3–1.5 μm (Figure 2F).

Having optimized the reaction conditions for the synthesis of PAAK-1 (polyaryllalkylketone), we studied the substrate scope of our methodology to understand the structure–property relationships. As described in Table 2 (entry 2), the coupling of 1,4-diacetylbenzene and 1,3-benzenedimethanol led to the formation of the corresponding polyaryllalkylketone in 77% yield. However, a lower yield of polyketone (41%) was obtained from the coupling of 1,4-diacetylbenzene and 1,4-cyclohexanedimethanol (entry 3). Remarkably, excellent yields of polyketones were obtained from the coupling of 1,3-diacetylbenzene with various diols (entries 4–6). To introduce ether functionality as in the case of polyaryletherketones (PAEKs), we used 4-acetylphenyl ether as a diketone feedstock. Remarkably, we were able to couple 4-acetylphenyl ether with various aromatic and aliphatic diols to make polyketones in moderate to excellent yields as described in Table 2, entries 7–12. Of particular significance is the use of *D*-Isosorbide as a diol (entry 12) that is a commercially available sugar derivative and can also be made from cellulose making the corresponding polyketone to be semirenewable.⁵⁸ The polymers were characterized by IR spectroscopy and ^{13}C CP/MAS solid-state NMR spectroscopy that showed signals corresponding to $\text{C}=\text{O}$, aromatic, and aliphatic groups (see SI, Section 1.5). Polyketone reported in entry 7, Table 2 (PAAK-7) was additionally analyzed with TGA-MS that showed the way this material decomposes. It was found that PAAK-7 starts decomposing at 320 °C with elimination of diketone-like components (m/z = 239 and 254 g/mol, Figure S151, SI), and xylene-derived components (m/z = 79, 91, 92, and 107 g/mol) become the major components of ion current at temperatures

Scheme 2. Synthesis of Polyketone PAAK-1 from 1,4-Benzenedimethanol Derived from the Waste Plastic Bottle



higher than 400 °C (Figure S150, SI). It confirms that both components of the reaction mixture are incorporated into the final product.

As mentioned earlier, the isolated materials showed no solubility in all of the attempted solvents (toluene, water, methanol, THF, CHCl_3 , DCM, DMF, DMSO, TFA, and HFIP) at room temperature or on heating (100 °C) which made analysis of the polymers by gel permeation chromatography (GPC) very challenging. However, we managed to partially dissolve the material in dichloroacetic acid (upon heating overnight at 120 °C) and the soluble part was analyzed by GPC in dichloroacetic acid/ CHCl_3 solvent mixture. Most of the dissolved polymers showed bimodal distribution with a low-molecular-weight component of 1.2–3.0 kDa ($\bar{D} = 1.2\text{--}1.6$) and a high-molecular-weight component of 51.1–58.5 kDa ($\bar{D} = 1.6\text{--}1.8$) (Table 2). Extremely broad polydispersities were observed for polymers reported in cases of entries 10 and 11, Table 2. Interestingly, monomodal distribution was obtained in cases of entries 6 and 9 (Table 2) when 1,4-cyclohexyldimethanol was utilized as a diol with $M_w = 59.6$ kDa ($\bar{D} = 1.6$) and 53.4 kDa ($\bar{D} = 1.7$), respectively. The same method was used to analyze molecular masses of commercial polyketones (Table S3, SI), POK and PEKK being completely soluble in dichloroacetic acid and PEEK only partially soluble. GPC showed that all of these polymers are monomodal ($\bar{D} = 2.2\text{--}7.5$) and have a higher molecular weight (63.3–126.8 kDa) than PAAK polymers reported herein.

The decomposition temperature (T_d), calculated as a temperature of 10% weight loss from TGA (thermogravimetric analysis), was found to be in the range of 321–383 °C as described in Table 2. This was lower than what was found for commercial PEEK and PEKK samples ($T_d = 581$ and 557 °C, respectively, see SI, Table S3) and close to the thermostability of commercial POK ($T_d = 387$ °C, see SI, Table S3). The powder XRD studies showed that all of the polyketones reported herein are amorphous in nature with some polymers containing an unidentified component of crystallinity (see SI, Section 1.5 for full details). This is consistent with the absence of any melting temperature in DSC traces of these polyketones. Additionally, DSC traces of PAAKs do not demonstrate any glass transition temperature which could be a sign of cross-linking in the material. It is known that a certain degree of cross-linking can increase the glass transition temperature of the polymer above the decomposition temperature.⁵² In support of this, the traces of terephthalic aldehyde-derived cross-linking were observed in the high-resolution mass spectrum of crude reaction mixture of small-molecule model reaction shown in Scheme 1A (Figure S1, SI). Presumably, since the glass transition temperature of aromatic polyketones is usually higher than 100 °C, even one

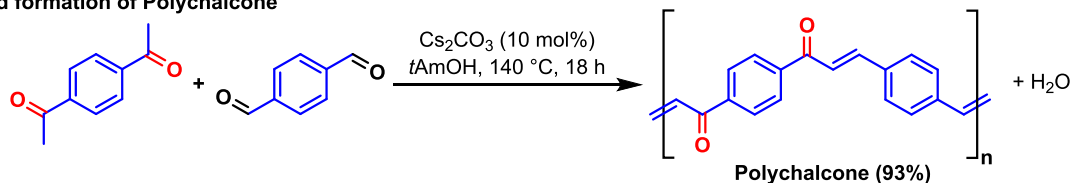
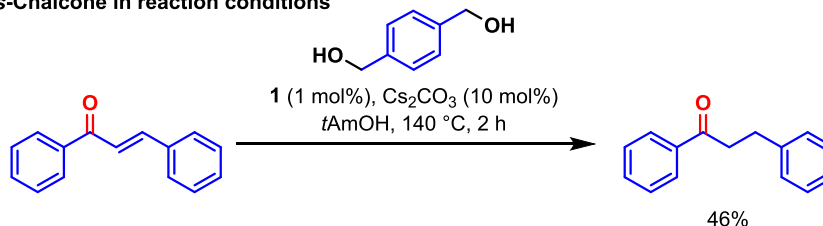
cross-link between two polymer chains could be enough to increase T_g above the decomposition temperature. The morphology of polyketones for most cases showed agglomerates of spherical particles in the range of 0.2–3 μm , as described in Table 2. In some cases, the particle sizes were more uniform (e.g., entry 1) than others (e.g., entry 4), whereas in some cases, nonhomogeneous agglomerates were observed (see SI, Section 1.18).

We envisioned that since the product precipitates out from the reaction medium whereas the catalyst is likely to remain soluble, this presents an opportunity to test the recyclability of the catalyst. After the reaction conducted as described in Table 2, entry 7 (coupling of 4-acetylphenyl ether (0.5 mmol) and 1,4-benzenedimethanol (0.5 mmol) that led to the isolation of polyketone in 89% yield), the mother liquor solution was transferred to another Young's flask containing 4-acetylphenyl ether (0.5 mmol), 1,4-benzenedimethanol (0.5 mmol), and Cs_2CO_3 (10 mol %). The reaction mixture was then refluxed at 140 °C for 2 h, resulting in the isolation of PAAK-7 in 55% yield showing an IR spectrum identical to that of the polymer isolated in the first batch (see Section 1.9 in the SI). Interestingly, when the recycling study was performed without adding base in the second stage, no precipitate was observed, suggesting the involvement of base in steps other than generating the active species from the precatalyst 1.

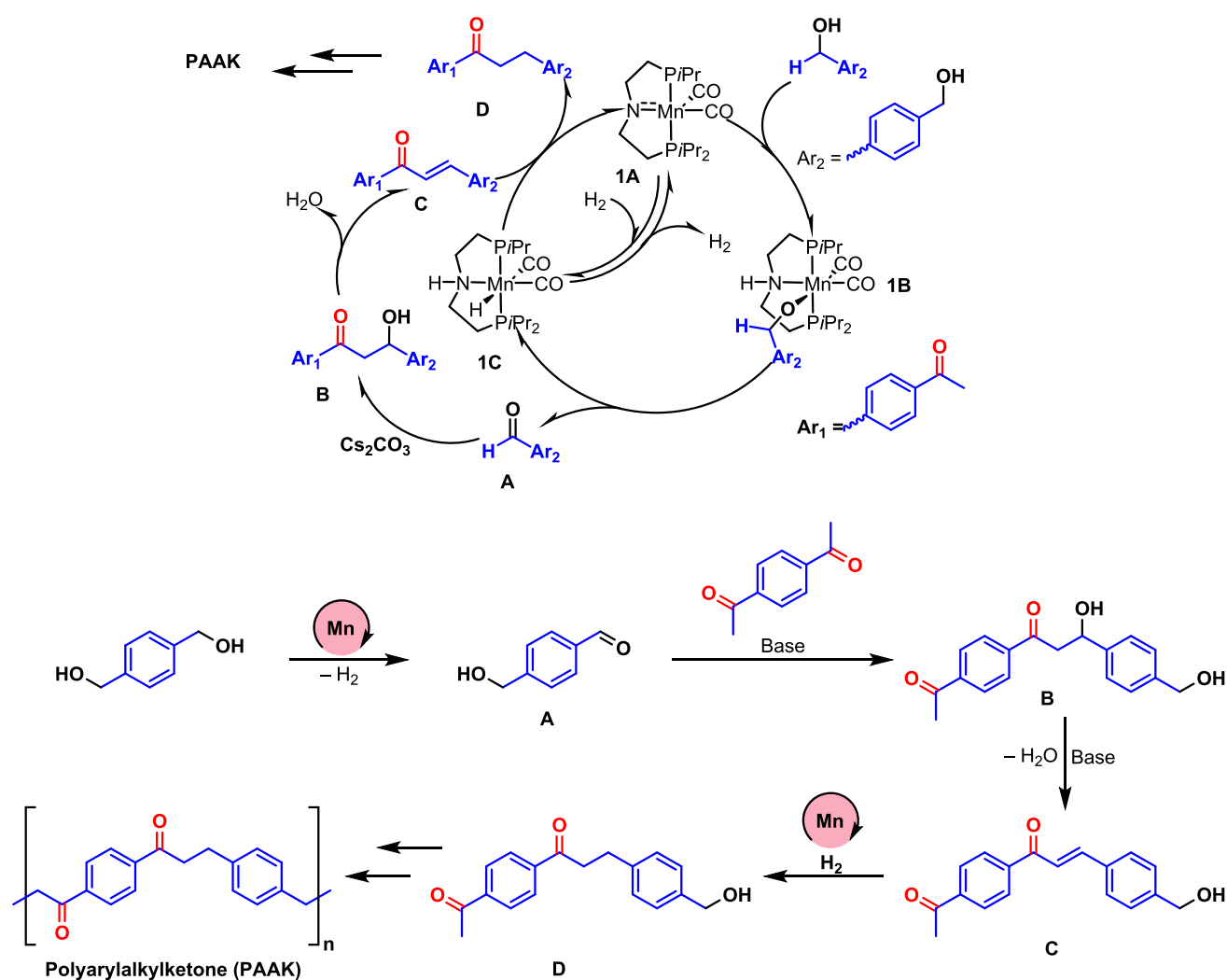
In pursuit of methods to make (semi)renewable plastics, we envisioned if a polyketone could be made from a diol sourced from the depolymerization of waste plastic such as poly(ethylene terephthalate) (PET). To achieve this, we carried out a two-step process where PET waste (sourced from plastic bottle) was first hydrogenatively depolymerized in a pressure reactor using the Milstein's ruthenium PNN catalyst (5, 2 mol %, and KOtBu , 10 mol %) in *t*AmOH solvent to form 1,4-benzenedimethanol and ethylene glycol in approximately quantitative yields as confirmed by the ^1H NMR spectroscopy (see Section 1.11 in SI). Analogous reaction on the hydrogenative depolymerization of PET has been reported previously by Robertson⁵⁹ and Klankermayer.⁶⁰ The mixture of 1,4-benzenedimethanol and *t*AmOH was then separated from ethylene glycol by extraction in DCM/water to which 1,4-diacetylbenzene, manganese complex 1 (1 mol %), and Cs_2CO_3 (10 mol %) were added and the reaction mixture was heated for 2 h at 140 °C as described in Table 2. This led to the isolation of PAAK-1 in 85% yield (Scheme 2). The reaction in the case when 1,4-benzenedimethanol was not separated from ethylene glycol led to the formation of a polyketone in only 21% yield that contained hydroxyl groups and double bonds according to IR spectroscopy.

Scheme 3. Control Experiments (A, B) and Proposed Pathway for the Formation of Polyketones (C)

A. Base-catalysed formation of Polychalcone

B. Hydrogenation of *trans*-Chalcone in reaction conditions

C. Proposed pathway for the synthesis of polyketones



Mechanisms for the coupling of ketone and alcohols to form alkylated ketones using analogous pincer complexes have been studied using both experiments and DFT computation.^{61,62} Based on the previous studies,⁴⁸ we hypothesize that the reaction proceeds via a “hydrogen-borrowing” mechanism

involving (i) metal-catalyzed dehydrogenation of the alcohol to aldehyde, (ii) base-catalyzed aldol condensation of the aldehyde with the ketone to form a chalcone-type derivative, and (iii) metal-catalyzed hydrogenation of the $\text{C}=\text{C}$ bond to form an alkylated ketone (Scheme 3C). We conducted a few

experiments to verify this proposal. First, performing a reaction of terephthalaldehyde with 1,4-diacetylbenzene in the presence of 10 mol % Cs_2CO_3 led to the formation of polychalcone in 93% yield (Scheme 3A). This suggests our proposal that Cs_2CO_3 is sufficient to catalyze the aldol condensation steps, whereas manganese is needed for the catalytic (de)hydrogenation steps. As described in the mechanism (Scheme 3C), a stoichiometric evolution of hydrogen gas is not observed, as it gets consumed in the subsequent hydrogenation step. In most cases, we observe less than 5 mL of gas. Analysis of this gas by the GC (thermal conductivity detector) confirmed it to be H_2 supporting our mechanistic proposal (see Section 1.10 in the SI). Furthermore, we also demonstrated that precatalyst **1** is capable of the hydrogenation of $\text{C}=\text{C}$ in chalcone by transfer hydrogenation from diol under the optimized reaction conditions making dihydrochalcone in 46% yield (Scheme 3B, Section 1.12 in the SI).

We then hypothesized that conducting the catalytic reactions in the presence of a hydrogen atmosphere (1 bar) might ensure the hydrogenation of any remaining $\text{C}=\text{C}$ bond in the polyketone chain and improve the yield and thermal properties of the polymers. Indeed, performing the synthesis of PAAK-1 in the presence of a hydrogen atmosphere (1 bar) resulted in a higher yield (95 vs 89%) and higher thermal stability ($T_d = 397$ vs 363°C) as described in Table 2, entry 1 (Section 1.8, see the SI). A similar trend was obtained for PAAK-7 (Table 2, entry 7, and Section 1.8 in the SI).

Based on the control experiments described above and mechanistic studies reported in the literature,⁴⁸ we have outlined a mechanism for the formation of polyketone (PAAK, Scheme 3C). The reaction starts with the dehydrogenation of 1,4-benzenedimethanol to a hydroxyaldehyde by the activated manganese complex **1A** that converts to the manganese hydride complex **1C** via an alkoxy complex **1B**. Based on previous studies,⁴⁸ it is likely that the dehydrogenation occurs through an “outer-sphere” mechanism. The formed hydroxyaldehyde can perform aldol condensation with 1,4-diacetylbenzene in the presence of base to form an alkene **C** via intermediate **B**. Alkene **C** can be hydrogenated by manganese hydride complex **1C** to form alkylated ketone. The continuation of this process would lead to the formation of polyketone (PAAK).

CONCLUSIONS

In conclusion, we have demonstrated the synthesis of a new class of polyketones called polyaryalkylketones (PAAK) using a new methodology based on the hydrogen-borrowing concept that has not been used for the synthesis of polyketones before. Among the studied catalysts, the manganese pincer complex **1** was found to be the best catalyst for this process, affording high yields using 0.5–1.0 mol % catalytic loading and in the reaction time as low as 2 h. Using this methodology, 12 new polyketones were synthesized using various diketones and diols including a renewable diol and a diol obtained from the depolymerization of waste plastic bottles. The isolated polymers were characterized by IR and solid-state NMR spectroscopy, GPC, powder XRD, SEM, and TGA/DSC studies. The elasticity modulus and Vickers hardness of PAAK-1 (a polyketone reported herein) estimated using nanoindentation were found to be comparable with a commercial sample of polyketone. Based on previous studies and conducted experiments herein, we suggest that the polymerization occurs via the hydrogen-borrowing mechanism, as outlined in Scheme 3C.

ASSOCIATED CONTENT

Data Availability Statement

The raw research data supporting this publication can be accessed at <https://doi.org/10.17630/3030ef3c-569c-45d9-ae6c-113de22d1db2>.

Supporting Information

The Supporting Information is available free of charge at <https://pubs.acs.org/doi/10.1021/acscatal.4c03019>.

Experimental details; characterization data; TGA, DSC curves; PXRD; and NMR spectra (PDF)

AUTHOR INFORMATION

Corresponding Author

Amit Kumar – EaStCHEM, School of Chemistry, University of St Andrews, St Andrews KY16 9ST, U.K.; orcid.org/0000-0002-8175-8221; Email: ak336@st-andrews.ac.uk

Authors

Pavel S. Kulyabin – EaStCHEM, School of Chemistry, University of St Andrews, St Andrews KY16 9ST, U.K.; orcid.org/0000-0003-2548-2117

Oxana V. Magdysyuk – EaStCHEM, School of Chemistry, University of St Andrews, St Andrews KY16 9ST, U.K.; orcid.org/0000-0003-3842-3239

Aaron B. Naden – EaStCHEM, School of Chemistry, University of St Andrews, St Andrews KY16 9ST, U.K.

Daniel M. Dawson – EaStCHEM, School of Chemistry, University of St Andrews, St Andrews KY16 9ST, U.K.; orcid.org/0000-0002-8110-4535

Ketan Pancholi – The Sir Ian Wood Building, Robert Gordon University, Aberdeen AB10 7GE, U.K.; orcid.org/0000-0001-7662-7764

Matthew Walker – Centre for the Cellular Microenvironment, Advanced Research Centre, University of Glasgow, Glasgow G11 6EW, U.K.; orcid.org/0000-0001-5119-9118

Massimo Vassalli – James Watt School of Engineering, University of Glasgow, Glasgow G12 8QQ, U.K.; orcid.org/0000-0002-3063-4376

Complete contact information is available at: <https://pubs.acs.org/doi/10.1021/acscatal.4c03019>

Author Contributions

The manuscript was written through contributions of all authors. All authors have given approval to the final version of the manuscript.

Notes

The authors declare no competing financial interest.

ACKNOWLEDGMENTS

This research was funded by a UKRI Future Leaders Fellowship (MR/W007460/1). The authors gratefully acknowledge funding from the EPSRC through grants EP/L017008/1, EP/R023751/1, and EP/T019298/1. They also thank Dr. Julia Payne for her assistance in initial powder XRD studies.

REFERENCES

- (1) Qin, L.; Yao, S.; Zhao, J.; Zhou, C.; Oates, T. W.; Weir, M. D.; Wu, J.; Xu, H. H. K. Review on Development and Dental Applications of Polyetheretherketone-Based Biomaterials and Restorations. *Materials* 2021, 14 (2), No. 408, DOI: 10.3390/ma14020408.

- (2) Vavasori, A.; Ronchin, L. Polyketones: Synthesis and Applications. In *Encyclopedia of Polymer Science and Technology*; Wiley: Hoboken, 2017; pp 1–41.
- (3) Sommazzi, A.; Garbassi, F. Olefin-Carbon Monoxide Copolymers. *Prog. Polym. Sci.* **1997**, *22* (8), 1547–1605.
- (4) Anselment, T. M. J.; Zintl, M.; Leute, M.; Nowack, R.; Rieger, B. Late Transition Metal Catalyzed Co- and Terpolymerization of α -Olefins with Carbon Monoxide. In *Handbook of Transition Metal Polymerization Catalysts*; Hoff, R., Ed.; John Wiley & Sons: Hoboken, NJ, 2018; pp 591–621.
- (5) Ballauf, F.; Bayer, O.; Leichmann, L. patent (Bayer AG). DE863711C1941.
- (6) (a) Reppe, W.; Mangini, A. patent (BASF SE). DE880297C1948. (b) Reppe, W.; Mangini, A. patent US2577208A, 1951.
- (7) Sen, A.; Lai, T. W. Novel Palladium(II)-Catalyzed Copolymerization of Carbon Monoxide with Olefins. *J. Am. Chem. Soc.* **1982**, *104* (12), 3520–3522.
- (8) Maloo, L. M.; Toshniwal, S. H.; Reche, A.; Paul, P.; Wanjar, M. B. A Sneak Peek Toward Polyaryletherketone (PAEK) Polymer: A Review. *Cureus* **2022**, *14* (11), No. e31042.
- (9) Ding, R.; Xu, L.; Li, J.; Liao, J.; Wang, J.; Wang, Z.; Ma, H. Investigation and Life Expectancy Prediction on Poly(Ether-Ether-Ketone) Cables for Thermo-Oxidative Aging in Containment Dome of Nuclear Power Plant. *Polym. Test.* **2021**, *103*, No. 107362.
- (10) Teng, R.; Wang, H.; Qu, M.; Zhou, G. Synthesis of Amorphous Poly (Aryl Ether Ketone) Resin and Its Anti-Irradiation Properties under Gamma Ray. *ChemistrySelect* **2023**, *8* (18), No. e202204784.
- (11) Flanagan, M.; Grogan, D. M.; Goggins, J.; Appel, S.; Doyle, K.; Leen, S. B.; Ó Brádaigh, C. M. Permeability of Carbon Fibre PEEK Composites for Cryogenic Storage Tanks of Future Space Launchers. *Composites, Part A* **2017**, *101*, 173–184.
- (12) Li, D.; Shi, D.; Feng, K.; Li, X.; Zhang, H. Poly (Ether Ether Ketone) (PEEK) Porous Membranes with Super High Thermal Stability and High Rate Capability for Lithium-Ion Batteries. *J. Membr. Sci.* **2017**, *530*, 125–131.
- (13) Yonezawa, N.; Okamoto, A. Synthesis of Wholly Aromatic Polyketones. *Polym. J.* **2009**, *41* (11), 899–928.
- (14) Gunanathan, C.; Milstein, D. Applications of Acceptorless Dehydrogenation and Related Transformations in Chemical Synthesis. *Science* **2013**, *341*, No. 1229712.
- (15) Trincado, M.; Bösen, J.; Grützmacher, H. Homogeneously Catalyzed Acceptorless Dehydrogenation of Alcohols: A Progress Report. *Coord. Chem. Rev.* **2021**, *443*, No. 213967.
- (16) Budweg, S.; Junge, K.; Beller, M. Catalytic Oxidations by Dehydrogenation of Alkanes, Alcohols and Amines with Defined (Non)-Noble Metal Pincer Complexes. *Catal. Sci. Technol.* **2020**, *10* (12), 3825–3842.
- (17) Zhang, J.; Leitus, G.; Ben-David, Y.; Milstein, D. Facile Conversion of Alcohols into Esters and Dihydrogen Catalyzed by New Ruthenium Complexes. *J. Am. Chem. Soc.* **2005**, *127* (31), 10840–10841.
- (18) Gunanathan, C.; Ben-David, Y.; Milstein, D. Direct Synthesis of Amides from Alcohols and Amines with Liberation of H₂. *Science* **2007**, *317* (5839), 790–792.
- (19) Daw, P.; Kumar, A.; Espinosa-Jalapa, N. A.; Ben-David, Y.; Milstein, D. Direct Synthesis of Amides by Acceptorless Dehydrogenative Coupling of Benzyl Alcohols and Ammonia Catalyzed by a Manganese Pincer Complex: Unexpected Crucial Role of Base. *J. Am. Chem. Soc.* **2019**, *141* (31), 12202–12206.
- (20) Kumar, A.; Espinosa-Jalapa, N. A.; Leitus, G.; Diskin-Posner, Y.; Avram, L.; Milstein, D. Direct Synthesis of Amides by Dehydrogenative Coupling of Amines with Either Alcohols or Esters: Manganese Pincer Complex as Catalyst. *Angew. Chem., Int. Ed.* **2017**, *56* (47), 14992–14996.
- (21) Hu, P.; Milstein, D. *Topics in Organometallic Chemistry*; Dixneuf, P. H.; Soulé, J.-F., Eds.; Springer: Cham, 2018; Vol. 63, pp 175–192.
- (22) Townsend, T. M.; Bernskoetter, W. H.; Hazari, N.; Mercado, B. Q. Dehydrogenative Synthesis of Carbamates from Formamides and Alcohols Using a Pincer-Supported Iron Catalyst. *ACS Catal.* **2021**, *11* (16), 10614–10624.
- (23) Kassie, A. A.; De la Torre, I. Y. C.; Remy, M. S.; Mukhopadhyay, S.; Kampf, J.; Qu, F.; Sanford, M. S. Metal Identity Effects in the Pincer Complex-Catalyzed Dehydrogenative Coupling of Formamides with Alcohols to Form Carbamates. *Organometallics* **2023**, *42* (10), 1030–1036, DOI: 10.1021/acs.organomet.3c00175.
- (24) Lane, E. M.; Hazari, N.; Bernskoetter, W. H. Iron-Catalyzed Urea Synthesis: Dehydrogenative Coupling of Methanol and Amines. *Chem. Sci.* **2018**, *9* (16), 4003–4008.
- (25) Bruffaerts, J.; Von Wolff, N.; Diskin-Posner, Y.; Ben-David, Y.; Milstein, D. Formamides as Isocyanate Surrogates: A Mechanistically Driven Approach to the Development of Atom-Efficient, Selective Catalytic Syntheses of Ureas, Carbamates, and Heterocycles. *J. Am. Chem. Soc.* **2019**, *141* (41), 16486–16493.
- (26) Kim, S. H.; Hong, S. H. Ruthenium-Catalyzed Urea Synthesis Using Methanol as the C1 Source. *Org. Lett.* **2016**, *18* (2), 212–215.
- (27) Gunanathan, C.; Milstein, D. Selective Synthesis of Primary Amines Directly from Alcohols and Ammonia. *Angew. Chem., Int. Ed.* **2008**, *47* (45), 8661–8664.
- (28) Ye, X.; Plessow, P. N.; Brinks, M. K.; Schelwies, M.; Schaub, T.; Rominger, F.; Paciello, R.; Limbach, M.; Hofmann, P. Alcohol Amination with Ammonia Catalyzed by an Acridine-Based Ruthenium Pincer Complex: A Mechanistic Study. *J. Am. Chem. Soc.* **2014**, *136* (16), 5923–5929.
- (29) Gunanathan, C.; Shimon, L. J. W.; Milstein, D. Direct Conversion of Alcohols to Acetals and H₂ Catalyzed by an Acridine-Based Ruthenium Pincer Complex. *J. Am. Chem. Soc.* **2009**, *131* (9), 3146–3147.
- (30) Gnanaprakasam, B.; Zhang, J.; Milstein, D. Direct Synthesis of Imines from Alcohols and Amines with Liberation of H₂. *Angew. Chem., Int. Ed.* **2010**, *49* (8), 1468–1471.
- (31) Maggi, A.; Madsen, R. Dehydrogenative Synthesis of Imines from Alcohols and Amines Catalyzed by a Ruthenium N-Heterocyclic Carbene Complex. *Organometallics* **2012**, *31* (1), 451–455.
- (32) Mondal, A.; Sharma, R.; Pal, D.; Srimani, D. Recent Progress in the Synthesis of Heterocycles through Base Metal-Catalyzed Acceptorless Dehydrogenative and Borrowing Hydrogen Approach. *Eur. J. Org. Chem.* **2021**, *2021* (26), 3690–3720.
- (33) Hunsicker, D. M.; Dauphinais, B. C.; Mc Ilrath, S. P.; Robertson, N. J. Synthesis of High Molecular Weight Polyesters via In Vacuo Dehydrogenation Polymerization of Diols. *Macromol. Rapid Commun.* **2012**, *33* (3), 232–236.
- (34) Malineni, J.; Keul, H.; Möller, M. An Efficient N-Heterocyclic Carbene-Ruthenium Complex: Application towards the Synthesis of Polyesters and Polyamides. *Macromol. Rapid Commun.* **2015**, *36* (6), 547–552.
- (35) Zeng, H.; Guan, Z. Direct Synthesis of Polyamides via Catalytic Dehydrogenation of Diols and Diamines. *J. Am. Chem. Soc.* **2011**, *133* (5), 1159–1161.
- (36) Gnanaprakasam, B.; Balaraman, E.; Gunanathan, C.; Milstein, D. Synthesis of Polyamides from Diols and Diamines with Liberation of H₂. *J. Polym. Sci., Part A: Polym. Chem.* **2012**, *50* (9), 1755–1765.
- (37) Guo, J.; Tang, J.; Xi, H.; Zhao, S.-Y.; Liu, W. Manganese Catalyzed Urea and Polyurea Synthesis Using Methanol as C1 Source. *Chin. Chem. Lett.* **2023**, *34* (4), No. 107731.
- (38) Langsted, C. R.; Paulson, S. W.; Bomann, B. H.; Suhail, S.; Aguirre, J. A.; Saumer, E. J.; Baclasky, A. R.; Salmon, K. H.; Law, A. C.; Farmer, R. J.; Furchtenicht, C. J.; Stankowski, D. S.; Johnson, M. L.; Corcoran, L. G.; Dolan, C. C.; Carney, M. J.; Robertson, N. J. Isocyanate-Free Synthesis of Ureas and Polyureas via Ruthenium Catalyzed Dehydrogenation of Amines and Formamides. *J. Appl. Polym. Sci.* **2022**, *139*, No. e52088.
- (39) Owen, A. E.; Preiss, A.; McLuskie, A.; Gao, C.; Peters, G.; Bühl, M.; Kumar, A. Manganese-Catalyzed Dehydrogenative Synthesis of Urea Derivatives and Polyureas. *ACS Catal.* **2022**, *12* (12), 6923–6933.
- (40) Brodie, C. N.; Owen, A. E.; Kolb, J. S.; Bühl, M.; Kumar, A. Synthesis of Polyethyleneimines from the Manganese-Catalysed

Coupling of Ethylene Glycol and Ethylenediamine. *Angew. Chem., Int. Ed.* **2023**, 62, No. e202306655, DOI: 10.1002/anie.202306655.

(41) Huang, F.; Liu, Z.; Yu, Z. C-Alkylation of Ketones and Related Compounds by Alcohols: Transition-Metal-Catalyzed Dehydrogenation. *Angew. Chem., Int. Ed.* **2016**, 55 (3), 862–875.

(42) Sharma, R.; Samanta, A.; Sardar, B.; Roy, M.; Srimani, D. Progressive Study on Ruthenium Catalysis for de(Hydrogenative) Alkylation and Alkenylation Using Alcohols as a Sustainable Source. *Org. Biomol. Chem.* **2022**, 20 (41), 7998–8030.

(43) Reed-Berendt, B. G.; Latham, D. E.; Dambatta, M. B.; Morrill, L. C. Borrowing Hydrogen for Organic Synthesis. *ACS Cent. Sci.* **2021**, 7 (4), 570–585.

(44) Reed-Berendt, B. G.; Polidano, K.; Morrill, L. C. Recent Advances in Homogeneous Borrowing Hydrogen Catalysis Using Earth-Abundant First Row Transition Metals. *Org. Biomol. Chem.* **2019**, 17 (7), 1595–1607.

(45) Irrgang, T.; Kempe, R. 3d-Metal Catalyzed N- and C-Alkylation Reactions via Borrowing Hydrogen or Hydrogen Autotransfer. *Chem. Rev.* **2019**, 119 (4), 2524–2549.

(46) Deibl, N.; Kempe, R. General and Mild Cobalt-Catalyzed C-Alkylation of Unactivated Amides and Esters with Alcohols. *J. Am. Chem. Soc.* **2016**, 138 (34), 10786–10789.

(47) Obora, Y. Recent Advances in α -Alkylation Reactions Using Alcohols with Hydrogen Borrowing Methodologies. *ACS Catal.* **2014**, 4 (11), 3972–3981.

(48) Peña-López, M.; Piehl, P.; Elangovan, S.; Neumann, H.; Beller, M. Manganese-Catalyzed Hydrogen-Autotransfer C–C Bond Formation: α -Alkylation of Ketones with Primary Alcohols. *Angew. Chem., Int. Ed.* **2016**, 55 (48), 14967–14971.

(49) Guo, J.; Ye, Y.; Gao, S.; Feng, Y. Synthesis of Polyketone Catalyzed by Pd/C Catalyst. *J. Mol. Catal. A: Chem.* **2009**, 307 (1), 121–127.

(50) Thiagarajan, S.; Sankar, R. V.; Gunanathan, C. Ruthenium-Catalyzed α -Alkylation of Ketones Using Secondary Alcohols to β -Disubstituted Ketones. *Org. Lett.* **2020**, 22 (20), 7879–7884, DOI: 10.1021/acs.orglett.0c02787.

(51) Baratta, W.; Bossi, G.; Putignano, E.; Rigo, P. Pincer and Diamine Ru and Os Diphosphane Complexes as Efficient Catalysts for the Dehydrogenation of Alcohols to Ketones. *Chem. – Eur. J.* **2011**, 17 (12), 3474–3481.

(52) Stevens, M. P. *Polymer Chemistry: An Introduction*, 3rd ed.; Oxford University Press: NY, 1999.

(53) Tebeta, R. T.; Fattahi, A. M.; Ahmed, N. A. Experimental and Numerical Study on HDPE/SWCNT Nanocomposite Elastic Properties Considering the Processing Techniques Effect. *Microsyst. Technol.* **2020**, 26 (8), 2423–2441.

(54) (a) Yan, Y.; Jiang, C.; Huo, Y.; Li, C. Preparation and Tribological Behaviors of Lubrication-Enhanced PEEK Composites. *Appl. Sci.* **2020**, 10 (21), No. 7536, DOI: 10.3390/app10217536.

(b) Liao, C.; Li, Y.; Tjong, S. C. Polyetheretherketone and Its Composites for Bone Replacement and Regeneration. *Polymers* **2020**, 12 (12), No. 2858, DOI: 10.3390/polym12122858.

(55) Hejmady, P.; van Breemen, L. C. A.; Anderson, P. D.; Cardinaels, R. A Processing Route to Spherical Polymer Particles via Controlled Droplet Retraction. *Powder Technol.* **2021**, 388, 401–411.

(56) Description of PolyKetone PK 5000 polymer can be found under 2024 <https://www.jabil.com/services/additive-manufacturing/additive-materials/compare-powders/pk-5000.html> (accessed: 3 January 2024).

(57) Pfister, A.; Müller, F.; Leuterer, M. Patent (EOS GmbH). U.S. Patent US8,299,208, 2010.

(58) Saxon, D. J.; Luke, A. M.; Sajjad, H.; Tolman, W. B.; Reineke, T. M. Next-Generation Polymers: Isosorbide as a Renewable Alternative. *Prog. Polym. Sci.* **2020**, 101, No. 101196.

(59) Krall, E. M.; Klein, T. W.; Andersen, R. J.; Nett, A. J.; Glasgow, R. W.; Reader, D. S.; Dauphinais, B. C.; Ilrath, S. P. M.; Fischer, A. A.; Carney, M. J.; Hudson, D. J.; Robertson, N. J. Controlled Hydrogenative Depolymerization of Polyesters and Polycarbonates Catalyzed

by Ruthenium(II) PNN Pincer Complexes. *Chem. Commun.* **2014**, 50 (38), 4884–4887, DOI: 10.1039/c4cc00541d.

(60) Westhues, S.; Idel, J.; Klankermayer, J. Molecular Catalyst Systems as Key Enablers for Tailored Polyesters and Polycarbonate Recycling Concepts. *Sci. Adv.* **2018**, 4 (8), No. eaat9669.

(61) Jana, A.; Das, K.; Kundu, A.; Thorve, P. R.; Adhikari, D.; Maji, B. A Phosphine-Free Manganese Catalyst Enables Stereoselective Synthesis of (1 + n)-Membered Cycloalkanes from Methyl Ketones and 1,n-Diols. *ACS Catal.* **2020**, 10 (4), 2615–2626.

(62) Chakraborty, S.; Daw, P.; Ben David, Y.; Milstein, D. Manganese-Catalyzed α -Alkylation of Ketones, Esters, and Amides Using Alcohols. *ACS Catal.* **2018**, 8 (11), 10300–10305.

Manganese Catalysed Synthesis of Polyketones using Hydrogen Borrowing Approach

Pavel Kulyabin,[†] Oxana V. Magdysyuk,[†] Aaron B Naden,[†] Daniel M Dawson,[†] Ketan Pancholi,^δ Matthew Walker,^γ Massimo Vassalli,^ζ and Amit Kumar^{†*}

[†]EaStCHEM, School of Chemistry, University of St Andrews, North Haugh, St Andrews, KY16 9ST, UK.

^δ The Sir Ian Wood Building, Robert Gordon University, Garthdee Rd, Garthdee, Aberdeen, AB10 7GE, UK.

^γCentre for the Cellular Microenvironment, Advanced Research Centre, University of Glasgow, Glasgow, G116EW, UK.

^ζ James Watt School of Engineering, University of Glasgow, Glasgow G12 8QQ, UK.

E-mail: ak336@st-andrews.ac.uk

Contents

1. Experimental Details	2
1.1 General Considerations	2
1.2 Synthesis of 3,3'-(1,4-phenylene)bis(1-phenylpropan-1-one) as a model substrate.....	4
1.3 Coupling of 1,4-diacetylbenzene and 1,4-benzenedimethanol.	6
1.4 NMR spectra of mother liquor from coupling reaction of 1,4-diacetylbenzene and 1,4-benzenedimethanol as described in Table S1.	29
1.5 Synthesis of polyketones from diketones and diols.	30
1.6 Syntheses of polychalcones from diketones and dialdehydes.....	69
1.7 Reaction 4-acetylphenyl ether and potassium <i>tert</i> -butoxide.	73
1.8 Syntheses of polyketones in the presence of hydrogen atmosphere.....	75
1.9 Catalyst reuse experiments.	79
1.10 Headspace gas analysis from the synthesis of polyketone PAAK-7.	80
1.11 Hydrogenative depolymerization of polyethyleneterephthalate (PET).	81
1.12 Hydrogenation of trans-Chalcone by transfer hydrogenation.	82
1.13 Mass spectroscopy investigation of mother liquor from reaction mixtures.	83
1.14 TGA and DSC analysis combined with mass-spectrometry.....	85
1.15 Infrared spectra of starting materials and commercially available compounds.	86
1.16 Thermal properties and GPC analysis of commercial polyketones.....	90
1.17 Powder XRD patterns of starting materials.	94
1.18 Scanning Electron Microscopy	96
1.19 Powder XRD and Scanning Electron Microscopy analysis	101
2. Mechanical properties.....	102
3. References	105

1. Experimental Details

1.1 General Considerations

All manipulations, unless otherwise stated, were performed under an argon atmosphere using standard Schlenk line and glove-box techniques. Glassware was oven-dried and flamed under vacuum prior to use. THF and toluene were dried using a Grubbs-type solvent purification system (Innovative Technologies SPS) equipped with a degasser. Pre-catalyst **1**^[1] was prepared in accordance with the literature procedure. Cs₂CO₃ (anhydrous) were stored at 80 °C and dried before use. Precatalysts **2–4**, Mn(CO)₅Br, triphenylphosphine, NMR solvents and iPr-PN^HP (10 wt% solution in THF) were purchased from Strem Chemicals and used as received. Polyolefinketone (POK), polyetherketoneketone (PEKK) and polyetheretherketone (PEEK) samples were purchased from Goodfellow Cambridge Limited and used as received.

Solution state NMR spectra were recorded on a Bruker AVIII-HD 400 MHz NMR spectrometer at 298 K unless otherwise specified. Residual protons of solvent were used as a reference for ¹H NMR spectra in deuterated solvent samples. All chemical shifts (δ) are quoted in ppm and coupling constants (J) in Hz.

Solid-state ¹³C NMR spectra were recorded using a Bruker Avance III spectrometer, equipped with a 9.4 T wide-bore superconducting magnet (¹H and ¹³C Larmor frequencies of 400.1 and 100.6 MHz, respectively). Some samples were submerged in liquid nitrogen and then ground to a powder. The remaining nitrogen and any condensed water were allowed to evaporate. Samples were packed into 4 mm zirconia magic angle spinning (MAS) rotors and rotated at a MAS rate of 12.5 kHz. ¹³C NMR spectra were recorded with cross polarisation (CP) from ¹H using a contact pulse (ramped for ¹H) of between 0.5 and 2 ms. Signal averaging was carried out for 2048 transients (NM118(II)) with a recycle interval of 2 s. High power ($\nu_1 \approx 100$ kHz) TPPM-15 decoupling of ¹H was applied during acquisition. Chemical shift is reported in ppm relative to (CH₃)₄Si using the CH₃ signal of L-alanine ($\delta = 20.5$ ppm) as a secondary solid reference.

Solid state ¹H MAS NMR spectra were recorded at 600.26 MHz using a Bruker Avance III spectrometer equipped with a 14.1 T wide-bore superconducting magnet. Samples were packed into a 1.9 mm zirconia rotors and rotated at the magic angle at a rate of 40 kHz. A rotor-synchronised spin echo pulse sequence ($\tau = 25$ μ s) was used to remove background signal. Signal averaging was carried out for 48 transients with a recycle interval of 5 s. Chemical shifts are reported in ppm relative to (CH₃)₄Si using the NH₃ signal of L-alanine ($\delta = 8.5$ ppm) as a secondary solid reference.

Infrared spectra (ATR-FTIR) were collected using a Shimadzu IRAffinity-1.

Thermogravimetric Analysis (TGA) was performed using Stanton Redcroft STA-780 Series Thermal Analyser between 30–900 °C at a heating rate of 10 °C/min under a flow of nitrogen gas (25 mL/min). Decomposition temperature (T_d , °C) was estimated as the temperature of 10% weight loss.

Differential Scanning Calorimetry (DSC) analyses were performed using a Netzsch DSC204 or Queens STA449 DSC217C between –80 or –10 to 250, 300 or 600 °C at a heating rate of 10 °C/min under a flow of nitrogen gas (20 mL/min) after an initial heat/cool cycle (25–120 °C at 10 °C/min with a 20-minute isothermal at 120 °C) to remove the thermal history of the sample.

Differential Scanning Calorimetry with Mass Spectroscopy (DSC-MS) analyses were performed using a Netzsch STA 449F5 30–600 °C at a heating rate of 10 °C/min under a flow of argon gas (20 mL/min).

Gel permeation chromatography (GPC) was performed on an Agilent 1260 InfinityLab II GPC fitted with a refractive index (RI) detector (35 °C). Two plus guard column Agilent PLgel-M 10 μ m MIXED-B columns setup was contained within an oven (35 °C). Mixture of chloroform (80%) and dichloroacetic acid (20%) was used as the eluent at a flow rate of 1.0 mL min^{–1}. The samples (30 mg) were heated in 4 mL of dichloroacetic acid at 120 °C overnight. Next, the samples were diluted to the required concentration of 0.2% (w/v) with chloroform and injected into a system running at temperature after filtration to remove

undissolved material. The calibration was conducted using a series of polystyrene ($M_n = 1,000 - 243,000 \text{ g mol}^{-1}$) standards obtained from Agilent Technologies.

Scanning electron microscopy (SEM) was performed on an FEI Scios dualbeam instrument operated at 3 kV, samples were prepared by dispersion onto adhesive carbon tape (Labtech International Ltd.) and sputter coated with a thin layer of gold to dissipate the charge.

Powder X-ray diffraction data was collected using Bruker AXS D8 Advance diffractometer with a Vantec detector, using Cu $K\alpha$ radiation. The data from powder samples were collected in the range of $2^\circ < 2\theta < 70$ or 90° . Some samples were measured on a PTFE pad which led to appearance of additional peaks (originated from PTFE) at high 2θ . Broad peak at $2\theta = 26^\circ$ in several samples originates from the polyester film that was used to cover the powder.

GC-MS data were collected as solutions in HPLC grade DCM using an Agilent 8860 GC system coupled to an Agilent 5977B EI instrument. EI spectra were collected as solutions in acetonitrile using a Micromass LCT spectrometer.

Headspace analysis was performed using an Agilent GC8860 with TCD. Gas separation is performed using dual columns (Agilent porous Polymer and Agilent Mol sieve). Gas sample (2.5 mL) is introduced to the columns using a gas tight syringe through a sample loop (0.25 mL).

1.2 Synthesis of 3,3'-(1,4-phenylene)bis(1-phenylpropan-1-one) as a model substrate.

A 15 mL pressure vessel was charged with pre-catalyst **1** (10 mg, 0.02 mmol, 2 mol%), 1,4-benzenedimethanol (138 mg, 1.0 mmol), acetophenone (240 mg, 2.0 mmol) and Cs₂CO₃ (33 mg, 0.10 mmol, 10 mol%). *tert*-Amyl alcohol (5 mL) was added, and the flask was sealed under a nitrogen atmosphere in a glove box before heating to 140 °C for 18 hours with stirring. After this period, the reaction vessel was allowed to cool to room temperature. Next, the crude was directly purified by flash chromatography on silica gel to afford, after concentration and high-vacuum drying, 284 mg (83%) of the product as a white solid. ¹H NMR (400 MHz, CDCl₃): δ 7.96 (m, 4H), 7.56 (m, 2H), 7.47 (m, 4H), 7.20 (s, 4H), 3.30 (m, 4H), 3.05 (m, 4H). ¹³C NMR (100 MHz, CDCl₃): δ 199.2, 139.0, 136.8, 133.0, 128.6, 128.0, 40.4, 29.9. IR (ATR-FTIR, cm⁻¹): ν 2920w (C-H), 1680s (C=O), 1593w, 1516w, 1447m, 1204m, 972m, 745s, 691s, 548m. [M+Na]⁺ Calcd for C₂₄H₂₂O₂²³Na, 365.1512; found: 365.1510.

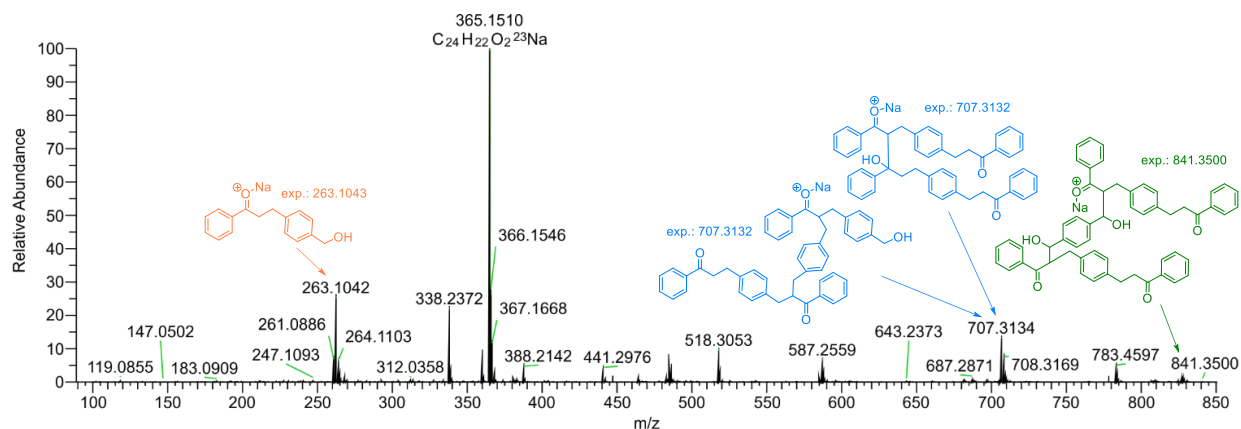


Figure S1. High Resolution Mass Spectrum (HRMS, ESI, MeCN) of crude reaction mixture after synthesis of 3,3'-(1,4-phenylene)bis(1-phenylpropan-1-one).

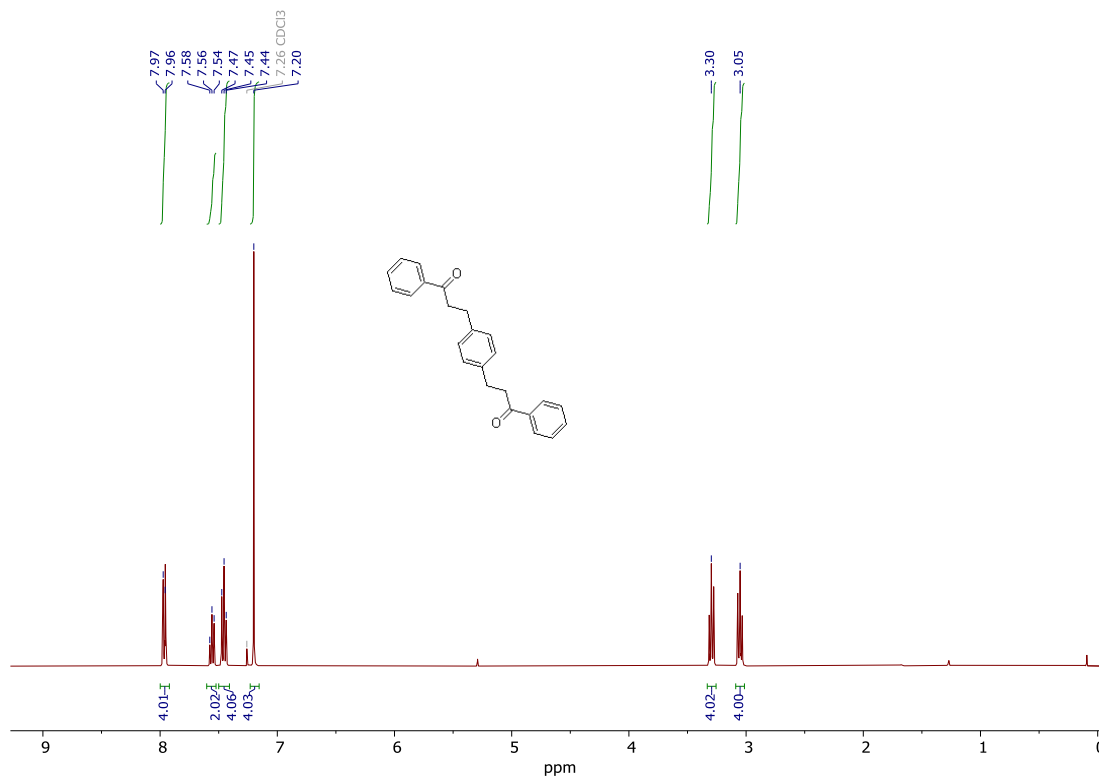


Figure S2. ¹H NMR (CDCl₃, 298 K) spectrum of 3,3'-(1,4-phenylene)bis(1-phenylpropan-1-one).

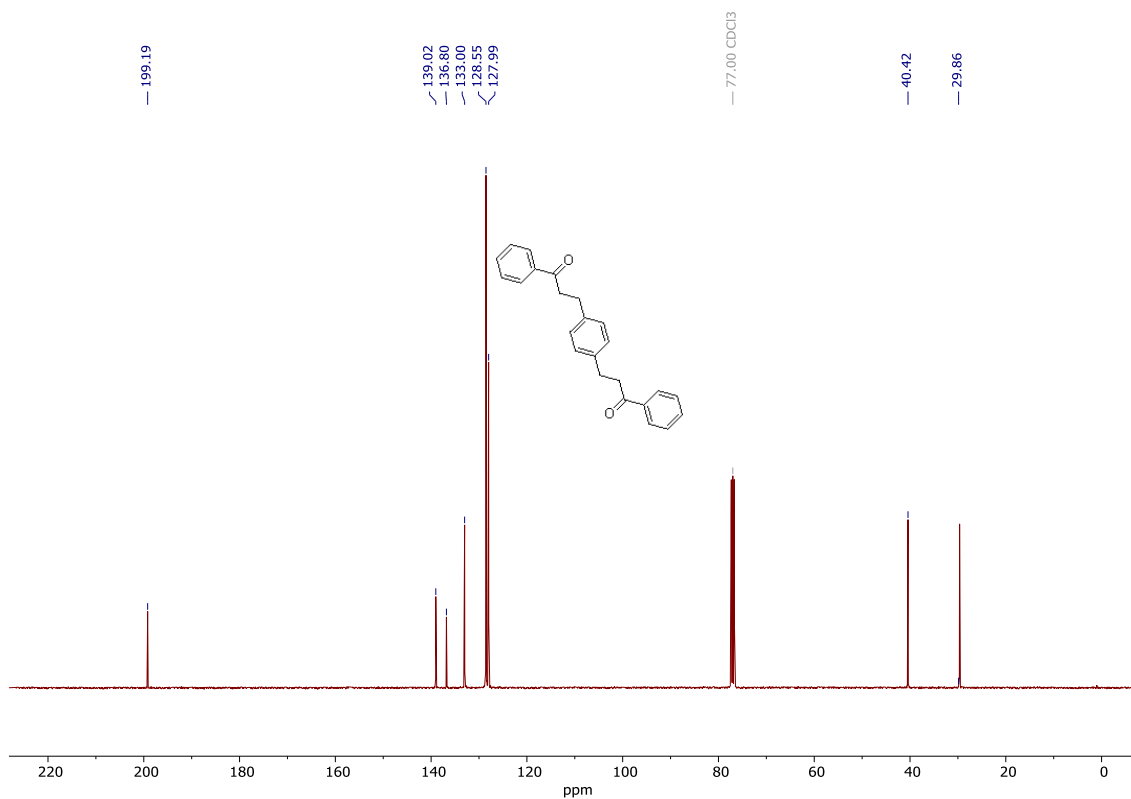


Figure S3. ¹³C{¹H} NMR (CDCl₃, 298 K) spectrum of 3,3'-(1,4-phenylene)bis(1-phenylpropan-1-one).

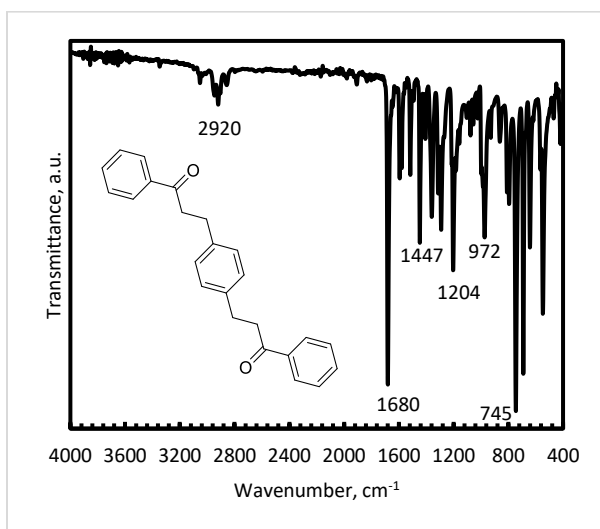


Figure S4. Infrared spectrum (ATR-FTIR) of 3,3'-(1,4-phenylene)bis(1-phenylpropan-1-one).

1.3 Coupling of 1,4-diacetylbenzene and 1,4-benzenedimethanol.

A 100 mL ampoule equipped with a J-Young's valve or a 15 mL pressure vessel was charged with pre-catalyst (e.g. **1**; 10 mg, 0.02 mmol, 2 mol%), 1,4-benzenedimethanol (138 mg, 1.0 mmol), 1,4-diacetylketone (162 mg, 1.0 mmol) and Cs₂CO₃ (e.g. 33 mg, 0.10 mmol, 10 mol%). *Tert*-amyl alcohol or toluene (e.g. 5 mL) was added and the flask was sealed under an argon atmosphere before heating to the desired temperature (e.g. 140 °C) for the desired length of time (e.g. 18 hours) with stirring. After this period, the reaction vessel was allowed to cool to room temperature and any gas evolved (presumably H₂) during the reaction measured using inverted cylinder in water method. To the resulting mixture, 5 mL of 1 M HCl was added and the flask had been heated at 90 °C for 1 h. The yellow precipitate was filtered and dried under reduced pressure at 120 °C.

Table S1. Polyketone synthesis from 1,4-diacetylbenzene and 1,4-benzenedimethanol.^a

Entry	Complex	mol%	Conc.	Base (mol%)	Time (h)	Isolated Yield (%)	T _d ^j (°C)
1 ^{b,c}	1	2	0.2 M	10%	18	58 ^d	325/266
2 ^b	1	2	0.2 M	10%	18	89	338
3 ^b	2	2	0.2 M	10%	18	< 5	n.d.
4 ^b	3	2	0.2 M	10%	18	51	353
5 ^b	4	2	0.2 M	10%	18	17	319
6 ^b	1	1	0.2 M	10%	18	87	356
7 ^b	1	0.5	0.2 M	10%	18	70	348
8	1	1	0.1 M	10%	18	85	373
9 ^c	1	1	0.1 M	10%	18	73	342
10	1	1	0.1 M	20%	18	90	369
11	1	1	0.1 M	3%	18	80	335
12 ^f	1	1	0.1 M	10%	18	67	328
13 ^g	1	1	0.25 M	10%	18	94	352
14 ^h	1	1	0.05 M	10%	18	86	342
15	1	1	0.1 M	10%	2	89	363
16	1	1	0.1 M	10%	1	81	343
17	1	1	0.1 M	3%	2	81	344
18	none	none	0.1 M	10%	18	8	396
19	1	1	0.1 M	none	18	none	—
20 ⁱ	1	1	0.1 M	1% ⁱ	18	none	—
21 ⁱ	1	1	0.1 M	2% ⁱ	18	< 5	—
22	5	1	0.1 M	10%	18	< 5	n.d.
23	6	1	0.1 M	10%	18	< 5	n.d.

1

2

3

4

5

6

^aGeneral reaction conditions: 1,4-diacetylbenzene (0.5 mmol), 1,4-benzenedimethanol (0.5 mmol), Cs₂CO₃, metal-complex, and 5 mL of *t*AmOH were placed into 100 mL ampoule with J-Young's valve under an argon atmosphere and heated at 140 °C for 18 h. ^b1 mmol of diol and diketone were used. ^cToluene was used instead of *t*AmOH. ^dThe reaction mixture consisted of two kinds of solid material: red chunk in the bottom (38%) and yellow brittle film on the edge of solution (20%) which were separated mechanically. ^eReaction was carried out in 15 mL pressure vessel. ^fReaction at 110°C. ^g2 mL of *t*AmOH were used. ^h10 mL of *t*AmOH were used. ⁱKOtBu was used for catalyst activation. ^jTemperature of degradation. Calculated from TGA as a temperature of 10% weight loss.

Table S1, Entry 1

Yellow solid (21%):

IR (ATR-FTIR, cm^{-1}): ν 3470w (O-H), 3049w (C-H), 2922w (C-H), 1674s (C=O), 1601m (C=C), 1506w, 1406m, 1265s, 1213s, 982s, 818s, 731s, 544m.

TGA: $T_d = 325\text{ }^\circ\text{C}$.

Red solid (38%):

3348m (O-H), 2924w (C-H), 1674s (C=O), 1605m (C-H), 1510w, 1373m, 1217m, 1213m, 1011m, 816s, 517s.

TGA: $T_d = 266\text{ }^\circ\text{C}$.

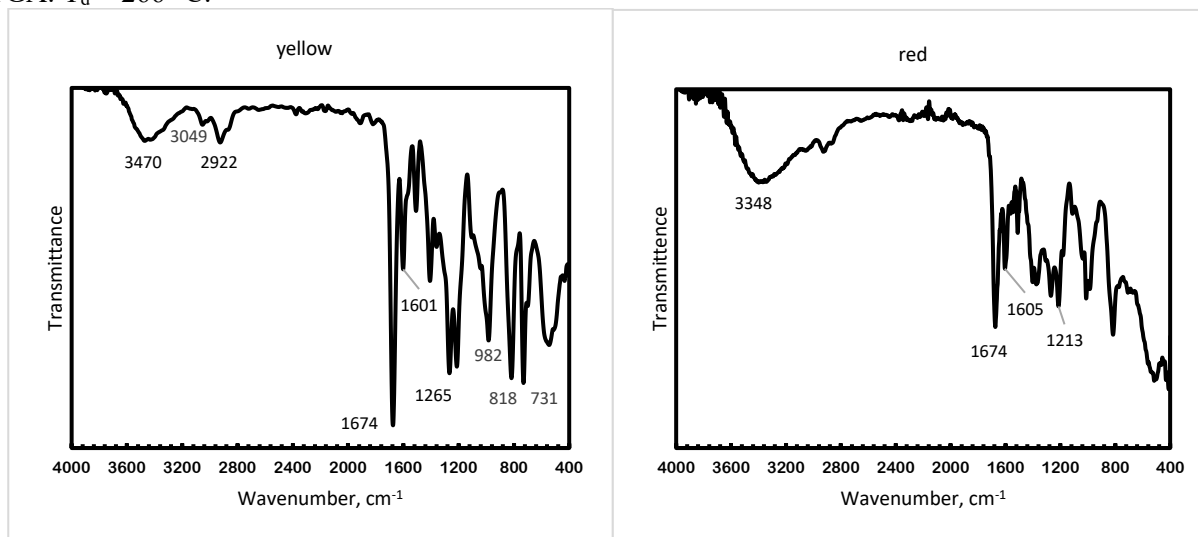


Figure S5. Infrared spectrum (ATR-FTIR) of the samples corresponding to Entry 1 in Table S1.

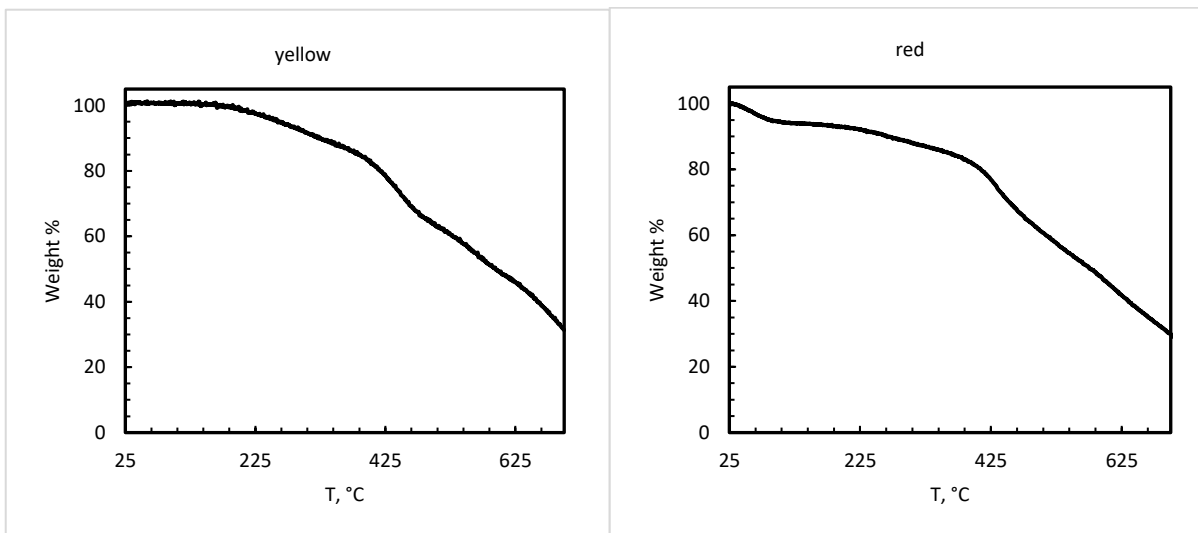


Figure S6. Mass loss as a function of temperature for samples corresponding to Entry 1 in Table S1.

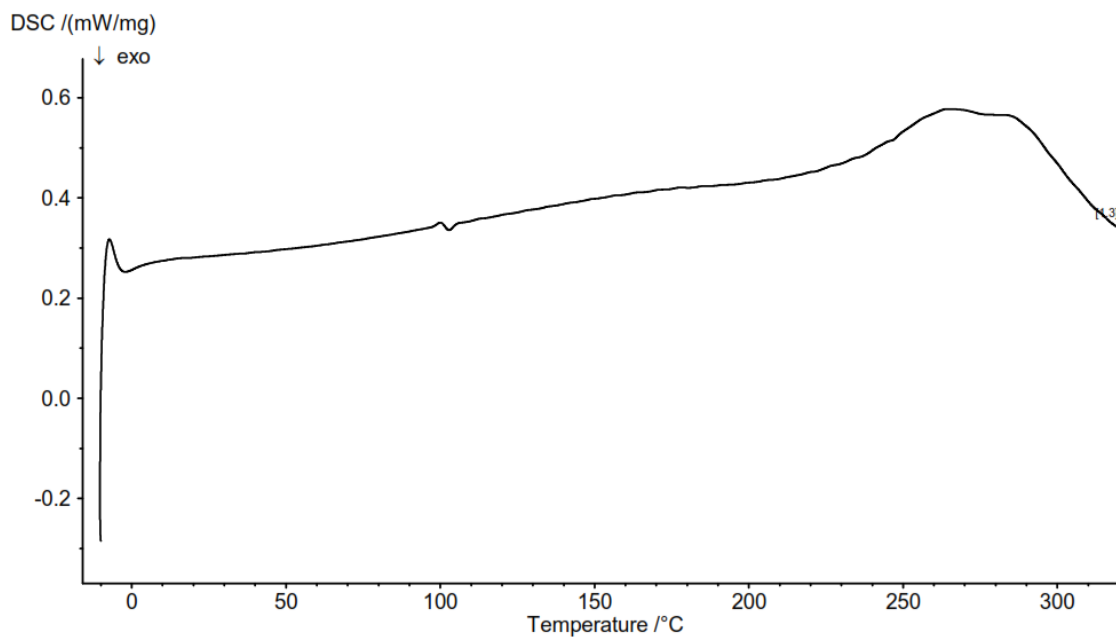


Figure S7. DSC trace corresponding to Entry 1 in Table S1, yellow solid.

Table S1, Entry 2

^{13}C CP MAS NMR (100.6 MHz): δ 199.5, 151.6, 139.9, 128.4, 75.7, 70.2, 64.4, 42.2, 29.3.

IR (ATR-FTIR, cm^{-1}): ν 3460w (O-H), 2926w (C-H), 1674s (C=O), 1603m (C=C), 1508w, 1406m, 1225s, 1211s, 982s, 818s, 546m.

TGA: $T_d = 338^\circ\text{C}$

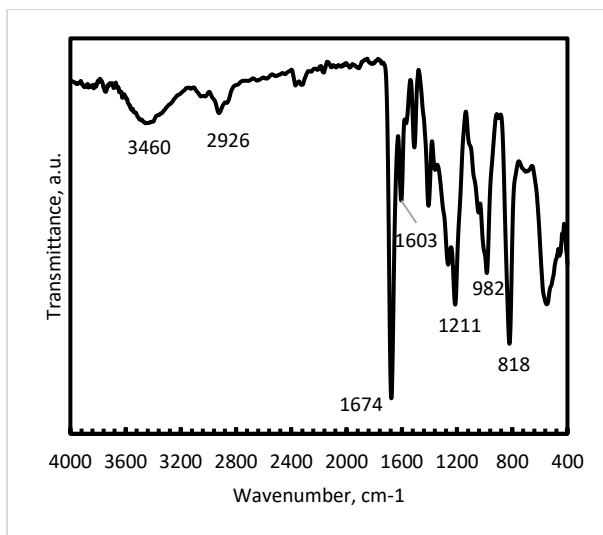


Figure S8. Infrared spectrum (ATR-FTIR) of the sample corresponding to Entry 2 in Table S1.

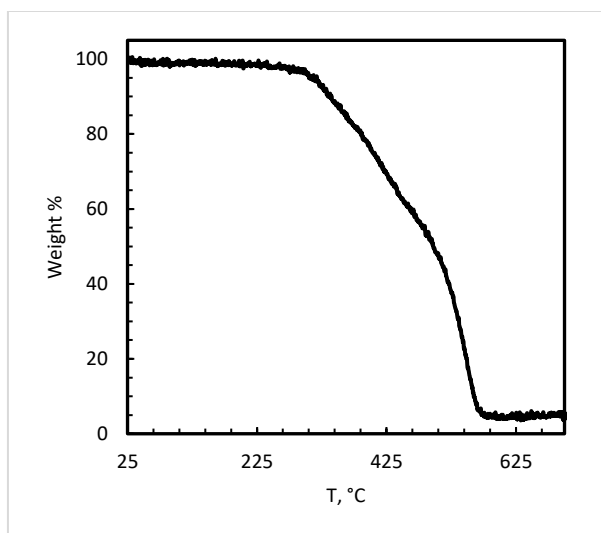


Figure S9. Mass loss as a function of temperature for sample corresponding to Entry 2 in Table S1.

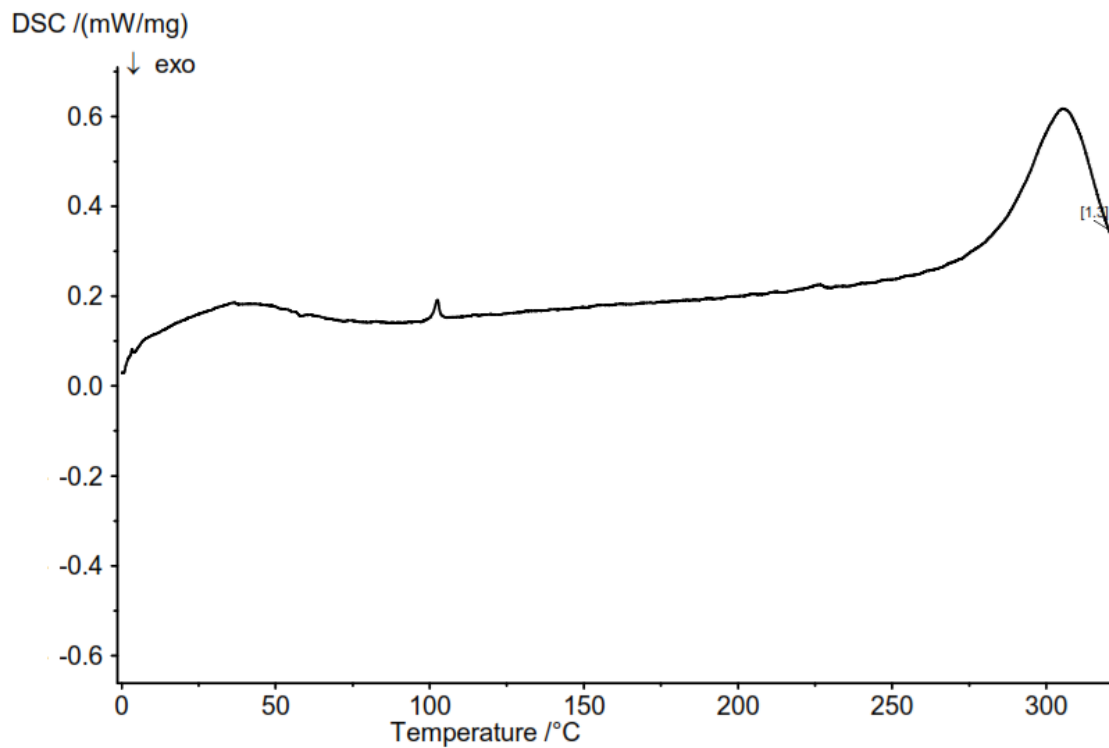


Figure S10. DSC trace corresponding to Entry 2 in Table S1.

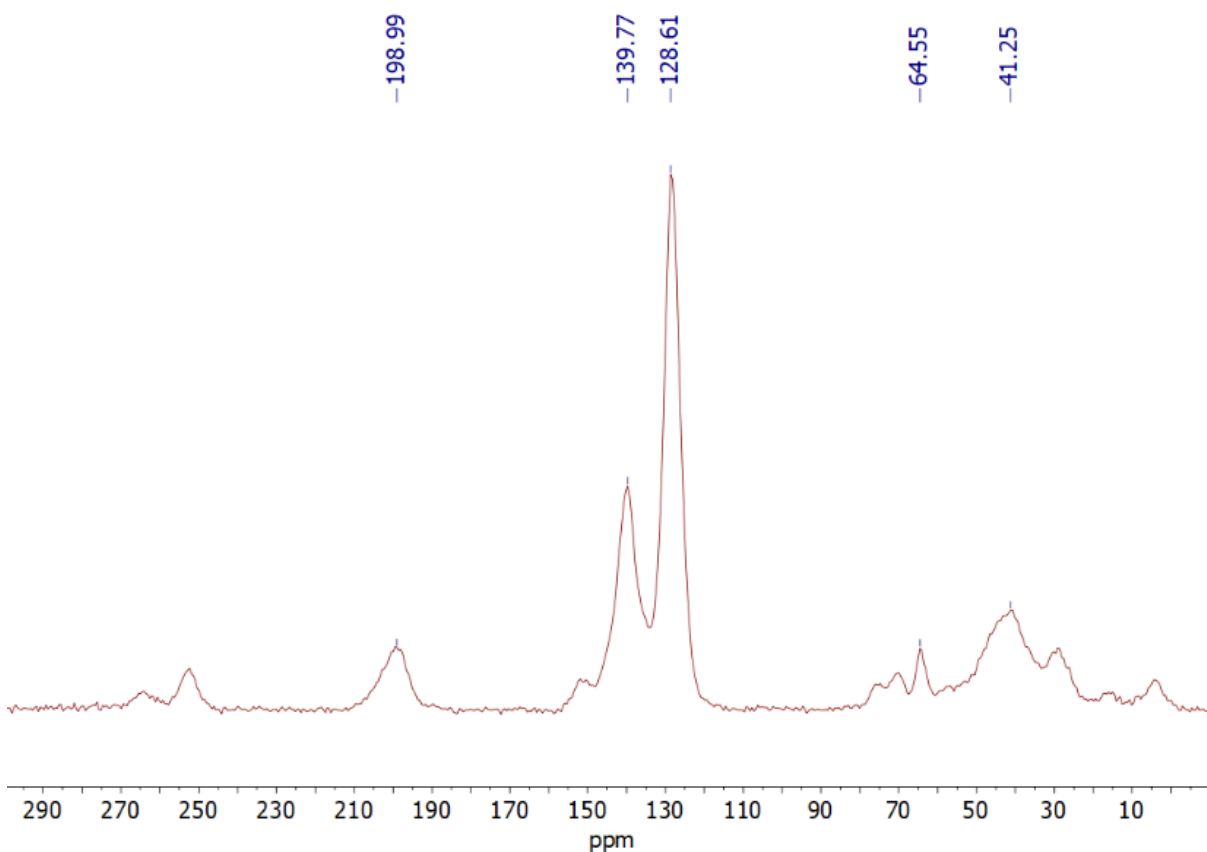


Figure S11. ^{13}C CP MAS NMR spectrum of the polymer corresponding to Entry 2 in Table S1.

Table S1, Entry 3

The isolated amount was not enough to perform analysis.

Table S1, Entry 4

IR (ATR-FTIR, cm^{-1}): ν 3368w (O-H), 2920w (C-H), 1690w, 1672s (C=O), 1607w (C=C), 1510w, 1400m, 1267s, 978m, 814s.

TGA: $T_d = 353\text{ }^\circ\text{C}$

DSC: $T_m = 215\text{ }^\circ\text{C}$

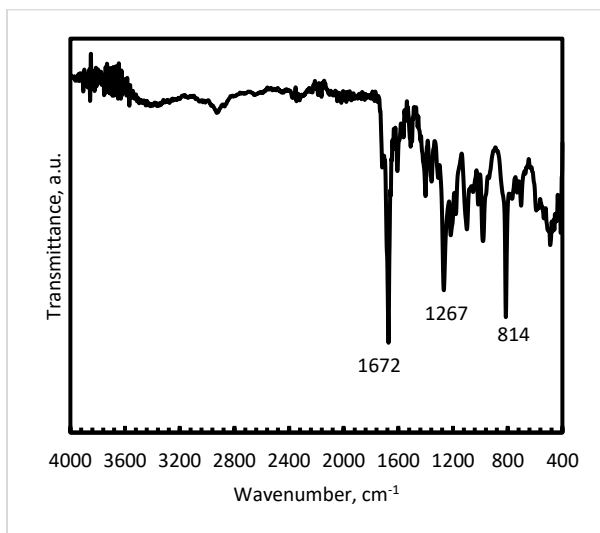


Figure S12. Infrared spectrum (ATR-FTIR) of the sample corresponding to Entry 4 in Table S1.

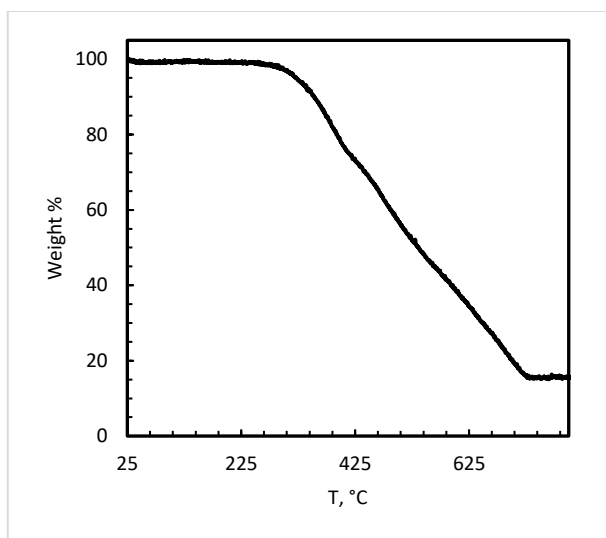


Figure S13. Mass loss as a function of temperature for sample corresponding to Entry 4 in Table S1.

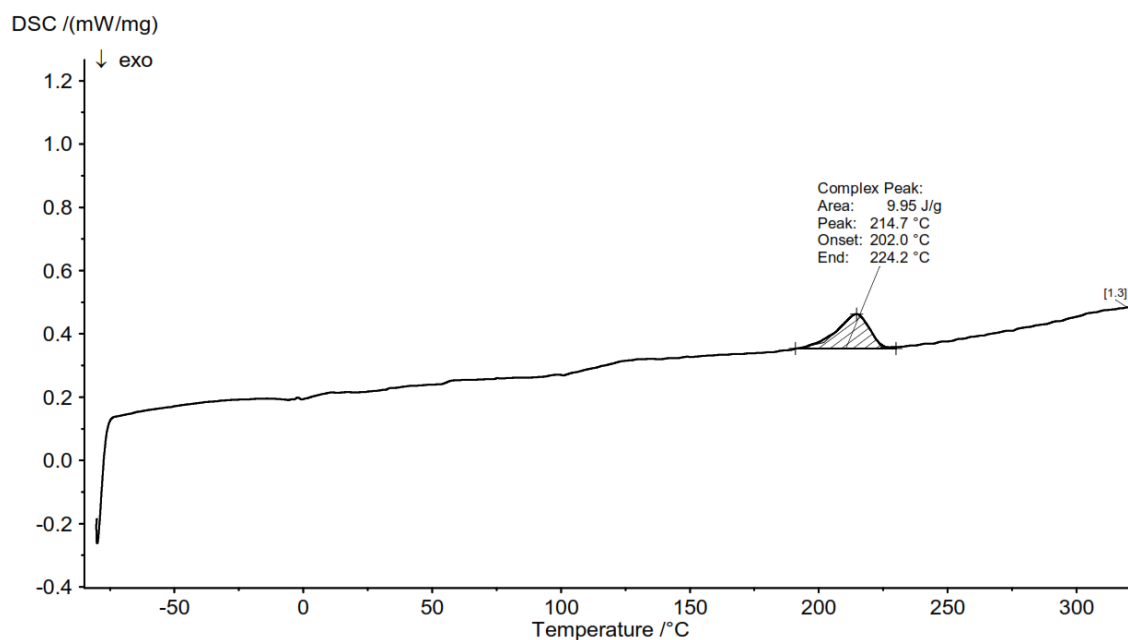


Figure S14. DSC trace corresponding to Entry 4 in Table S1.

Table S1, Entry 5

IR (ATR-FTIR, cm^{-1}): ν 3416w (O-H), 2911w (C-H), 1676s (C=O), 1605m (C=C), 1506s, 1402m, 1265s, 1213s, 988s, 820s.

TGA: $T_d = 319^\circ\text{C}$

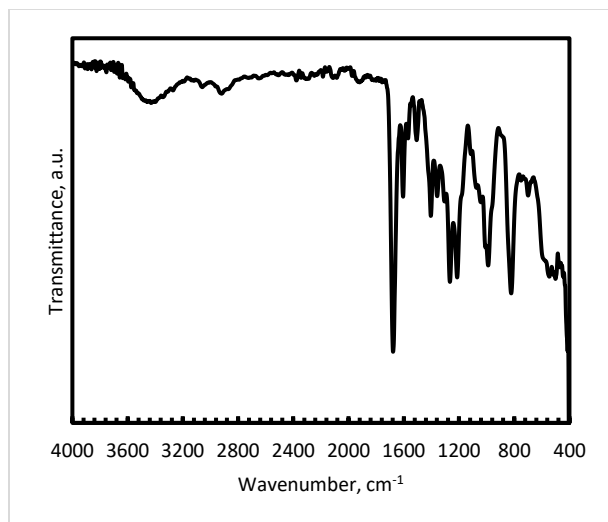


Figure S15. Infrared spectrum (ATR-FTIR) of the sample corresponding to Entry 5 in Table S1.

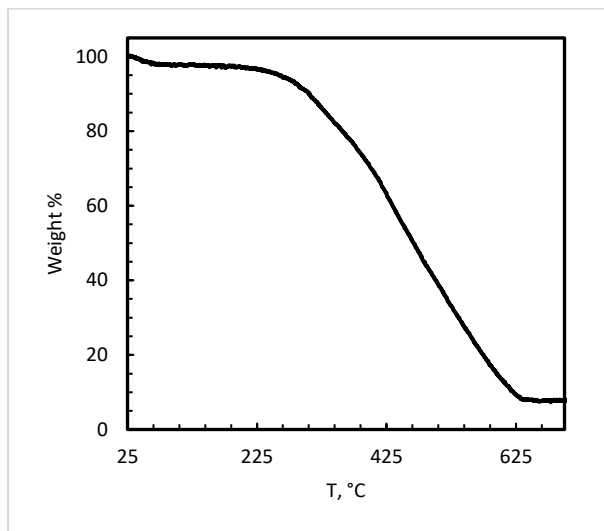


Figure S16. Mass loss as a function of temperature for sample corresponding to Entry 5 in Table S1.

Table S1, Entry 6

IR (ATR-FTIR, cm^{-1}): ν 3424w (O-H), 2924w (C-H), 1676s (C=O), 1605m (C=C), 1510s, 1402m, 1225m, 1213s, 984m, 818s, 542m.

TGA: $T_d = 356^\circ\text{C}$

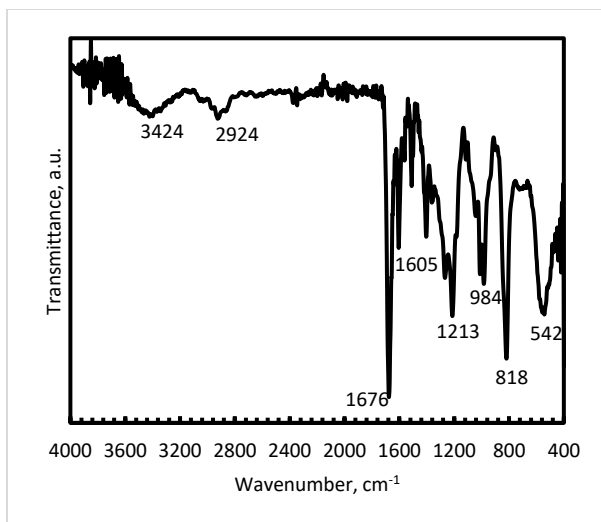


Figure S17. Infrared spectrum (ATR-FTIR) of the sample corresponding to Entry 6 in Table S1.

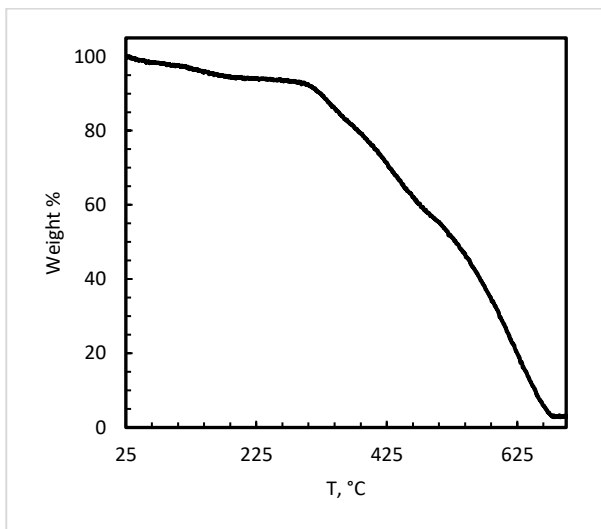


Figure S18. Mass loss as a function of temperature for sample corresponding to Entry 6 in Table S1.

Table S1, Entry 7

IR (ATR-FTIR, cm^{-1}): ν 3420w (O-H), 2918w (C-H), 1674s (C=O), 1603m (C=C), 1422w, 1402m, 1265m, 1211s, 982s, 818s, 550m.

TGA: $T_d = 348^\circ\text{C}$

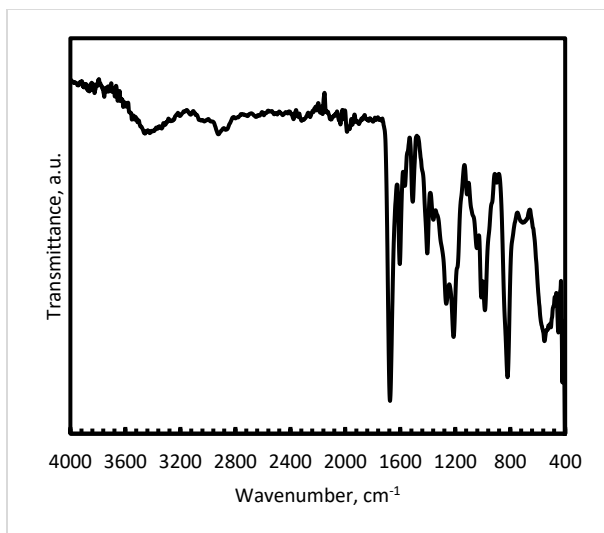


Figure S19. Infrared spectrum (ATR-FTIR) of the sample corresponding to Entry 7 in Table S1.

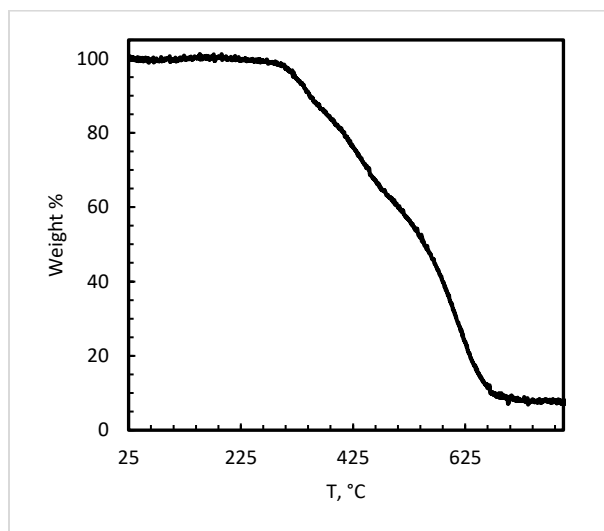


Figure S20. Mass loss as a function of temperature for sample corresponding to Entry 7 in Table S1.

Table S1, Entry 8

IR (ATR-FTIR, cm^{-1}): ν 3402w (O-H), 2914w (C-H), 1674s (C=O), 1603m (C=C), 1510w, 1402m, 1225m, 1211s, 982m, 818s, 550m.

TGA: $T_d = 373^\circ\text{C}$

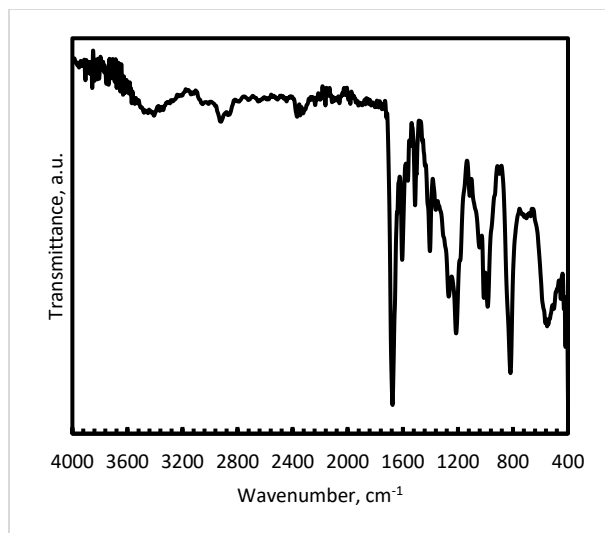


Figure S21. Infrared spectrum (ATR-FTIR) of the sample corresponding to Entry 8 in Table S1.

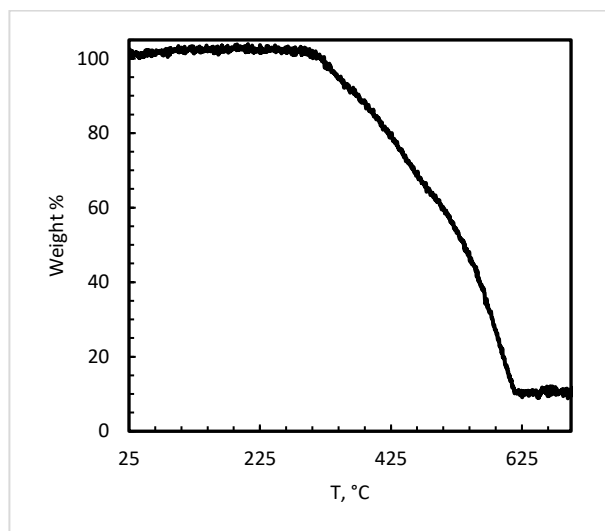


Figure S22. Mass loss as a function of temperature for sample corresponding to Entry 8 in Table S1.

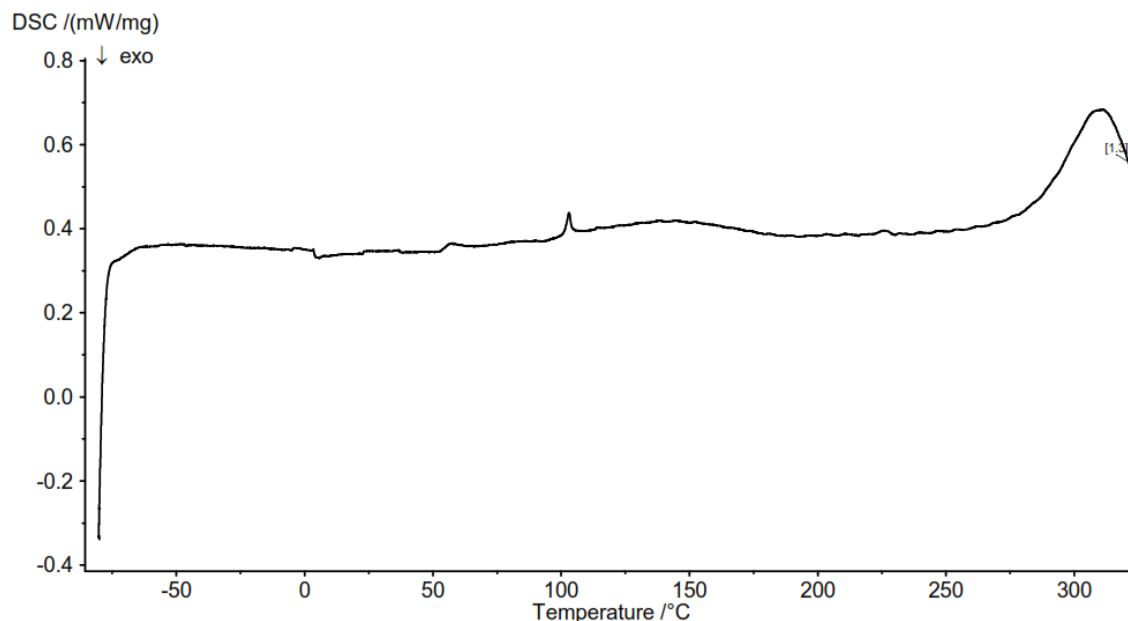


Figure S23. DSC trace corresponding to Entry 8 in Table S1.

Table S1, Entry 9

IR (ATR-FTIR, cm^{-1}): ν 3449w (O-H), 2911w (C-H), 1676s (C=O), 1605m (C=C), 1510w, 1402m, 1221m, 1211s, 982s, 818s.

TGA: $T_d = 342\text{ }^{\circ}\text{C}$

DSC: $T_g = 247\text{ }^{\circ}\text{C}$

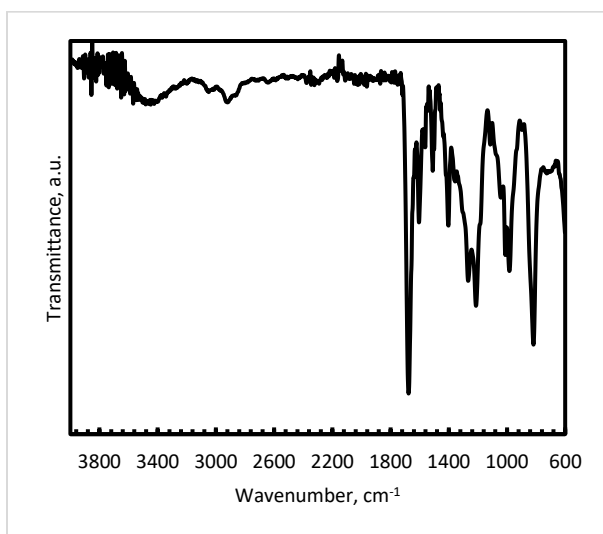


Figure S24. Infrared spectrum (ATR-FTIR) of the sample corresponding to Entry 9 in Table S1.

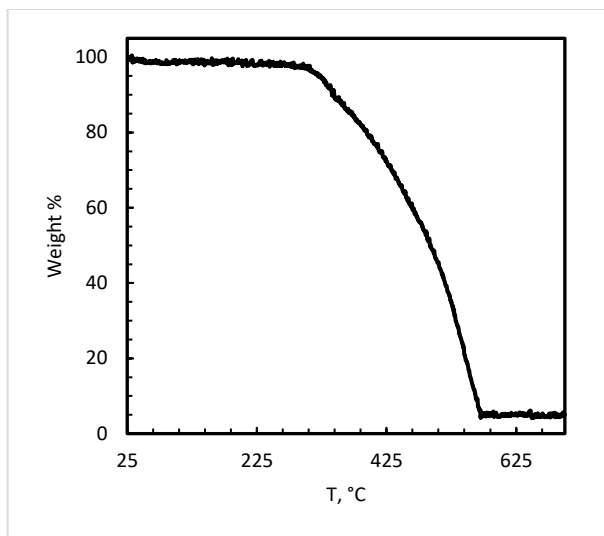


Figure S25. Mass loss as a function of temperature for sample corresponding to Entry 9 in Table S1.

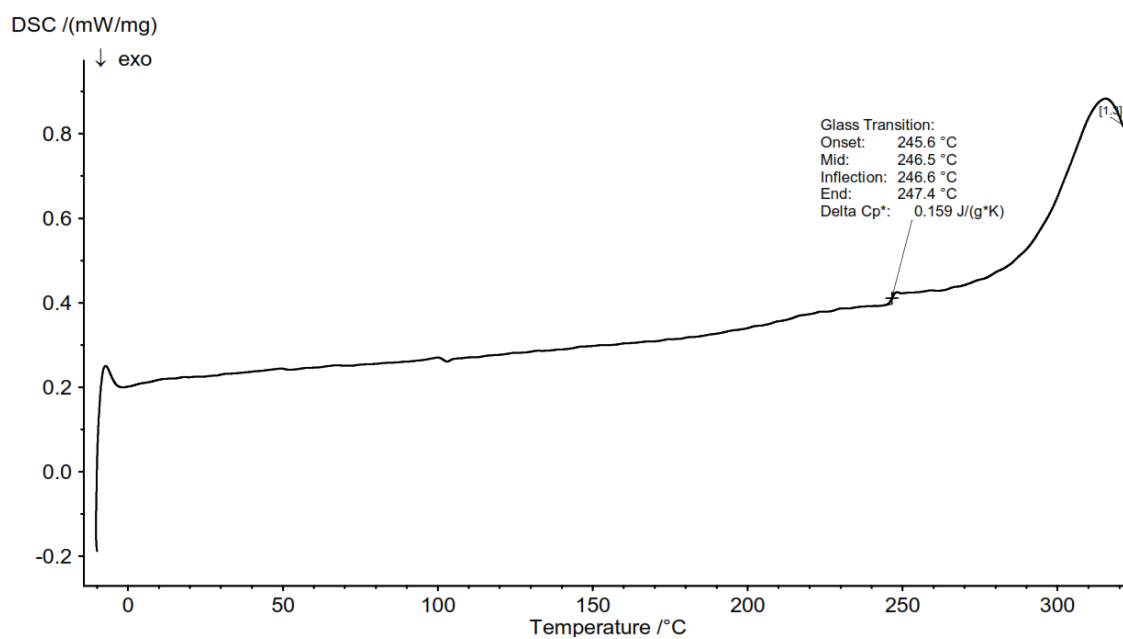


Figure S26. DSC trace corresponding to Table S1; Entry 9.

Table S1, Entry 10

IR (ATR-FTIR, cm^{-1}): ν 3464w (O-H), 2922w (C-H), 1676s (C=O), 1605m (C=C), 1418w, 1404m, 1220m, 1213s, 984m, 818s.

TGA: $T_d = 369\text{ }^\circ\text{C}$

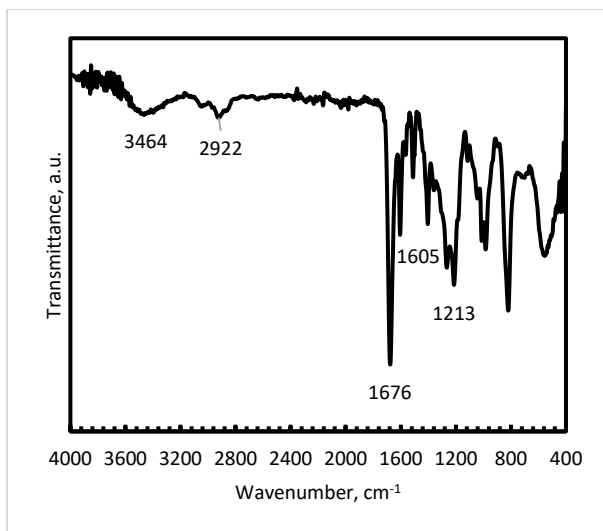


Figure S27. Infrared spectrum (ATR-FTIR) of the sample corresponding to Entry 10 in Table S1.

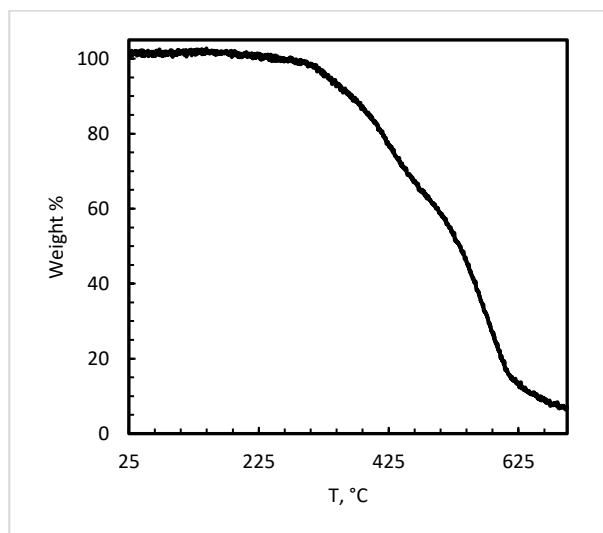


Figure S28. Mass loss as a function of temperature for sample corresponding to Entry 10 in Table S1.

Table S1, Entry 11

IR (ATR-FTIR, cm^{-1}): ν 3400w (O-H), 2924w (C-H), 1676s (C=O), 1604m (C=C), 1510w, 1402m, 1222m, 1213s, 983m, 818s.

TGA: $T_d = 335\text{ }^\circ\text{C}$

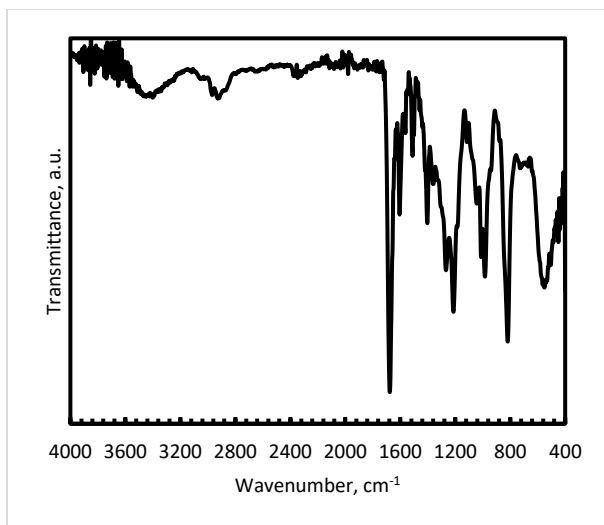


Figure S29. Infrared spectrum (ATR-FTIR) of the sample corresponding to Entry 11 in Table S1.

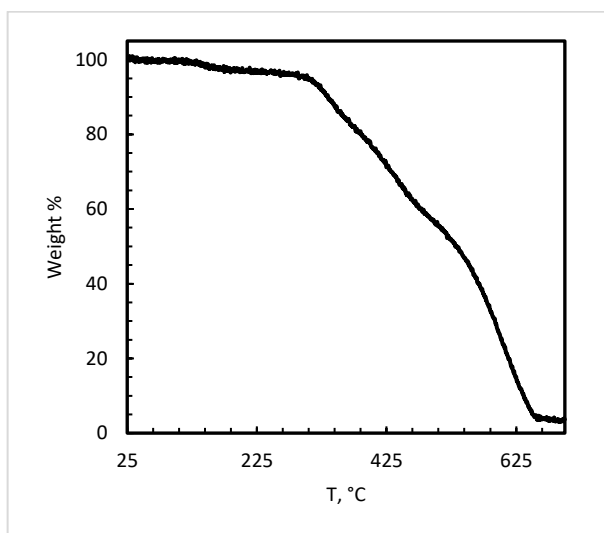


Figure S30. Mass loss as a function of temperature for sample corresponding to Entry 11 in Table S1.

Table S1, Entry 12

IR (ATR-FTIR, cm^{-1}): ν 3389w (O-H), 2907w (C-H), 1676s (C=O), 1604m (C=C), 1508w, 1402m, 1225m, 1211s, 983m, 818s.

TGA: $T_d = 328\text{ }^\circ\text{C}$

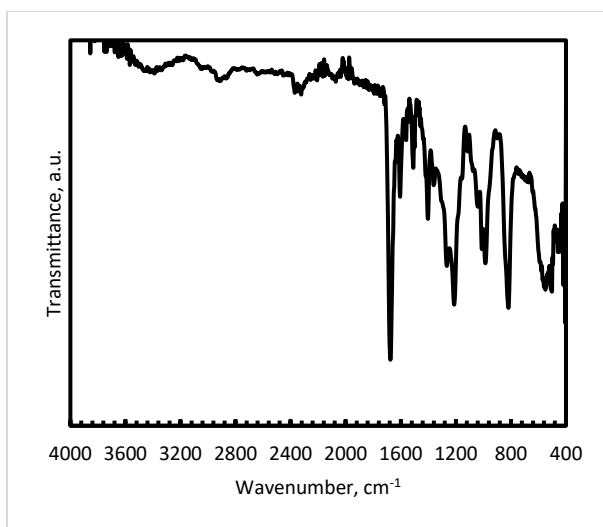


Figure S31. Infrared spectrum (ATR-FTIR) of the sample corresponding to Entry 12 in Table S1.

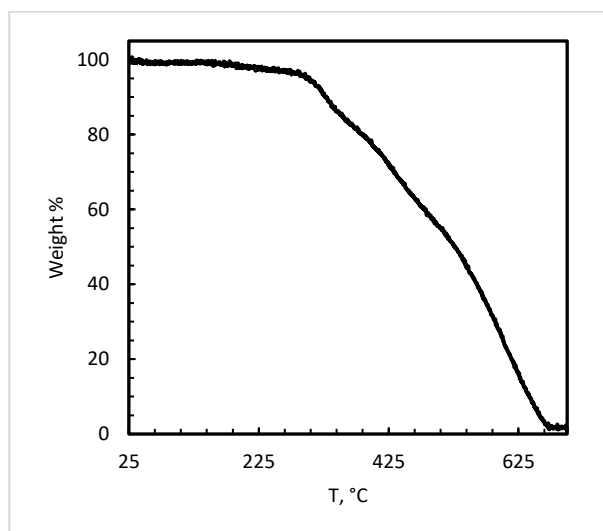


Figure S32. Mass loss as a function of temperature for sample corresponding to Entry 12 in Table S1.

Table S1, Entry 13

IR (ATR-FTIR, cm^{-1}): ν 3401w (O-H), 2926w (C-H), 1676s (C=O), 1605m (C=C), 1510w, 1404m, 1225m, 1213s, 982s, 818s, 555w.

TGA: $T_d = 352\text{ }^\circ\text{C}$

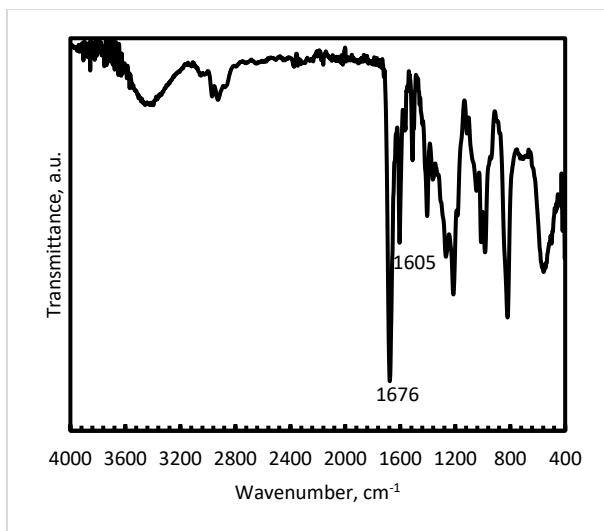


Figure S33. Infrared spectrum (ATR-FTIR) of the sample corresponding to Entry 13 in Table S1.

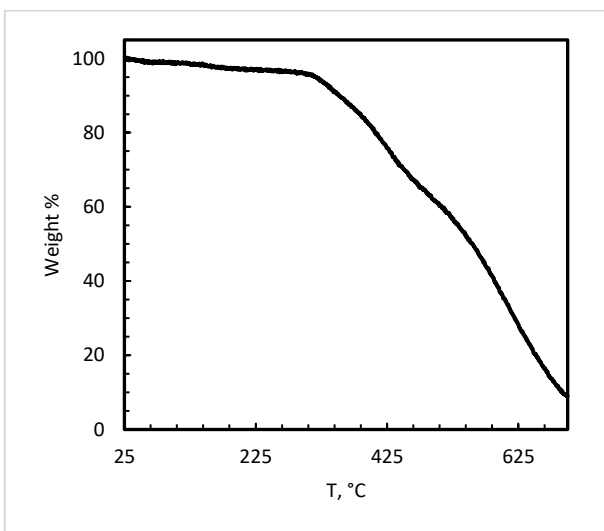


Figure S34. Mass loss as a function of temperature for sample corresponding to Entry 13 in Table S1.

Table S1, Entry 14

IR (ATR-FTIR, cm^{-1}): ν 3427w (O-H), 2918w (C-H), 1676s (C=O), 1601m (C=C), 1506w, 1404m, 1228s, 1211s, 982m, 820s, 542m.

TGA: $T_d = 342\text{ }^\circ\text{C}$

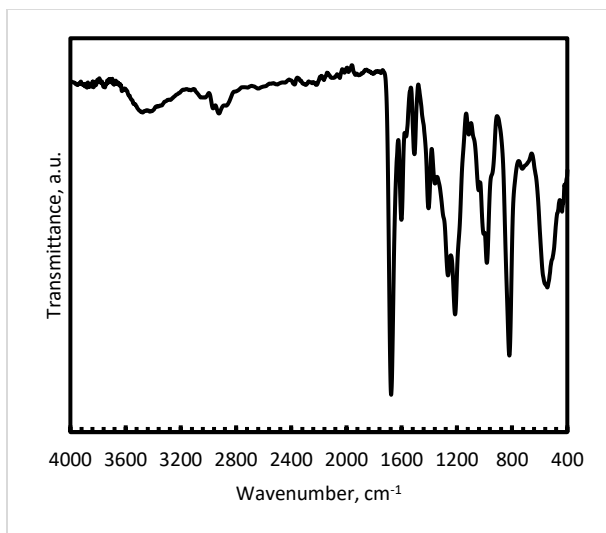


Figure S35. Infrared spectrum (ATR-FTIR) of the sample corresponding to Entry 14 in Table S1.

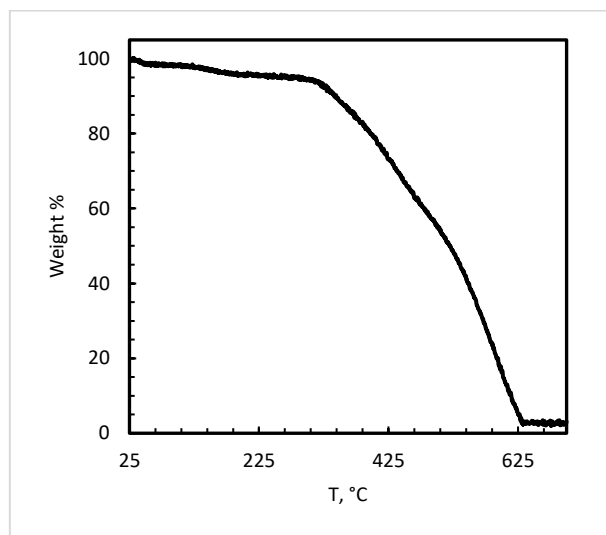


Figure S36. Mass loss as a function of temperature for sample corresponding to Entry 14 in Table S1.

Table S1, Entry 15

IR (ATR-FTIR, cm^{-1}): ν 3445w (O-H), 2918w (C-H), 1678s (C=O), 1605m (C=C), 1510w, 1402m, 1263m, 1213s, 981s, 818s, 550m.

TGA: $T_d = 363^\circ\text{C}$

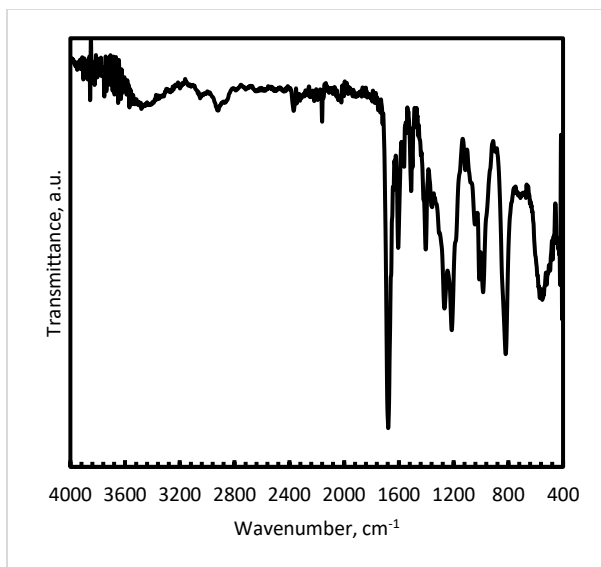


Figure S37. Infrared spectrum (ATR-FTIR) of the sample corresponding to Entry 15 in Table S1.

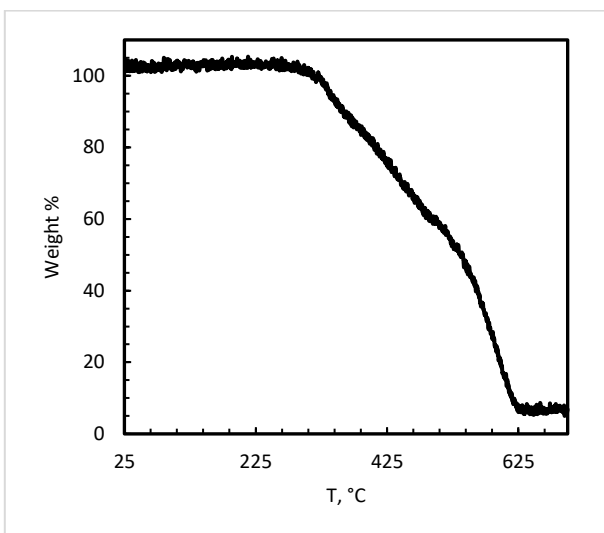


Figure S38. Mass loss as a function of temperature for sample corresponding to Entry 15 in Table S1.

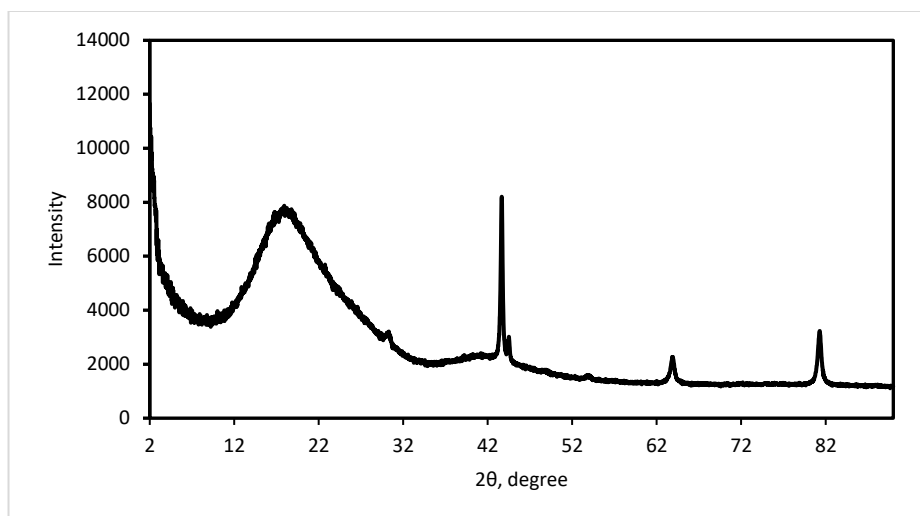


Figure S39. Experimental powder XRD patterns of the sample corresponding to Entry 15 in Table S1. Crystalline peaks are from Teflon substrate.

Table S1, Entry 16

IR (ATR-FTIR, cm^{-1}): ν 3404w (O-H), 2911w (C-H), 1676s (C=O), 1603m (C=C), 1508w, 1402m, 1267s, 1211s, 984m, 818s, 555m.

TGA: $T_d = 343\text{ }^\circ\text{C}$

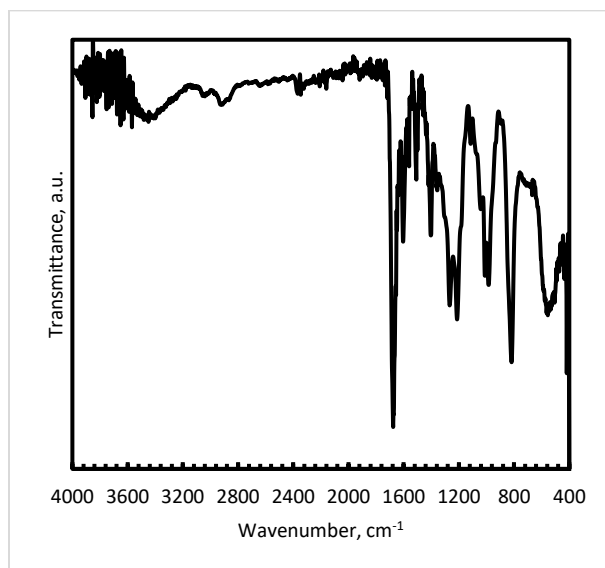


Figure S40. Infrared spectrum (ATR-FTIR) of the sample corresponding to Entry 16 in Table S1.

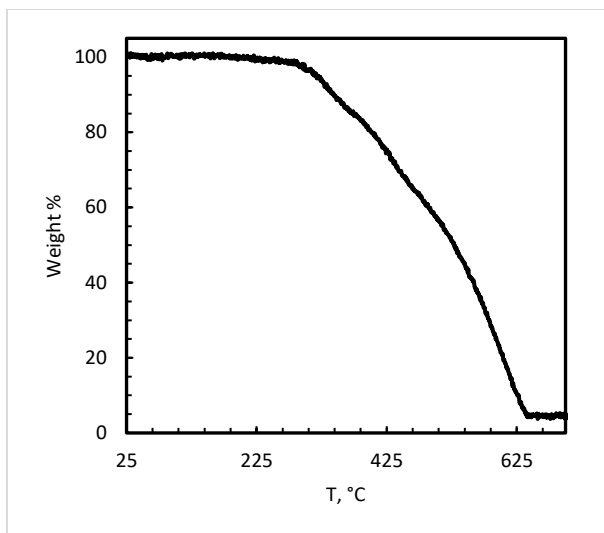


Figure S41. Mass loss as a function of temperature for sample corresponding to Entry 16 in Table S1.

Table S1, Entry 17

IR (ATR-FTIR, cm^{-1}): ν 3449w (O-H), 2914w (C-H), 1676s (C=O), 1604m (C=C), 1510w, 1402m, 1267s, 1213s, 983m, 818s, 548m.

TGA: $T_d = 344\text{ }^\circ\text{C}$

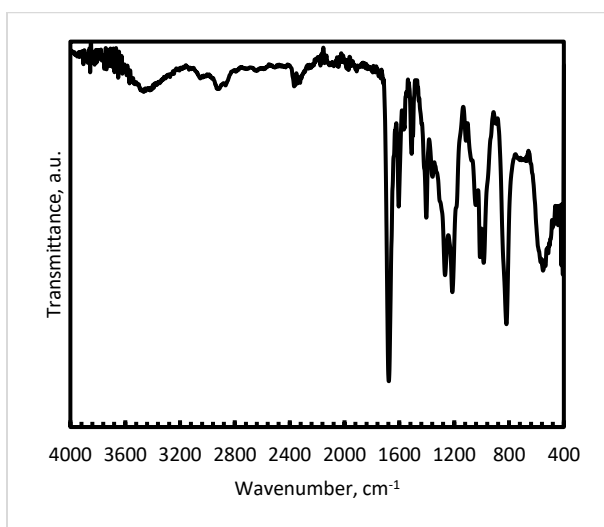


Figure S42. Infrared spectrum (ATR-FTIR) of the sample corresponding to Entry 17 in Table S1.

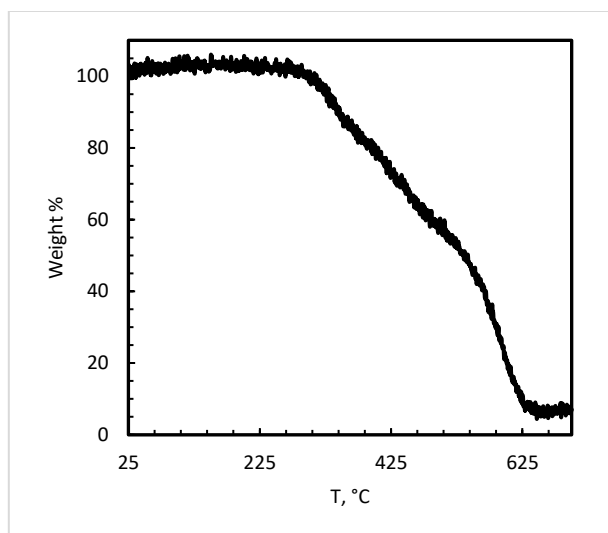


Figure S43. Mass loss as a function of temperature for sample corresponding to Entry 17 in Table S1.

Table S1, Entry 18

IR (ATR-FTIR, cm^{-1}): ν 3424w (O-H), 2924w (C-H), 1672s (C=O), 1599s (C=C), 1287m, 1267s, 1015m, 824s.

TGA: $T_d = 396\text{ }^{\circ}\text{C}$

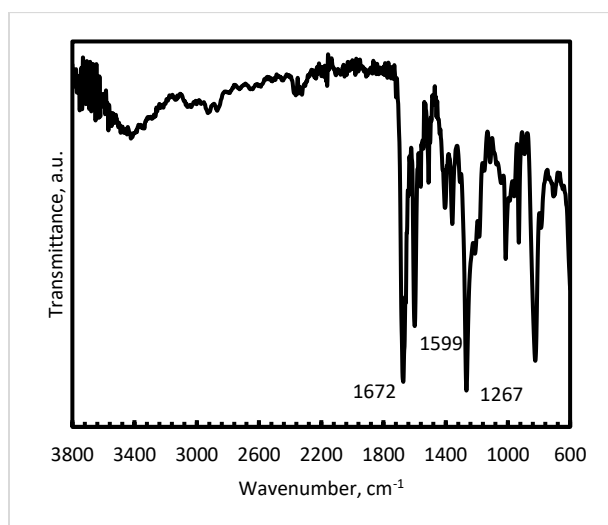


Figure S44. Infrared spectrum (ATR-FTIR) of the sample corresponding to Entry 18 in Table S1.

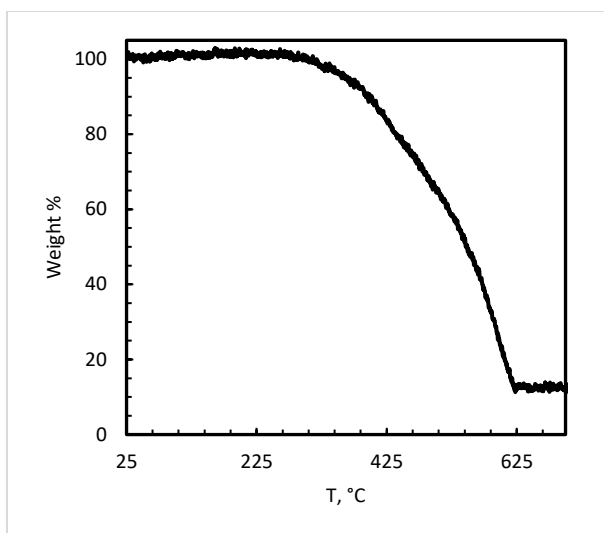


Figure S45. Mass loss as a function of temperature for sample corresponding to Entry 18 in Table S1.

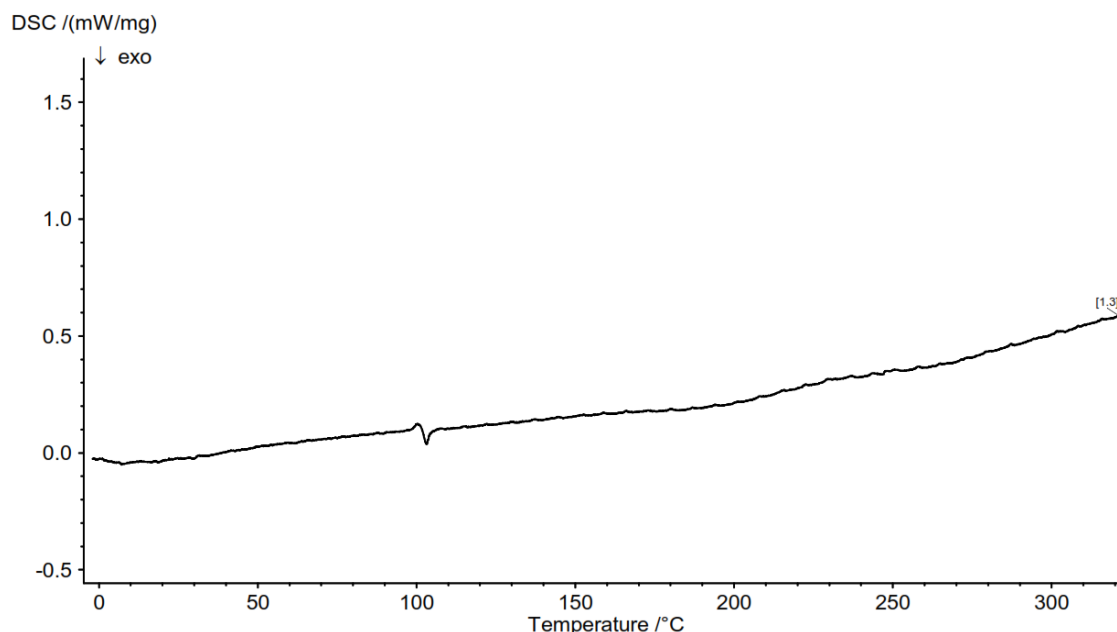


Figure S46. DSC trace corresponding to Entry 18 in Table S1.

Table S1, Entry 19

A 100 mL ampoule equipped with a J-Young's valve was refilled with argon, charged with pre-catalyst **1** (2.5 mg, 0.005 mmol, 1 mol%), 5 mL of dry THF and solution of KO^tBu (0.5 mL of 0.01 M in THF, 1 mol%). The mixture was stirred at room temperature for 1 h and then the volatiles were evaporated. To the resulting mixture 1,4-benzenedimethanol (69 mg, 0.5 mmol) and 1,4-diacetylketone (81 mg, 0.5 mmol) were added. *tert*-Amyl alcohol was added and the flask was sealed under an argon atmosphere before heating to 140 °C for 18 hours. To the resulting mixture, 5 mL of 1 M HCl was added and the flask had been heated at 90 °C for 1 h.

The isolated amount was not enough to perform analysis.

Table S1, Entry 20

A 100 mL ampoule equipped with a J-Young's valve was refilled with argon, charged with pre-catalyst **1** (2.5 mg, 0.005 mmol, 1 mol%), 5 mL of dry THF and solution of KO^tBu (1.0 mL of 0.01 M in THF, 2 mol%).

The mixture was stirred at room temperature for 1 h and then the volatiles were evaporated. To the resulting mixture 1,4-benzenedimethanol (69 mg, 0.5 mmol) and 1,4-diacetylketone (81 mg, 0.5 mmol) were added. *tert*-Amyl alcohol was added and the flask was sealed under an argon atmosphere before heating to 140 °C for 18 hours. To the resulting mixture, 5 mL of 1 M HCl was added and the flask had been heated at 90 °C for 1 h.

The isolated amount was not enough to perform analysis.

Table S1, Entry 21

The isolated amount was not enough to perform analysis.

Table S1, Entry 22

The isolated amount was not enough to perform analysis.

1.4 NMR spectra of mother liquor from coupling reaction of 1,4-diacetylbenzene and 1,4-benzenedimethanol as described in Table S1.

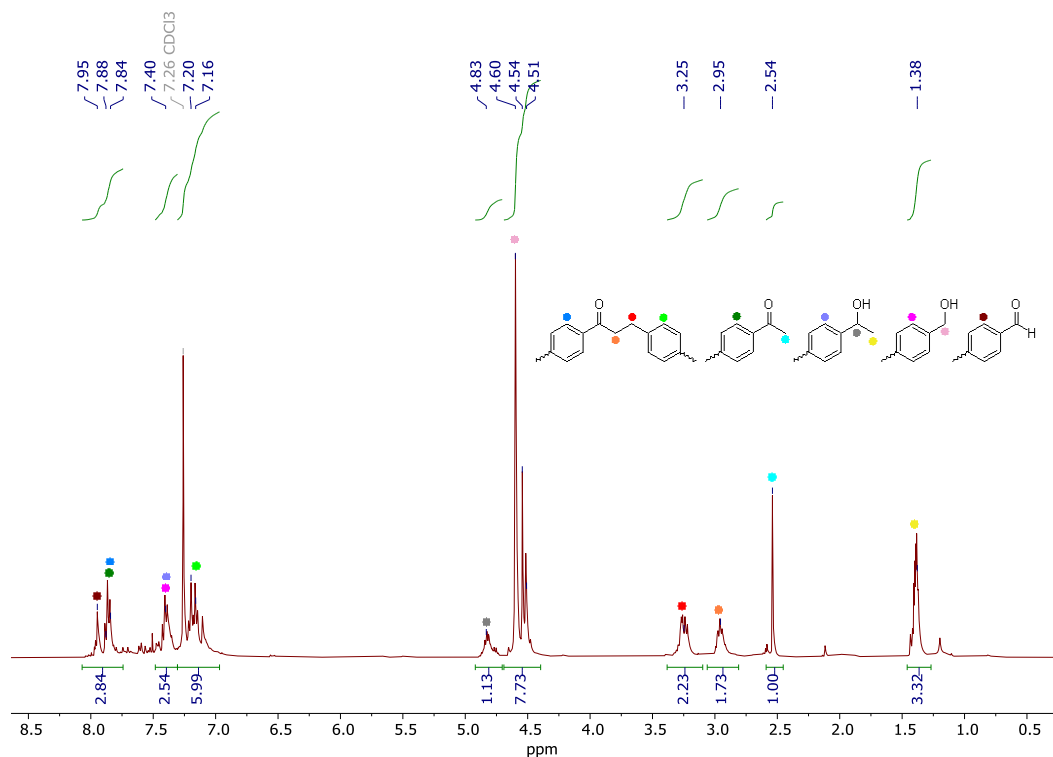


Figure S47. ¹H NMR spectrum of mother liquor after polymer precipitation from the reaction Table S1; Entry 7 in CDCl₃/CD₃OD = 3/1 at room temperature.

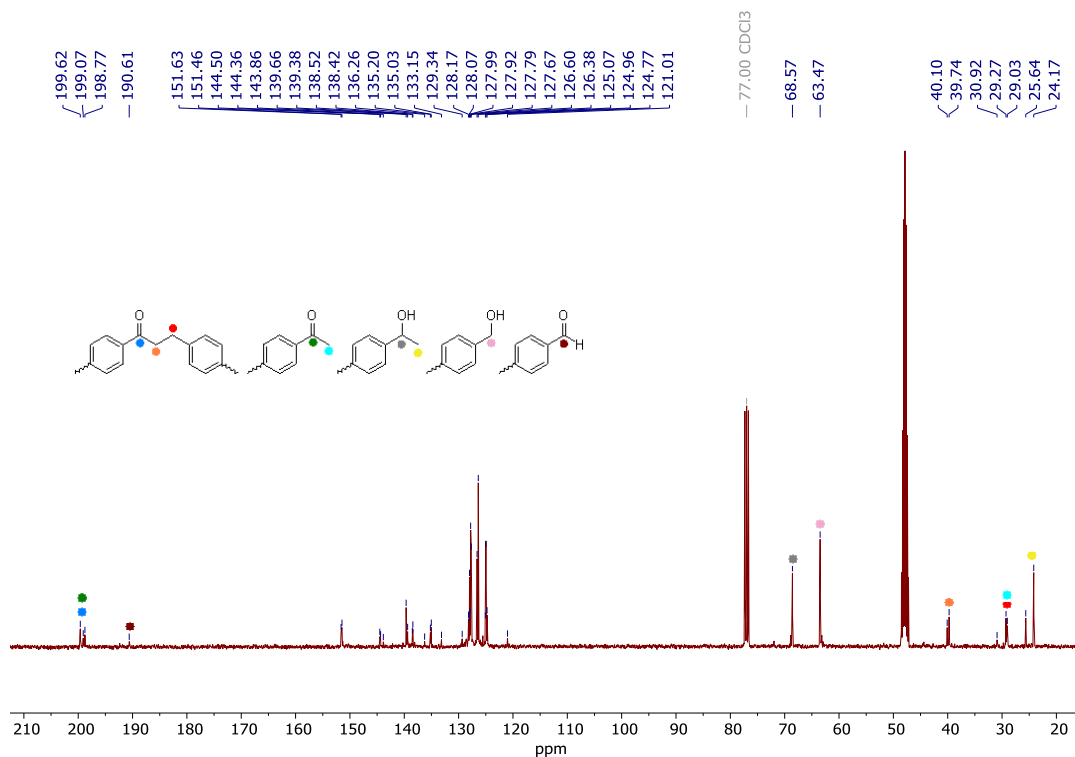


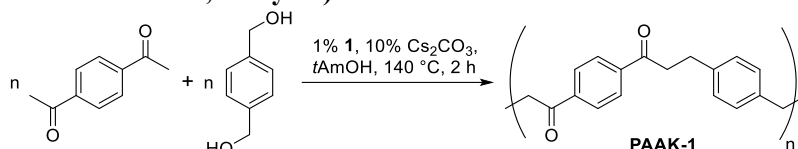
Figure S48. ¹³C{¹H} NMR spectrum of mother liquor after polymer precipitation from the reaction Entry 7 in Table S1 in CDCl₃/CD₃OD = 3/1 at room temperature.

1.5 Synthesis of polyketones from diketones and diols.

General method for the coupling of diketones and 1,4-benzenedimethanol, 1,3-benzenedimethanol and 1,4-cyclohexanedimethanol:

A 100 mL ampoule equipped with a J-Young's valve was charged with pre-catalyst **1** (2.5 mg, 0.005 mmol, 1 mol%) and Cs₂CO₃ (16.5 mg, 0.05 mmol, 10 mol%) or KO^tBu (56 mg, 0.5 mmol, 100 mol%), diol (0.5 mmol) and diketone (0.5 mmol). The flask was sealed under an argon atmosphere and *tert*-amyl alcohol (5 mL) was added before heating to 140 °C for 2 or 18 h with stirring. After this period, the reaction vessel was allowed to cool to room temperature and any gas evolved (presumably H₂) during the reaction was measured when possible. To the resulting mixture 5 mL of 1 M HCl were added and the flask had been heated at 90 °C for 1 h. The precipitate was filtered and dried under reduced pressure at 120 °C.

PAAK-1 (corresponds to Table S1, entry 15)



1,4-Dimethanolbenzene (69 mg, 0.5 mmol) and 1,4-diacetylbenzene (81 mg, 0.5 mmol) were used. The polymer was obtained in 89% yield (117 mg) as a yellow solid.

IR (ATR-FTIR, cm⁻¹): ν 3445w (O-H), 2918w (C-H), 1678s (C=O), 1605m (C=C), 1510w, 1402m, 1263m, 1213s, 981s, 818s, 550m.

TGA: T_d = 363 °C

GPC: bimodal: MW(1) = 1.5 kDa, PDI = 1.3; MW(2) = 51.1 kDa, PDI = 1.6.

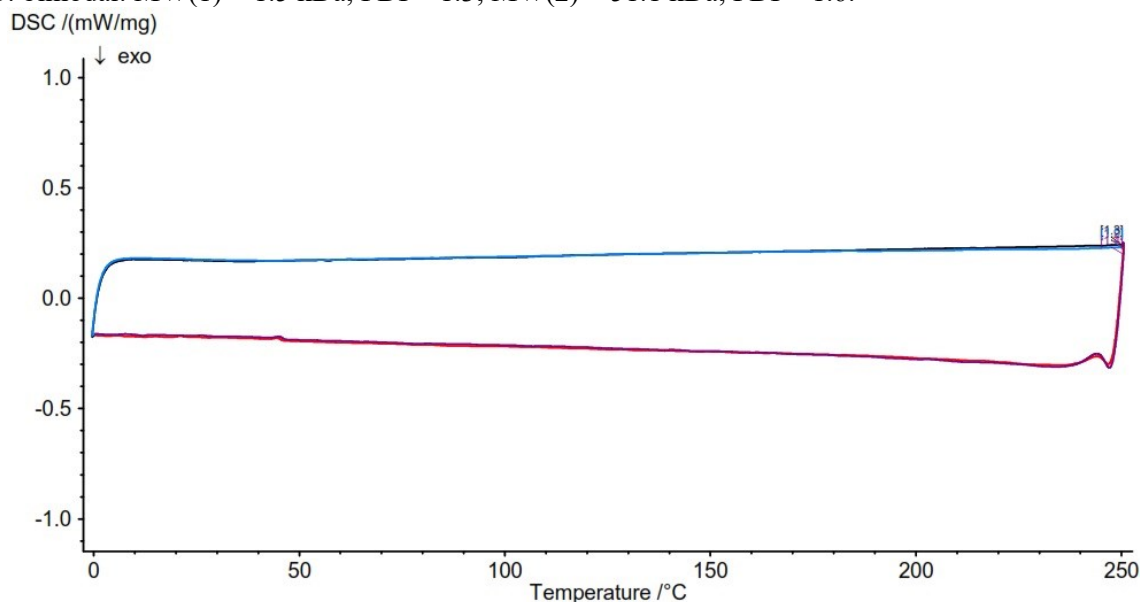


Figure S49. DSC trace corresponding to PAAK-1.

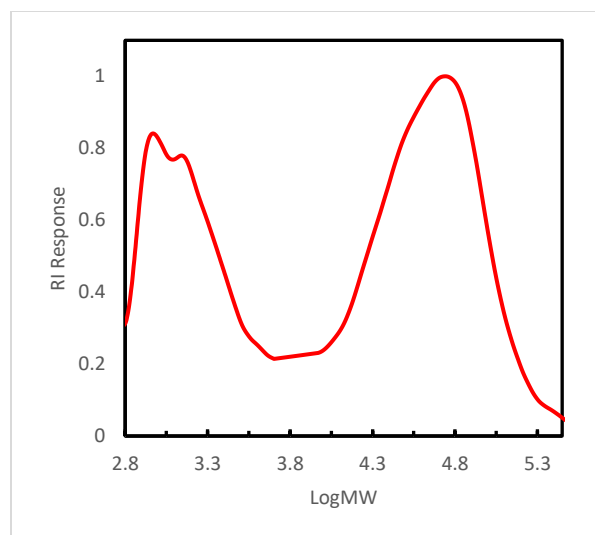
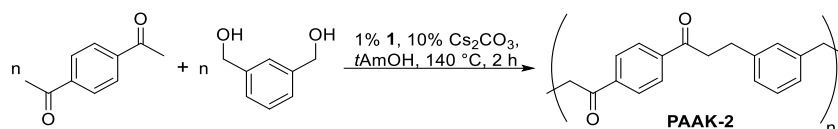


Figure S50. GPC chromatograph corresponding to **PAAK-1**.

PAAK-2



1,3-benzenedimethanol (69 mg, 0.5 mmol) and 1,4-diacetylbenzene (81 mg, 0.5 mmol) were used. The polymer was obtained with 77% yield (101 mg) as a yellow solid.

^{13}C CP MAS NMR (100.6 MHz): δ 199.4, 151.3, 141.1, 128.2, 70.8, 64.5, 41.1, 36.2, 28.8.

IR (ATR-FTIR, cm^{-1}): ν 3422w (O-H), 2918w (C-H), 1678s (C=O), 1605m (C=C), 1449w, 1402m, 1265m, 1211s, 984s, 793m, 704s.

TGA: $T_d = 351\text{ }^\circ\text{C}$

GPC: bimodal: $\text{MW}(1) = 1.2\text{ kDa}$, $\text{PDI} = 1.2$; $\text{MW}(2) = 54.1\text{ kDa}$, $\text{PDI} = 1.6$.

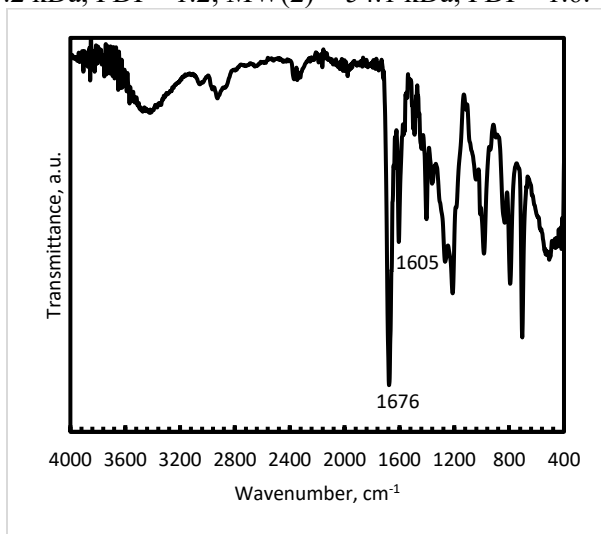


Figure S51. Infrared spectrum (ATR-FTIR) of polyketone PAAK-2.

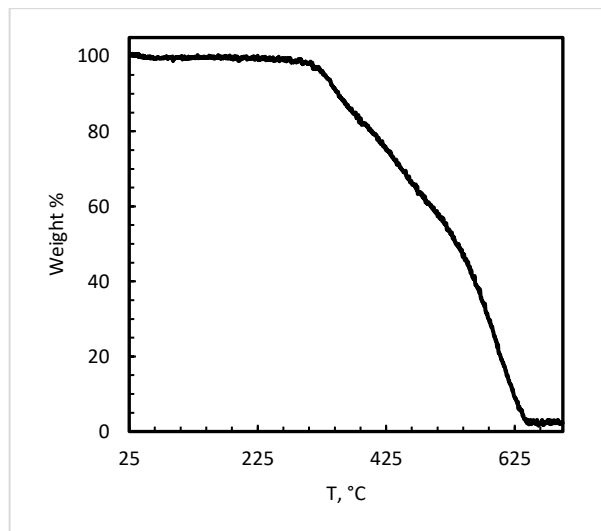


Figure S52. Mass loss as a function of temperature for polyketone PAAK-2.

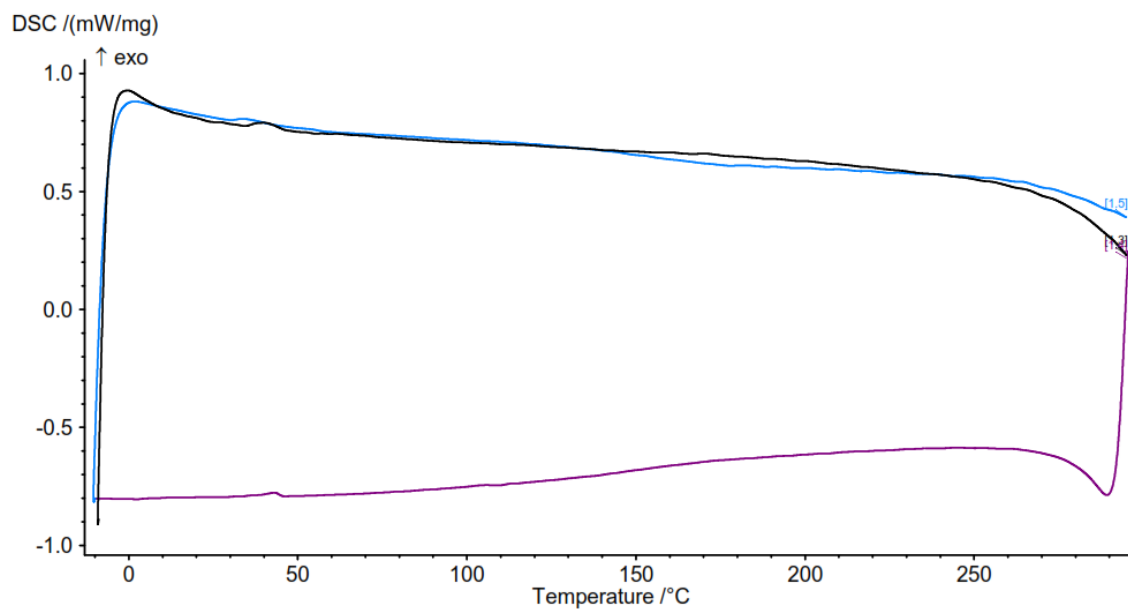


Figure S53. DSC trace corresponding to **PAAK-2**.

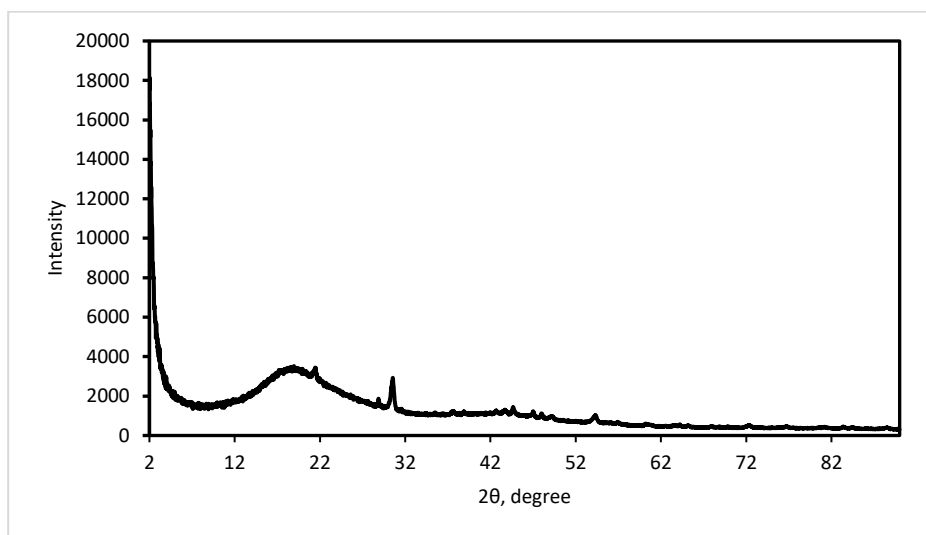


Figure S54. Experimental powder XRD patterns of **PAAK-2**. Crystalline peaks were indexed in the small-volume unit cell which remains unidentified.

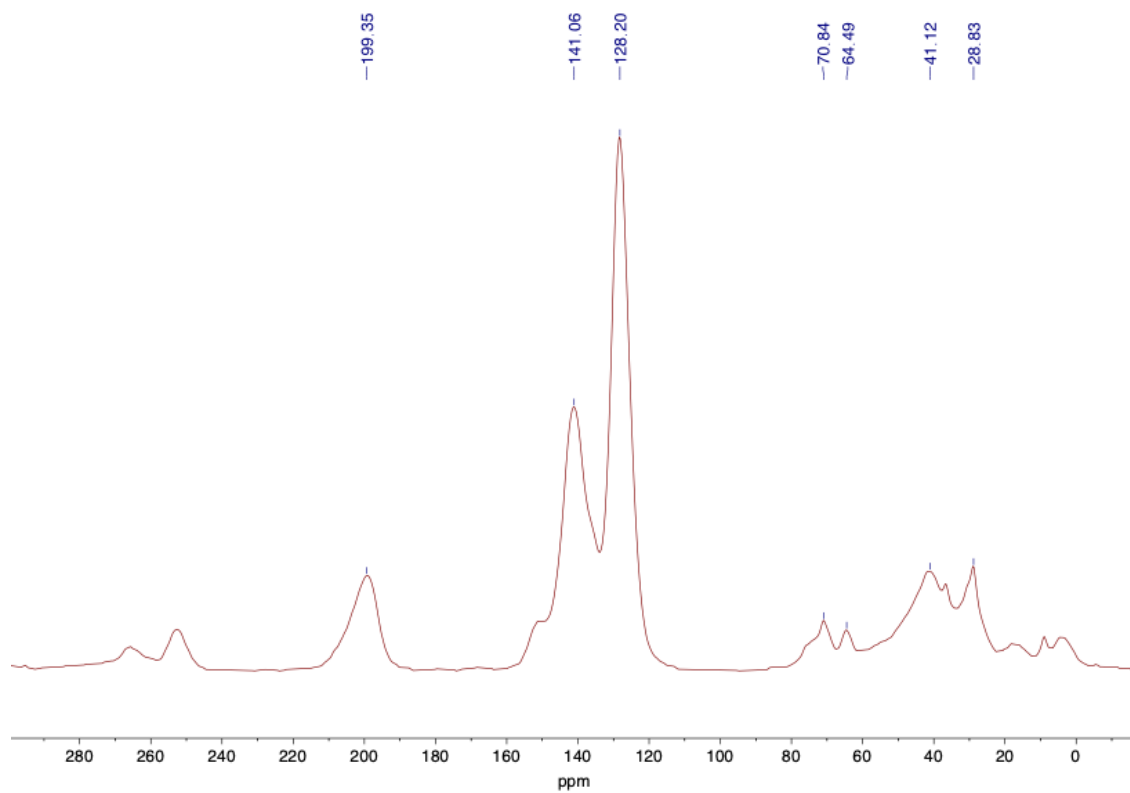


Figure S55. ^{13}C CP MAS NMR spectrum of **PAAK-2**.

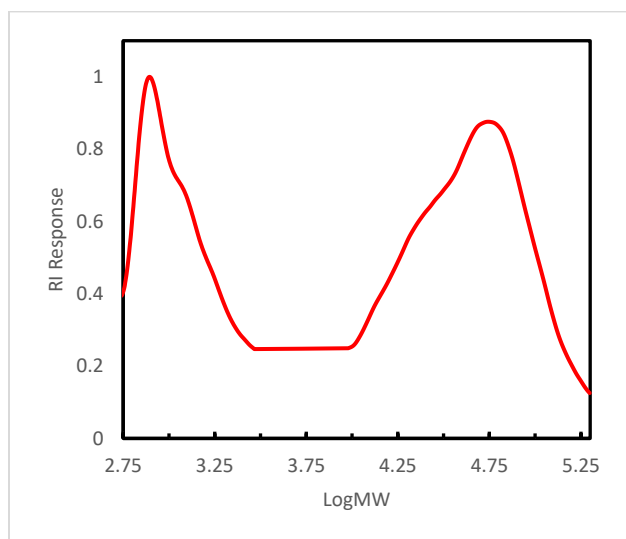
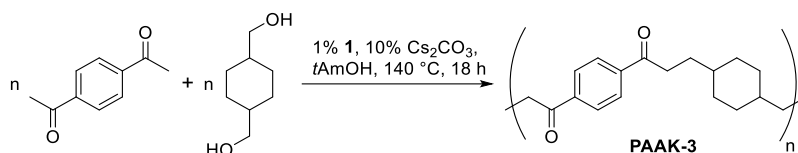


Figure S56. GPC chromatograph corresponding to **PAAK-2**.

PAAK-3



^{13}C CP MAS NMR (100.6 MHz): δ 199.9, 148.1, 140.2, 128.4, 75.8, 68.4, 48.5, 36.7, 41.1, 30.7.

IR (ATR-FTIR, cm^{-1}): ν 3482w (O-H), 2918m (C-H), 2853m (C-H), 1676s (C=O), 1605m (C=C), 1402m, 1269m, 1217m, 1011m, 829m, 503m.

TGA: $T_d = 369^\circ\text{C}$

GPC: bimodal: MW(1) = 1.6 kDa, PDI = 1.3; MW(2) = 52.9 kDa, PDI = 1.7.

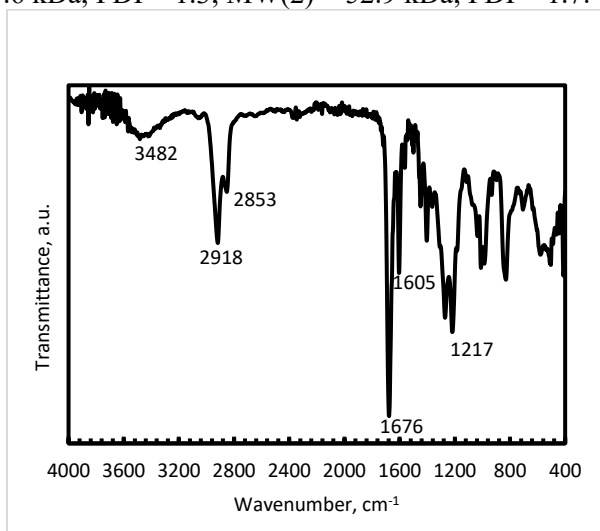


Figure S57. Infrared spectrum (ATR-FTIR) of polyketone PAAK-3.

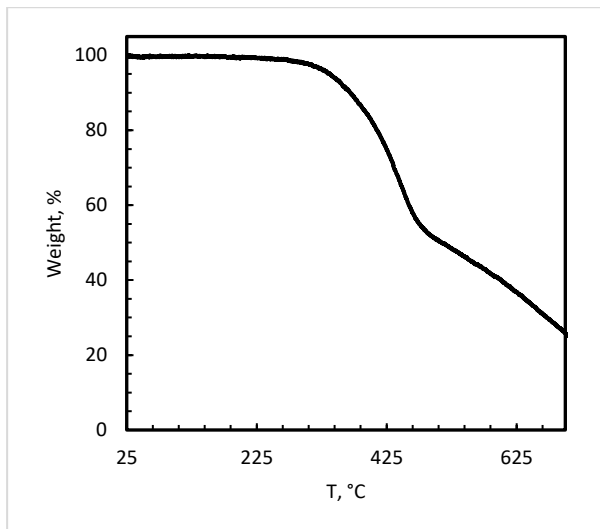


Figure S58. Mass loss as a function of temperature for polyketone PAAK-3.

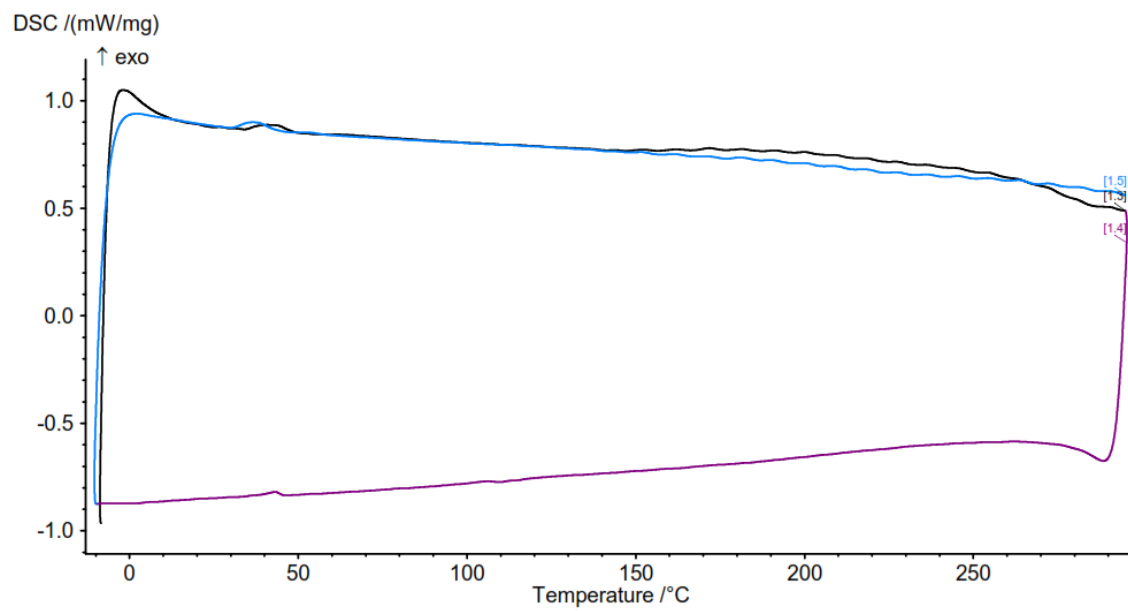


Figure S59. DSC trace corresponding to **PAAK-3**.

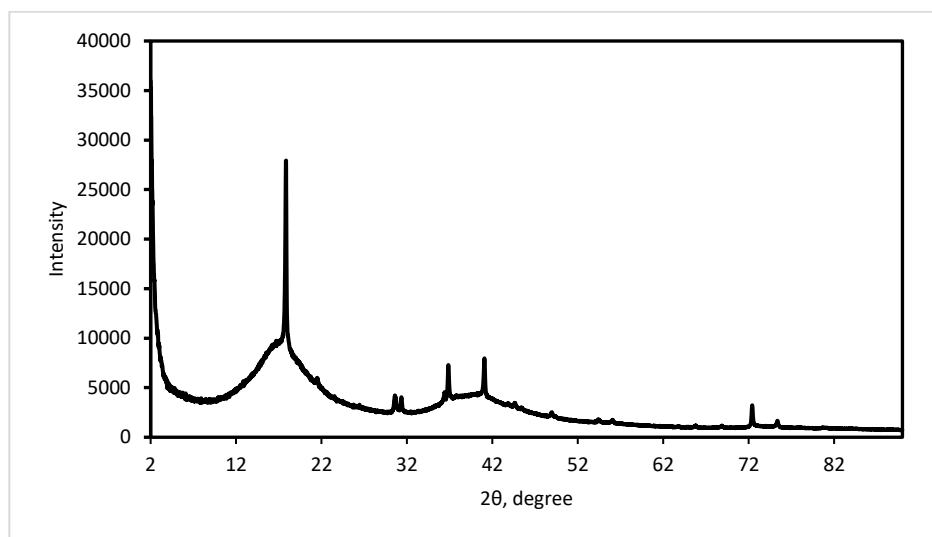


Figure S60. Experimental powder XRD patterns of **PAAK-3**. Unidentifiable crystalline phases are present.

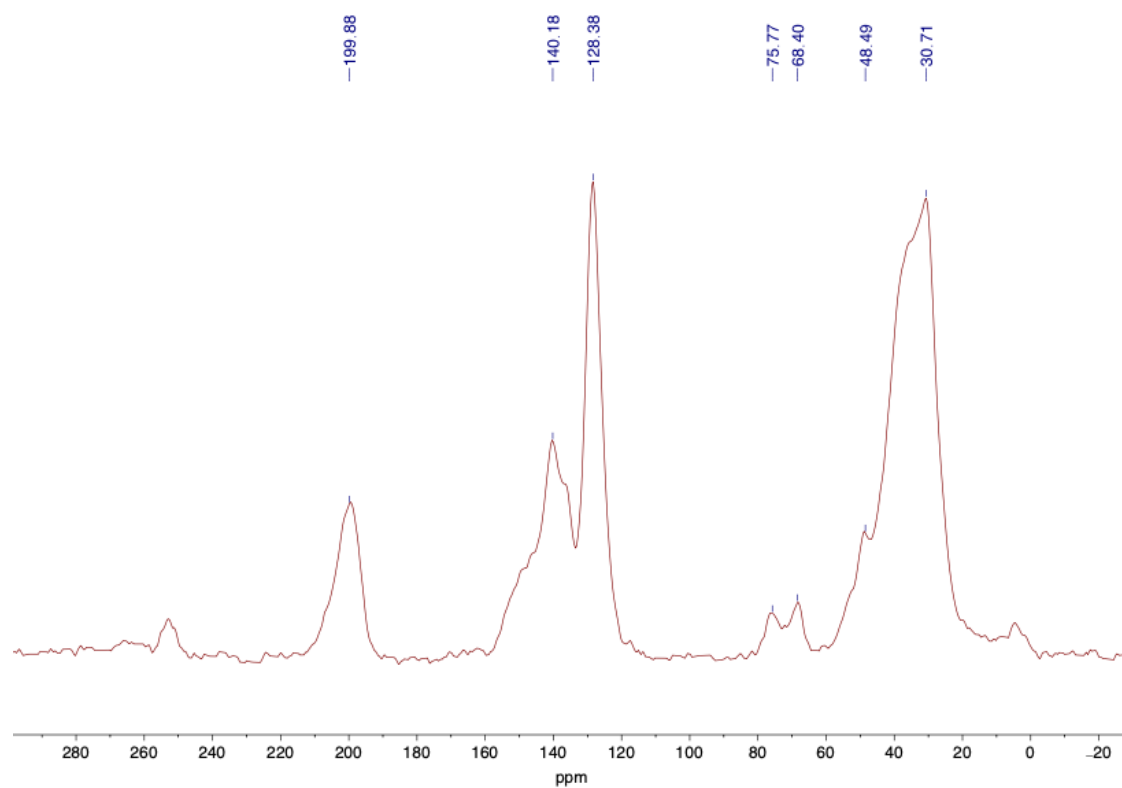


Figure S61. ^{13}C CP MAS NMR spectrum of **PAAK-3**.

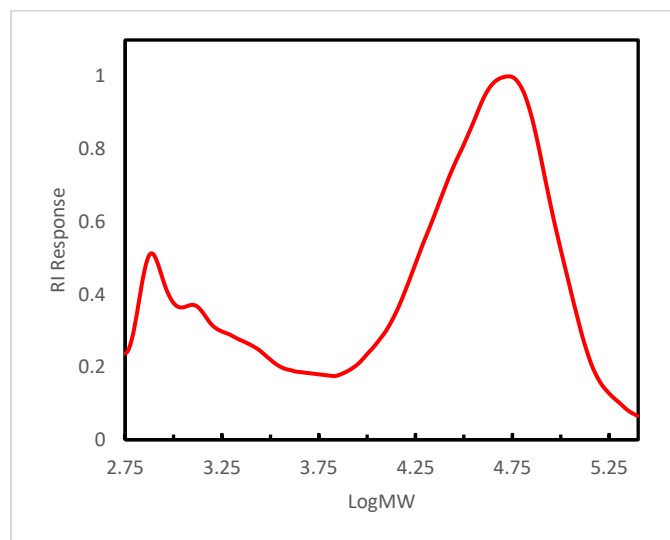
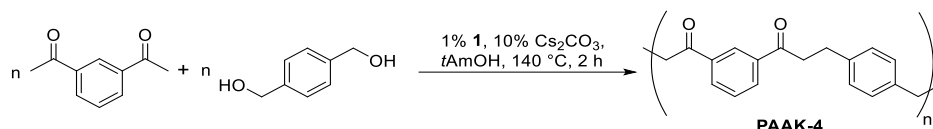


Figure S62. GPC chromatograph corresponding to **PAAK-3**.

PAAK-4



1,4-Benzenedimethanol (69 mg, 0.5 mmol) and 1,3-diacetylbenzene (81 mg, 0.5 mmol) were used. The polymer was obtained in 98 % yield (129 mg) as a yellow solid.

^{13}C CP MAS NMR (100.6 MHz): δ 199.5, 141.0, 137.9, 128.6, 75.1, 71.0, 64.5, 41.2, 37.2, 29.1.

IR (ATR-FTIR, cm^{-1}): ν 3472w (O-H), 3059w, 2920w (C-H), 1680s (C=O), 1597m, 1171m, 999w, 795m, 704m.

TGA: $T_d = 350^\circ\text{C}$

GPC: bimodal: MW(1) = 1.4 kDa, PDI = 1.3; MW(2) = 51.1 kDa, PDI = 1.7.

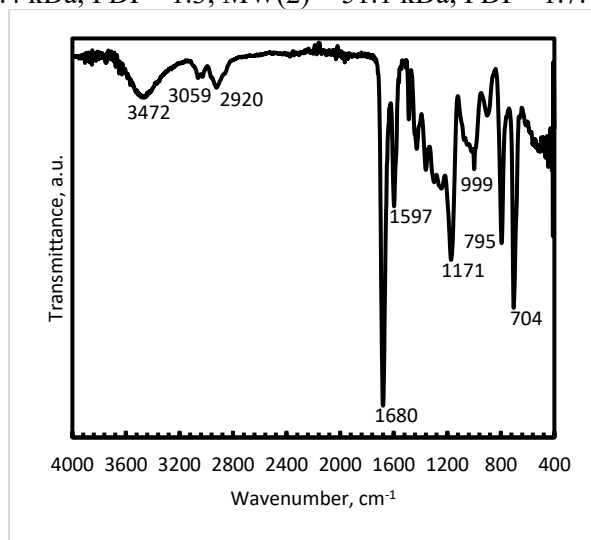


Figure S63. Infrared spectrum (ATR-FTIR) of polyketone PAAK-4.

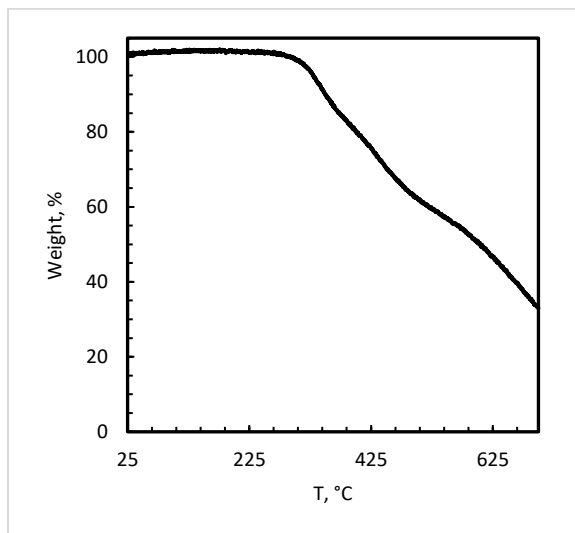


Figure S64. Mass loss as a function of temperature for polyketone PAAK-4.

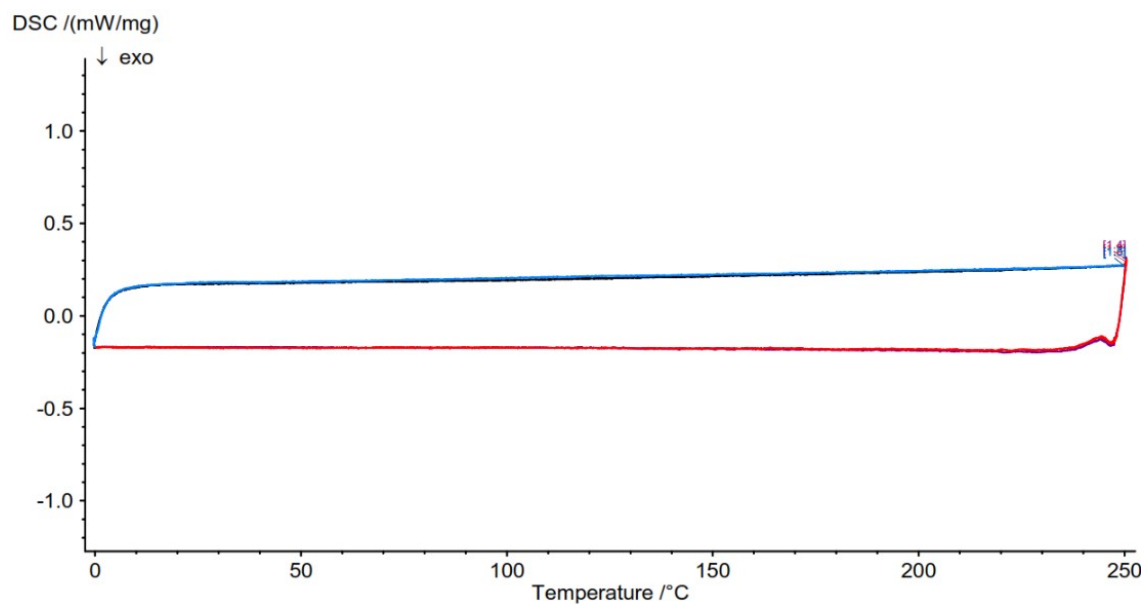


Figure S65. DSC trace corresponding to **PAAK-4**.

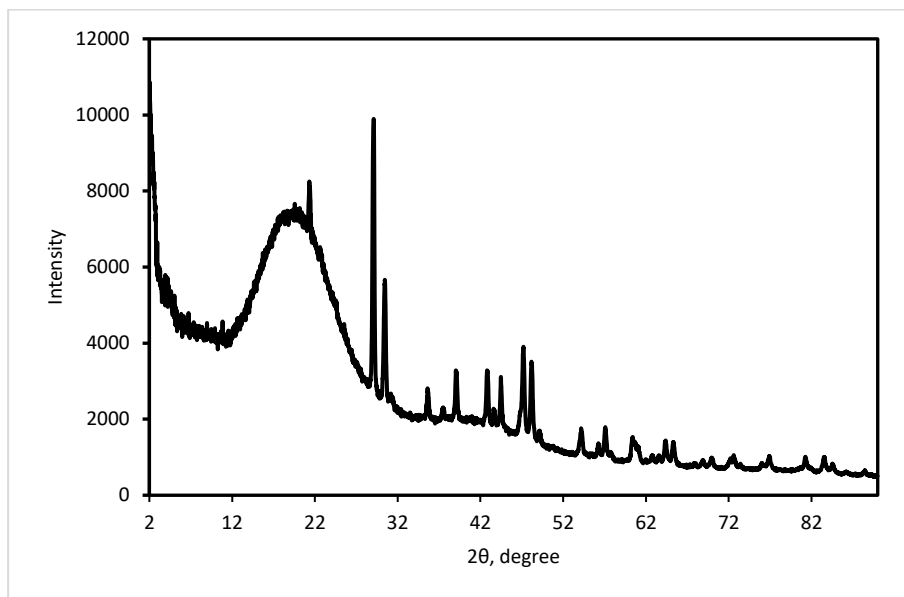


Figure S66. Experimental powder XRD patterns of **PAAK-4**. Unidentifiable crystalline phase present.

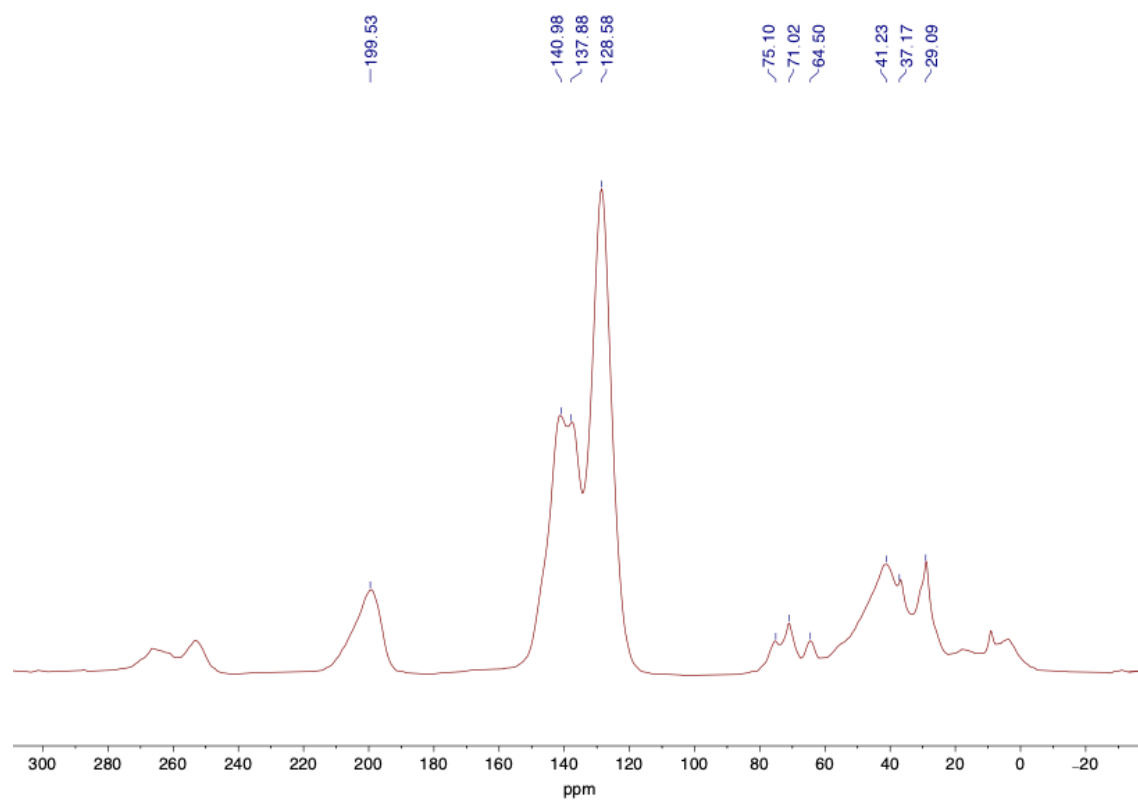


Figure S67. ^{13}C CP MAS NMR spectrum of **PAAK-4**.

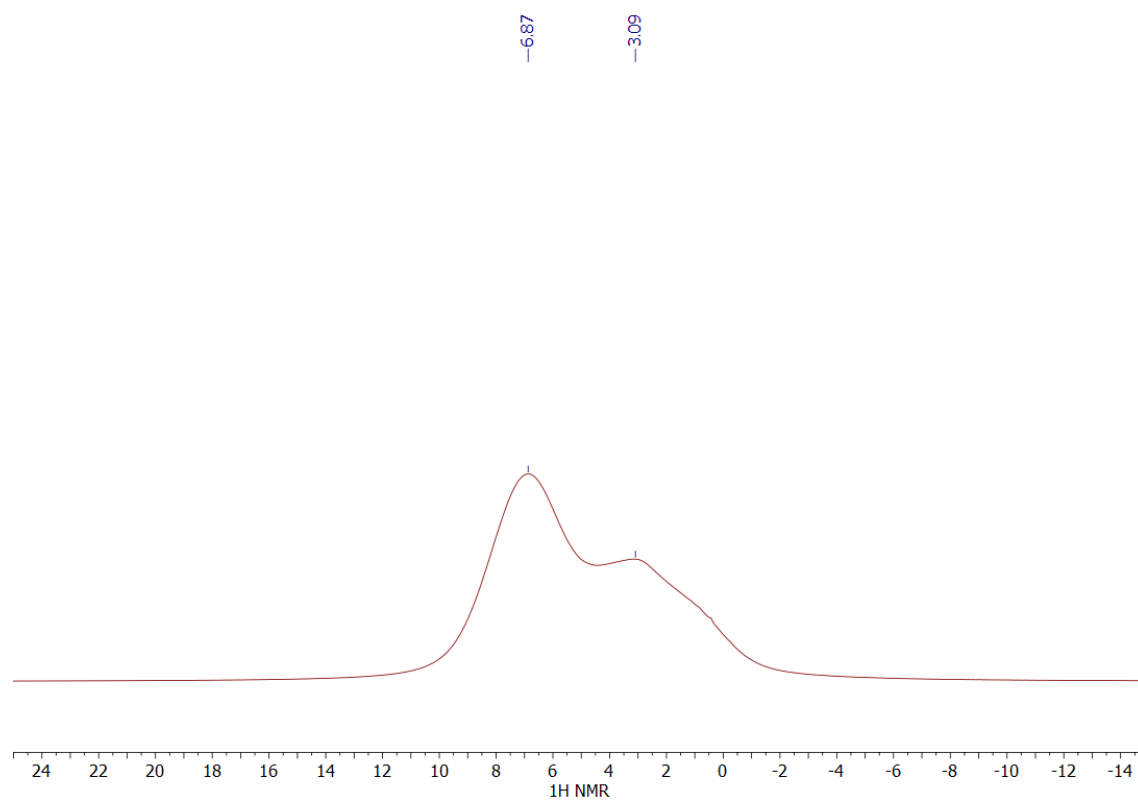


Figure S68. ^1H CP MAS NMR spectrum of **PAAK-4**.

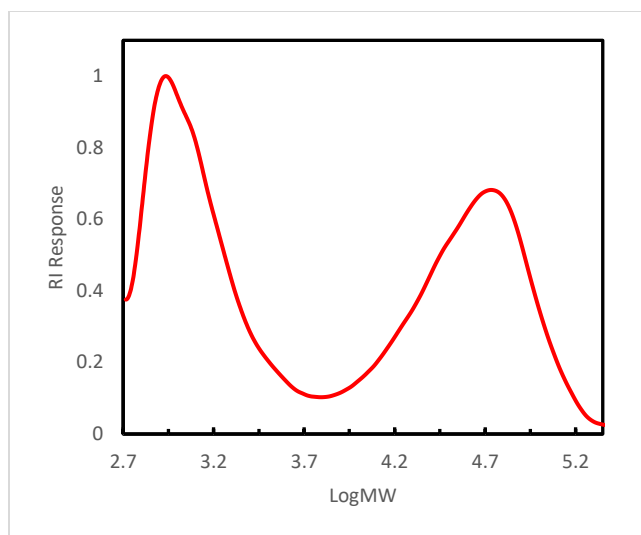
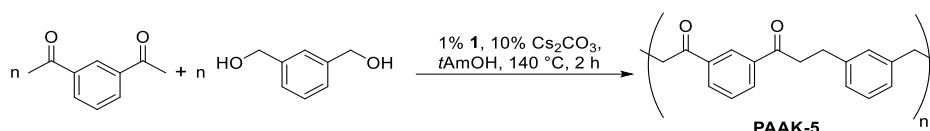


Figure S69. GPC chromatograph corresponding to **PAAK-4**.

PAAK-5



^{13}C CP MAS NMR (100.6 MHz): δ 199.5, 138.3, 128.9, 75.1, 70.9, 64.2, 41.4, 29.0.

IR (ATR-FTIR, cm^{-1}): ν 3422w (O-H), 3049w, 2914w (C-H), 1678s (C=O), 1597m, 1171m, 1016w, 804m, 696w, 554m.

TGA: $T_d = 365\text{ }^\circ\text{C}$

GPC: bimodal: $\text{MW}(1) = 2.1\text{ kDa}$, $\text{PDI} = 1.6$; $\text{MW}(2) = 53.7\text{ kDa}$, $\text{PDI} = 1.6$.

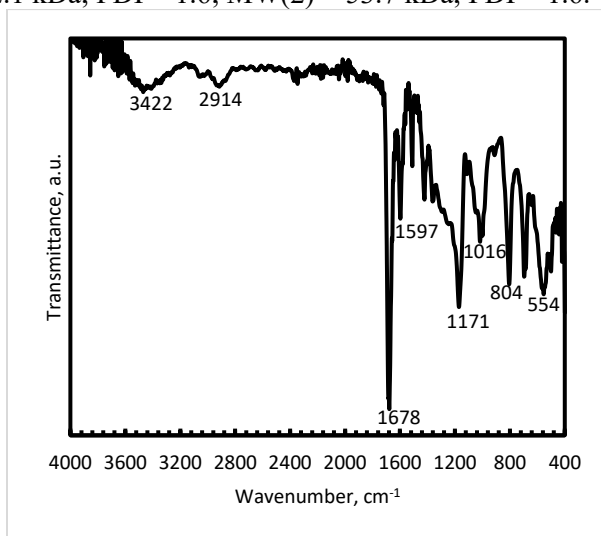


Figure S70. Infrared spectrum (ATR-FTIR) of polyketone **PAAK-5**.

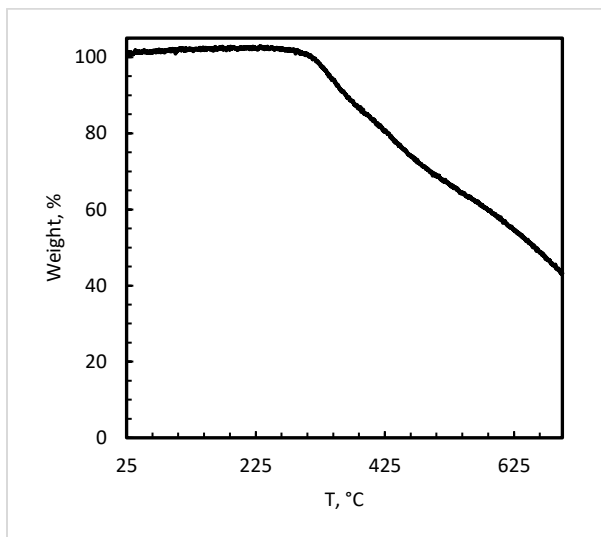


Figure S71. Mass loss as a function of temperature for polyketone **PAAK-5**.

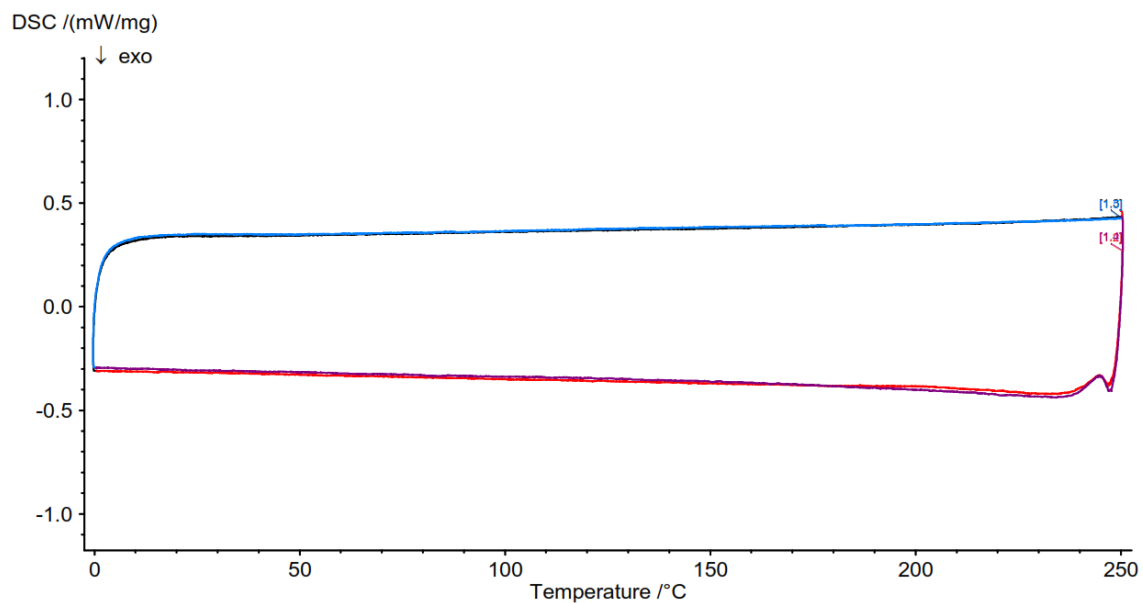


Figure S72. DSC trace corresponding to **PAAK-5**.

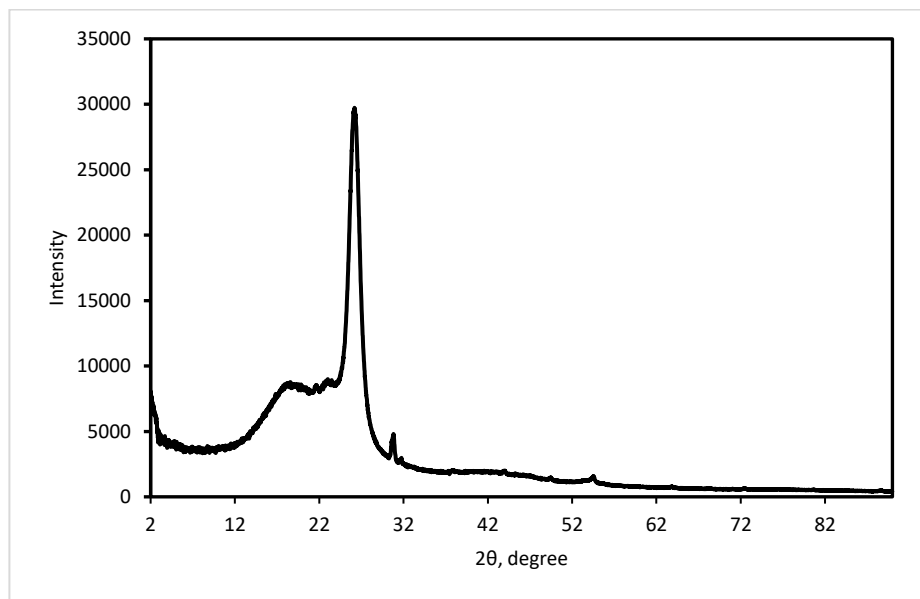


Figure S73. Experimental powder XRD patterns of **PAAK-5**. Crystalline peaks were indexed in the small-volume unit cell which remains unidentified. Tall thin amorphous halo is from polyester films used for measurements of small amount of sample.

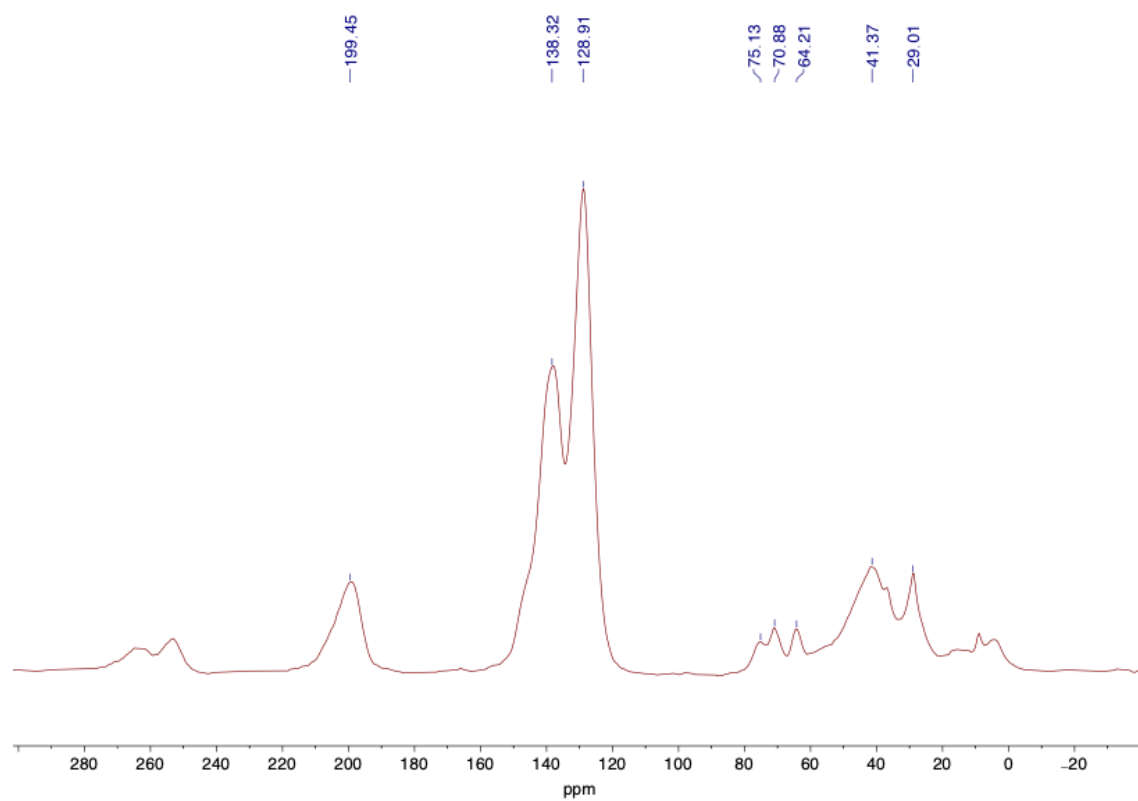


Figure S74. ¹³C CP MAS NMR spectrum of PAAK-5.

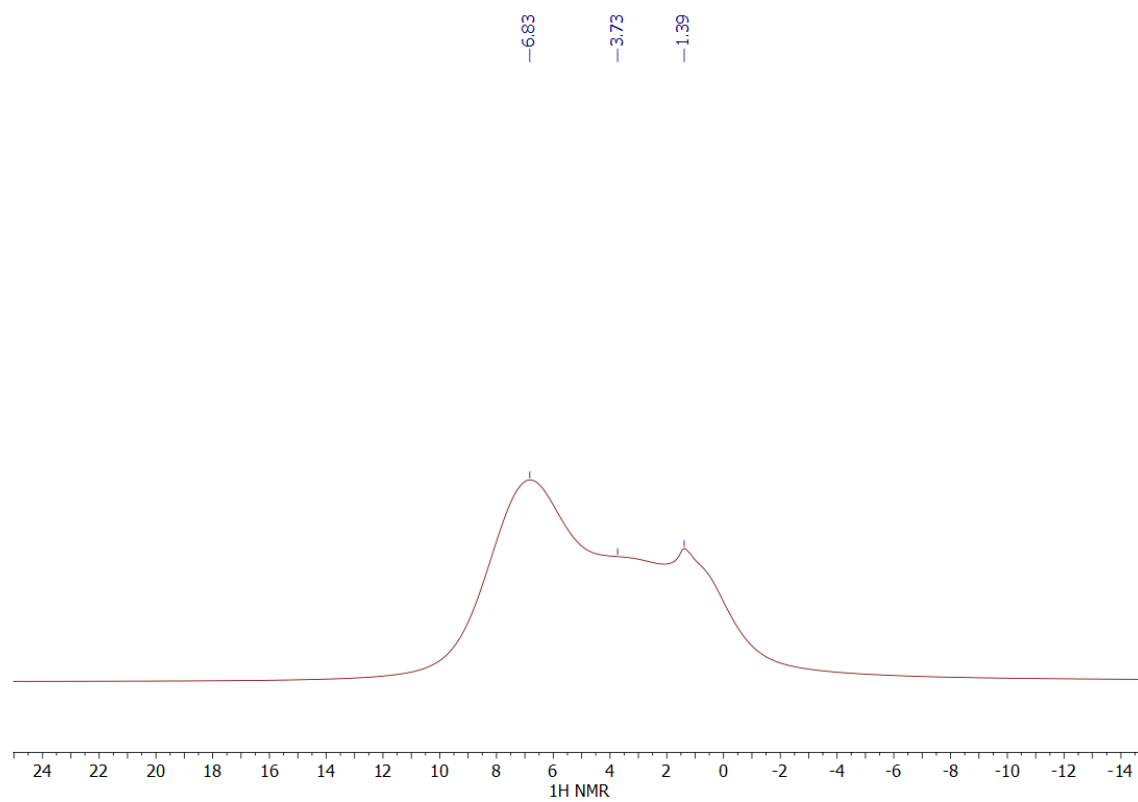


Figure S75. ¹H CP MAS NMR spectrum of PAAK-5.

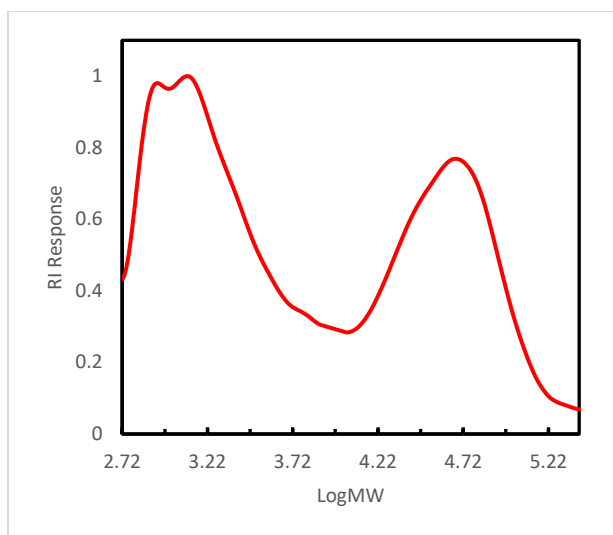
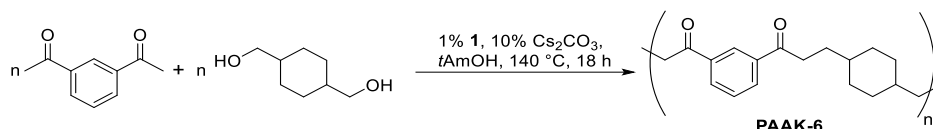


Figure S76. GPC chromatograph corresponding to **PAAK-5**.

PAAK-6



1,4-Cyclohexanedimethanol (72 mg, 0.5 mmol) and 1,3-diacetylbenzene (81 mg, 0.5 mmol) were used. The polymer was obtained in 99 % yield (134 mg) as a yellowish solid.

^{13}C CP MAS NMR (100.6 MHz): δ 199.9, 146.9, 137.5, 128.8, 74.4, 71.0, 47.9, 36.4, 34.0, 29.3.

IR (ATR-FTIR, cm^{-1}): ν 3485w (O-H), 2926s (C-H), 2851m (C-H), 1678s (C=O), 1597m, 1449m, 1269m, 1167s, 799m, 696s.

TGA: $T_d = 380\text{ }^\circ\text{C}$

GPC: monomodal: $\text{MW}(1) = 59.6\text{ kDa}$, $\text{PDI} = 1.6$.

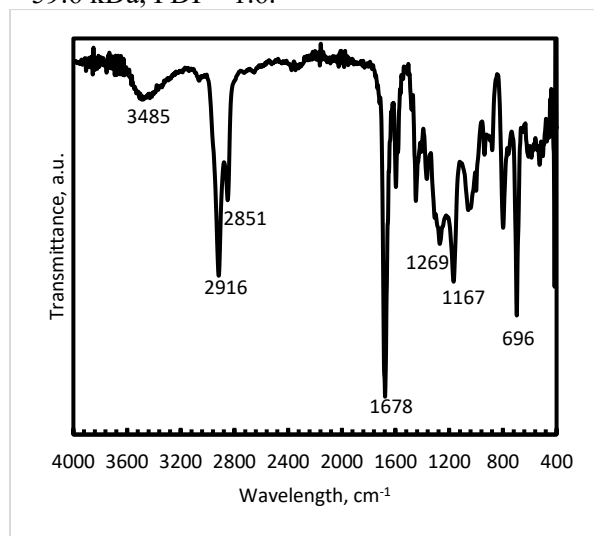


Figure S77. Infrared spectrum (ATR-FTIR) of polyketone **PAAK-6**.

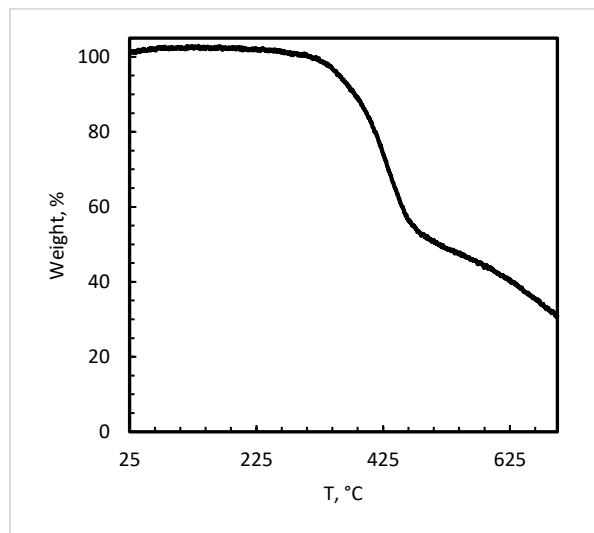


Figure S78. Mass loss as a function of temperature for polyketone **PAAK-6**.

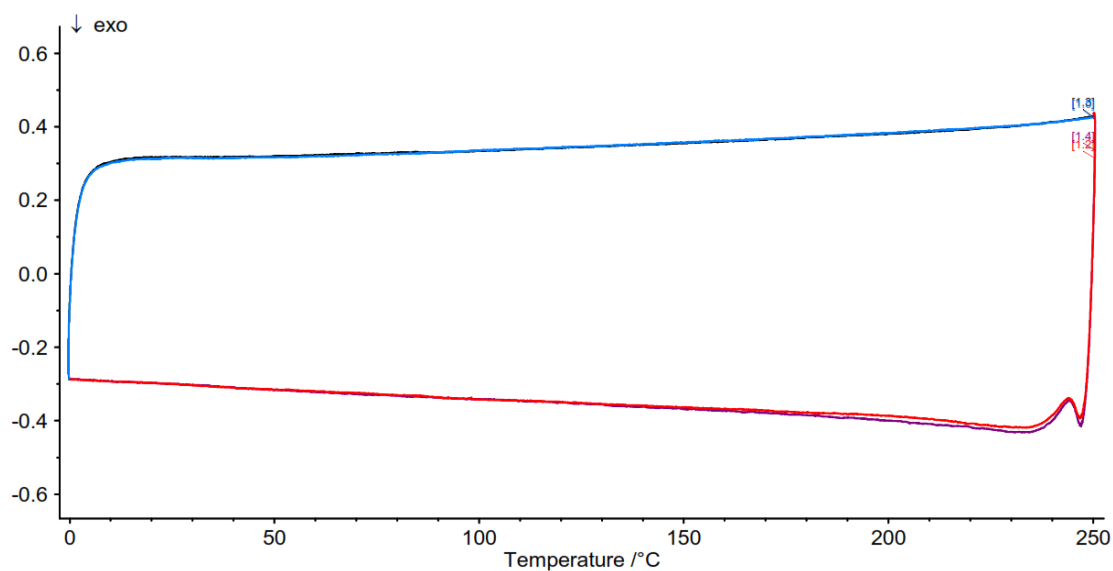


Figure S79. DSC trace corresponding to **PAAK-6**.

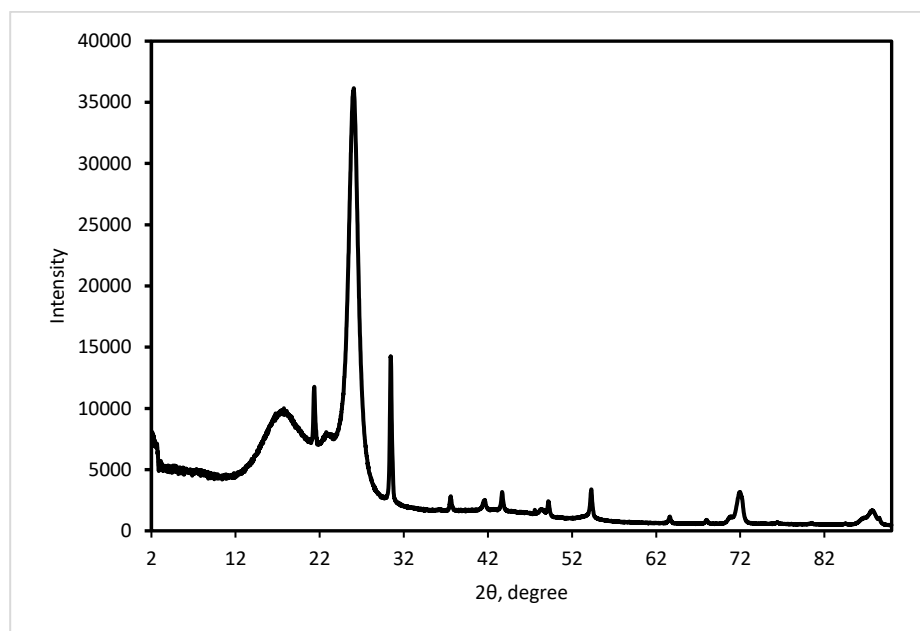


Figure S80. Experimental powder XRD patterns of **PAAK-6**. Crystalline peaks were indexed in the small-volume unit cell which remains unidentified. Tall thin amorphous halo is from polyester films used for measurements of small amount of sample.

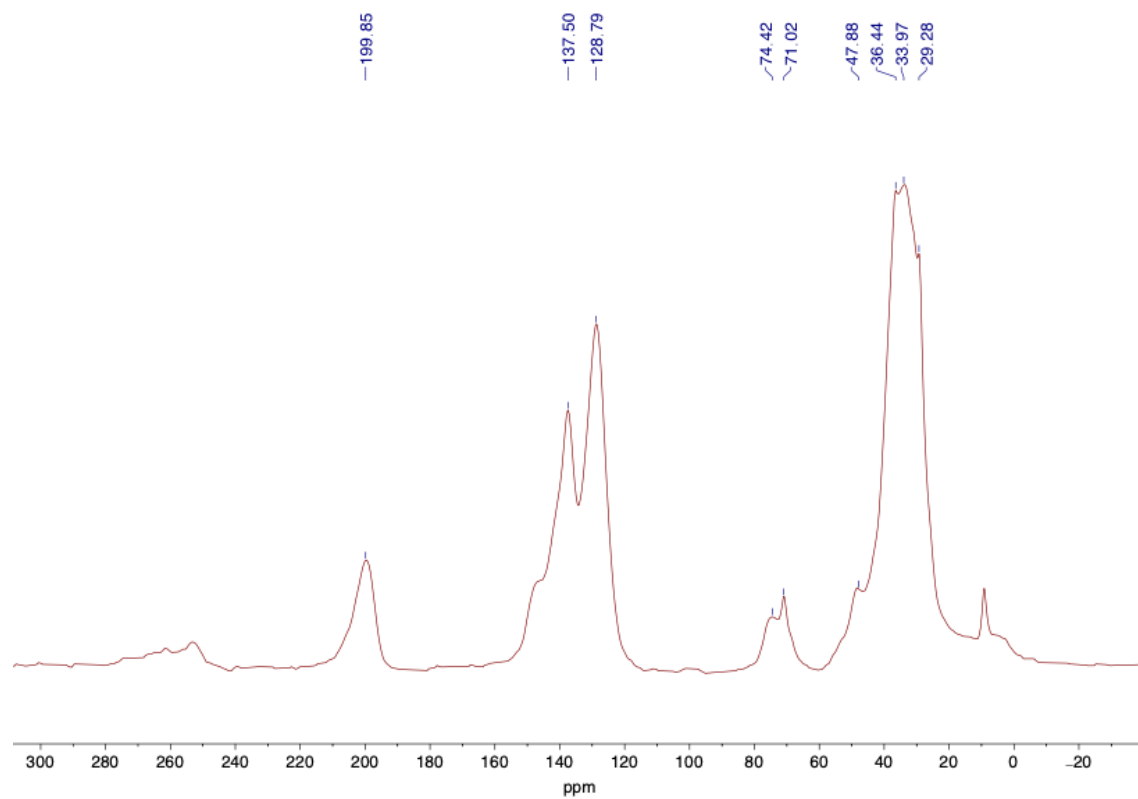


Figure S81. ^{13}C CP MAS NMR spectrum of **PAAK-6**.

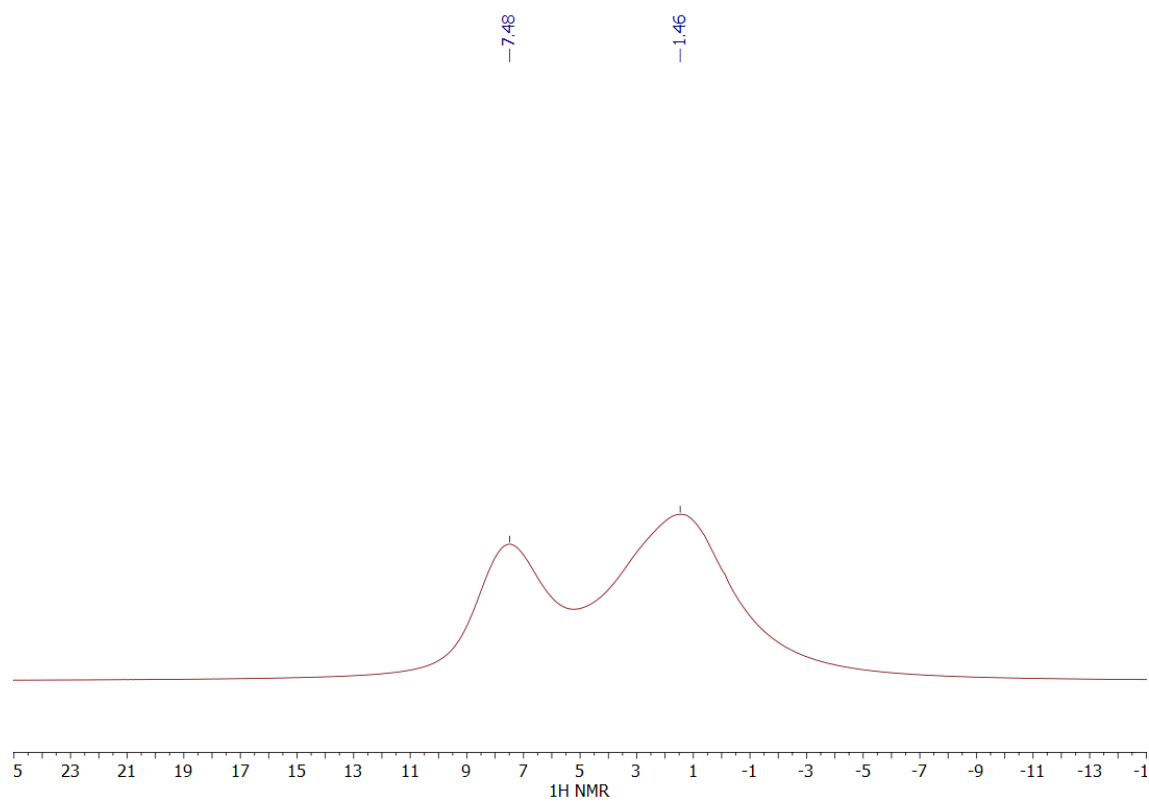


Figure S82. ^1H CP MAS NMR spectrum of **PAAK-6**.

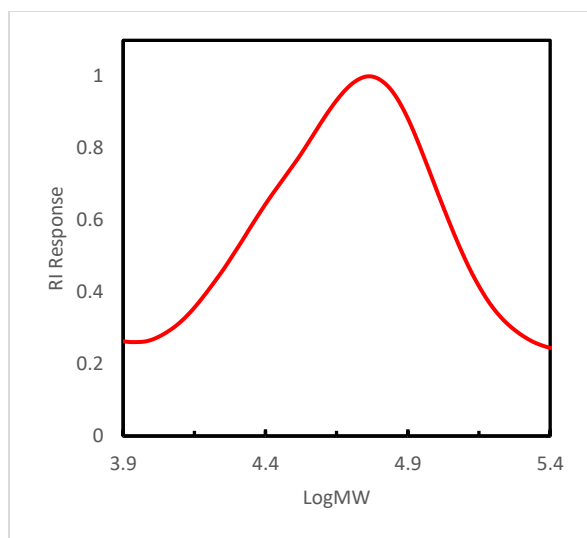
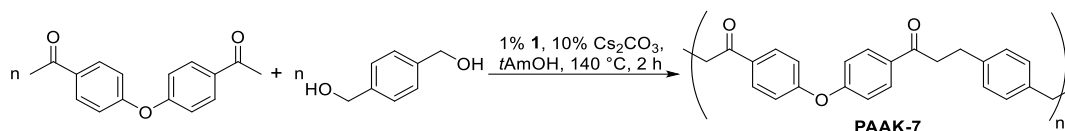


Figure S83. GPC chromatograph corresponding to **PAAK-6**.

PAAK-7



^{13}C CP MAS NMR (100.6 MHz): δ 198.1, 160.1, 140.3, 130.8, 121.0, 75.3, 64.4, 42.7.

IR (ATR-FTIR, cm^{-1}): ν 3466w (O-H), 3055w, 2922w (C-H), 1672s (C=O), 1587s (C=C), 1497s, 1411w, 1233s (C-O), 1163s, 983m, 833s, 554m.

TGA: $T_d = 362\text{ }^\circ\text{C}$

GPC: bimodal: $\text{MW}(1) = 2.4\text{ kDa}$, $\text{PDI} = 1.4$, $\text{MW}(2) = 58.5\text{ kDa}$, $\text{PDI} = 1.8$.

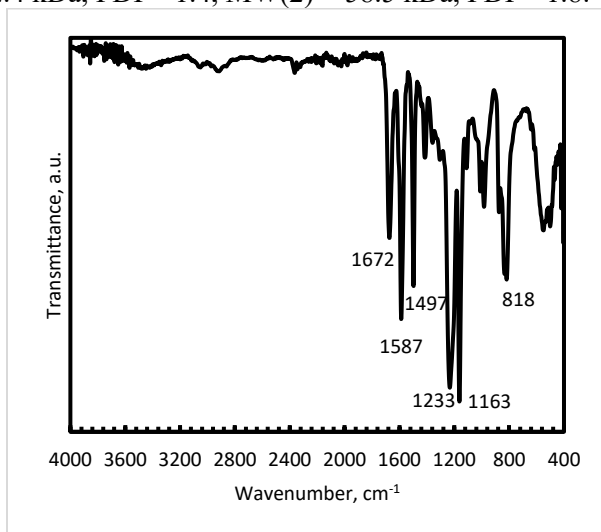


Figure S84. Infrared spectrum (ATR-FTIR) of polyketone PAAK-7.

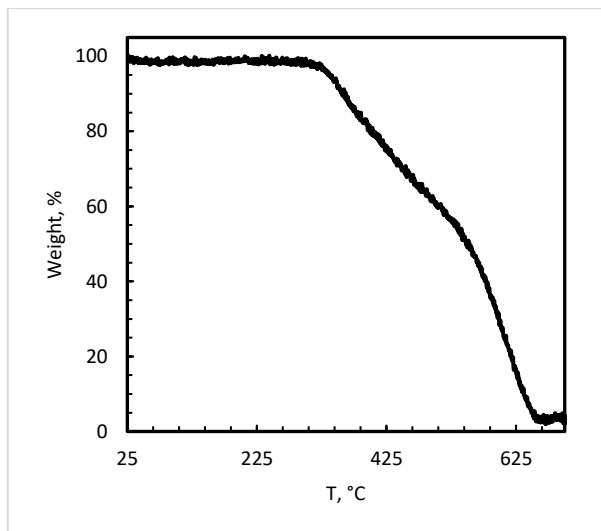


Figure S85. Mass loss as a function of temperature for polyketone PAAK-7.

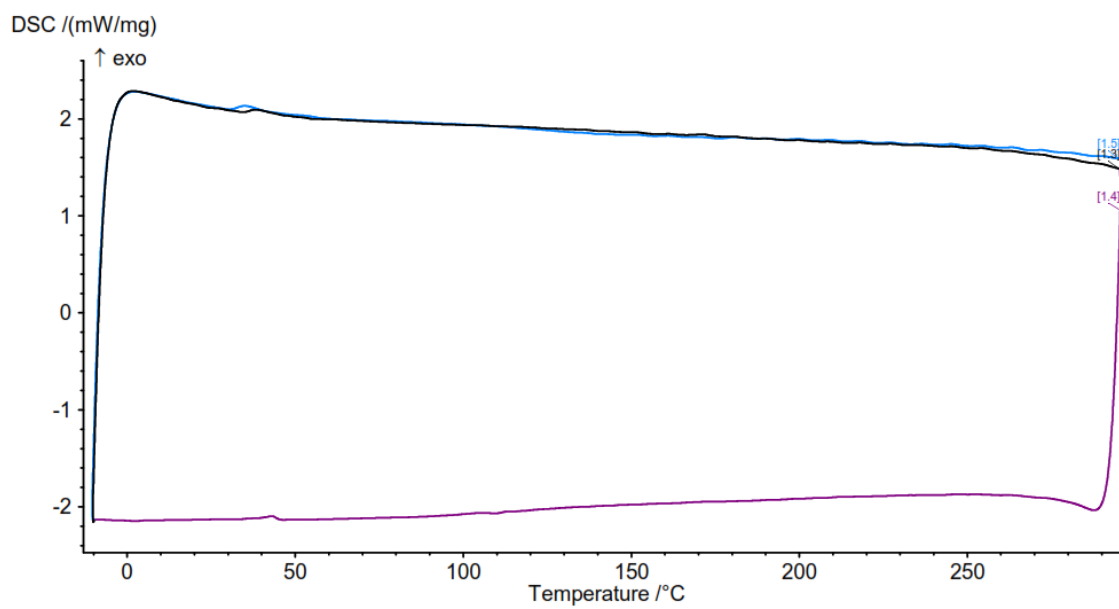


Figure S86. DSC trace corresponding to **PAAK-7**.

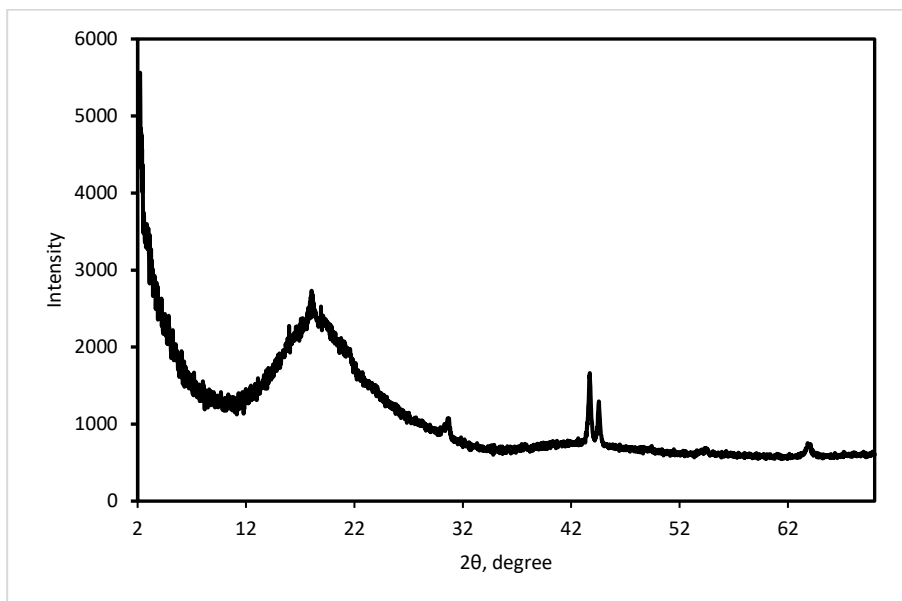


Figure S87. Experimental powder XRD patterns of **PAAK-7**. Unidentifiable crystalline phase presents. Peaks at high angles are from crystalline Teflon substrate.

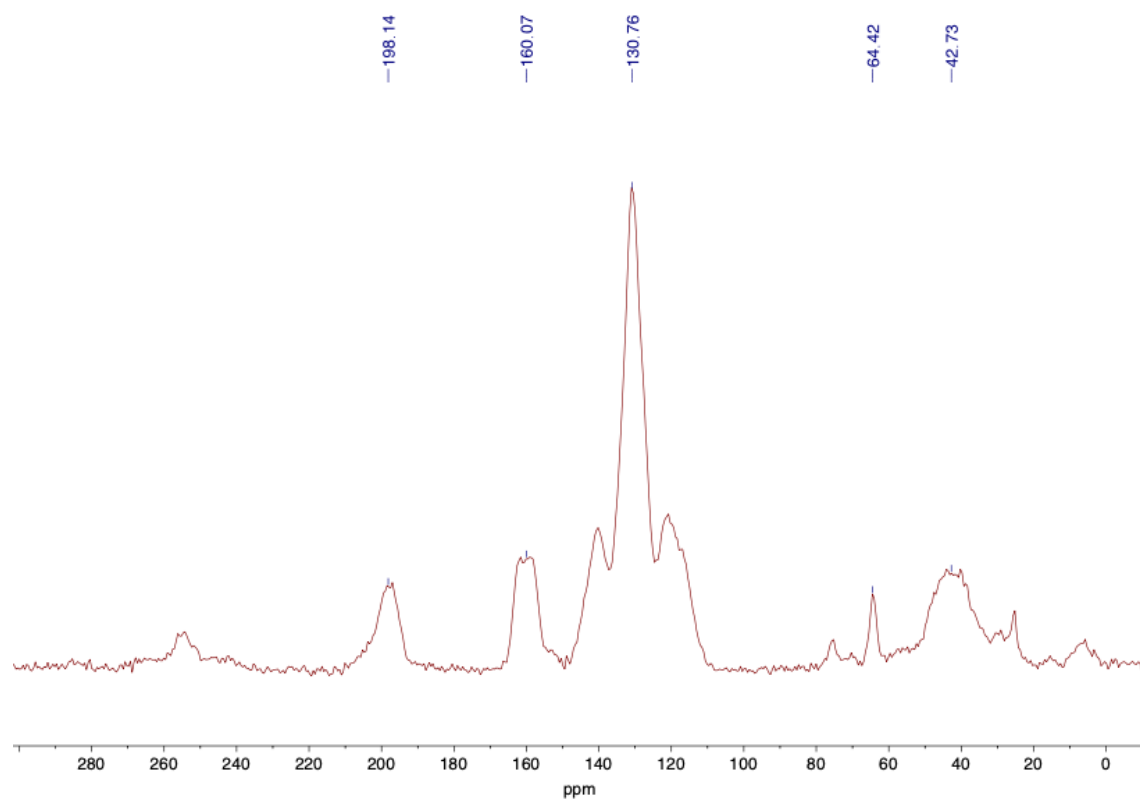


Figure S88. ^{13}C CP MAS NMR spectrum of **PAAK-7**.

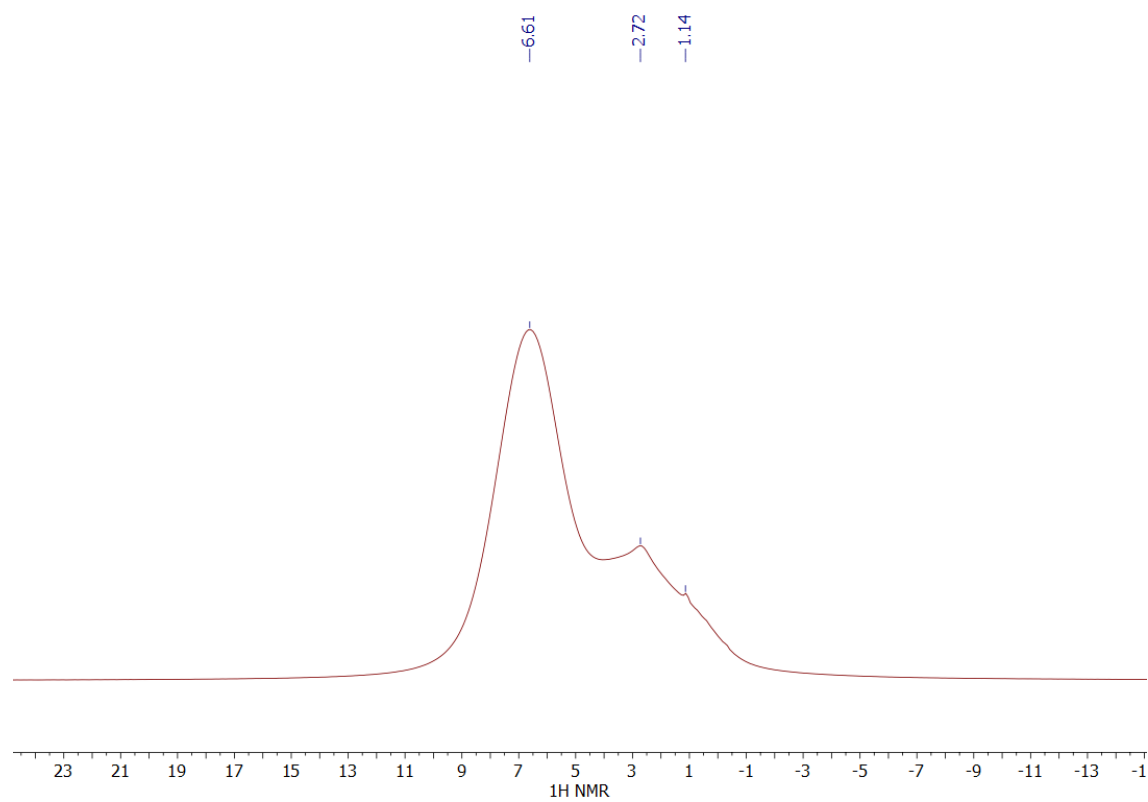


Figure S89. ^1H CP MAS NMR spectrum of **PAAK-7**.

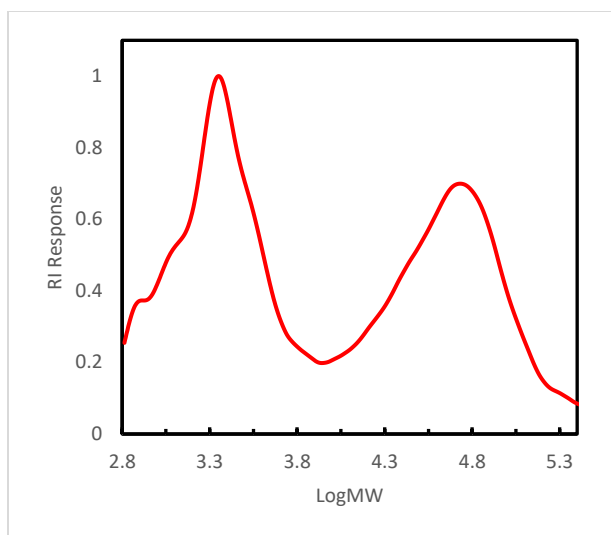
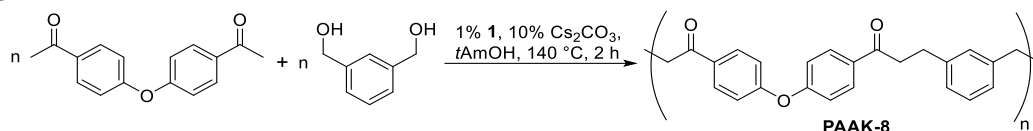


Figure S90. GPC chromatograph corresponding to **PAAK-7**.

PAAK-8



1,3-Dimethanolbenzene (69 mg, 0.5 mmol) and 4-acetylphenylether (127 mg, 0.5 mmol) were used. The polymer was obtained in 79% yield (140 mg) as a white solid.

^{13}C CP MAS NMR (100.6 MHz): δ 198.0, 162.1, 158.9, 142.2, 131.0, 121.6, 75.3, 64.5, 41.7.

IR (ATR-FTIR, cm^{-1}): ν 3066w (C-H), 2904w (C-H) 1674m (C=O), 1587s (C=C), 1499s, 1410w, 1234s, 1163s, 984w, 835m, 704w, 501w.

TGA: $T_d = 365^\circ\text{C}$

GPC: bimodal: $\text{MW}(1) = 1.6$ kDa, $\text{PDI} = 1.3$, $\text{MW}(2) = 53.9$ kDa, $\text{PDI} = 1.4$.

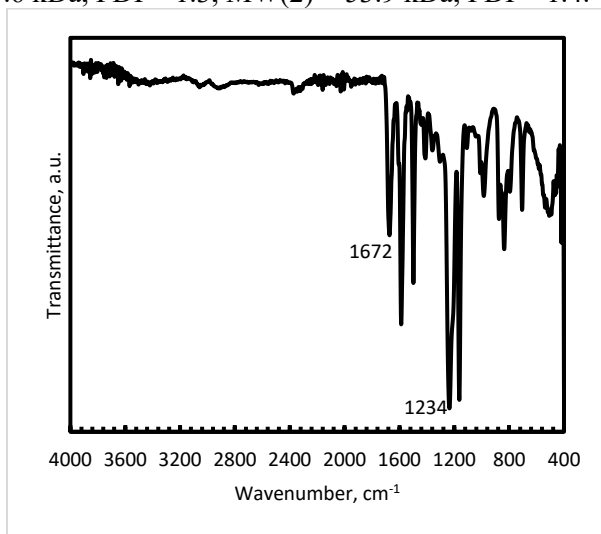


Figure S91. Infrared spectrum (ATR-FTIR) of polyketone PAAK-8.

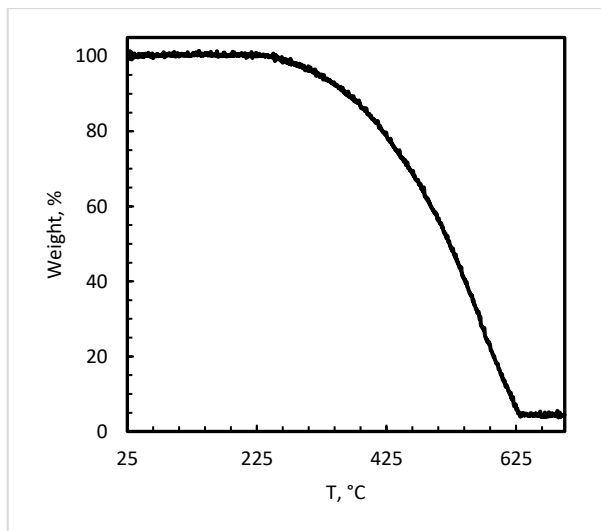


Figure S92. Mass loss as a function of temperature for polyketone PAAK-8.

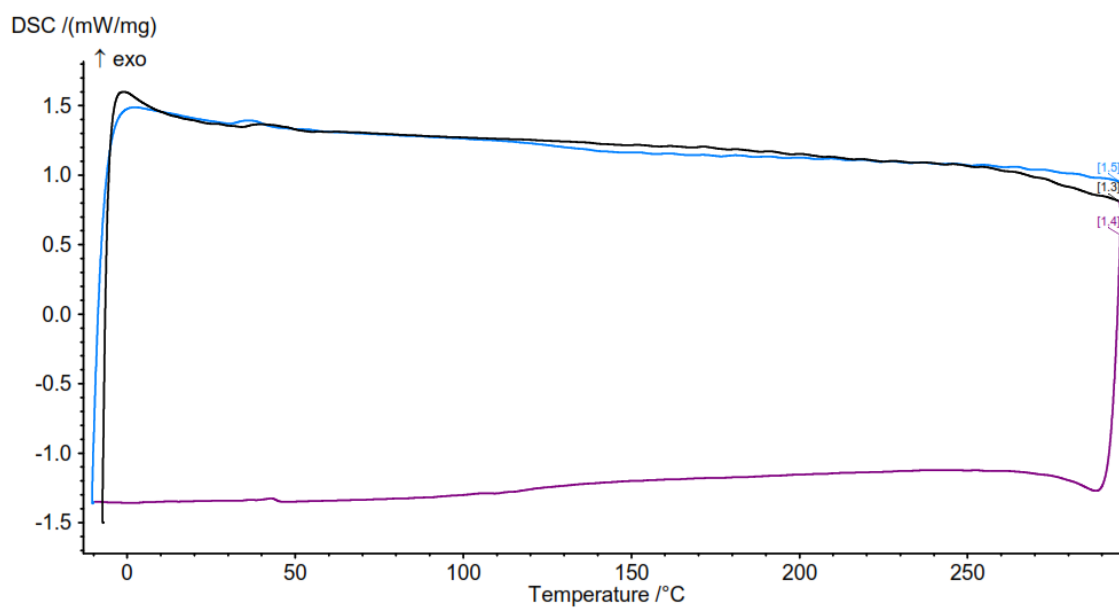


Figure S93. DSC trace corresponding to **PAAK-8**.

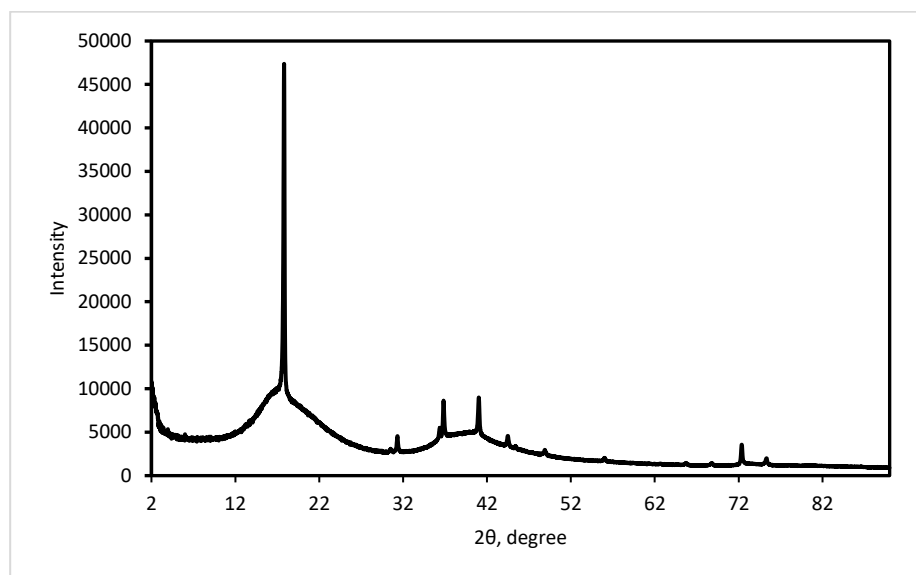


Figure S94. Experimental powder XRD patterns of **PAAK-8**. Unidentifiable crystalline phase present.

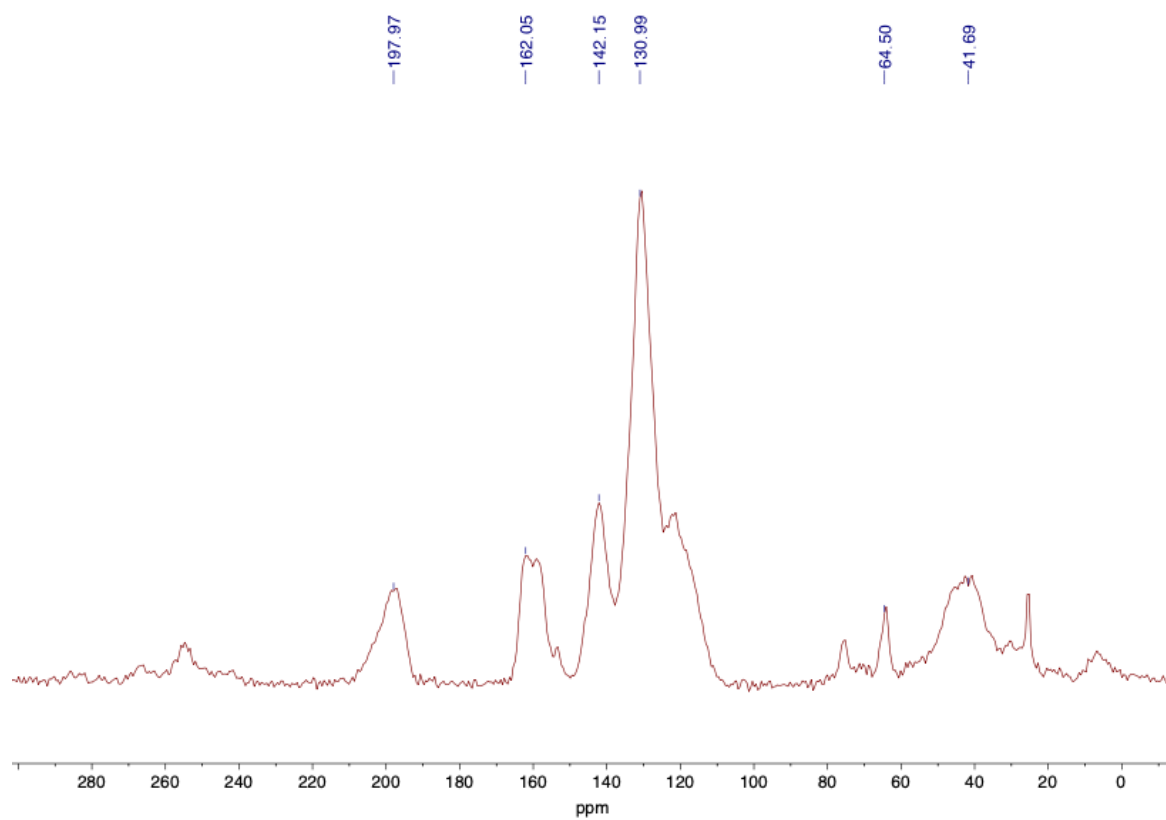


Figure S95. ^{13}C CP MAS NMR spectrum of **PAAK-8**.

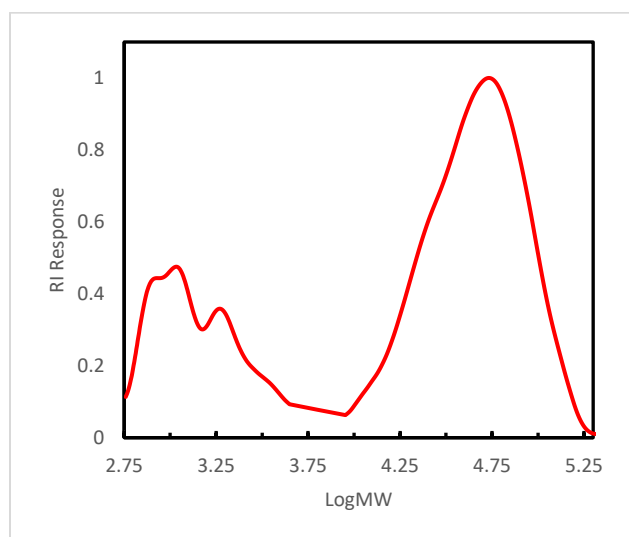
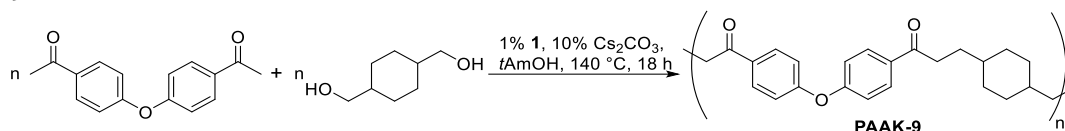


Figure S96. GPC chromatograph corresponding to **PAAK-8**.

PAAK-9



^{13}C CP MAS NMR (100.6 MHz): δ 198.6, 161.7, 159.1, 153.9, 131.6, 120.5, 76.4, 68.4, 48.4, 36.5, 32.3, 30.8.

IR (ATR-FTIR, cm^{-1}): ν 2916w (C-H), 2851w (C-H), 1674s (C=O), 1589s (C=C), 1499s, 1412w, 1236s (C-O), 1163s, 1011w, 835m, 567w.

TGA: $T_d = 383\text{ }^\circ\text{C}$

GPC: monomodal: MW = 53.4 kDa, PDI = 1.7.

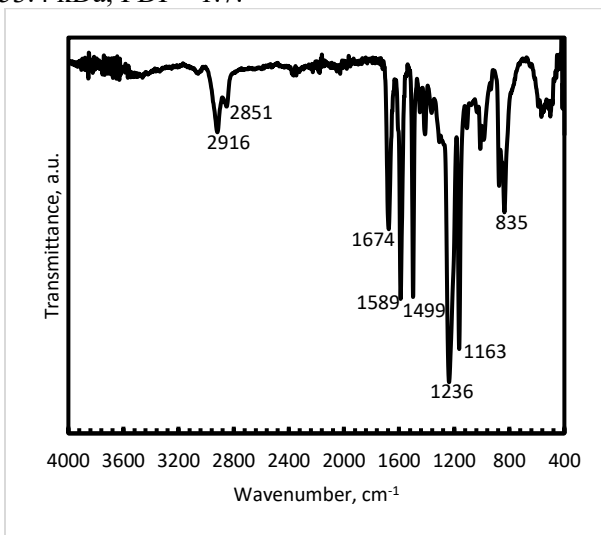


Figure S97. Infrared spectrum (ATR-FTIR) of polyketone **PAAK-9**.

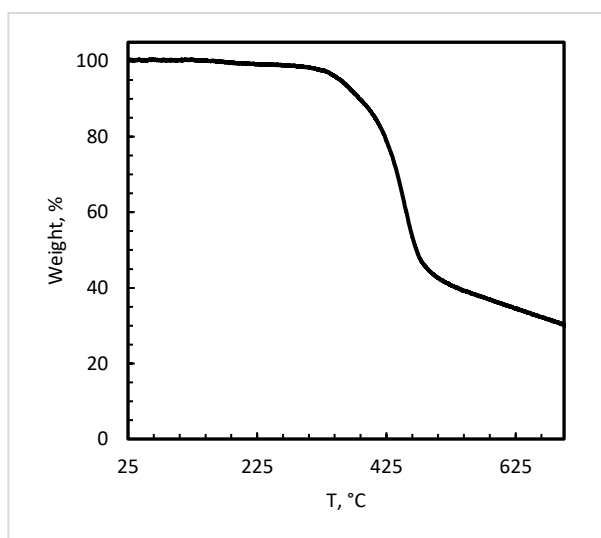


Figure S98. Mass loss as a function of temperature for polyketone **PAAK-9**.

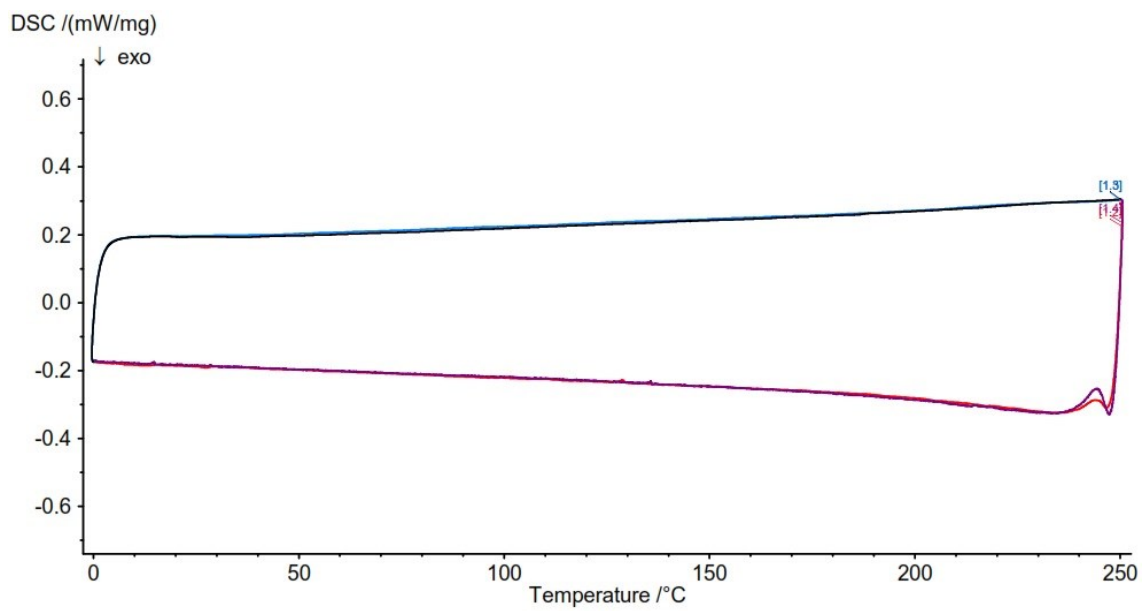


Figure S99. DSC trace corresponding to **PAAK-9** .

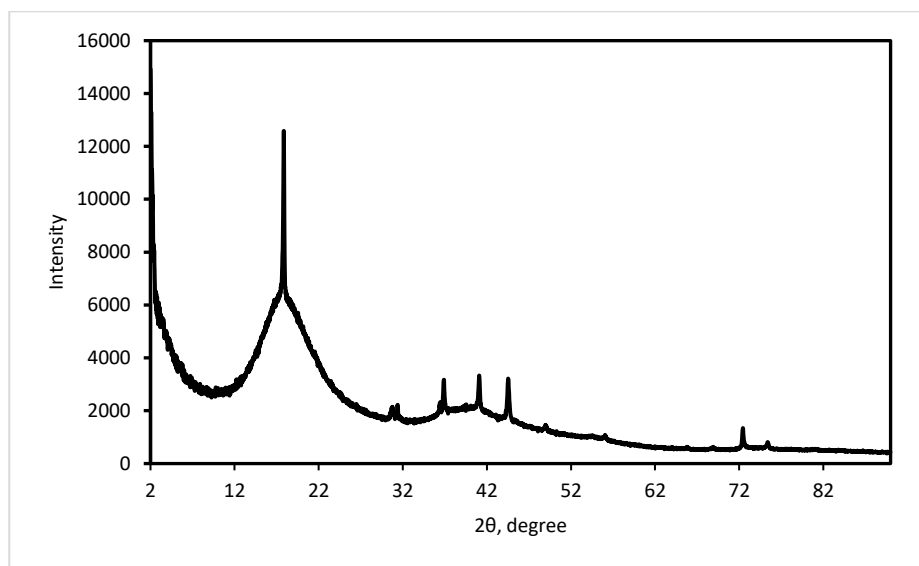


Figure S100. Experimental powder XRD patterns of **PAAK-9**. Unidentifiable crystalline phase present.

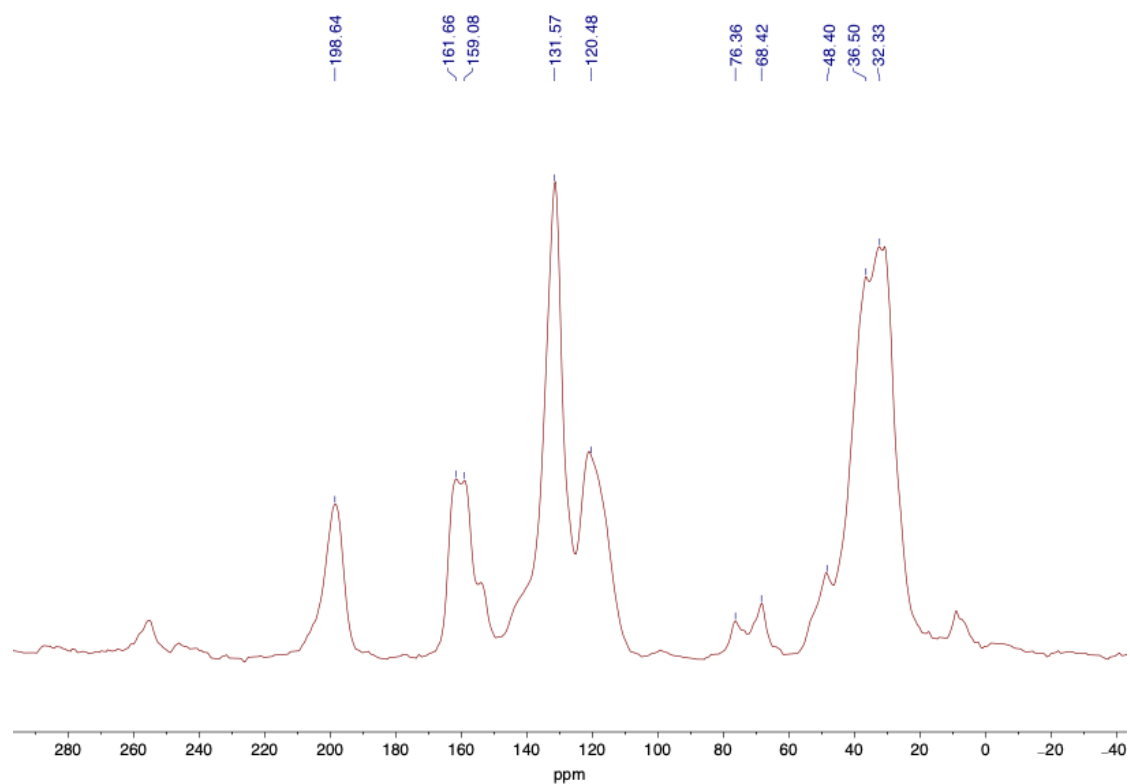


Figure S101. ^{13}C CP MAS NMR spectrum of **PAAK-9**.

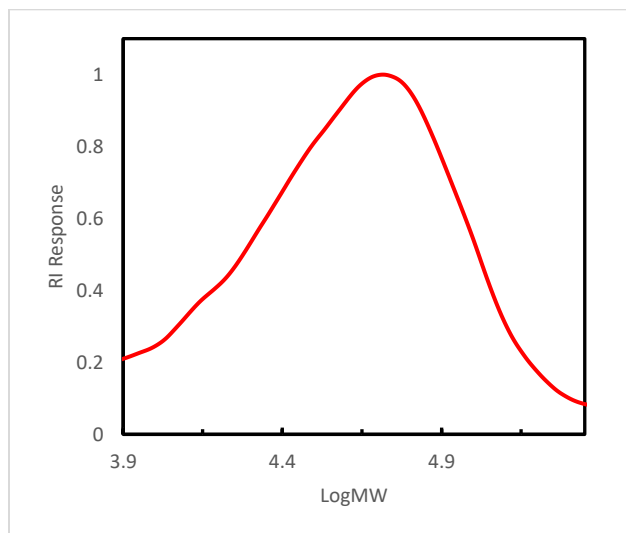
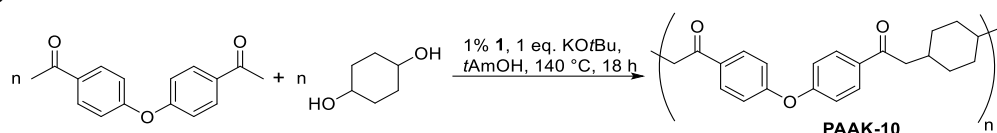


Figure S102. GPC chromatograph corresponding to **PAAK-9**.

PAAK-10



Cyclohexane-1,4-diol (58 mg, 0.5 mmol) and 4-acetylphenylether (127 mg, 0.5 mmol) were used. The polymer was obtained in 57% yield (95 mg) as a yellow solid.

^{13}C CP MAS NMR (100.6 MHz): δ 197.9, 157.6, 154.7, 129.8, 121.7, 71.5, 35.6, 28.7.

IR (ATR-FTIR, cm^{-1}): ν 3346w (O-H), 2918w (C-H), 1676w (C=O), 1591m (C=C), 1497s, 1231s (C-O), 1161s, 1013m, 826m, 509m.

TGA: $T_d = 363\text{ }^\circ\text{C}$

GPC: broad dispersity, outside calibration curve: MW = 621.6 kDa, PDI = 108.6.

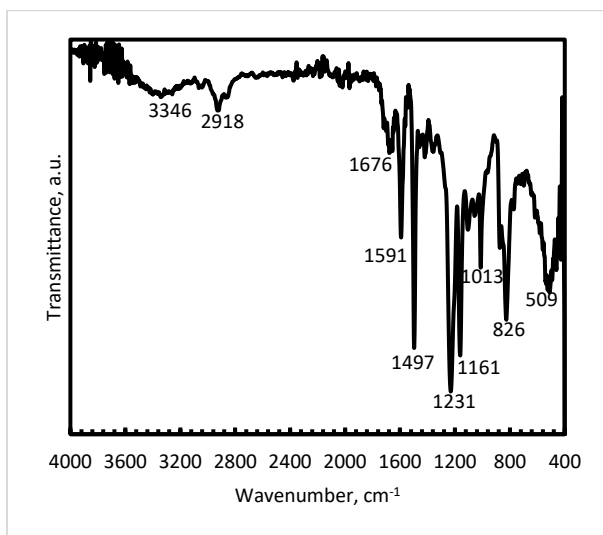


Figure S103. Infrared spectrum (ATR-FTIR) of polyketone **PAAK-10**.

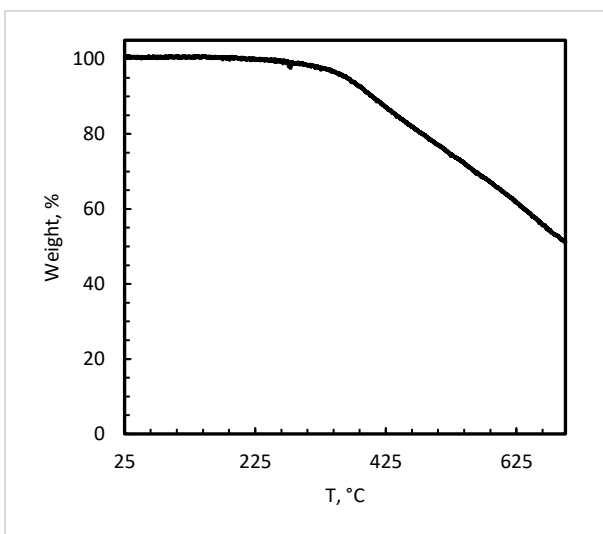


Figure S104. Mass loss as a function of temperature for polyketone **PAAK-10**.

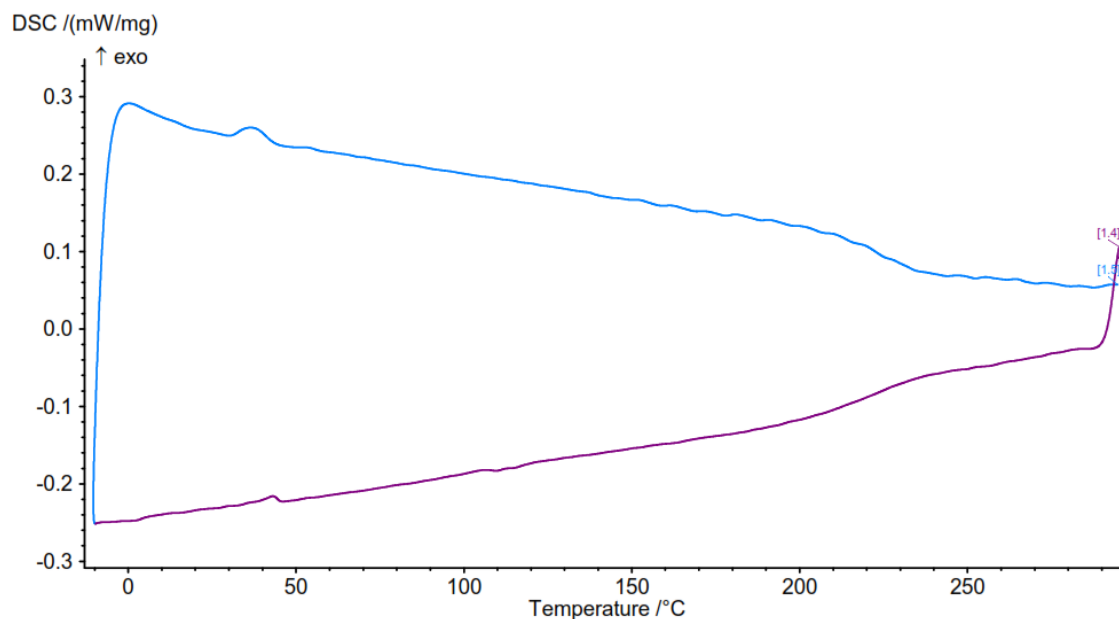


Figure S105. DSC trace corresponding to **PAAK-10**.

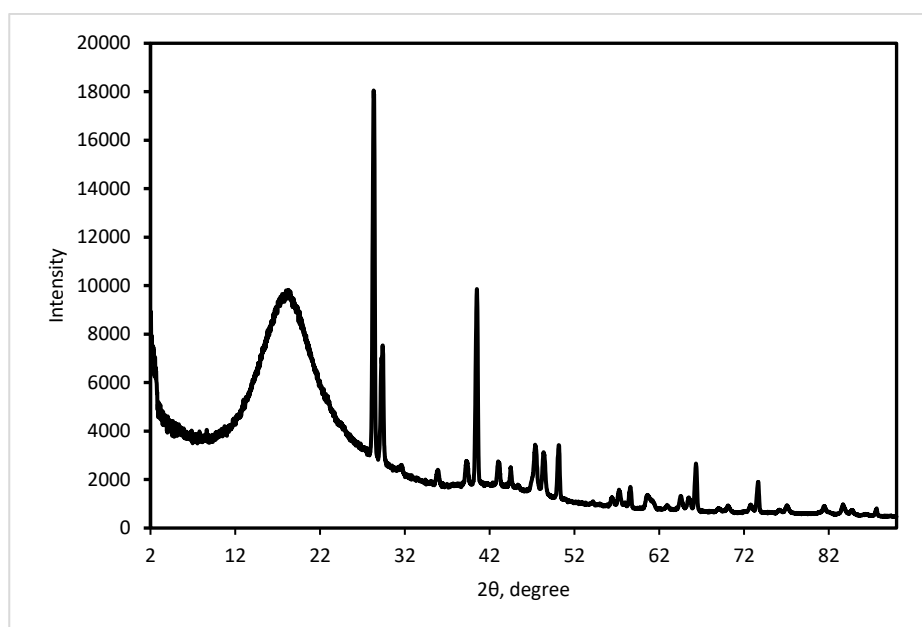


Figure S106. Experimental powder XRD patterns of **PAAK-10**. Crystalline peaks were indexed in the small-volume unit cell which remains unidentified.

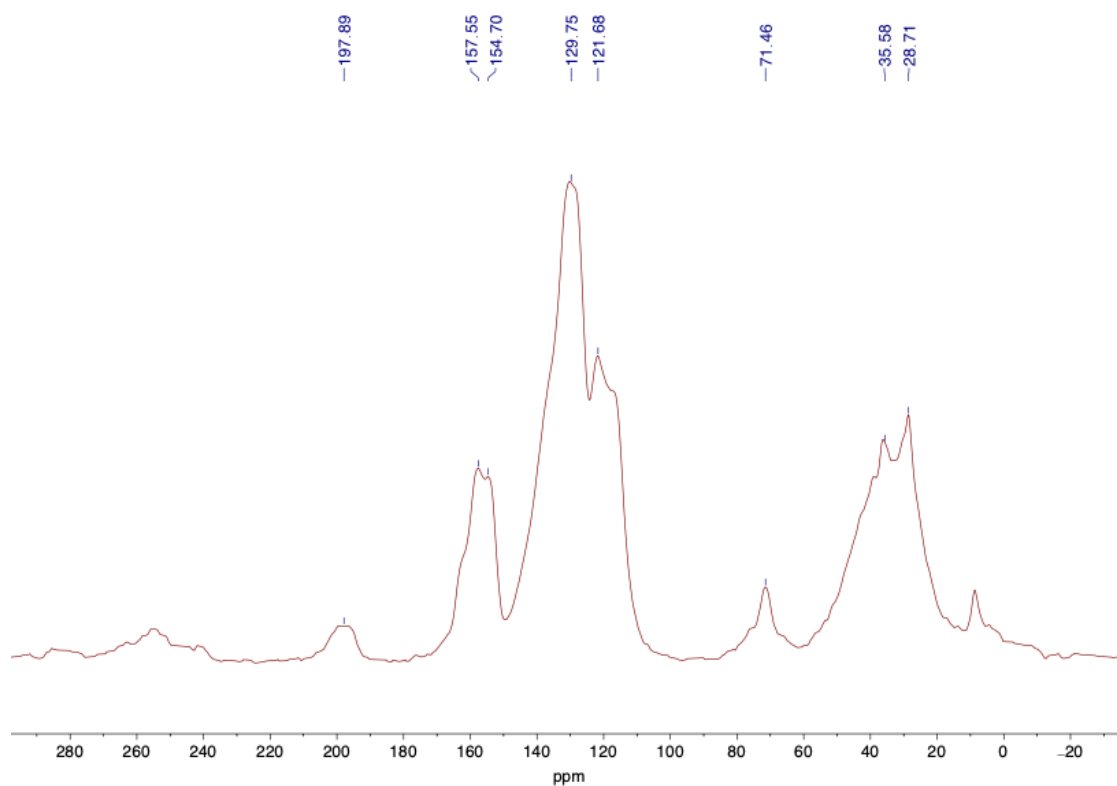


Figure S107. ^{13}C CP MAS NMR spectrum of **PAAK-10**.

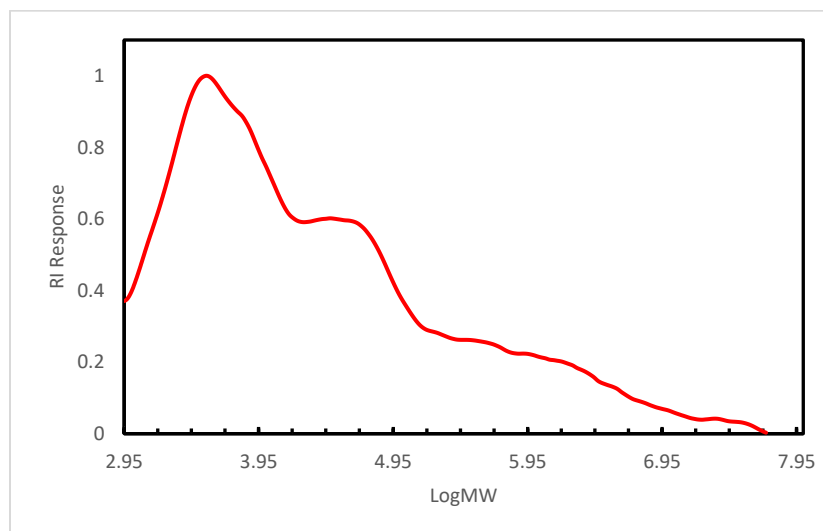
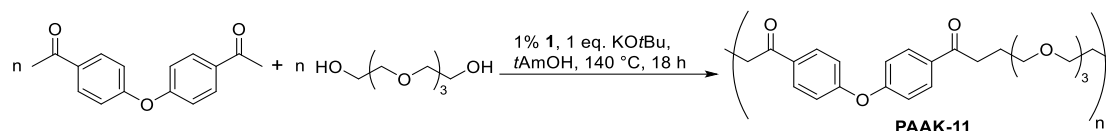


Figure S108. GPC chromatograph corresponding to **PAAK-10**.

PAAK-11



Tetraethylene glycol (115 mg, 0.6 mmol) and 4-acetylphenylether (127 mg, 0.5 mmol) were used. The polymer was obtained in 64 % yield (131 mg) as an orange solid.

^{13}C CP MAS NMR (100.6 MHz): δ 196.8, 162.8, 157.9, 130.8, 116.0, 70.3, 67.8, 39.4.

IR (ATR-FTIR, cm^{-1}): ν 2922w (C-H), 2868w (C-H), 1655w (C=O), 1595s, 1501s, 1233s (C-O), 1096s, 827s, 507m.

TGA: $T_d = 375\text{ }^\circ\text{C}$

GPC: broad dispersity, outside calibration curve: MW = 899.1 kDa, PDI = 148.8.

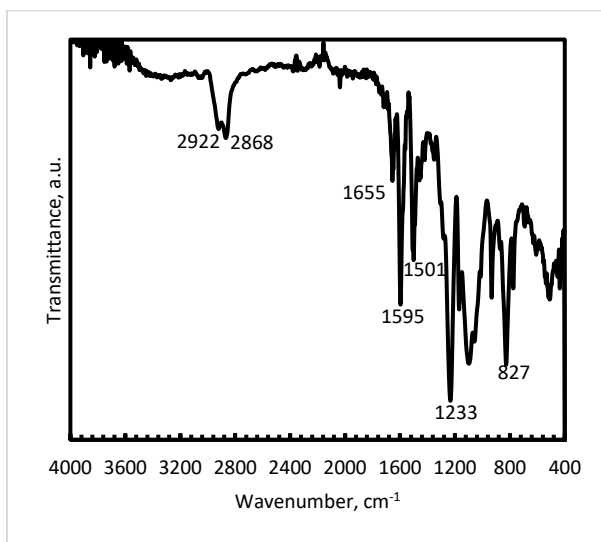


Figure S109. Infrared spectrum (ATR-FTIR) of polyketone PAAK-11.

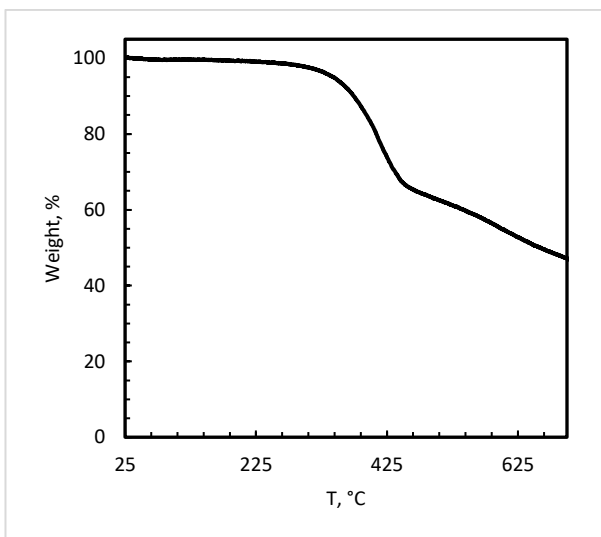


Figure S110. Mass loss as a function of temperature for polyketone PAAK-11.

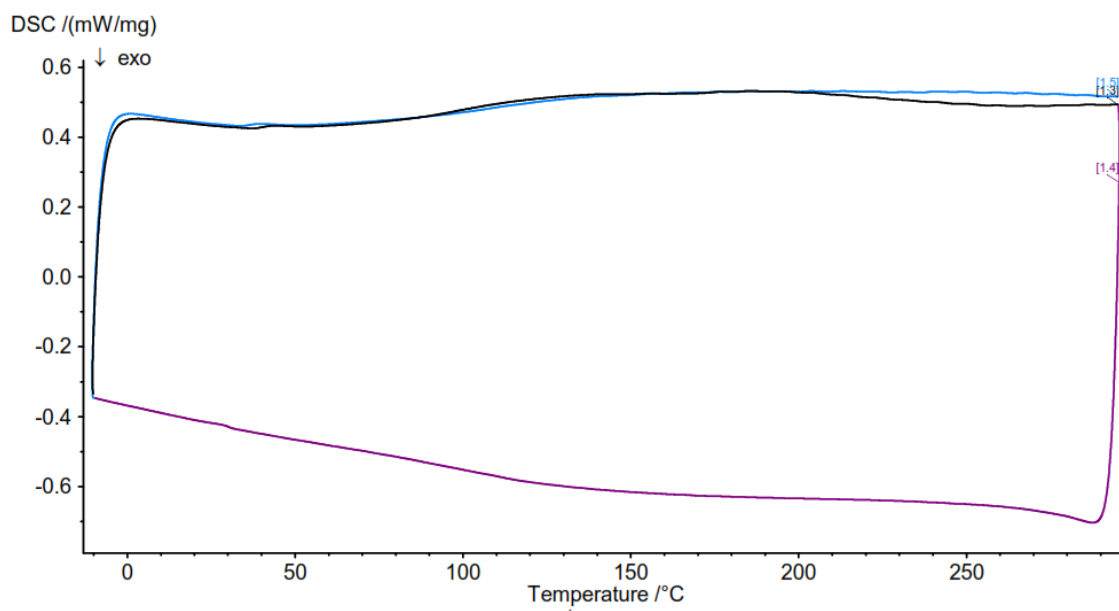


Figure S111. DSC trace corresponding to **PAAK-11**.

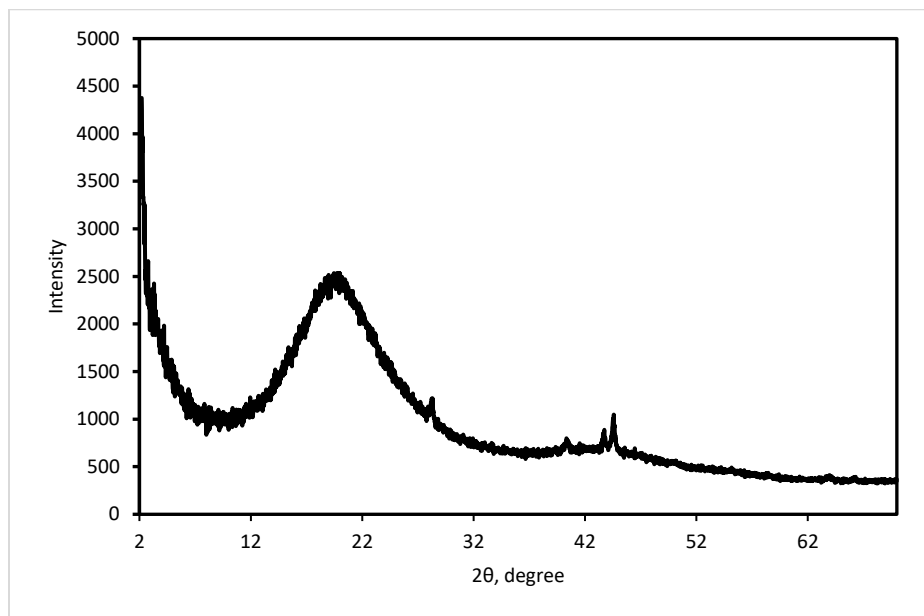


Figure S112. Experimental powder XRD patterns of **PAAK-11**. Some small crystalline peaks are from Teflon substrate, other were indexed in the small-volume unit cell which remains unidentified.

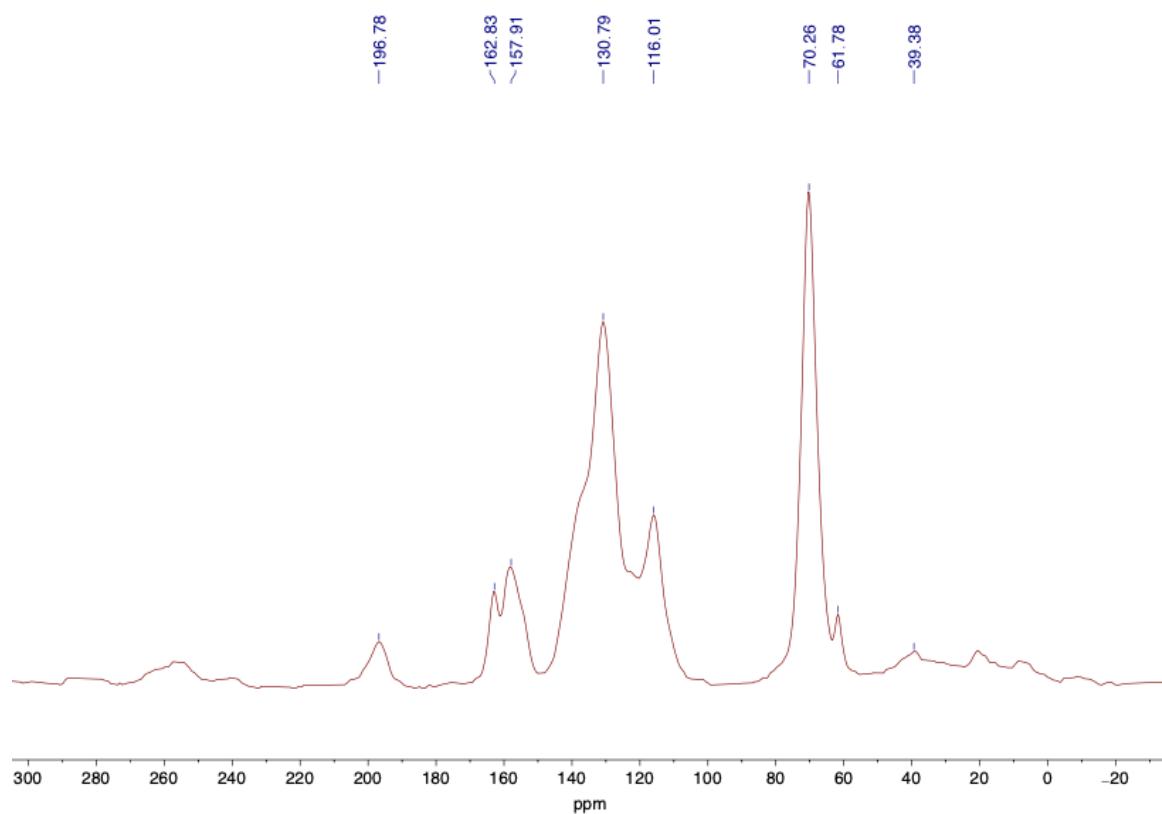


Figure S113. ^{13}C CP MAS NMR spectrum of **PAAK-11** coupling product.

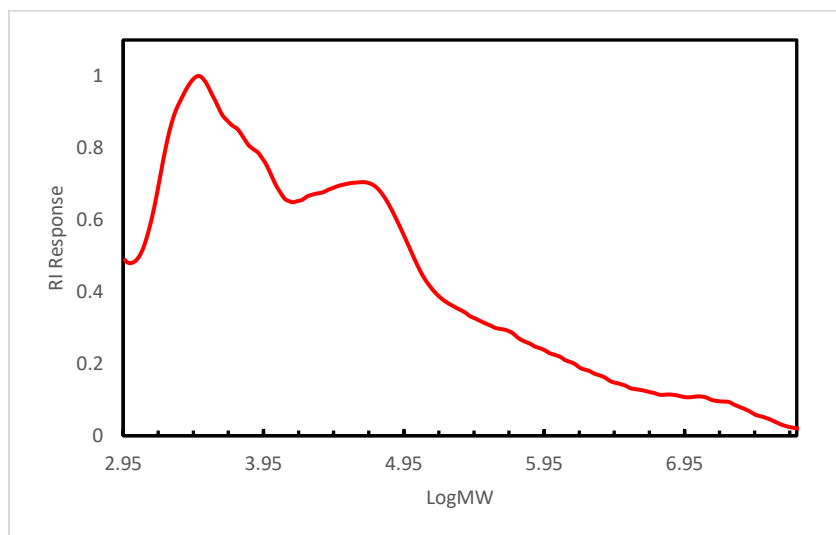
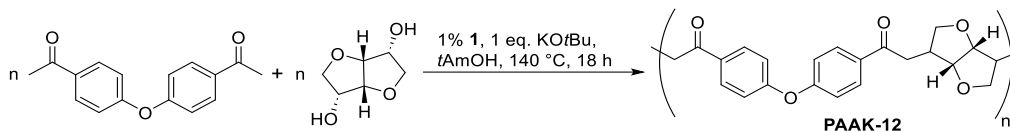


Figure S114. GPC chromatograph corresponding to **PAAK-11**.

PAAK-12



D-isosorbide (73 mg, 0.5 mmol) and 4-acetylphenylether (127 mg, 0.5 mmol) were used. The polymer was obtained in 52% yield (94 mg) as an orange solid.

^{13}C CP MAS NMR (100.6 MHz): δ 196.4, 158.1, 130.3, 120.5, 75.8, 39.9, 27.0.

IR (ATR-FTIR, cm^{-1}): ν 2963w (C-H), 1676w (C=O), 1591m (C=C), 1497s, 1231s (C-O), 1161s, 1013m, 827m, 527m.

TGA: $T_d = 381$ °C

GPC: bimodal: MW(1) = 3.0 kDa, PDI = 1.3, MW(2) = 53.6 kDa, PDI = 1.7.

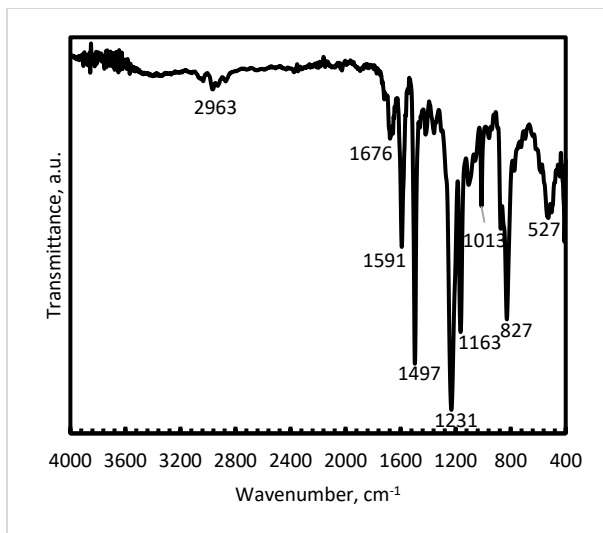


Figure S115. Infrared spectrum (ATR-FTIR) of polyketone PAAK-12.

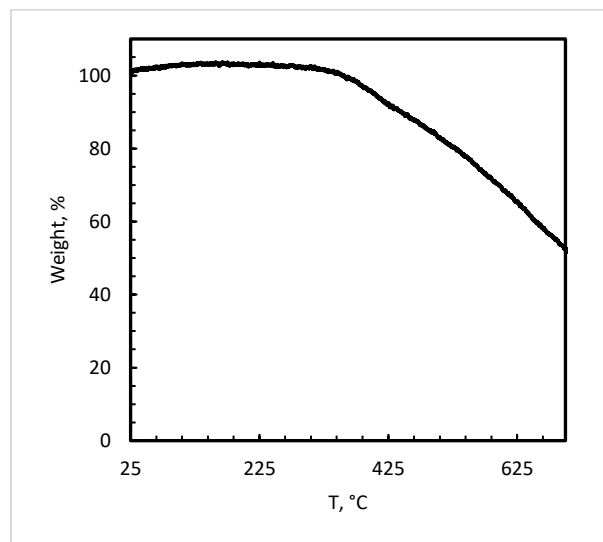


Figure S116. Mass loss as a function of temperature for polyketone PAAK-12.

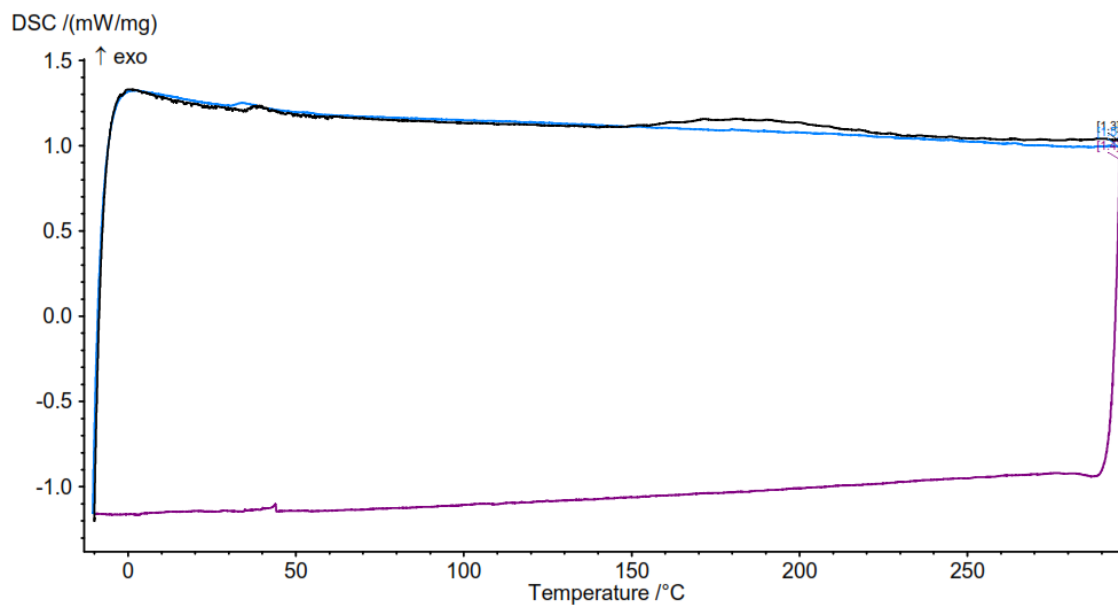


Figure S117. DSC trace corresponding to **PAAK-12**.

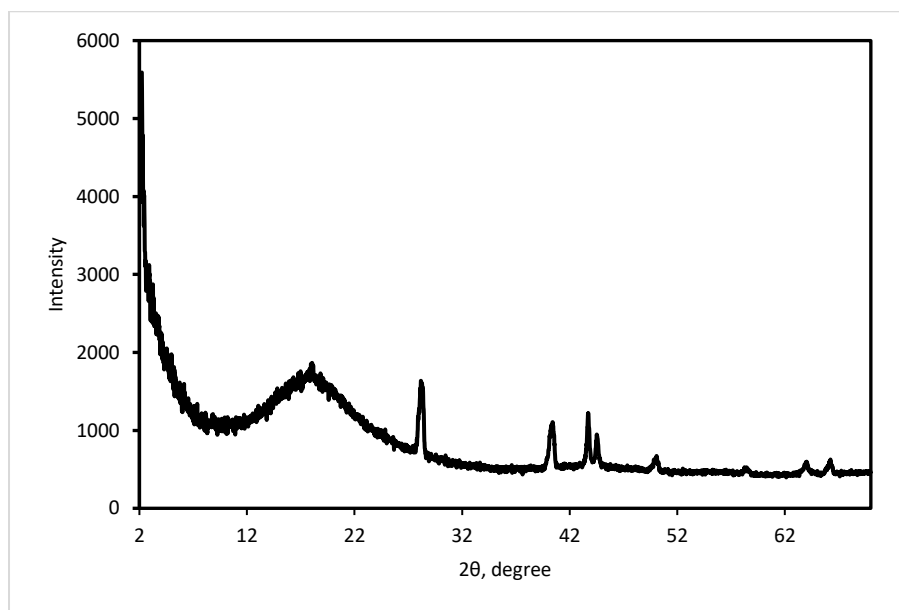


Figure S118. Experimental powder XRD patterns of **PAAK-12**. Crystalline peaks are either from Teflon substrate or were indexed in the small-volume unit cell which remains unidentified.

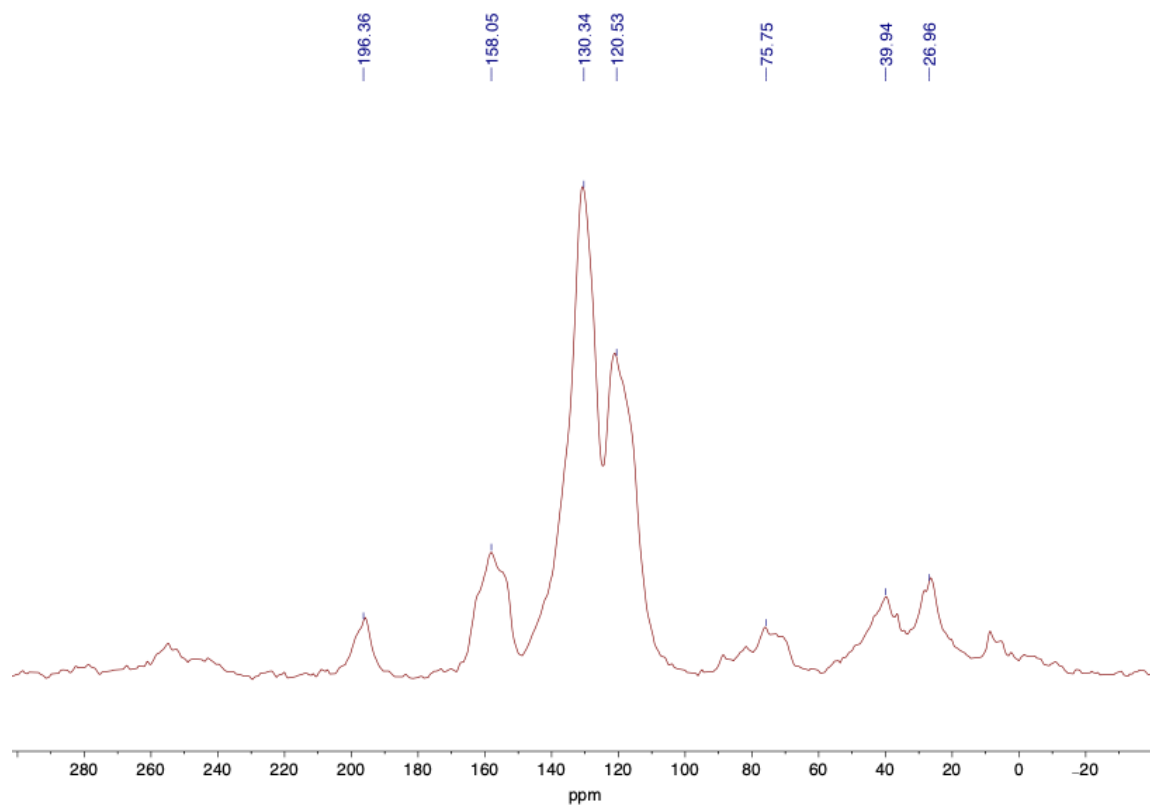


Figure S119. ^{13}C CP MAS NMR spectrum of **PAAK-12**.

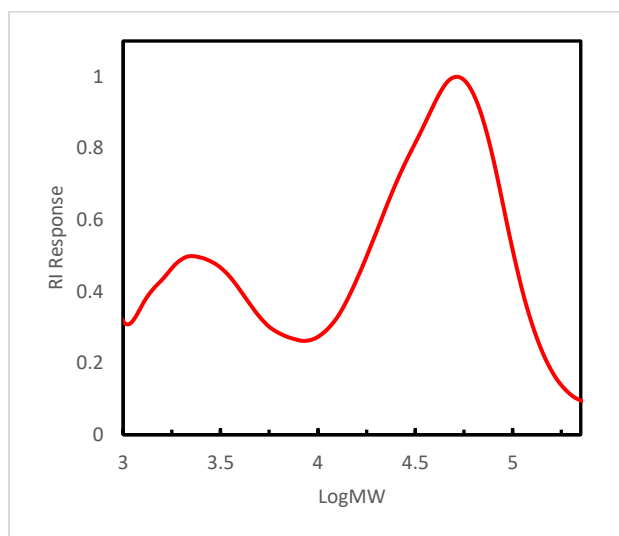


Figure S120. GPC chromatograph corresponding to **PAAK-12**.

1.6 Syntheses of polychalcones from diketones and dialdehydes

A 100 mL ampoule equipped with a J-Young's valve was charged with Cs_2CO_3 (16.5 mg, 0.05 mmol, 10 mol%), dialdehyde (0.5 mmol) and diketone (0.5 mmol). The flask was sealed under an argon atmosphere and *tert*-amyl alcohol (5 mL) was added before heating to 140 °C for 18 h with stirring. After this period, the reaction vessel was allowed to cool to room temperature. To the resulting mixture, 5 mL of water was added and the flask was heated at 90 °C for 1 h. The precipitate was filtered and dried under reduced pressure at 120 °C.

PCH-1



Terephthalaldehyde (68 mg, 0.5 mmol) and 1,4-diacetylbenzene (81 mg, 0.5 mmol) were used. The polymer was obtained with 93% yield (121 mg) as a yellow solid.

IR (ATR-FTIR, cm^{-1}): ν 3472w (C-H), 3036w, 2834w, 1657m (C=O), 1599s (C=C), 1566m, 1501w, 1402w, 1327m, 1211s, 980m, 810s.

TGA: Td = 365 °C

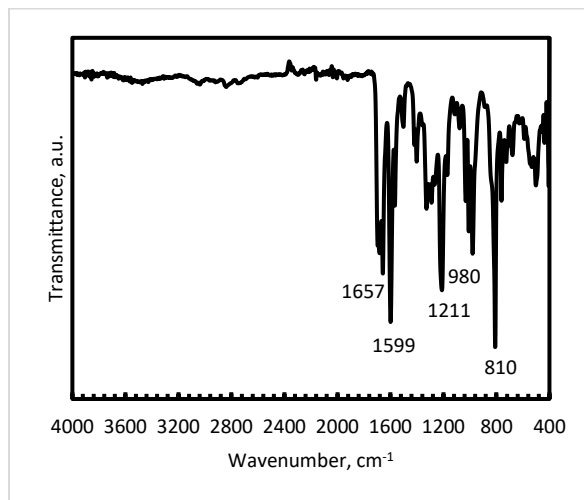


Figure S121. Infrared spectrum (ATR-FTIR) for polychalcone **PCH-1**.

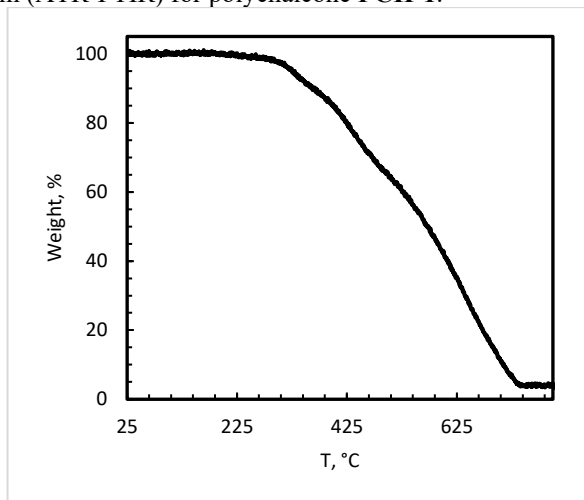


Figure S122. Mass loss as a function of temperature for polychalcone **PCH-1**.

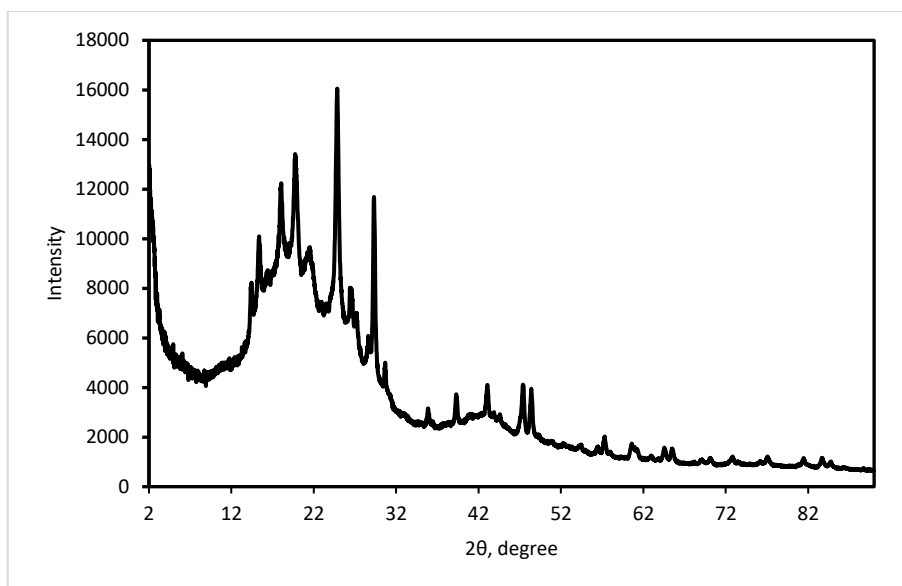
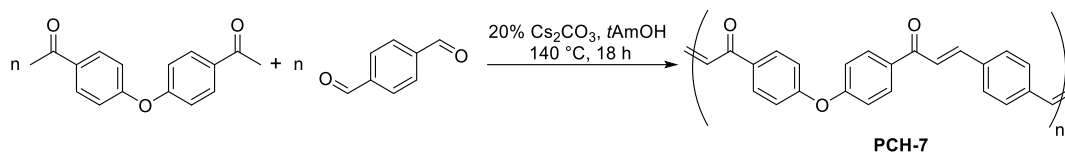


Figure S123. Experimental powder XRD patterns of polychalcone **PCH-1**.

PCH-7



Terephthalaldehyde (68 mg, 0.5 mmol) and 4-acetylphenyl ether (127 mg, 0.5 mmol) were used. The polymer was obtained in 91% yield (161 mg) as a yellow solid.

IR (ATR-FTIR, cm^{-1}): ν 3460w (C-H), 3044w, 1657m (C=O), 1589s (C=C), 1499m, 1418w, 1333m, 1215s, 1163s, 978w, 818s, 500m.

TGA: $T_d = 393\text{ }^{\circ}\text{C}$

DSC: $T_m = 248\text{ }^{\circ}\text{C}$

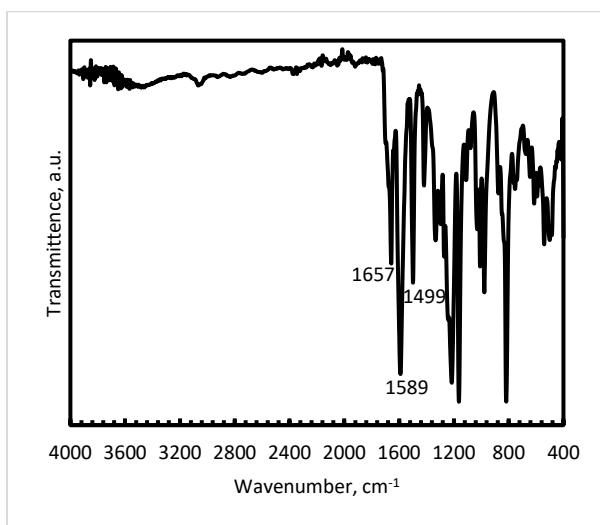


Figure S124. Infrared spectrum (ATR-FTIR) of polychalcone **PCH-7**.

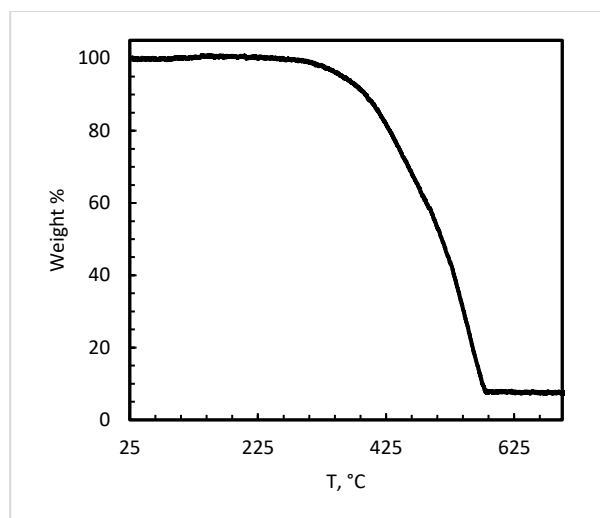


Figure S125. Mass loss as a function of temperature for polychalcone **PCH-7**.

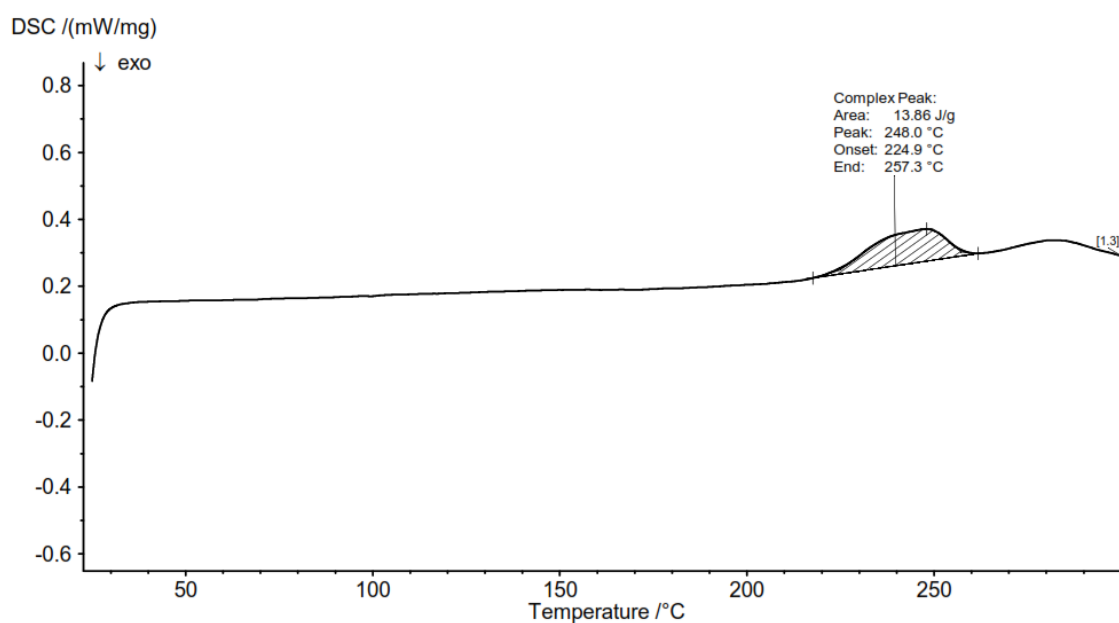


Figure S126. DSC trace corresponding to **PCH-7**.

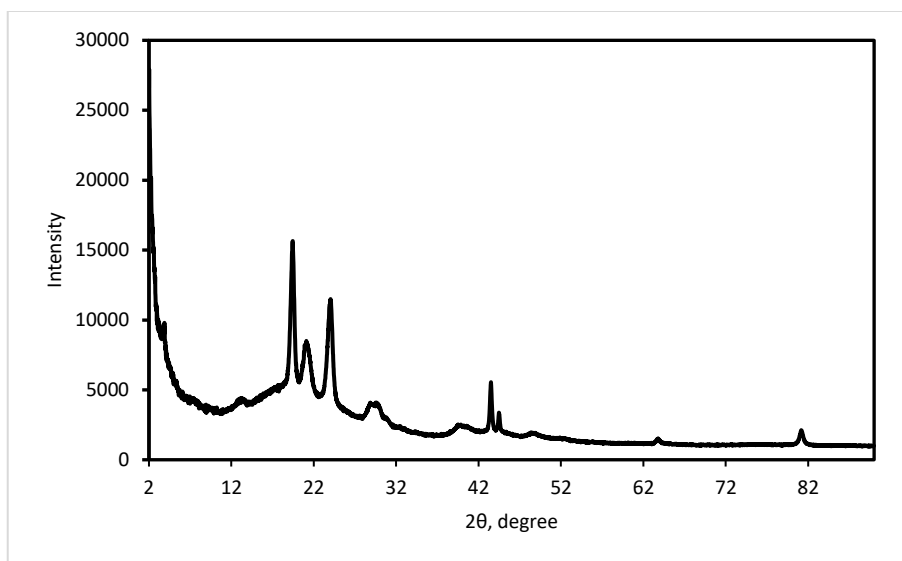


Figure S127. Experimental powder XRD patterns of polychalcone **PCH-7**.

1.7 Reaction 4-acetylphenyl ether and potassium *tert*-butoxide.

A 50 mL ampoule equipped with a J-Young's valve was charged with KO^tBu (56 mg, 0.5 mmol, 1 eq. mol%), 4-acetylphenyl ether (127 mg, 0.5 mmol). The flask was sealed under an argon atmosphere and *tert*-amyl alcohol (5 mL) was added before heating to 140 °C for 18 h with stirring. After this period, the reaction vessel was allowed to cool to room temperature. To the resulting mixture, 5 mL of 1 M solution of HCl was added and the flask was heated at 90 °C for 1 h. The precipitate was filtered, washed with water, acetone and dichloromethane and dried under reduced pressure at 120 °C giving the product (55 mg, 50% yield) as a white solid.

IR (ATR-FTIR, cm⁻¹): ν 1680w, 1591w, 1495s, 1233s, 1163m, 826m, 507w.

TGA: T_d = 455 °C

DSC: T_g = 230 °C

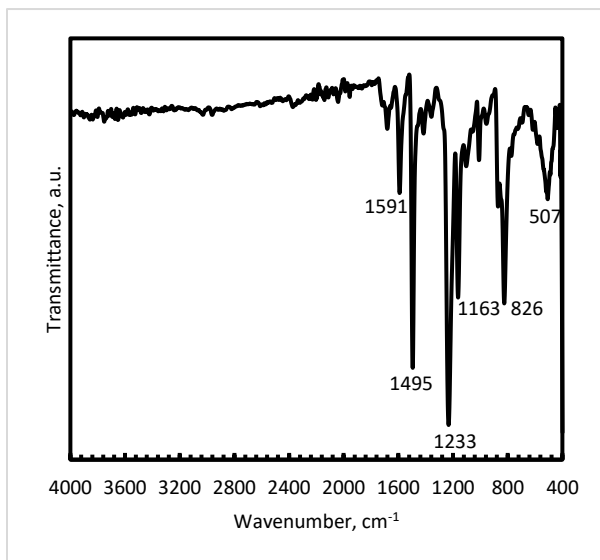


Figure S128. Infrared spectrum (ATR-FTIR) of the reaction product of 4-acetylphenyl ether and potassium *tert*-butoxide.

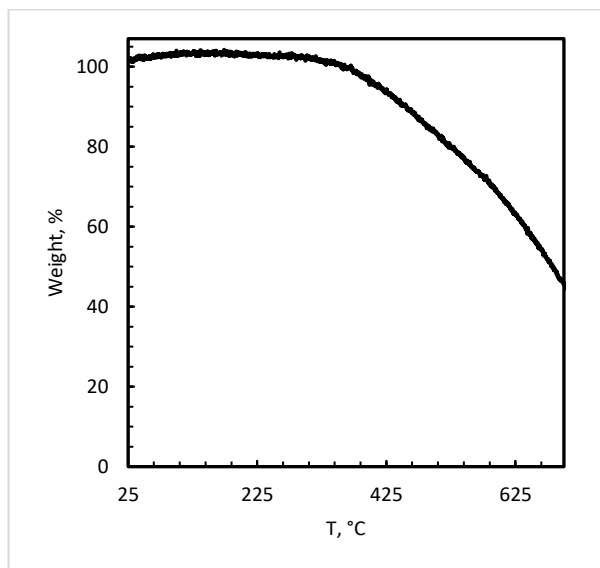


Figure S129. Mass loss as a function of temperature for the reaction product of 4-acetylphenyl ether and potassium *tert*-butoxide.

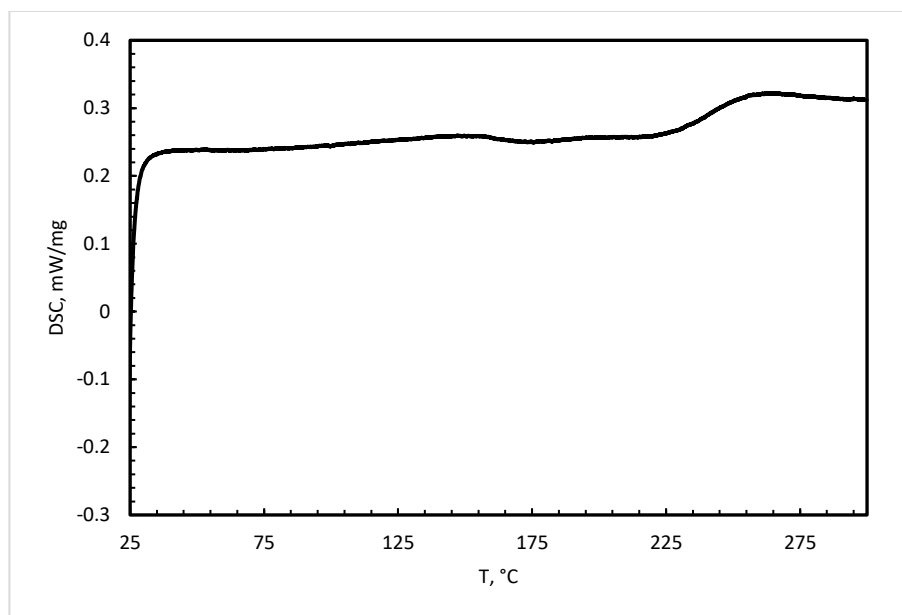


Figure S130. DSC trace corresponding to the reaction product of 4-acetylphenyl ether and potassium *tert*-butoxide.

1.8 Syntheses of polyketones in the presence of hydrogen atmosphere.

Synthesis of PAAK-1 in the presence of hydrogen atmosphere.

A 100 mL ampoule equipped with a J-Young's valve was charged with pre-catalyst **1** (2.5 mg, 0.005 mmol, 1 mol%), 1,4-benzenedimethanol (69 mg, 0.5 mmol), 1,4-diacetylketone (81 mg, 0.5 mmol) and Cs_2CO_3 (16.5 mg, 0.05 mmol, 10 mol%). *tert*-Amyl alcohol (5 mL) was added and the flask was sealed under a hydrogen atmosphere before heating to 140 °C for 18 h with stirring. After this period, the reaction vessel was allowed to cool to room temperature. To the resulting mixture, 5 mL of 1 M HCl was added and the flask had been heated at 90 °C for 1 h. The yellow precipitate (126 mg, 95% yield) was filtered and dried under reduced pressure at 120 °C.

IR (ATR-FTIR, cm^{-1}): ν 3476w (O-H), 2920w (C-H), 1676s (C=O), 1605m (C=C), 1510w, 1402m, 1267m, 1211s, 982m, 818s, 550m.

TGA: Td = 397 °C

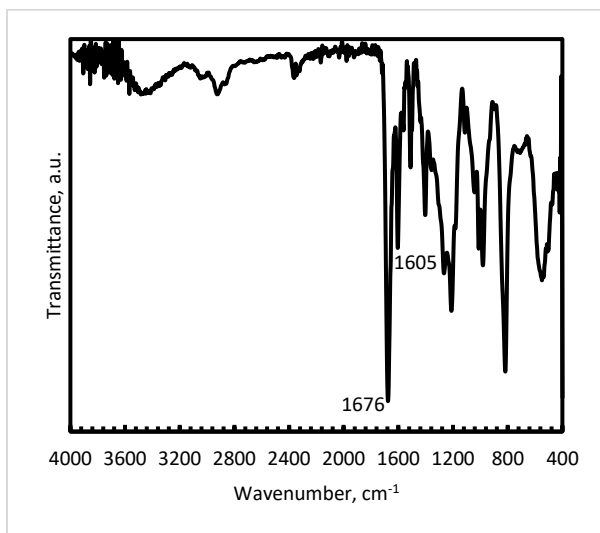


Figure S131. Infrared spectrum (ATR-FTIR) of polyketone **PAAK-1** obtained in the atmosphere of hydrogen.

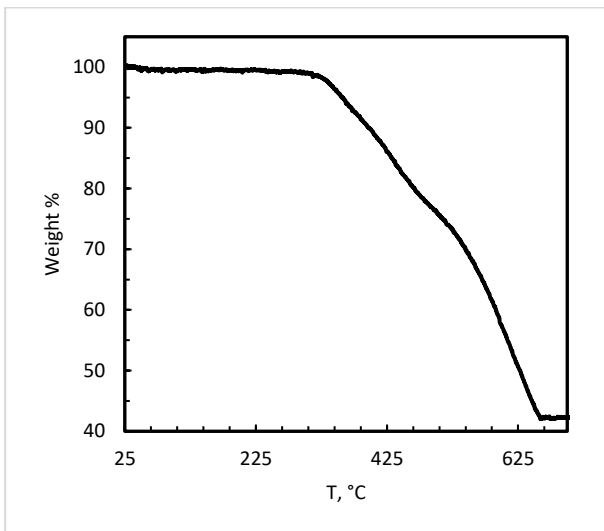


Figure S132. Mass loss as a function of temperature for polyketone **PAAK-1** obtained in the atmosphere of hydrogen.

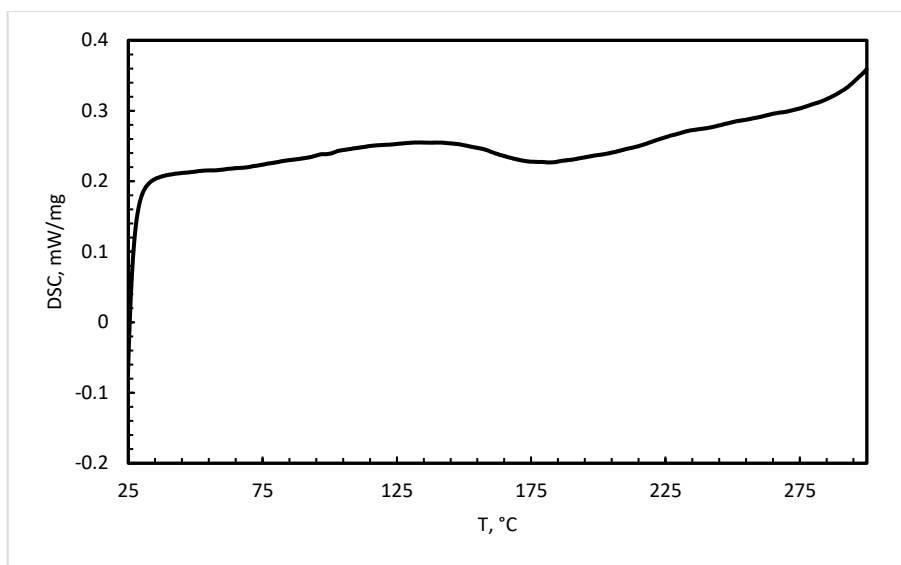


Figure S133. DSC trace corresponding to polyketone **PAAK-1** obtained in the atmosphere of hydrogen.

Synthesis of PAAK-7 in the presence of hydrogen atmosphere.

A 100 mL ampoule equipped with a J-Young's valve was charged with pre-catalyst **1** (2.5 mg, 0.005 mmol, 1 mol%), 1,4-benzenedimethanol (69 mg, 0.5 mmol), 4-acetylphenyl ether (127 mg, 0.5 mmol) and Cs_2CO_3 (16.5 mg, 0.05 mmol, 10 mol%). *tert*-Amyl alcohol (5 mL) was added and the flask was sealed under a hydrogen atmosphere before heating to 140 °C for 18 h with stirring. After this period, the reaction vessel was allowed to cool to room temperature. To the resulting mixture, 5 mL of 1 M HCl was added and the flask had been heated at 90 °C for 1 h. The white precipitate (177 mg, 99% yield) was filtered and dried under reduced pressure at 120 °C.

IR (ATR-FTIR, cm^{-1}): ν 2914w (C-H), 1674m (C=O), 1585s (C=C), 1497m, 1233s, 1163s, 822m, 548m.

TGA: Td = 371 °C

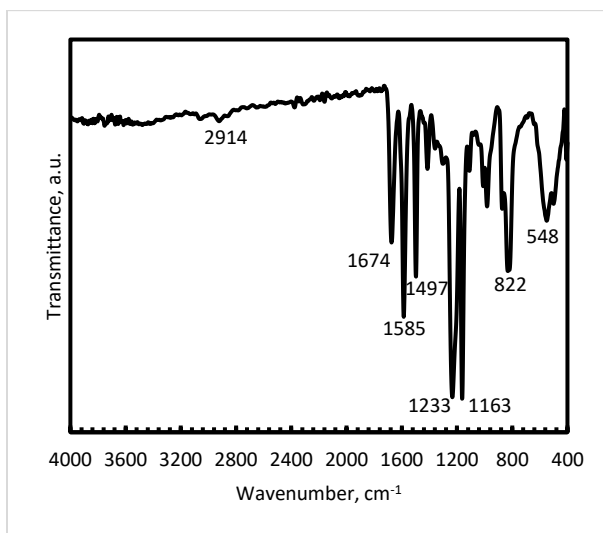


Figure S134. Infrared spectrum (ATR-FTIR) of polyketone **PAAK-7** obtained in the atmosphere of hydrogen.

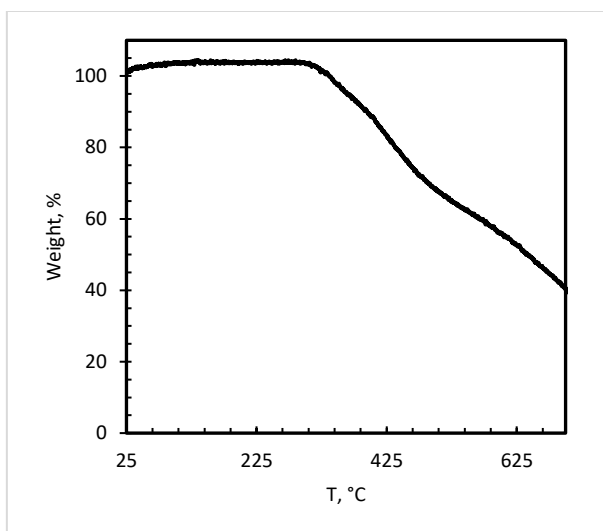


Figure S135. Mass loss as a function of temperature for polyketone **PAAK-7** obtained in the atmosphere of hydrogen.

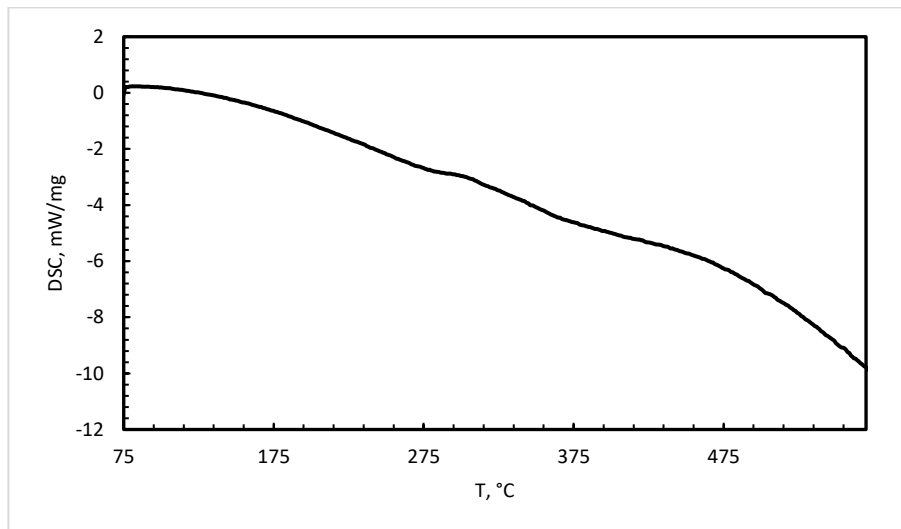


Figure S136. DSC trace corresponding to **PAAK-7** obtained in the atmosphere of hydrogen.

Synthesis of PAAK-9 in the presence of hydrogen atmosphere.

A 100 mL ampoule equipped with a J-Young's valve was charged with pre-catalyst **1** (2.5 mg, 0.005 mmol, 1 mol%), 1,4-cyclohexanedimethanol (72 mg, 0.5 mmol), 4-acetylphenyl ether (127 mg, 0.5 mmol) and Cs_2CO_3 (16.5 mg, 0.05 mmol, 10 mol%). *tert*-Amyl alcohol (5 mL) was added and the flask was sealed under a hydrogen atmosphere before heating to 140 °C for 18 h with stirring. After this period, the reaction vessel was allowed to cool to room temperature. To the resulting mixture, 5 mL of 1 M HCl was added and the flask had been heated at 90 °C for 1 h. The white precipitate (178 mg, 98% yield) was filtered and dried under reduced pressure at 120 °C.

IR (ATR-FTIR, cm^{-1}): ν 2916w (C-H), 2853w (C-H), 1674m (C=O), 1587m (C=C), 1497m, 1234s, 1163s, 835m.

TGA: Td = 384 °C

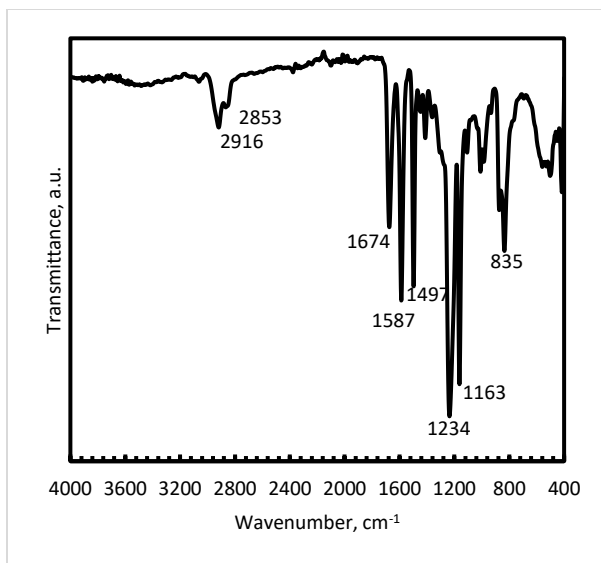


Figure S137. Infrared spectrum (ATR-FTIR) of polyketone **PAAK-9** obtained in the atmosphere of hydrogen.

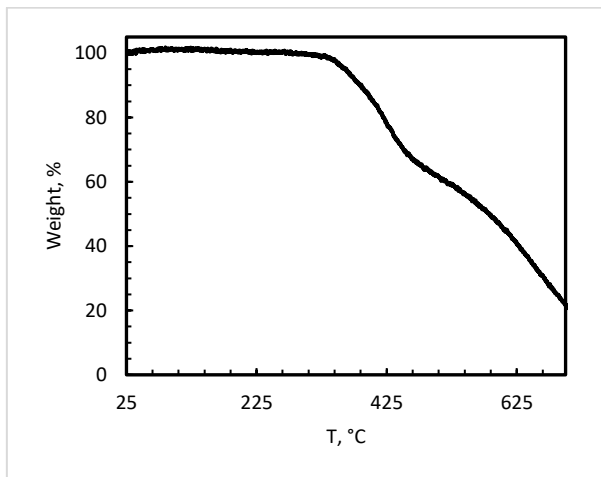


Figure S138. Mass loss as a function of temperature for polyketone **PAAK-9** obtained in the atmosphere of hydrogen.

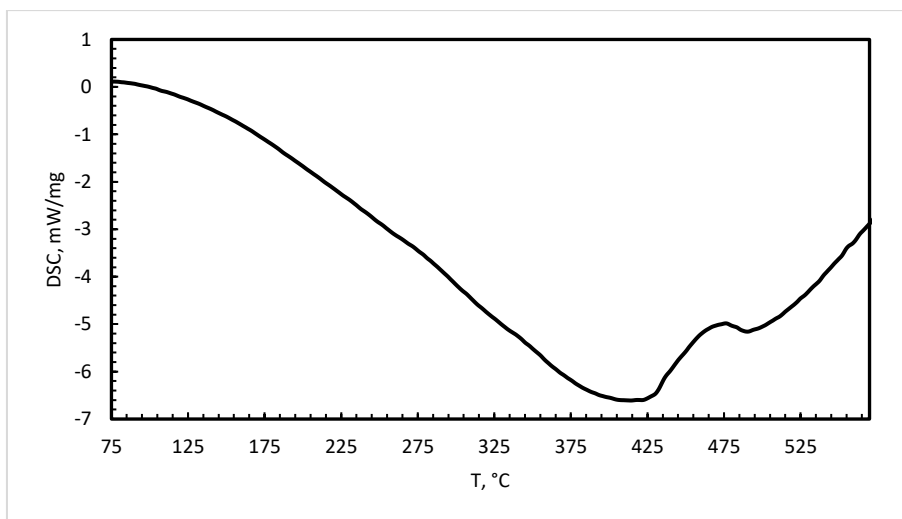


Figure S139. DSC trace corresponding to **PAAK-9** obtained in the atmosphere of hydrogen.

1.9 Catalyst reuse experiments.

Catalyst reuse after synthesis of PAAK-7.

A 100 mL ampoule equipped with a J-Young's valve was charged with pre-catalyst **1** (2.5 mg, 0.005 mmol, 1 mol%) and Cs_2CO_3 (16.5 mg, 0.05 mmol, 10 mol%), 1,4-benzenedimethanol (69 mg, 0.5 mmol) and 4-acetylphenyl ether (127 mg, 0.5 mmol). The flask was sealed under an argon atmosphere and *tert*-amyl alcohol (5 mL) was added before heating to 140 °C for 2 h with stirring. After this period, the reaction vessel was allowed to cool to room temperature. The reaction mixture consisted of a white precipitate (175 mg, 89%) and a yellowish solution. The ampoule was connected to the Schlenk line and the yellowish solution was transferred to another 100 mL ampoule charged with fresh portion of 1,4-benzenedimethanol (69 mg, 0.5 mmol) and 4-acetylphenyl ether (127 mg, 0.5 mmol) under argon. The freshly charged ampoule was sealed and heating to 140 °C for 2 h with stirring. After this period, the reaction vessel was allowed to cool to room temperature. No precipitate was observed after the second iteration.

Catalyst reuse after synthesis of PAAK-7 with addition of base.

A 100 mL ampoule equipped with a J-Young's valve was charged with pre-catalyst **1** (2.5 mg, 0.005 mmol, 1 mol%) and Cs_2CO_3 (16.5 mg, 0.05 mmol, 10 mol%), 1,4-benzenedimethanol (69 mg, 0.5 mmol) and 4-acetylphenyl ether (127 mg, 0.5 mmol). The flask was sealed under an argon atmosphere and *tert*-amyl alcohol (5 mL) was added before heating to 140 °C for 2 h with stirring. After this period, the reaction vessel was allowed to cool to room temperature. The reaction mixture consisted of a white precipitate (161 mg, 90%) and a yellowish solution. The ampoule was connected to the Schlenk line and the yellowish solution was transferred to another 100 mL ampoule charged with fresh portion of Cs_2CO_3 (16.5 mg, 0.05 mmol, 10 mol%), 1,4-benzenedimethanol (69 mg, 0.5 mmol) and 4-acetylphenyl ether (127 mg, 0.5 mmol) under argon. The freshly charged ampoule was sealed and heating to 140 °C for 2 h with stirring. After this period, the reaction vessel was allowed to cool to room temperature. To the resulting mixture, 5 mL of 1 M HCl was added and the flask had been heated at 90 °C for 1 h. The precipitate was filtered and dried under reduced pressure at 120 °C giving the product (98 mg, 55% yield) as a white solid.

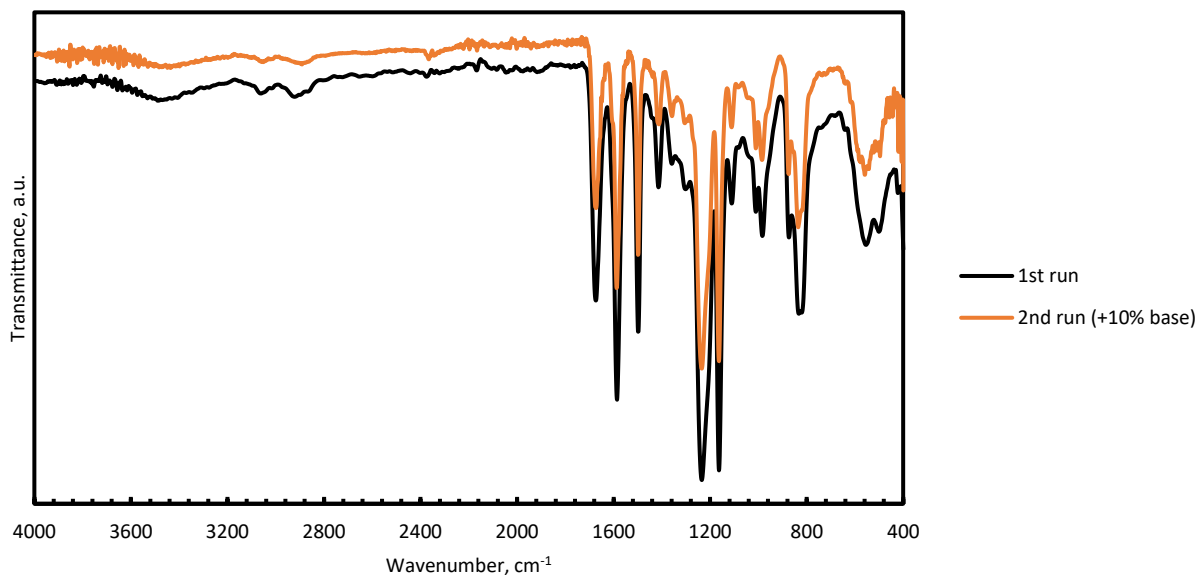


Figure S140. Infrared spectrum (ATR-FTIR) of PAAK-7 obtained by fresh catalyst (black) and reused reaction solution with addition of 10% base (orange).

1.10 Headspace gas analysis from the synthesis of polyketone PAAK-7.

A 100 mL ampoule equipped with a J-Young's valve was charged with pre-catalyst **1** (2.5 mg, 0.005 mmol, 1 mol%) and Cs_2CO_3 (16.5 mg, 0.05 mmol, 10 mol%), 1,4-benzenedimethanol (69 mg, 0.5 mmol) and 4-acetylphenyl ether (127 mg, 0.5 mmol). The flask was sealed under an argon atmosphere and *tert*-amyl alcohol (5 mL) was added before heating to 140 °C for 2 h with stirring. After this period, the reaction vessel was allowed to cool to room temperature. A sample of the headspace was extracted using a gas tight syringe and analysed using GC-TCD. It was demonstrated that the injected gas consisted mainly from Hydrogen (from the reaction itself) and Nitrogen (from the reaction inert atmosphere) with some Oxygen originated from the atmosphere during sample preparation and injection (see Figure below).

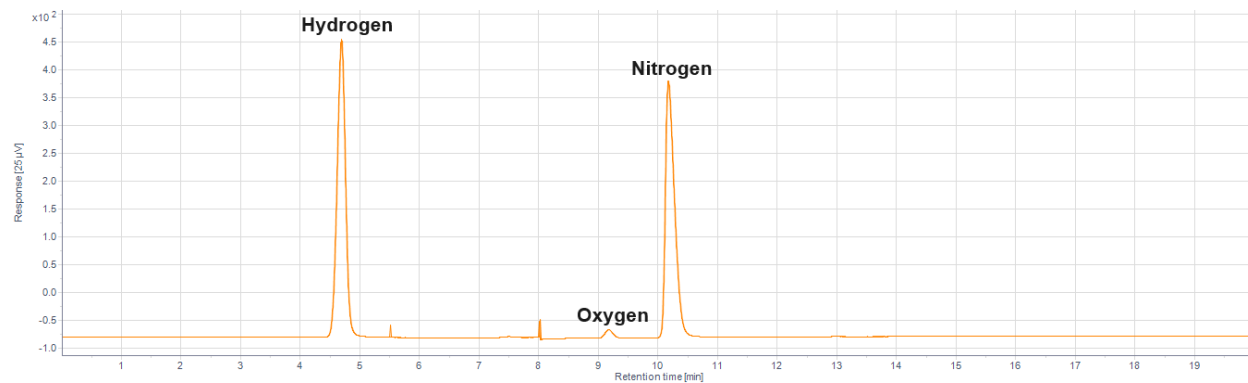
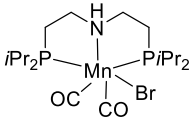
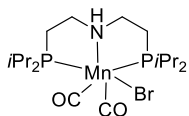
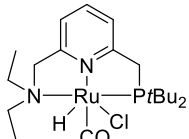


Figure S141. GC-TCD chromatograph of the reaction headspace from synthesis of PAAK-7.

1.11 Hydrogenative depolymerization of polyethyleneterephthalate (PET).

Table S2. Tested conditions for hydrogenative depolymerization of PET.^a

Entry	Amount of catalyst	Catalyst	Base	Amount of base	Conversion ^b	Yield of 1,4-benzenedimethanol ^c
1	1%		KOtBu	10%	0%	0%
2	3%		KOtBu	30%	0%	0%
3	2%		KOtBu	10%	quant.	97%

^a Polyethylene terephthalate (192.2 mg, 1 mmol, 1 eq., taken from a plastic bottle), a catalyst (1–3%) and KOtBu (10–30%), were weighed under air, placed into an 8 mL glass ampoule, a stir bar was added, and the ampoule was sealed with a cap, containing a septum. The ampoule was backfilled with argon and 5 mL of anhydrous *tert*-amyl alcohol was added via syringe. The ampoules were placed inside a 150 mL autoclave with some metal beans to ensure thermocunductivity. The autoclave was purged with argon, then sealed, purged with H₂, pressurized with 50 bar of H₂, and placed in an oil bath. The reaction was stirred at 140 °C for 88 hours. After that, the autoclave was cooled down to room temperature in an ice bath and carefully vented to atmosphere. ^b Conversion was calculated as 100% minus amount of unreacted PET flakes. ^c Yield was calculated via ¹H NMR employing mesitylene as internal standard. Hence, 200–300 mg of the reaction solution and 10 mg mesitylene were weighed in a NMR tube followed by the addition of methanol-d₄ (0.3 mL).

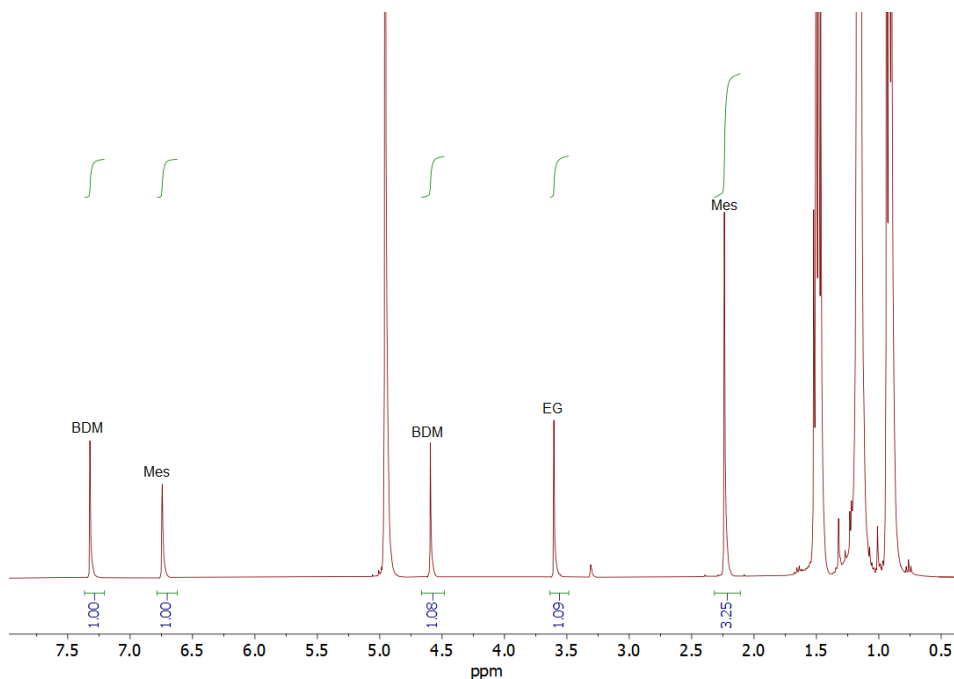


Figure S142. ¹H NMR spectrum of reaction mixture from Entry 3 in Table S2 in methanol-d₄ at room temperature. BDM – 1,4-benzenedimethanol, EG – ethylene glycol, Mes – mesitylene. The remaining signals correspond to *tert*-amyl alcohol and methanol-d₄.

1.12 Hydrogenation of *trans*-Chalcone by transfer hydrogenation.

A 100 mL ampoule equipped with a J-Young's valve was charged with **1** (2.5 mg, 0.005 mmol, 1 mol%), 1,4-benzenedimethanol (69 mg, 0.5 mmol), *trans*-chalcone (104 mg, 0.5 mmol) and Cs₂CO₃ (16.5 mg, 0.10 mmol, 10 mol%). The flask was refilled with argon and *tert*-amyl alcohol (5 mL) was added. The flask was sealed and heated 140 °C for 2 h with stirring. After this period, the reaction vessel was allowed to cool to room temperature and the resulting mixture was analysed with GC-MS and NMR (with CDCl₃ as a solvent) using mesitylene as an internal standard. The yield was estimated to be 46%. The NMR spectrum of 1,3-diphenylpropan-1-one corresponds to the literature data [2].

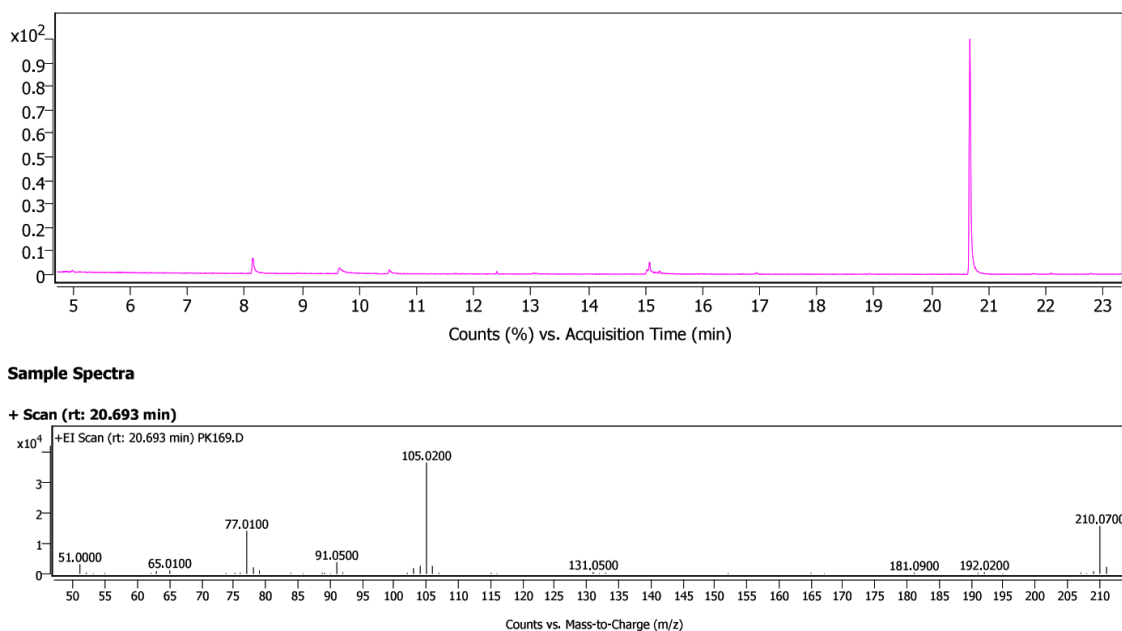


Figure S143. GC chromatogram of the products of transfer hydrogenation of *trans*-chalcone (above) and mass spectrum (EI) of 1,3-diphenylpropan-1-one extracted from the chromatogram.

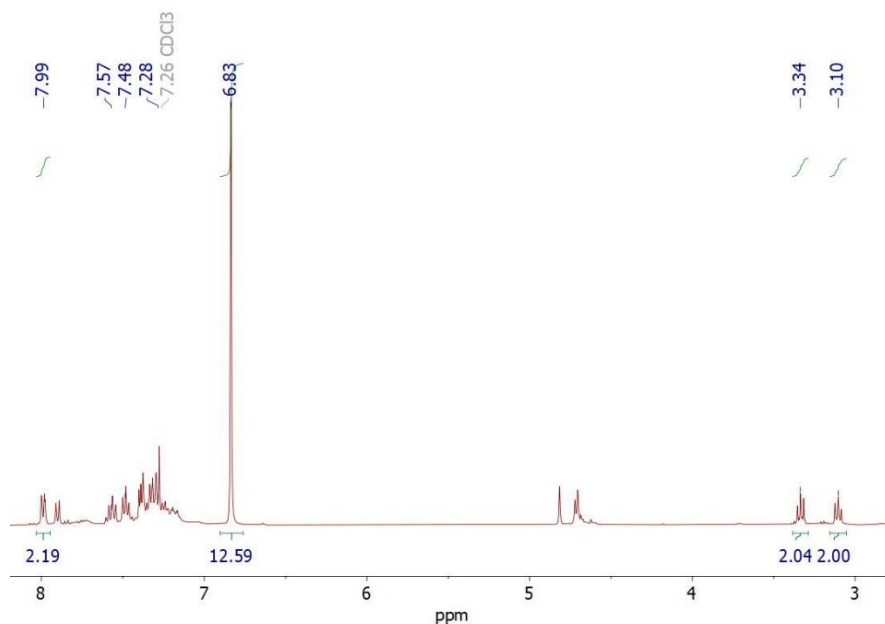


Figure S144. Fragment of ¹H NMR (400 MHz, CDCl₃) of the reaction mixture of transfer hydrogenation of *trans*-chalcone in the presence of 1,4-benzenedimethanol.

1.13 Mass spectroscopy investigation of mother liquor from reaction mixtures.

PK268_2pos #1-152 RT: 0.01-1.02 AV: 152 NL: 1.73E8
T: FTMS + p ESI Full ms [100.0000-1400.0000]

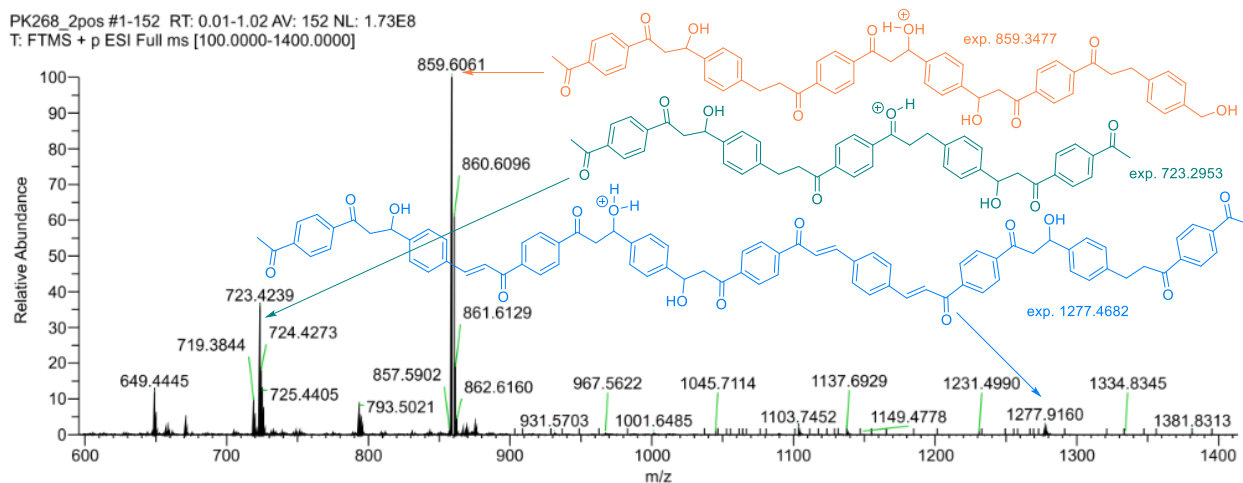


Figure S145. HRMS (EI, MeCN) spectrum for mother liquor from reaction mixture after synthesis of **PAAK-1**. The peak assignment is illustrative and might not represent the precise structure.

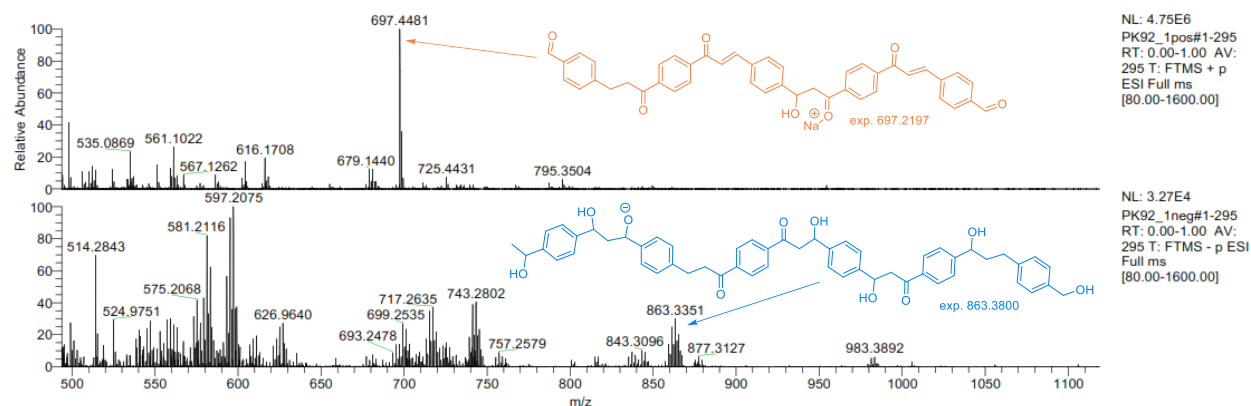


Figure S146. HRMS (EI, MeCN) spectrum for mother liquor from reaction mixture after synthesis of **PAAK-1** corresponding to Entry 10, Table S1. The peak assignment is illustrative and might not represent the precise structure.

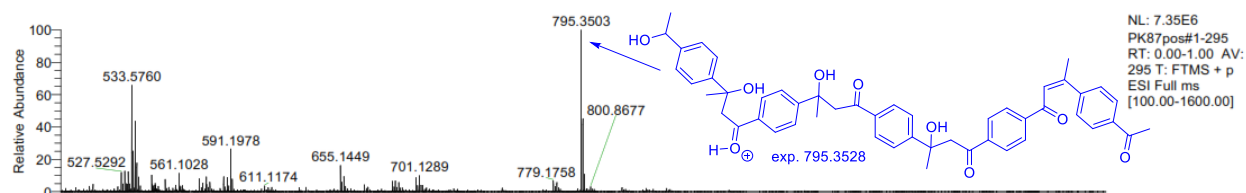


Figure S147. HRMS (EI, MeCN) spectrum for mother liquor from reaction mixture after synthesis of **PAAK-1** corresponding to Entry 18, Table S1. The peak assignment is illustrative and might not represent the precise structure.

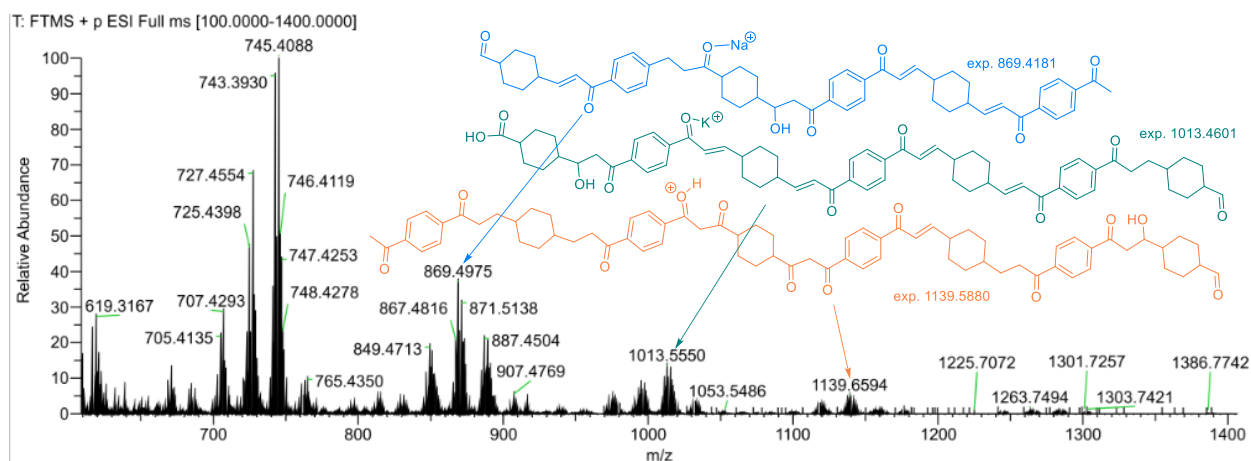


Figure S148. HRMS (EI, MeCN) spectrum for mother liquor from reaction mixture after synthesis of **PAAK-3**. The peak assignment is illustrative and might not represent the precise structure.

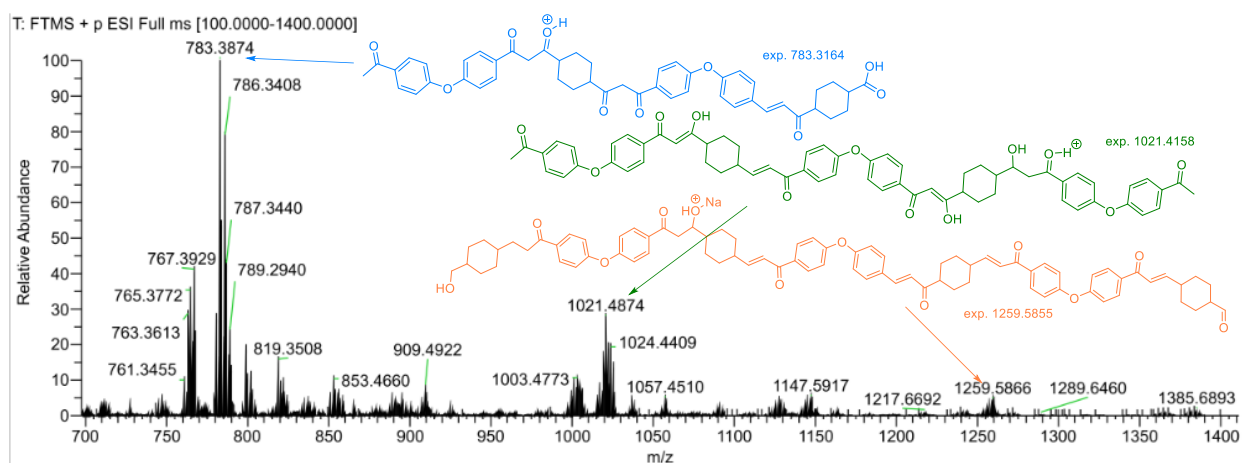


Figure S149. HRMS (EI, MeCN) spectrum for mother liquor from reaction mixture after synthesis of **PAAK-9**. The peak assignment is illustrative and might not represent the precise structure.

1.14 TGA and DSC analysis combined with mass-spectrometry.

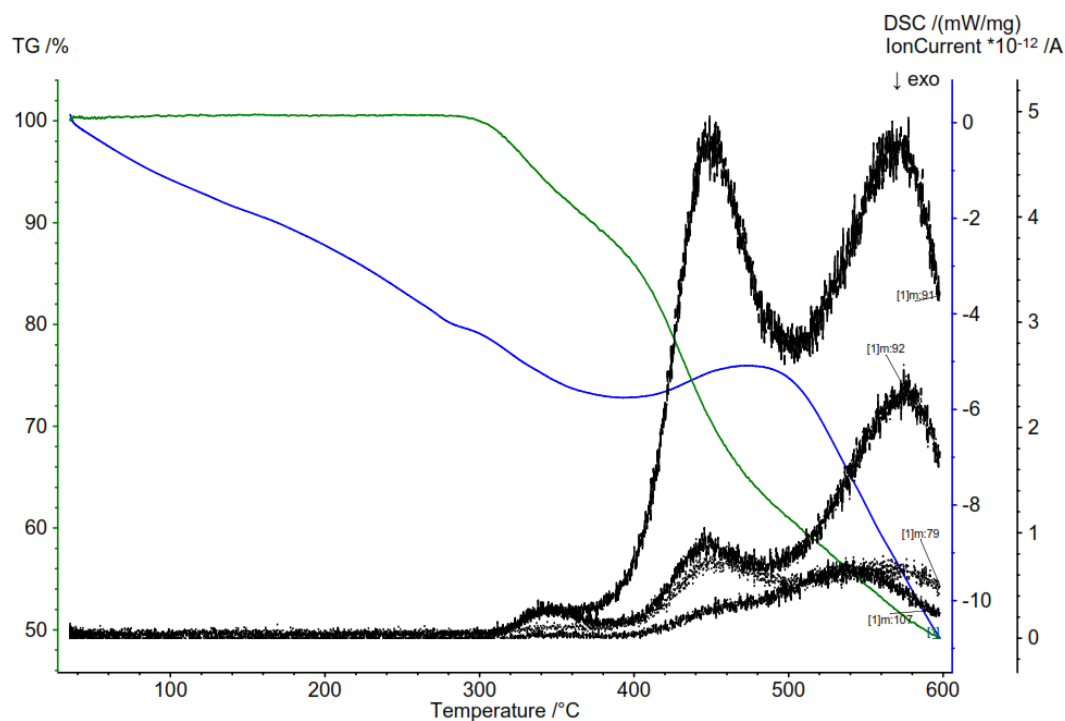


Figure S150. TGA curve (green), DSC trace (blue) and ion current (black) at temperatures 30–600 °C corresponding to PAAK-7. Ion current for $m=79$; 91; 92 and 107 g/mol is shown which corresponds to 1,4-benzenedimethanol-derived fragments in the polymer.

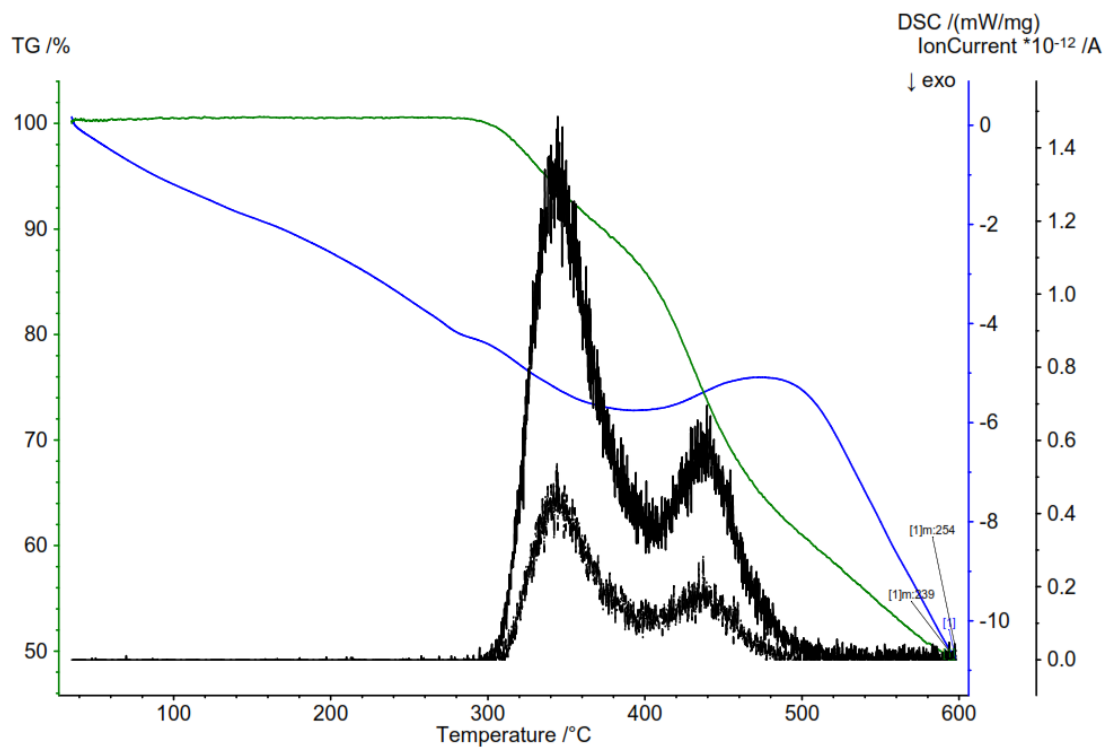


Figure S151. TGA curve (green), DSC trace (blue) and ion current (black) at temperatures 30–600 °C corresponding to PAAK-7. Ion current for $m=239$ and 254 g/mol is shown which corresponds to 4-acetylphenyl ether-derived fragments in the polymer.

1.15 Infrared spectra of starting materials and commercially available compounds.

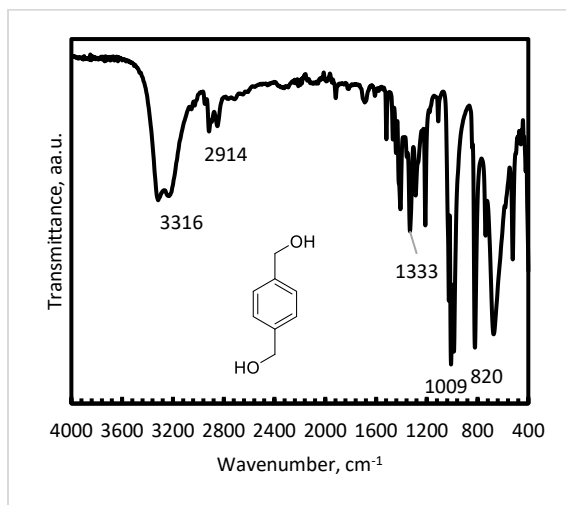


Figure S152. Infrared spectrum (ATR-FTIR) of 1,4-benzenedimethanol.

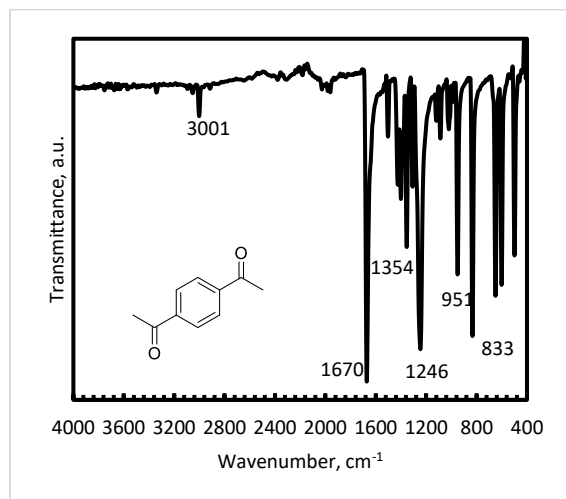


Figure S153. Infrared spectrum (ATR-FTIR) of 1,4-diacetylbenzene.

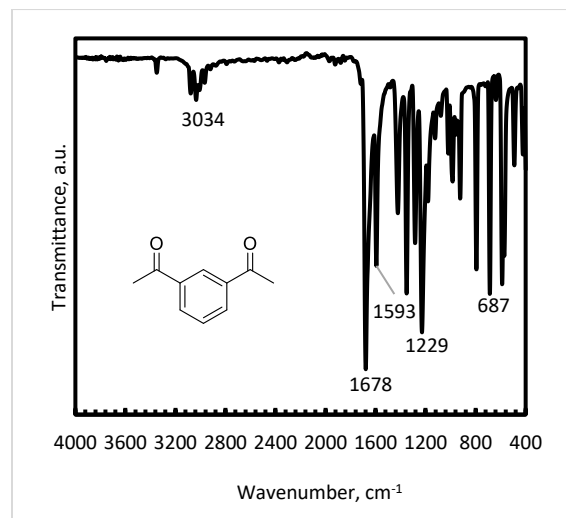


Figure S154. Infrared spectrum (ATR-FTIR) of 1,3-diacetylbenzene.

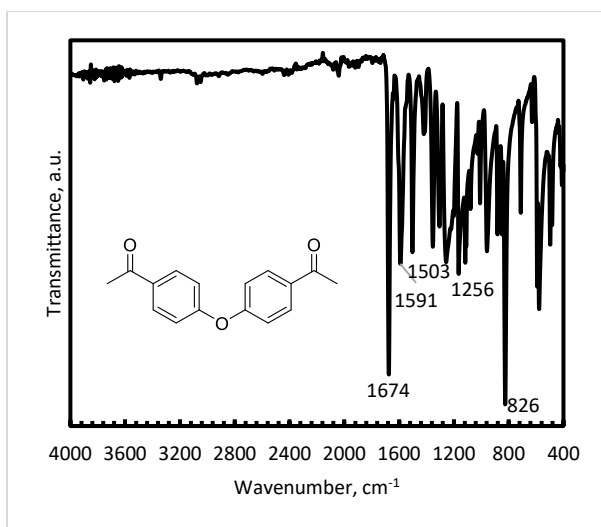


Figure S155. Infrared spectrum (ATR-FTIR) of 4-acetylphenyl ether.

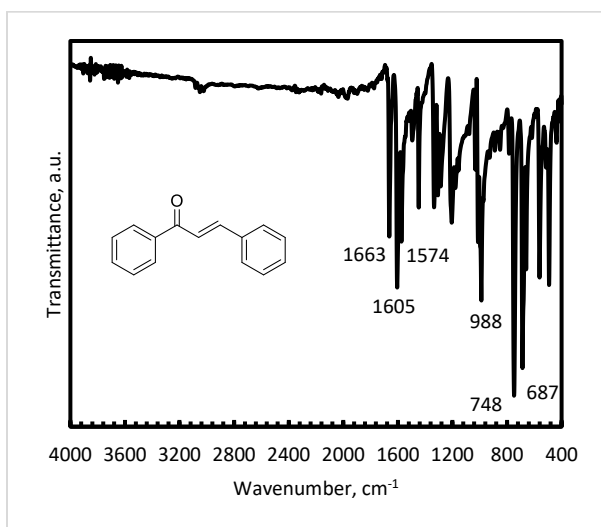


Figure S156. Infrared spectrum (ATR-FTIR) of *trans*-chalcone.

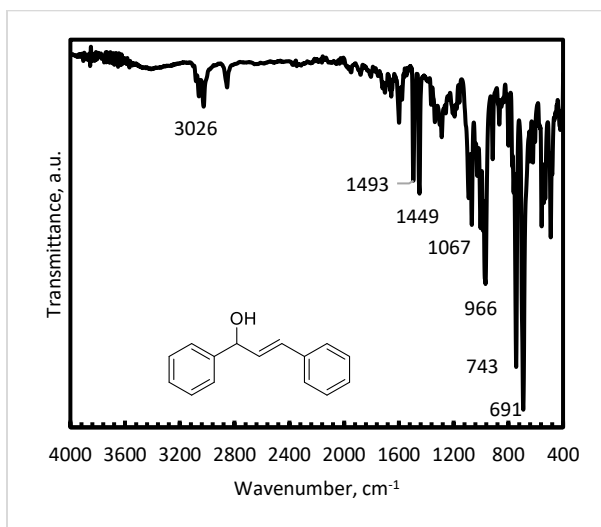


Figure S157. Infrared spectrum (ATR-FTIR) of (*E*)-1,3-diphenylprop-2-en-1-ol.

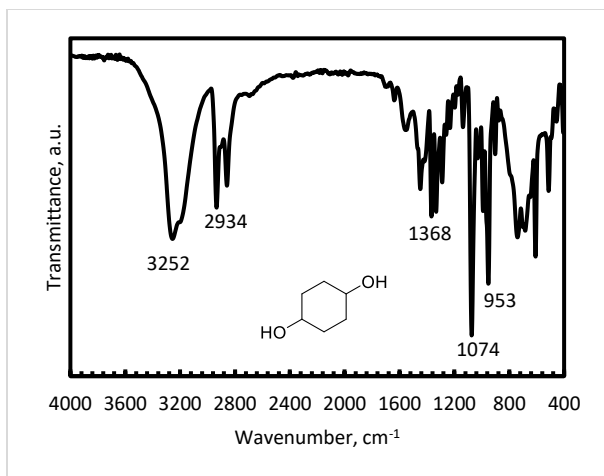


Figure S158. Infrared spectrum (ATR-FTIR) of 1,4-cyclohexanediol.

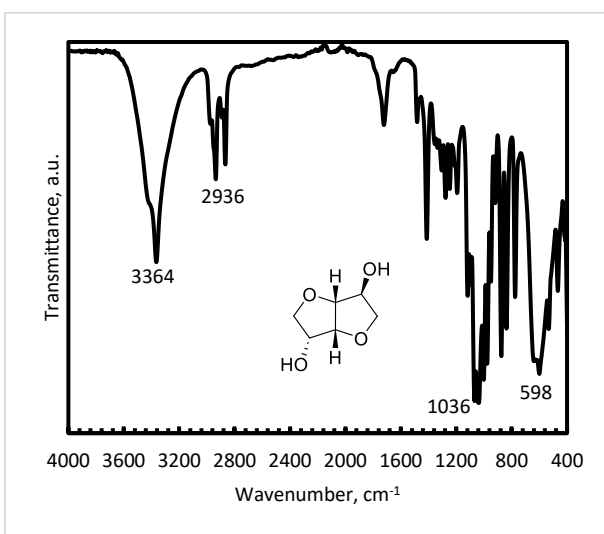


Figure S159. Infrared spectrum (ATR-FTIR) of D-isosorbide.

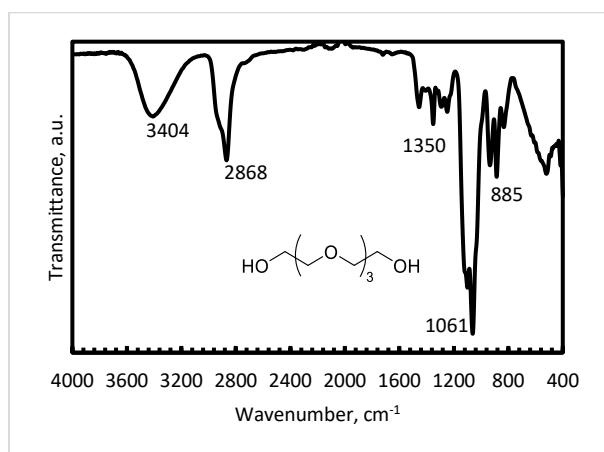


Figure S160. Infrared spectrum (ATR-FTIR) of tetraethylene glycol.

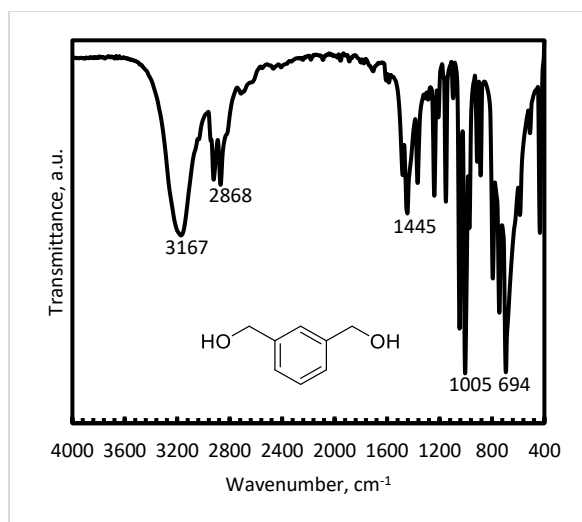


Figure S161. Infrared spectrum (ATR-FTIR) of 1,3-benzenedimethanol.

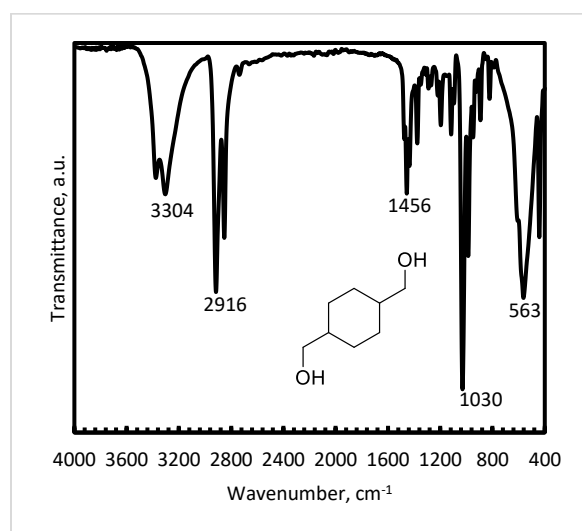


Figure S162. Infrared spectrum (ATR-FTIR) of 1,4-cyclohexanedimethanol.

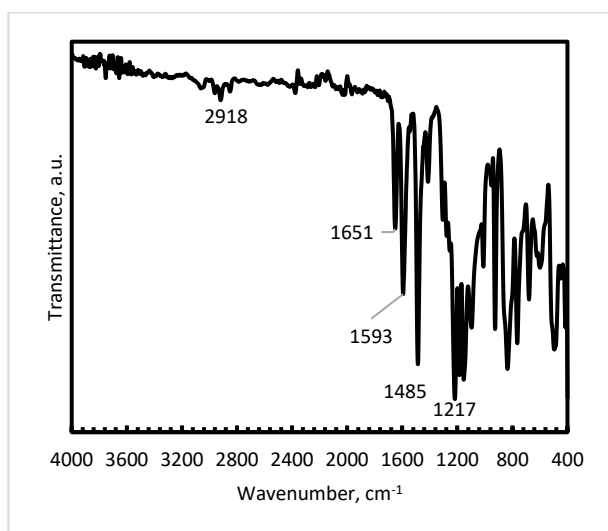


Figure S163. Infrared spectrum (ATR-FTIR) of commercial polymer PEEK.

1.16 Thermal properties and GPC analysis of commercial polyketones.

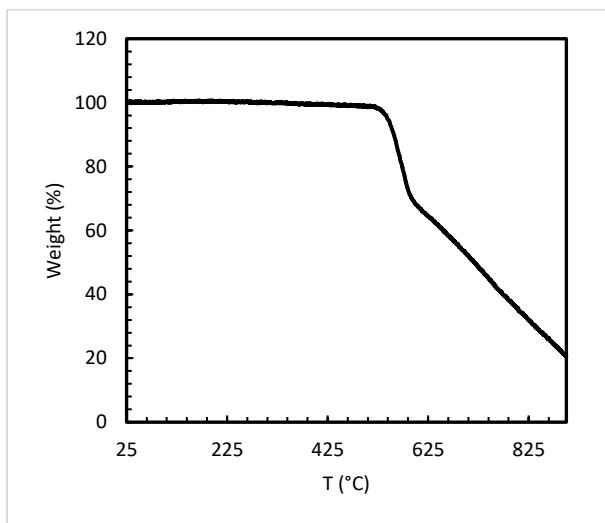


Figure S164. Mass loss as a function of temperature for commercial PEEK.

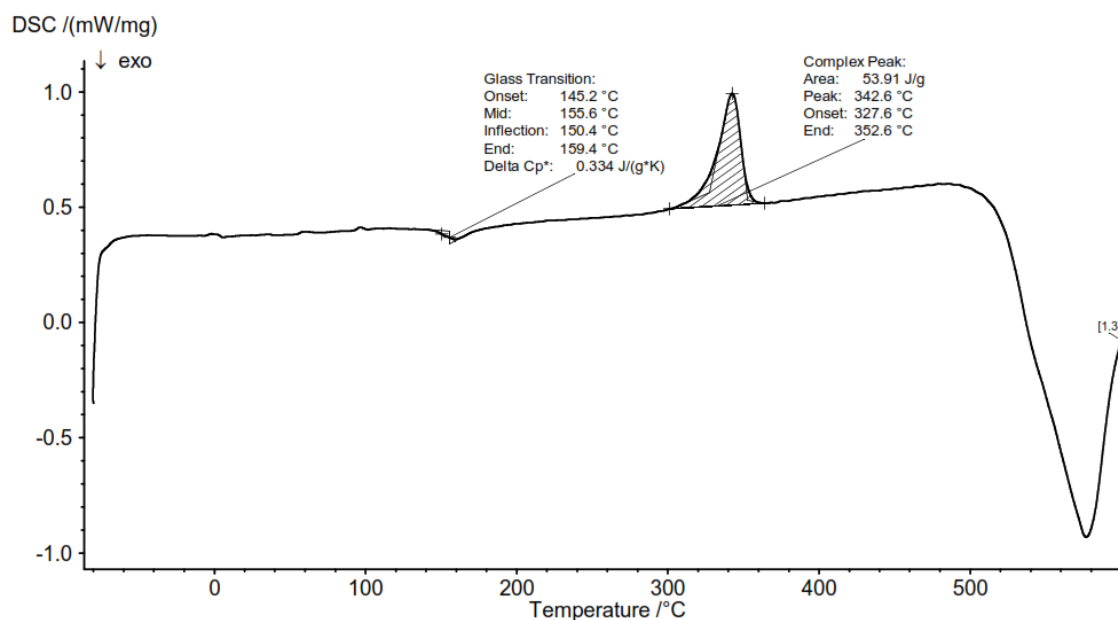


Figure S165. DSC trace corresponding to commercial PEEK.

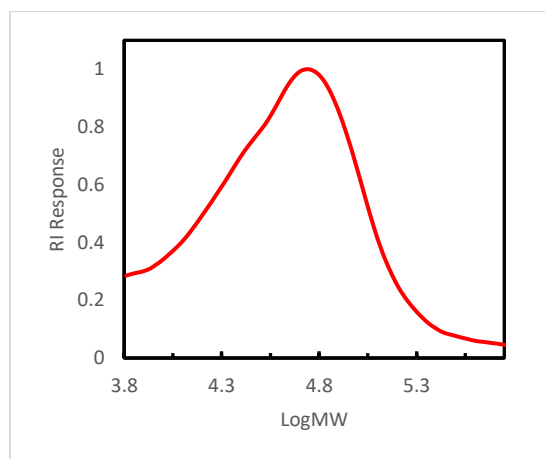


Figure S166. GPC chromatogram corresponding to commercial PEEK.

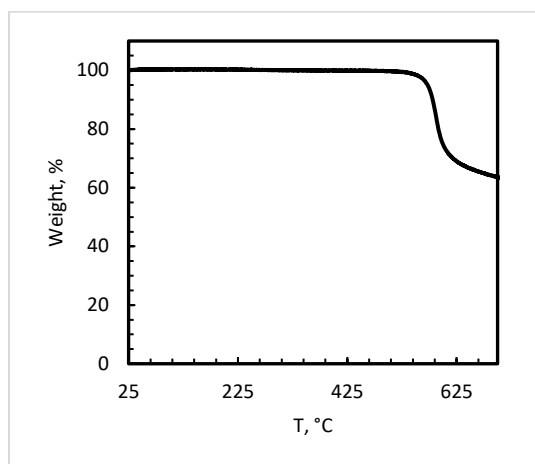


Figure S167. Mass loss as a function of temperature for commercial PEKK.

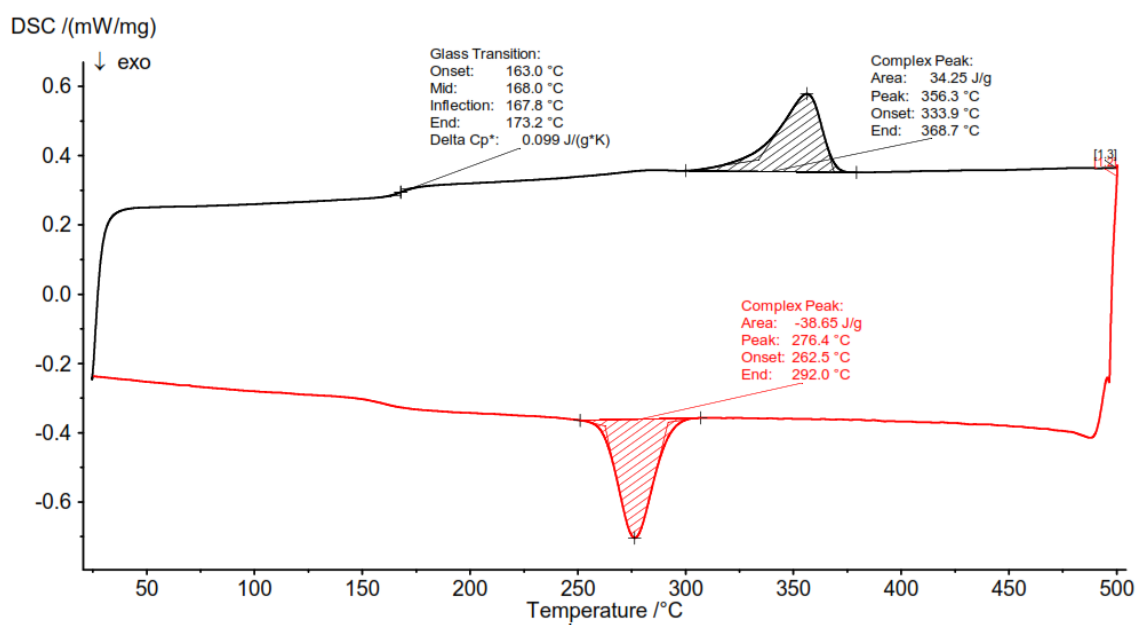


Figure S168. DSC trace corresponding to commercial PEKK.

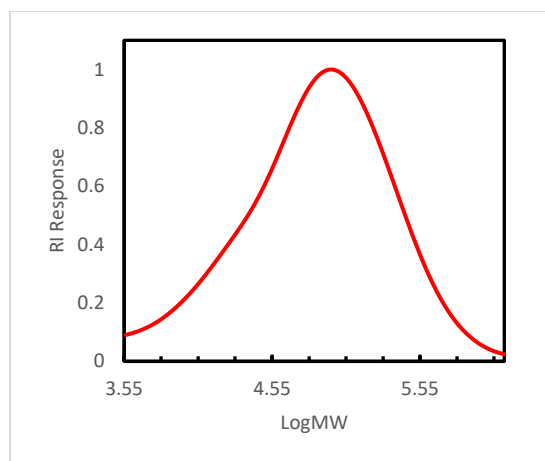


Figure S169. GPC chromatogram corresponding to commercial PEKK.

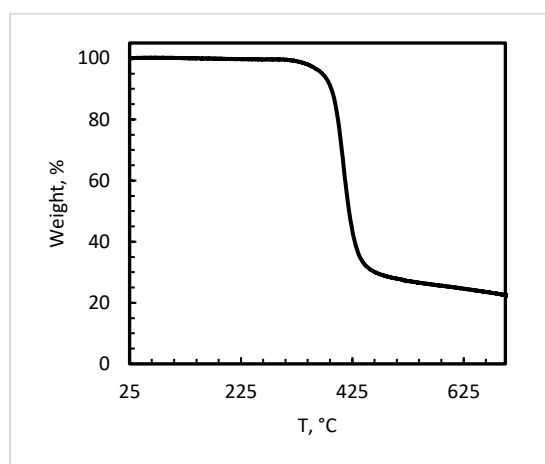


Figure S170. Mass loss as a function of temperature for commercial aliphatic polyketone POK.

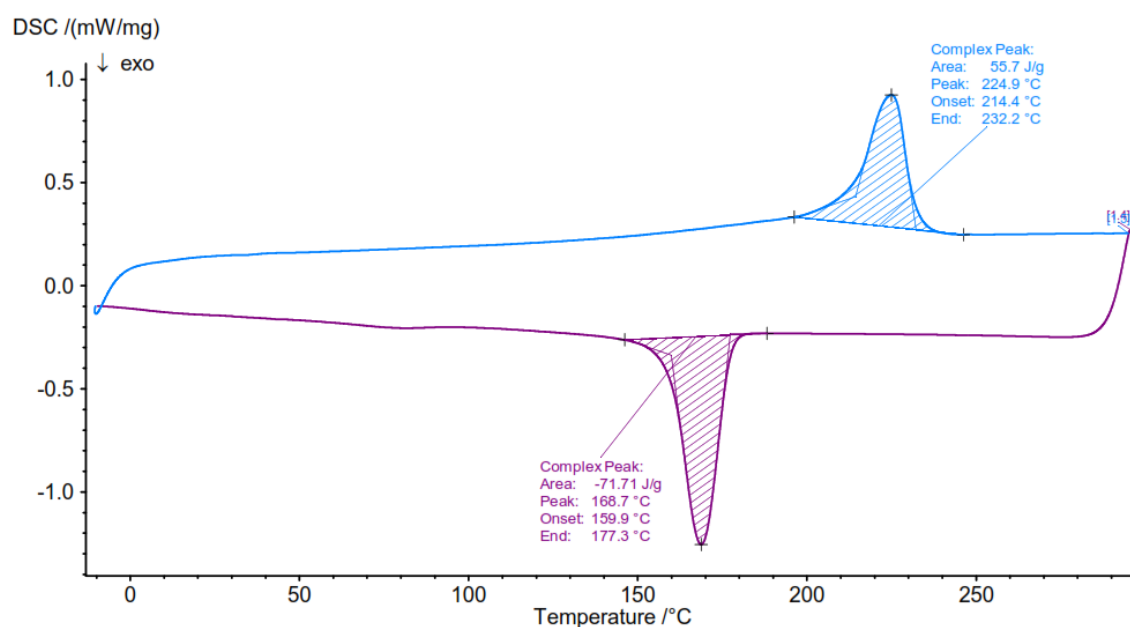


Figure S171. DSC trace corresponding to commercial POK.

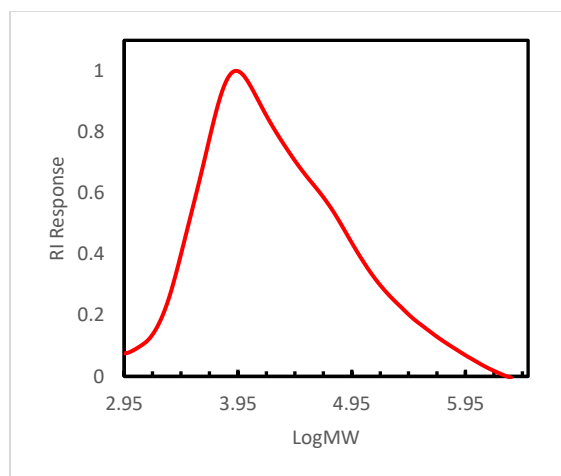


Figure S172. GPC chromatogram corresponding to commercial POK.

Table S3. Thermal properties and molecular weight of the commercial polyketones.

Entry	Polymer	T _d , °C	T _m , °C	T _c , °C	T _g , °C	Mw, kDa	<i>D</i>
1	POK	387	225	169	n.d.	66.2	7.5
2	PEEK	557	343	276	156	63.3	2.2
3	PEKK	581	356	n.d.	168	126.8	3.4

1.17 Powder XRD patterns of starting materials.

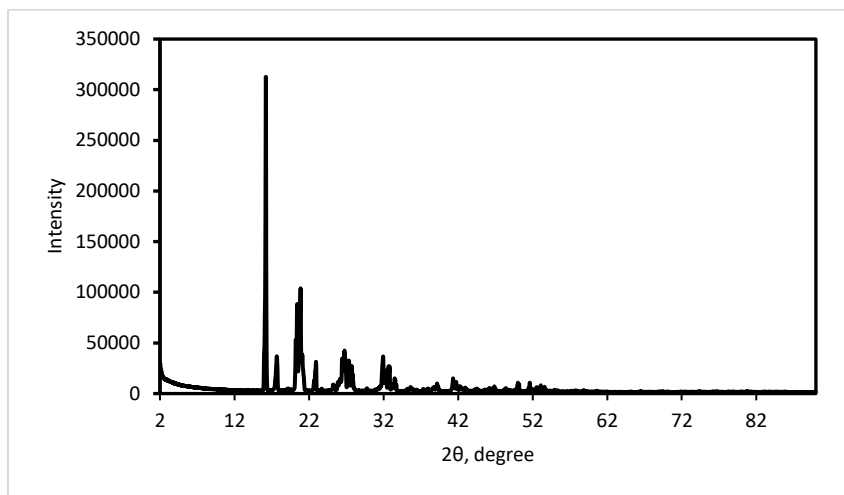


Figure S173. Experimental powder XRD patterns of 1,4-diacetylbenzene.

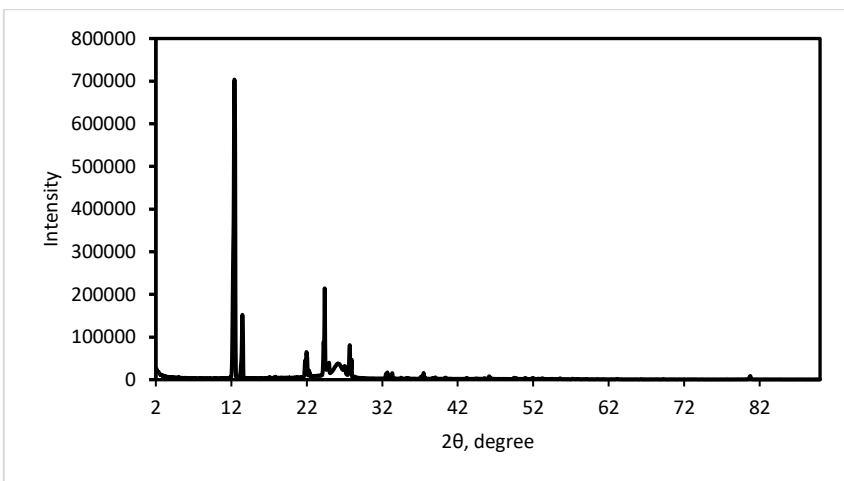


Figure S174. Experimental powder XRD patterns of 1,3-diacetylbenzene.

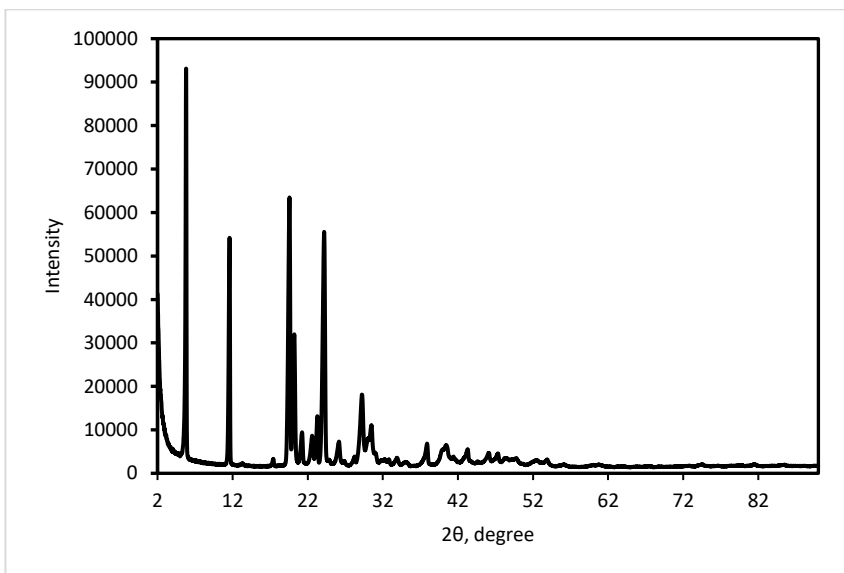


Figure S175. Experimental powder XRD patterns of 4-acetylphenyl ether.

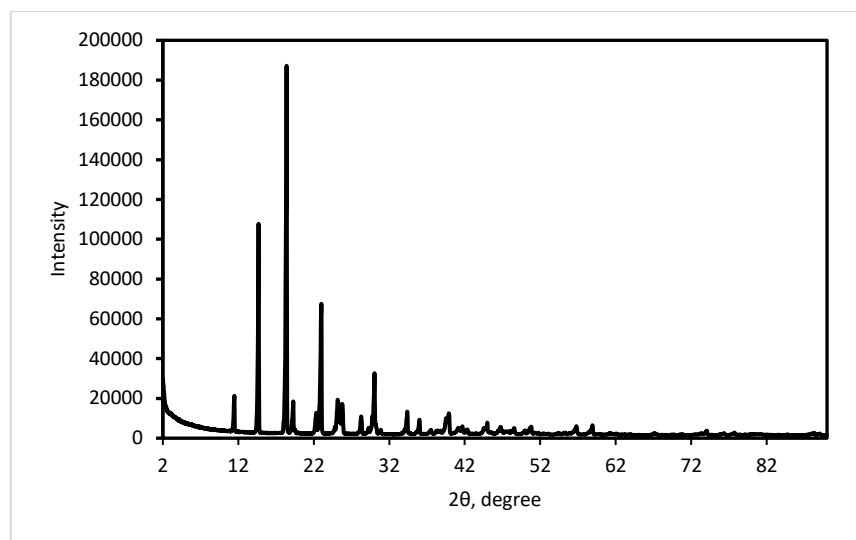


Figure S176. Experimental powder XRD patterns of 1,4-benzenedimethanol.

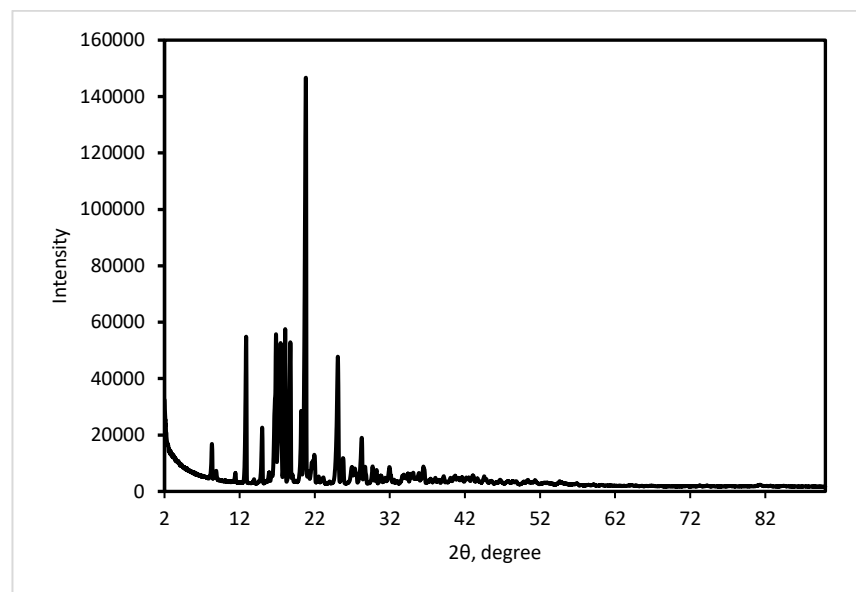
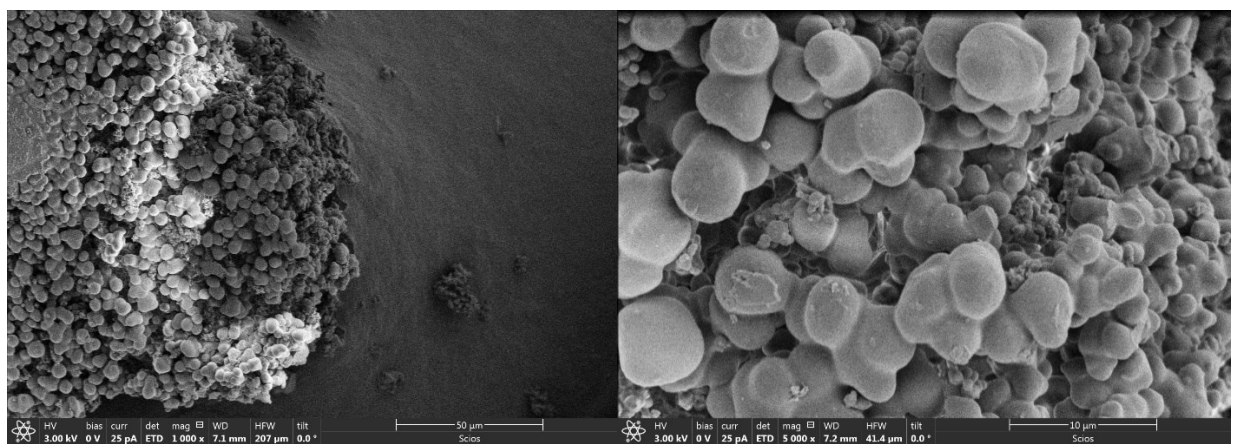
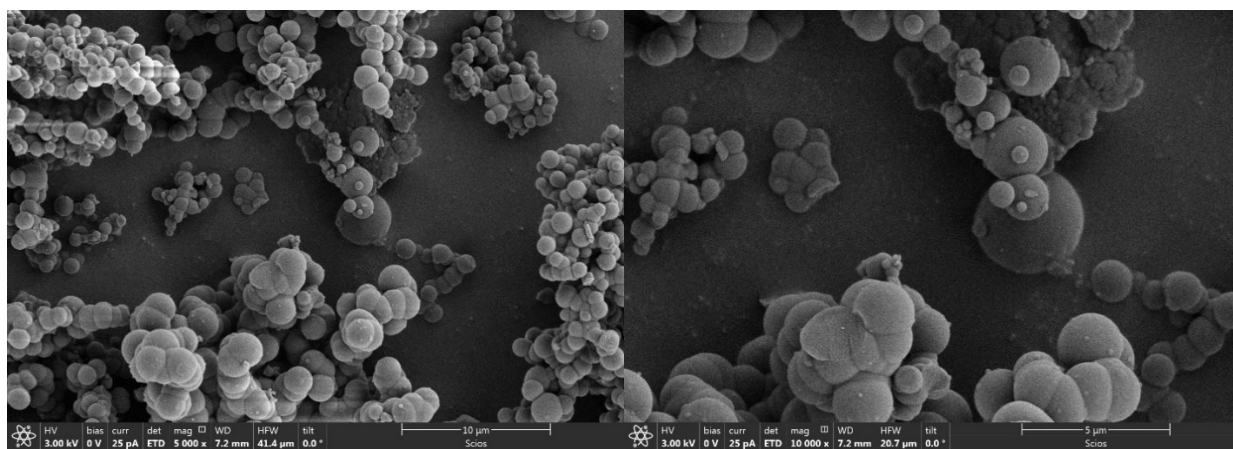
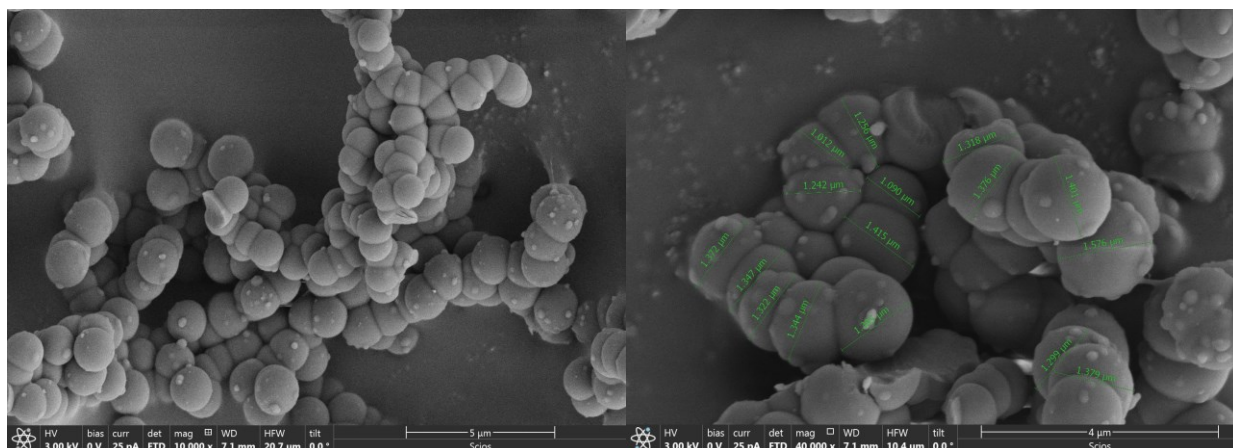


Figure S177. Experimental powder XRD patterns of 1,4-cycloheanedimethanol.

1.18 Scanning Electron Microscopy



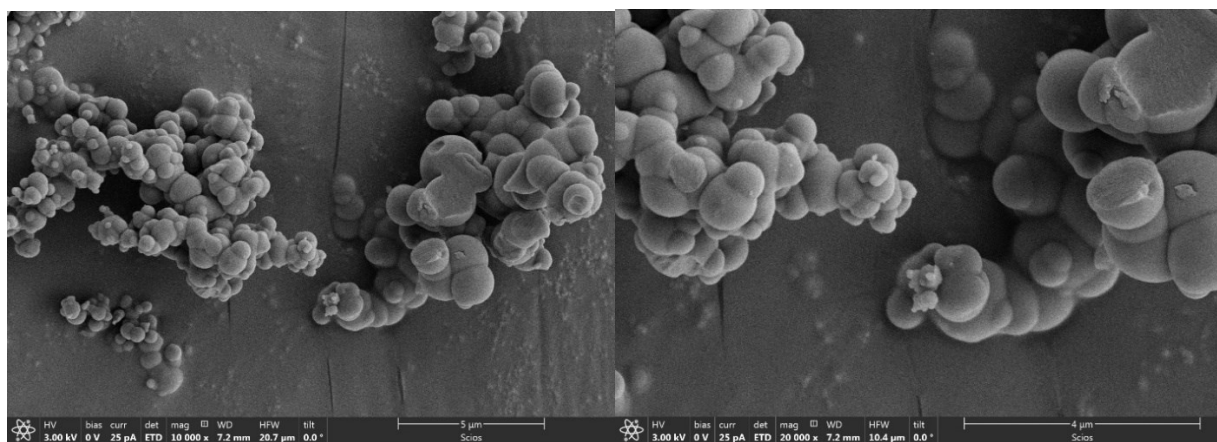


Figure S181. SEM micrographs of polyketone **PAAK-4**.

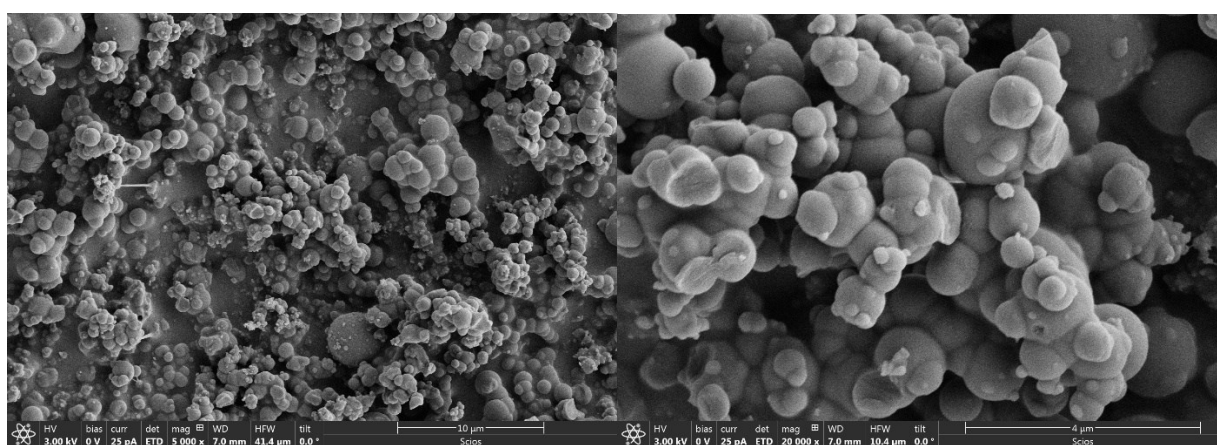


Figure S182. SEM micrographs of polyketone **PAAK-5**.

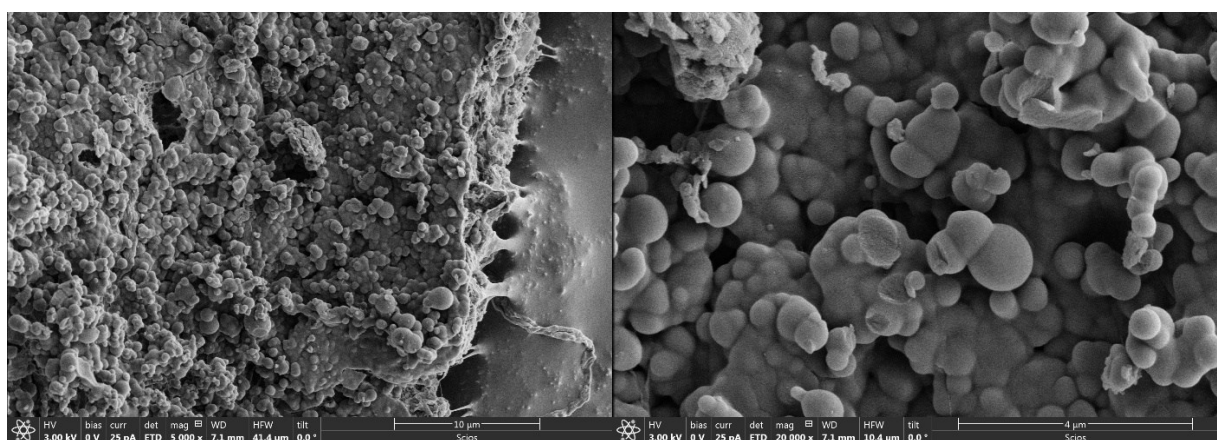


Figure S183. SEM micrographs of polyketone **PAAK-6**.

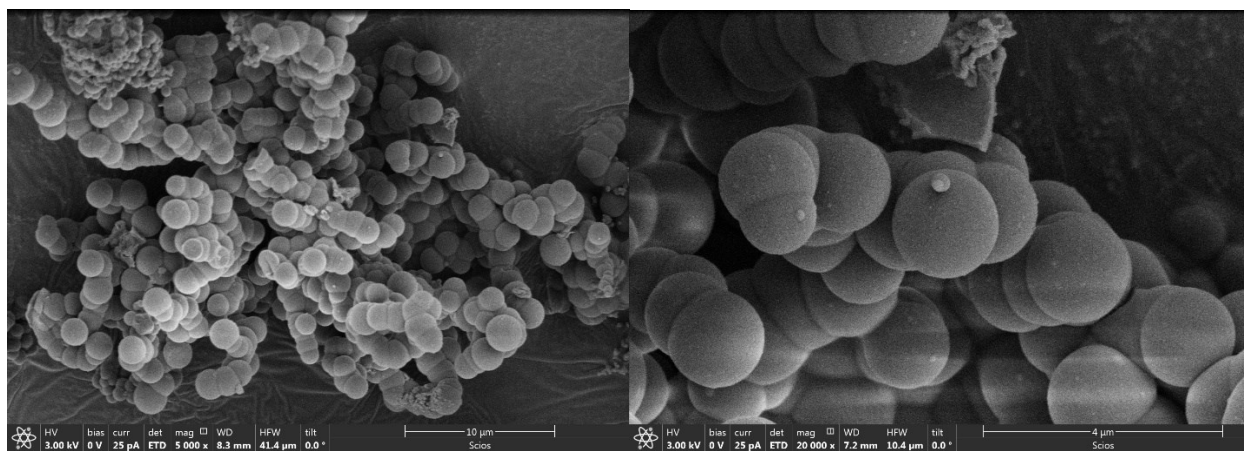


Figure S184. SEM micrographs of polyketone PAAK-7.

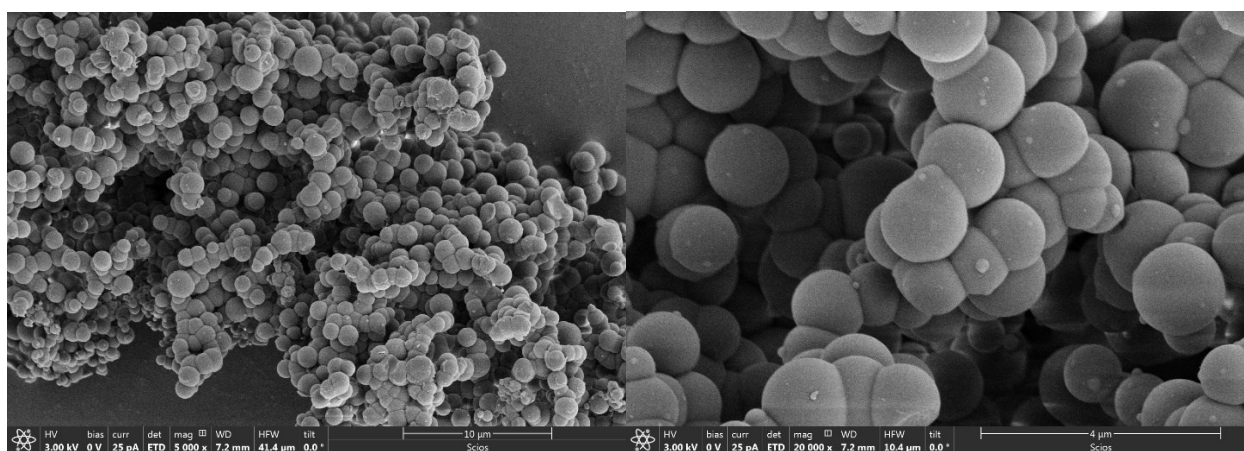


Figure S185. SEM micrographs of polyketone PAAK-8.

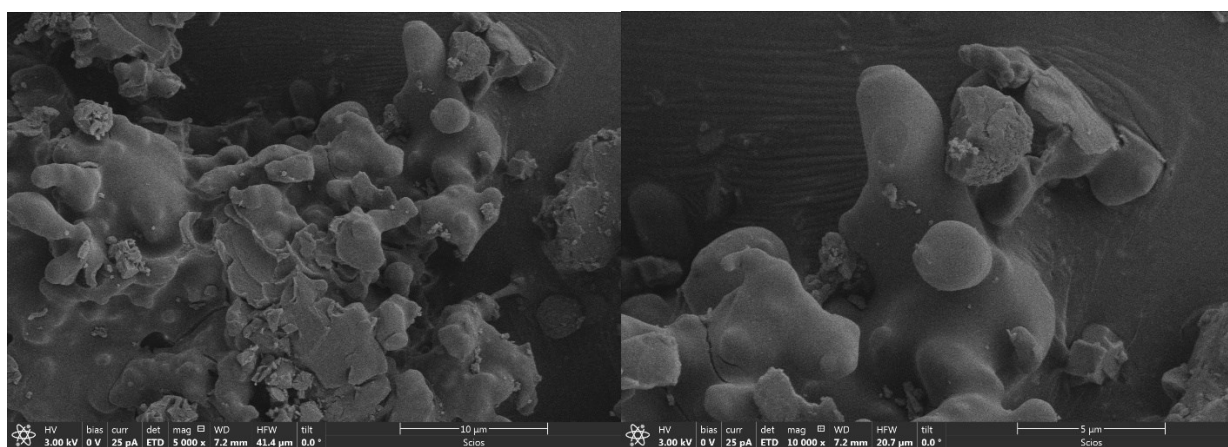


Figure S186. SEM micrographs of polyketone PAAK-9.

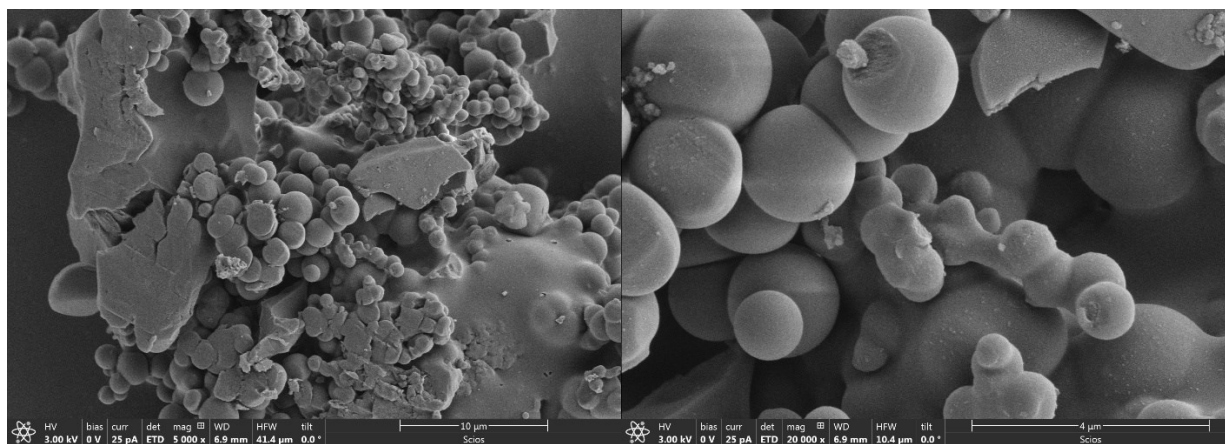


Figure S187. SEM micrographs of polyketone **PAAK-10**.

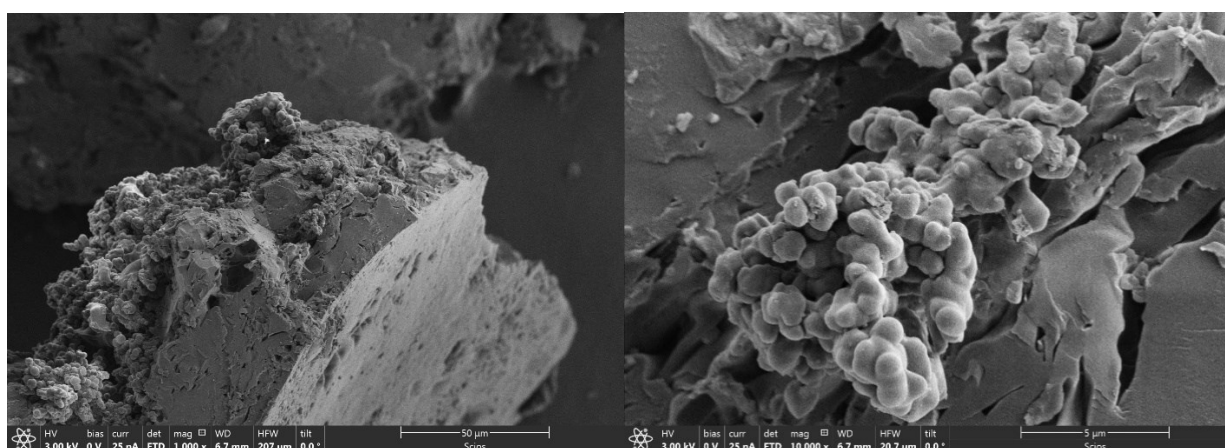


Figure S188. SEM micrographs of polyketone **PAAK-11**.

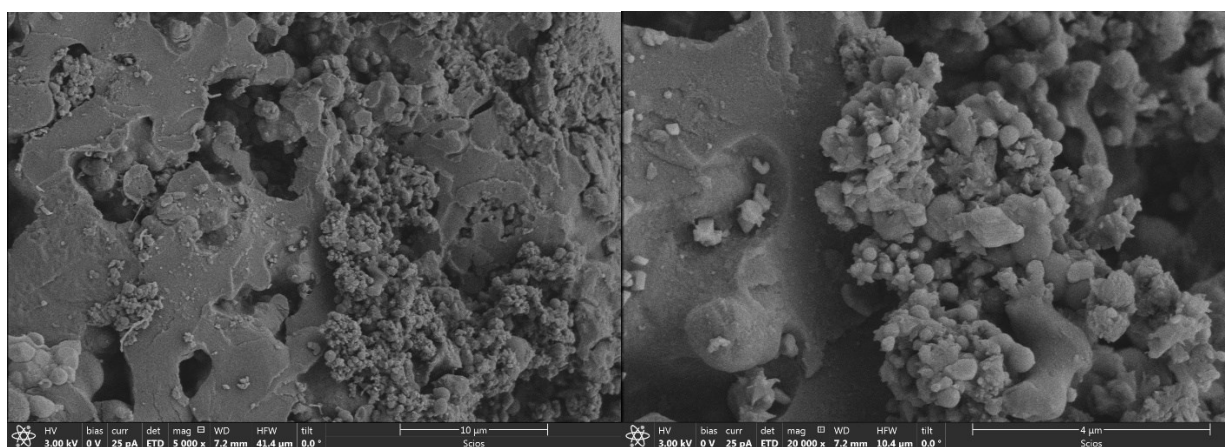


Figure S189. SEM micrographs of polyketone **PAAK-12**.

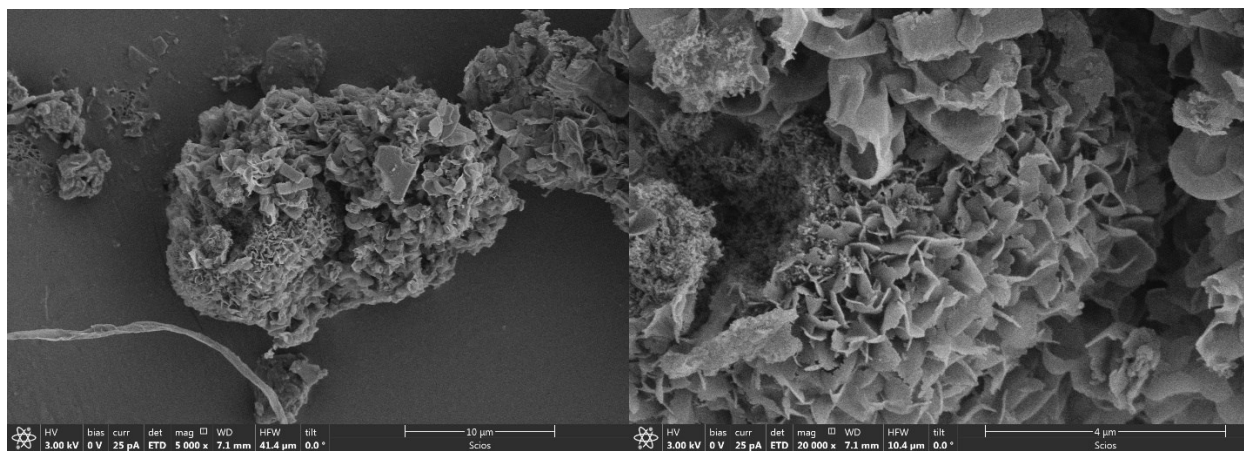


Figure S190. SEM micrographs of polychalcone **PCH-1**.

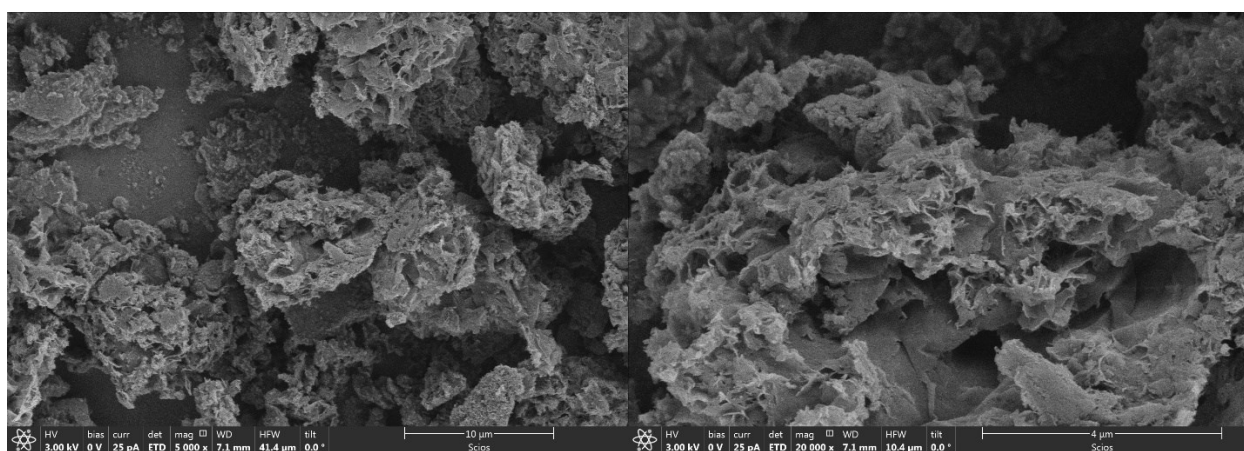


Figure S191. SEM micrographs of polychalcone **PCH-7**.

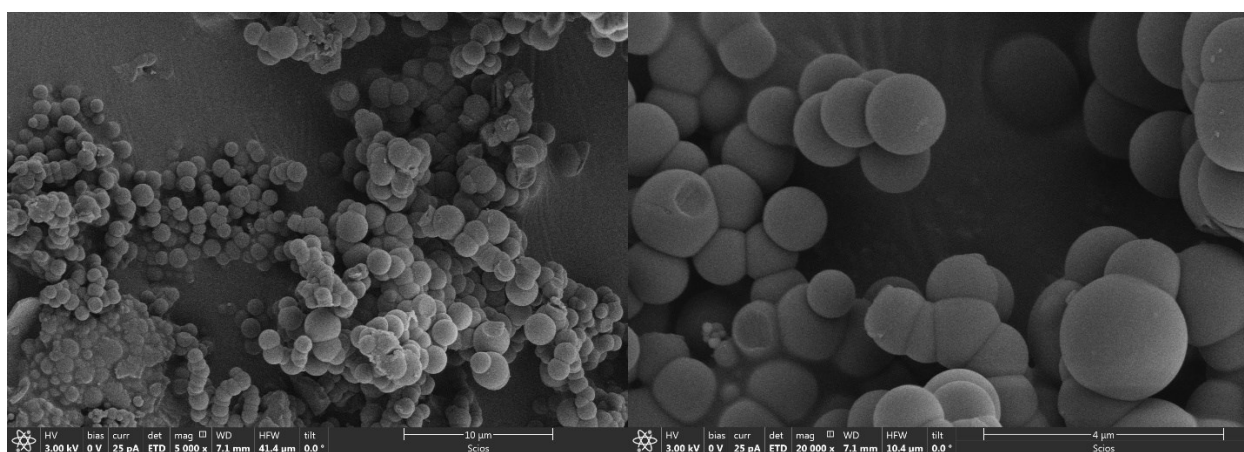


Figure S192. SEM micrographs of polyketone **PAAK-1** obtained in atmosphere of hydrogen.

1.19 Powder XRD and Scanning Electron Microscopy analysis

Table S4. Comments on the analysis of the obtained polymers with SEM and pXRD

Entry	Polymer	SEM	Powder XRD	
			Crystalline state	d-spacing of the largest amorphous bump
1	PAAK-1	Spherical agglomerates (size ~1.5 μm)	Amorphous phase clearly formed; size < 2 nm	4.94 \AA
2	PAAK-2	Spherical agglomerates (size ~0.5 μm)	Amorphous phase clearly formed; size < 2 nm	4.90 \AA
3	PAAK-3	Inhomogeneous agglomerates with spherical particles (size ~3 μm)	Amorphous phase clearly formed; size < 2 nm	5.19 \AA
4	PAAK-4	Spherical agglomerates (0.2-2 μm)	Amorphous phase clearly formed; size < 2 nm	4.51 \AA
5	PAAK-5	Spherical agglomerates (0.1-2 μm)	Amorphous phase clearly formed; size < 2 nm	4.90 \AA
6	PAAK-6	Inhomogeneous agglomerates with spherical particles (0.1-1 μm)	Amorphous phase clearly formed; size < 2 nm	5.02 \AA
7	PAAK-7	Spherical agglomerates (size ~2 μm)	Amorphous phase clearly formed; size < 2 nm	4.88 \AA
8	PAAK-8	Spherical agglomerates (size ~1 μm)	Amorphous phase clearly formed; size < 2 nm	5.18 \AA
9	PAAK-9	Inhomogeneous agglomerates with spherical particles	Amorphous phase clearly formed; size < 2 nm	5.01 \AA
10	PAAK-10	Complex inhomogeneous agglomerates With incorporated spherical agglomerates (size ~2 μm)	Amorphous phase clearly formed; size < 2 nm	4.52 \AA
11	PAAK-11	Complex inhomogeneous agglomerates	Amorphous phase clearly formed; size < 2 nm	4.52 \AA
12	PAAK-12	Complex inhomogeneous agglomerates	Amorphous phase clearly formed; size < 2 nm	4.97 \AA
13	PCH-1	Flakes-like crystallites	Semicrystalline material with large unit cell. Peaks are very broad so not possible to index.	
14	PAAK-1 obtained in H_2	Spherical agglomerates (size ~0.7–2.1 μm)	Amorphous phase clearly formed; size < 2 nm	4.84 \AA

2. Mechanical properties

PAAK-1 was prepared according to the method described in Table 2, entry 1 (main paper). The commercial sample of PEEK (450g rod, 300 mm length and 6mm diameter) studied here was purchased from the RS (<https://uk.rs-online.com/web/>). The commercial HDPE sample (granule, 2-4 mm particle, density: 0.930 g/cm³) studied here was purchased from the Goodfellow (<https://www.goodfellow.com/>).

Processing of PAAK-1: The polymer sample was immersed in liquid nitrogen for 30 minutes and pulverised. The polymer was then immersed in THF solvent overnight. Subsequently, the polymer was subjected to vacuum oven drying at 60°C for one hour to achieve complete solvent removal. The dried polymer powder was carefully sandwiched between the bottom and top plates of the mould, ensuring proper alignment. The assembled mould was then transferred to the heated surface of the Specac constant film maker (set to 300 °C). A constant pressure of 1900 N was applied to the mould for a minimum of one minute to induce the film formation. Upon completion of the film formation process, the mould was removed from the heating surface and allowed to cool completely. Once the mould had cooled, the film was carefully peeled off from the plates. The mould was specifically designed to create a cavity between the top and bottom plates, enabling the formation of a 2 mm film of uniform thickness.

Similarly, HDPE granules and PEEK samples were employed to fabricate 2 mm thick films through compression at the respective temperatures.

Measurement of mechanical properties: The mechanical properties were estimated using nanoindentation method. Nanoindentation techniques are widely employed to assess the mechanical properties of both materials and thin films. It enables the direct measurement of load applied to a sharp indenter and its displacement as a function of indentation depth. The values of hardness and elastic modulus can be extracted from the load-displacement curves obtained during loading and unloading cycles. All three films were individually mounted on a flat magnetic surface of the Nanoindenter. All measurements were conducted using a Nanoindenter Optics11 Chiaro instrument, employing a continuous stiffness method at a frequency of 25 Hz and a suitable displacement amplitude. A spherical indenter with a diameter of 18 µm and a stiffness of 39.53 N/m was utilised. Prior to the measurements, the equipment was calibrated using spherical indenter. Load-displacement curves were analysed using the Oliver and Pharr method [2] to extract mechanical properties. The elastic modulus was calculated based to the following relation. Further changes in equations are used as discussed in [3].

$$S = 2\beta E \sqrt{\frac{A}{\pi}}$$

where A, E, and S represent the contact area, elastic modulus, and contact stiffness, respectively. The geometric correction factor b was assumed to be unity [4]. Given the direct proportionality between the contact area and the square of the contact depth, its value was estimated through calibration using known polymer properties. The proportionality constant provided both the contact area and contact depth values in accordance with the methodology proposed in [5]. The contact stiffness value was determined by measuring the initial slope of the unloading curve, as depicted in **Figure S193** and **Figure S194**. The computed elastic moduli for each polymer are depicted in **Figure S195**. Additionally, the Vickers hardness (HV) values for each polymer were measured using a Mitutoyo series 810 HM 210/220 instrument and reported in **Figure S196**. The obtained values are consistent with previously reported values [6–9].

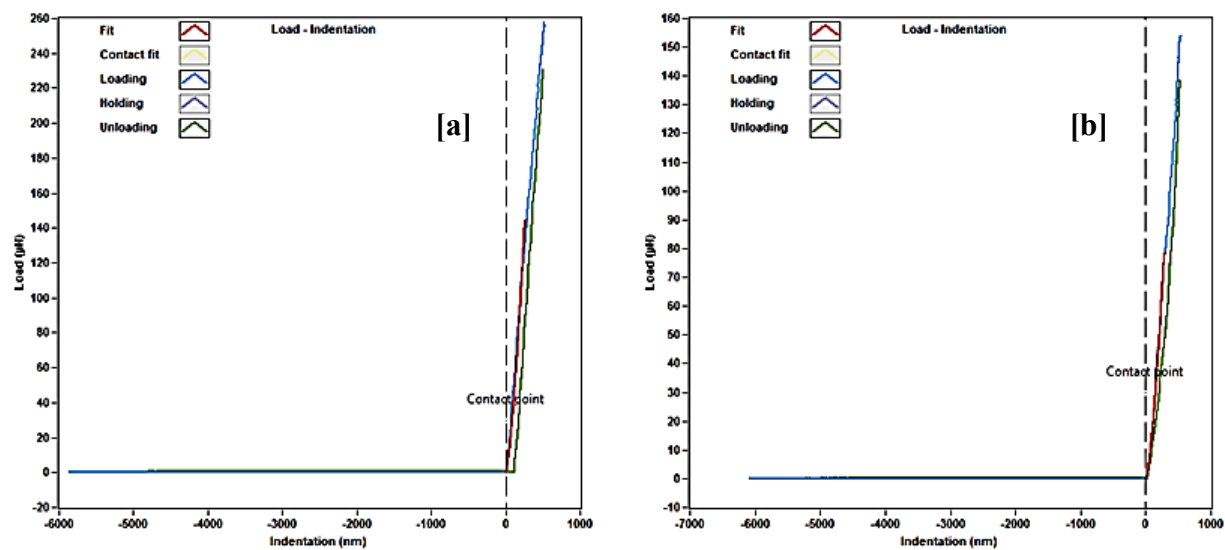


Figure S193. Loading and unloading curves for [a] PEEK and [b] HDPE.

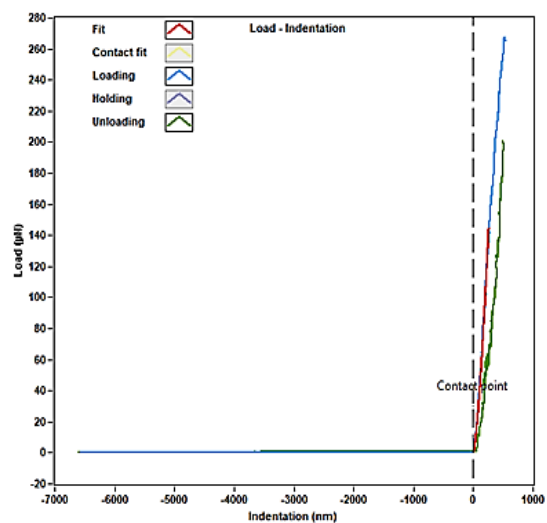


Figure S194. Loading and unloading curves for Polyketone PAAK-1.

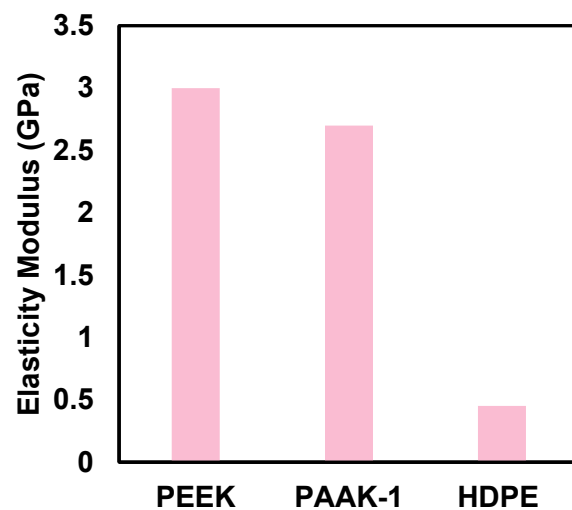


Figure S195. Elasticity modulus of polymers PEEK, PAAK-1 and HDPE.

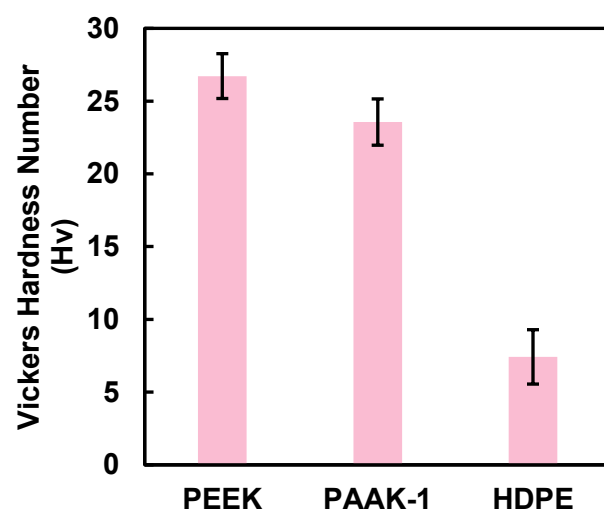


Figure S196. Vickers hardness number of polymers PEEK, PAAK-1 and HDPE.

3. References

- [1] Peña-López, M.; Piehl, P.; Elangovan, S.; Neumann, H.; Beller, M. “Manganese-Catalyzed Hydrogen-Autotransfer C–C Bond Formation: α -Alkylation of Ketones with Primary Alcohols.” *Angew. Chem. Int. Ed.* **2016**, 55, 14967-14971.
- [2] Liu, J.; Hu, K.-F.; Qu, J.-P.; Kang, Y.-B. “Organopromoted Selectivity-Switchable Synthesis of Polyketones” *Org. Lett.* **2017** 19 (20), 5593-5596.
- [3] Carl, O. C W.; Pharr G. M. “An improved technique for determining hardness and elastic modulus using load and displacement sensing indentation experiments.” *Journal of materials research* **1992**, 7(6), 1564-1583.
- [4] Fischer-Cripps, A. C. “Examples of nanoindentation testing.” *Nanoindentation* **2002**, 159.
- [5] Hochstetter, G.; Jimenez, A; Loubet, J. L. “Strain-rate effects on hardness of glassy polymers in the nanoscale range. Comparison between quasi-static and continuous stiffness measurements. *J. Macromol. Sci. Phys.* **1999**, 38(5-6), 681-692.
- [6] Chengzhu, L.; Li, Y.; Tjong, S. C. “Polyetheretherketone and its composites for bone replacement and regeneration.” *Polymers* **2020**, 12 (12), 2858.
- [7] Yutao, Y.; Jiang, C.; Huo, Y.; Li C. “Preparation and tribological behaviors of lubrication-enhanced PEEK composites.” *Applied Sciences* **2020**, 10 (21), 7536.
- [8] Tebeta, R. T.; Fattahi, A. M.; Ahmed N. A. “Experimental and numerical study on HDPE/SWCNT nanocomposite elastic properties considering the processing techniques effect.” *Microsystem Technologies* 2020, 26, 2423-2441.
- [9] Nectarios, V.; Petousis M.; Maniadi A. “Sustainable Additive Manufacturing: Mechanical Response of High-Density Polyethylene over Multiple Recycling Processes.” *Recycling* **2021**, 6(1), 4.